Sea Level, Ice Sheets and Climate during Marine Isotope Sub-stages 5a and 5c

Emma-Kate Potter

Research School of Earth Sciences
Australian National University

A thesis submitted for the degree of
Doctor of Philosophy of The Australian National University.

November 2002

Statement

This thesis is an account of my research undertaken during the period March 1999 to November 2002 while I was a full-time student in the Research School of Earth Sciences at the Australian National University. Except as otherwise indicated in the text, the work described is my own. This thesis has never been submitted to another university or similar institution.

Emma-Kate Potter

Canberra

November 2002

...they are ill discoverers that think there is no land when they can see nothing but sea.
Francis Bacon (1561-1626)

Acknowledgments

There are so many people who deserve recognition for their contributions to this thesis and to my life during the last few years. First of all I would like to thank my supervisor Kurt Lambeck for his support, guidance and his talent for always knowing the right questions to ask! Thanks also to Tezer Esat for our animated discussions and for teaching me the 'ins and outs' of U-Th mass spectrometry. Thanks to John Chappell for sharing his expertise on 'all things Huon Peninsula'. A special thank you Herb McQueen for always being there, whether it be for a laugh or as a shoulder to cry on, and for being a true mentor (thanks also for the *secret* stash of snacks in the top drawer of your filing cabinet...).

Thanks to those 'geodynamites' who have come and gone and those who have been there all along: Jean, Derek, Paul T, Clementine, Yusuke, David, Georg, Susanne; to Paul J and Tony for patiently answering endless questions about 'glacio-hydro-isostasy'; to Richard and Frédéric for making me the 'senior' student; to Kevin for the cakes; to Julie and Nerilie for the therapeutic 'girl' chats; and to Jonathon for our deep philosophical discussions about life, the universe and PhDs. Thanks also to the rest of the lunchtime crowd including Todd, Malcolm S, Stewart and Nick. A huge thank you to Lois for being a true friend and for always making me smile. Thanks also to Graham for teaching me everything I know about U-Th chemistry. Many thanks to Helen, Gael, Juan, John M., Wolfgang and many others for their professional and personal support. I am also deeply grateful for the assistance of Ulrich Radtke, Gerhard Schellmann and Eugene Wallensky during the Barbados and PNG fieldwork.

Before the dreaded 'writing-up phase' I seem to recall having a bit of a life outside my office and lab that was made worthwhile thanks to the friendship of Helen, Gerard, Susie, Matt, Todd, Pip, Carrie and Darren and Co. Thanks also to Linda, Jess and Ben for our 'Purple Pickle' lunches.

Thanks to mum and dad for your constant love and encouragement - I never would have made it this far without you. (Thanks also for moving overseas and trusting me with the house, car, and access to the bank account !!!)

And finally, to my best friend and husband Steve - without your love and support (and proof-reading skills) this thesis may not have made it to the printer. Thank you for believing in me even when I did not believe in myself.

Abstract

The timing and magnitude of marine isotope sub-stage (MIS) 5a and 5c sea-level oscillations have been determined by U-Th dating of more than 80 coral samples from the uplifted reef terraces at Barbados. At least three distinct periods of coral growth during sub-stages 5a and 5c have been identified and are associated with morphologically distinct reef deposits. The 'classic' sub-stage 5c and 5a deposits were found to have ages of ~101 ka and ~84 ka respectively. An additional period of coral growth during sub-stage 5a was found to occur at ~77 ka BP. This is the first time a distinct sea-level feature of this age has been clearly established. The extensive U-Th data set has also enabled an examination of the processes influencing the reliability of U-Th dating, including the possibility of changes in oceanic δ^{234}U and the effects of diagenetic alteration on a coral's U-Th system.

The sea levels associated with the classic sub-stage 5c and 5a deposits and the additional 5a feature at Barbados are -15±4 m, -19±4 m and -19±4 m respectively. Further estimates of sub-stage 5a sea level at sites throughout the Caribbean range from -19 m at Barbados to above present sea level on the US East Coast. These estimates are reconciled in the current study by taking into account the effects of glacio-hydro-isostasy. The comparison of sea-level observations with glacio-hydro-isostatic model predictions provides constraints on both the melting history of the Laurentide Ice Sheet (LIS) during MIS 5 and on the effective viscoelastic rheology of the Earth. In particular, the modelling results suggest that the LIS may have been centred further north and that it contributed a smaller proportion to the global ice volume during MIS 5 compared to MIS 3 or the last glacial maximum. The results also point to a high viscosity for the upper mantle beneath the LIS and surrounding region ($>4\times10^{20}$ Pa s) and a high viscosity for the lower mantle ($>1\times10^{22}$ Pa s).

The new Barbados sea-level record established in this thesis implies that the sea-level change during sub-stages 5a and 5c is more complex than suggested by some previous studies. A similar complexity is also implied by the MIS 5 uplifted coral reefs at Huon Peninsula, PNG. A comparison of these sea-level observations with other proxy records of climate change indicates that climate variability during MIS 5 is the result of a complex interplay between insolation forcing and intrinsic climate instability.

Contents

Chapter 1

Introduction

Climate change during the late Quaternary has been dominated by large scale oscillations between glacial and interglacial conditions. Ice volume and sea level are a direct measure of the state of climate, so precisely defining the timing and magnitude of global ice-volume variations during the last glacial cycle can aid in illuminating the mechanisms involved in the control of climate change. The focus of this study is sea-level change during marine isotope sub-stages 5a and 5c. These events are of importance because they represent the transition between the interglacial conditions of sub-stage 5e, similar to the Earth's present state, and the more heavily glaciated period leading into the last glacial maximum. In this thesis I will demonstrate that by interpreting sea-level observations in the context of glacio-hydro-isostatic models and other proxy records of climate change, a coherent picture of climate can be established.

Estimates of global ice volume can be made from $\delta^{18}O$ records derived from shells of foraminifera in deep sea cores (Shackleton and Opdyke, 1973). However, foraminifera not only measure changes in global oceanic $\delta^{18}O$, but are also a function of temperature changes and local variations in water $\delta^{18}O$. Instead of using this proxy, direct estimates of changes in global ice volume can be made from the preserved evidence of past sea levels. Indicators of paleo-sea level include coral reefs, wave cut notches, marine facies, beach deposits and periodically submerged speleothems. Late Pleistocene coral reefs, where they are well preserved and accessible, can be dated using high precision U-Th techniques to provide a very useful record of the timing and magnitude of sea-level change.

This study focuses on the sea-level oscillations during marine isotope sub-stages (MIS) 5a and 5c, which immediately follow the last interglacial period (sub-stage 5e). In most parts of the world, coral reefs and other sea-level indicators that formed during these

events are presently submerged and have often been overprinted during the subsequent post-glacial sea-level transgression. However, at rapidly uplifting coastlines (such as Barbados, West Indies, and Huon Peninsula, Papua New Guinea), coral reefs that formed when sea level was below present are now exposed above present sea level (Veeh and Chappell, 1970; Mesolella *et al.*, 1969). Subsequent studies have established that the uplifted coral terraces of Barbados and Huon Peninsula record each of the major interstadials and interglacial events identified in the deep sea core $\delta^{18}O$ records over at least the last 400-500 ka (Chappell, 1974; Bender *et al.*, 1979; Schellmann and Radtke, 2001).

Previous studies at Barbados suggest there were two distinct periods of reef growth corresponding to the 'classic' sub-stage 5a and 5c events identified in marine $\delta^{18}O$ records (Gallup *et al.*, 1994; Ku *et al.* 1990; Edwards *et al.*, 1987b; Bard *et al.*, 1990). Recent revised morphostratigraphic mapping of the southern Barbados coral terraces reveals a number of additional, morphologically distinct sub-reefs (Schellmann and Radtke, 2001). These observations imply a more complex sea-level history than has previously been proposed for that period, but the timing of these events have not been well established. High precision U-Th ages are required for the purposes of calculating precise sea levels associated with each of these deposits and for comparison with other proxy climate records.

Typical analytical precision for U-Th age analyses is 200-400 years for 80-100 ka samples.[1] Additional uncertainties may be introduced by the effects of sub-aerial weathering and diagenetic alteration, which can lead to the mobilisation of uranium and thorium isotopes. The effects of subtle diagenetic alteration on the U-Th system in corals are not well understood (Gallup *et al.*, 1994; Hamelin *et al.*, 1991; Bar-Matthews *et al.*, 1993; Fruijtier *et al.*, 2000; Thompson *et al.*, 2002). A comparison of the calculated initial $\delta^{234}U$ of a coral sample[2] with that of modern corals is regarded as one of the most important criteria for judging of the reliability of the measured U-Th age (Gallup *et al.* 1994; Stirling *et al.*, 1995). This criterion is based on the assumption that the $\delta^{234}U$ of ocean water remains unchanged over time-scales of several hundred thousand years (Henderson, 2002). However, there is a growing body of evidence that suggests ocean water $\delta^{234}U$ may have changed during the last glacial cycle (see chapter 3 for references). This may complicate the use of $\delta^{234}U$ as a test of closed system behaviour and has implications for the interpretation of

[1] This quoted uncertainty does not include uncertainty in the decay constants of the radioactive uranium and thorium isotopes.

[2] $\delta^{234}U$ is a conventional expression of the permil excess of ^{234}U over ^{238}U compared to an equilibrium state.

U-Th ages. By extensively sampling and dating a large number of samples from each site, the issues of oceanic δ^{234}U and the effects of diagenetic alteration can be addressed more comprehensively. This sampling strategy also minimises the assignment of erroneous ages and may be as important as other physical, chemical and isotopic criteria in determining the reliability of dating results.

Milankovitch's (1941) orbital forcing model postulates that global ice volume and climate are dependent on orbitally-driven changes in seasonal solar insolation received at high northern latitudes. The main periods of climate oscillation predicted by insolation variations (~20-100 ka, Berger, 1988; Berger and Loutre, 1991) are present in many records of climate change (Hays *et al.*, 1976). However, a more complex picture of sea level and climate change has emerged in recent studies. In particular, climate variability at frequencies higher than predicted by Milankovitch's orbital forcing model are also present. This 'suborbital' period climate variability is evident in MIS 3 Greenland ice core δ^{18}O records (proxy for atmospheric temperature changes, Dansgaard *et al.*, 1993; Bond *et al.*, 1993) and in North Atlantic Ocean sediment records (episodes of enhanced ice-rafted debris (IRD) deposition and interruptions to the thermohaline circulation, Heinrich, 1988; Bond and Lotti, 1995; Chapman *et al.*, 2000). The major ice-rafting episodes during MIS 3, known as Heinrich events, occur every 5-7 ka and also appear to be associated with rapid sea-level oscillations identified at Huon Peninsula (Yokoyama *et al.*, 2001b; Chappell, 2002). The mechanisms leading to these periodic climate oscillations are not yet well established. Internal instability and collapse of the Laurentide Ice Sheet has been suggested as a trigger for the periodic interruptions of North Atlantic thermohaline circulation (MacAyeal, 1993a,b). Other external forcing mechanisms have been proposed that involve non-linear interactions between the atmosphere-ocean system (Cane, 1998). Variations of a similar frequency to Heinrich events are also evident in MIS 5 ice core and oceanic records (Chapman and Shackleton, 1998, 1999; McManus *et al.*, 1994; Oppo *et al.*, 2001; Oppo and Lehman, 1995). Because the distribution of ice in the North Atlantic region at this time was different to that of MIS 3 (Clark *et al.*, 1993), a comparison of the climate instabilities in these two periods can give an insight into the behaviour of climate in different mean states.

At first glance, estimates of stage 5a sea level from the Caribbean and surrounding region appear to be inconsistent (see figure 1.1). In Barbados, at the peak of stage 5a, sea level reached ~19 m below present (this study). Dodge *et al.* (1983) estimated that the stage 5a sea level at Haiti was ~13 m below present. Further north, in the Bahamas, stage

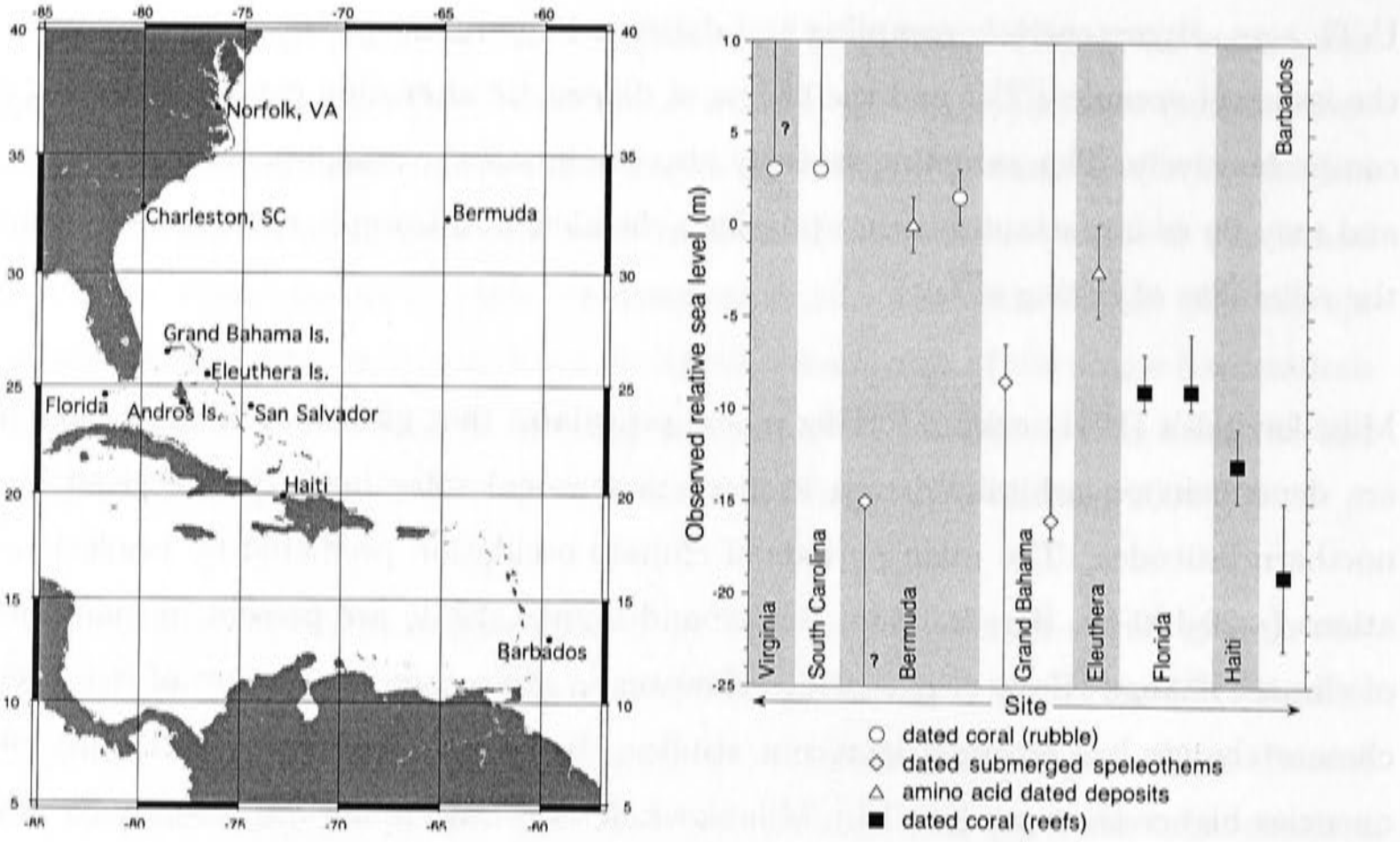

Figure 1.1: Summary of sub-stage 5a sea-level estimates and locations in the Caribbean region. See text for references. Observations summarised in detail in section 4.5 of chapter 4.

5a beach deposits above present sea level indicate that local sea level rose to above 5m below present at that time (Hearty, 1998; Hearty and Kindler, 1994; Hearty and Kaufman, 2000; Kindler and Hearty, 1996). Dating of a submerged speleothem at Lucayan Caverns near Grand Bahama Island suggests that sea level remained below -8.5 m during stage 5a (Lundberg and Ford, 1994; Toscano and Lundberg, 1999). Submerged sub-stage 5a coral reefs off the south-east Florida Keys indicate that sea level at that time was between 6-10 m below present, allowing for subsidence (Ludwig *et al.*, 1996; Toscano and Lundberg, 1999). At Bermuda, stratigraphic considerations, amino acid racemisation dating and U-Th dating of samples from a coral rubble deposit above present sea level suggest that sea level may have been near or above present during sub-stage 5a (Hearty and Vacher, 1994; Ludwig *et al.*, 1996; Muhs *et al.*, 2001). On the US East coast, marine facies deposits, including coral rubble have been identified at elevations of greater than 3 m above present suggesting that sea level reached that point during sub-stage 5a (Szabo, 1985; Cronin *et al.*, 1981; J. Wehmiller, pers. comm.). These different estimates are generally attributed to poor sample quality, non *in situ* sample collection, uncertainties in tectonic setting and/or poor stratigraphic context.

Observations of relative sea levels do not simply record changes in ice-equivalent sea level.[3]

[3]Ice-equivalent sea level is defined as an ocean averaged change in sea level associated with melting a volume of ice (see chapter 5).

Instead, local sea-level change reflects not only changes in global ice volume but also the effects of the deformation of the Earth and perturbation of the geoid in response to changing ice and water surface loads. Collectively, these latter effects are termed glacio-hydro-isostasy. The sites mentioned above span the outer intermediate-field region associated with the Laurentide Ice Sheet and therefore experience different glacio-hydro-isostatic effects. For this reason, the relative sea-level histories at these sites differ. Past changes in local sea level are a function of the glacio-hydro-isostatic state of the earth at the time of interest relative to the present day and depend on both the Earth's viscoelastic rheology and the melting history of global ice sheets. For Caribbean sites, the melting history of the Laurentide Ice Sheet prior to and after the time of interest are important factors in determining the relative sea level at that time. A spatially and temporally distributed data set of sea-level observations can be used to place constraints on the earth and ice model parameters.

The aims of this thesis are to: (i) constrain the timing and magnitude of the classic sub-stage 5a and 5c sea-level oscillations at Barbados; (ii) investigate the validity of the δ^{234}U criterion as a test of reliability of U-Th age measurements; (iii) examine the relationships between global ice volume and North Atlantic region sub-orbital climate variability during MIS 5; (iv) use glacio-hydro-isostatic considerations to reconcile estimates of relative sea level at Barbados and Huon Peninsula with those from other sites in the Caribbean region; and (v) place constraints on the global ice volume variations and Laurentide Ice Sheet distribution during MIS 5.

The thesis is divided into 2 parts. Part 1 (chapters 2, 3 and 4) deals with the observations of sub-stage 5a and 5c relative sea level at Barbados, Huon Peninsula (PNG) and other sites in the Caribbean and surrounding region. Chapter 2 presents an overview of the selection criteria and analytical techniques involved in the U-Th dating of coral. The results of the U-Th analyses of over 80 Barbados coral samples are presented in chapter 3. Chapter 3 also discusses potential mechanisms for changing ocean water δ^{234}U as well as models of open system U-Th behaviour in corals and highlights how these influence the interpretation of U-Th ages. Chapter 4 presents the calculation of relative sea levels for each of the features identified at Barbados and a sea-level curve based on the Huon Peninsula uplifted coral terraces is also presented. In addition, the implications of sub-orbital sea-level oscillations are discussed in the context of the factors controlling climate change, such as insolation forcing and ice sheet instability. Finally, chapter 4 contains a detailed summary of the published estimates of sub-stage 5a relative sea level from sites in the

Caribbean and surrounding region. In Part 2, (chapters 5 and 6), I review the concepts of glacio-hydro-isostasy and present the results of numerical models which reconcile the seemingly conflicting estimates of sea level during sub-stage 5a. This is followed by a discussion of the constraints placed by these observations on the Earth's rheological structure and the melting history of the Laurentide Ice Sheet.

Part I

Relative Sea-Level Observations

Chapter 2

U-Th Age Analysis

2.1 Introduction

U-Th dating, based on the decay series of ^{238}U-^{234}U-^{230}Th, is the most commonly used technique in the analysis of late Quaternary-age carbonate material. This dating method is applicable to coral samples that were deposited less than 200 years ago (Edwards *et al.*, 1987a) and extends beyond the approximately ~50 ka upper dating limit of ^{14}C to as early as 500-600 ka BP (Stirling *et al.*, 2001).[1] Using thermal ionisation mass spectrometry (TIMS) analysis techniques, a precision of better than 0.5% can be routinely achieved for samples of 100 ka age. The focus of this study is the dating of late Pleistocene-age coral samples, of mainly sub-stage 5a and 5c age (~80-100 ka), from the uplifted coral terraces at Barbados.

U-Th dating is based on the following decay series:

$$^{238}U \xrightarrow{\tau_{1/2}^{238}} {}^{234}U \xrightarrow{\tau_{1/2}^{234}} {}^{230}Th \xrightarrow{\tau_{1/2}^{230}} \cdots \longrightarrow {}^{206}Pb \tag{2.1}$$

where the decay half-lives, $\tau_{1/2}^{238}$, $\tau_{1/2}^{234}$ and $\tau_{1/2}^{230}$ are 4.49×10^9 yr, 2.48×10^5 yr and 7.5×10^4 yr respectively.

Physical and geochemical processes can lead to the separation of daughter nuclides of this decay chain from their parents, producing a state of isotopic disequilibrium (Faure, 1986). The half-life of the parent, ^{238}U, is several orders of magnitude larger than that of its daughters, ^{234}U and ^{230}Th. Hence, if there is an excess of one of the daughter isotopes in this decay chain (such as ^{234}U) the decay of that daughter will occur more rapidly

[1] For samples younger than ~50 ka, both U-Th and ^{14}C dating techniques can be used, however the relationship between the radiocarbon time-scale and true calendar age is not well known prior to 20 ka BP as the production rate of ^{14}C in the atmosphere has not been constant.

than its formation from the decay of ^{238}U, and the system will approach a state of secular equilibrium. In this state, the activity of all of the radioactive daughters of the decay chain are equal to the activity of ^{238}U:

$$Activity = \lambda_{238} N_{238} = \lambda_{234} N_{234} = \lambda_{230} N_{230} \tag{2.2}$$

where N is the concentration and λ is the decay constant of each isotope ($\lambda \propto 1/\tau_{\frac{1}{2}}$). Therefore, in a state of secular equilibrium, the abundance of each isotope is directly proportional to its half-life.

U-Th dating of corals is possible because the ^{238}U-^{234}U-^{230}Th system is in disequilibrium in corals. As the carbonate skeleton of coral forms, it incorporates and concentrates elements from the surrounding seawater. Uranium and thorium exhibit different chemical behaviour and are highly chemically fractionated in seawater. Uranium is readily oxidised to the highly soluble uranyl (U^{6+}) ion and is easily dissolved in seawater under oxidising conditions. Thorium, however, is highly insoluble, and readily adsorbed onto the surfaces of particulate matter and quickly removed from the water column. Immediately after deposition, a coral skeleton contains ~3 ppm of uranium and virtually no thorium.

In an unaltered fossil coral sample, the only ^{230}Th that is present has been formed solely by the *in-situ* decay of its parent, ^{234}U. Thus, the activity of ^{230}Th increases until the system approaches secular equilibrium (figure 2.1). The concentrations (N) of the isotopes, ^{238}U-^{234}U-^{230}Th, at some time (T) after the deposition of the coral skeleton can be expressed as:

$$\begin{aligned} \frac{dN_{238}}{dT} &= -\lambda_{238} N_{238} \\ \frac{dN_{234}}{dT} &= \lambda_{238} N_{238} - \lambda_{234} N_{234} \\ \frac{dN_{230}}{dT} &= \lambda_{234} N_{234} - \lambda_{230} N_{230} \end{aligned} \tag{2.3}$$

The relative concentrations of these isotopes are, therefore, a measure of the time elapsed since the deposition of the coral skeleton. This is only true if the coral skeleton has remained a closed system with respect to uranium and thorium, meaning that no addition or removal of these isotopes has occurred other than by the process of radioactive decay.

The half-life of ^{238}U decay is several orders of magnitude larger than that of its daughters, so $\lambda_{238} \ll \lambda_{234}, \lambda_{230}$ and the change in concentration of ^{238}U over the time-scale of the dating technique can be considered negligible ($N_{238}(t) \approx$ constant). Using these assumptions, the system of differential equations (2.3) can be used to relate the time (T) since the

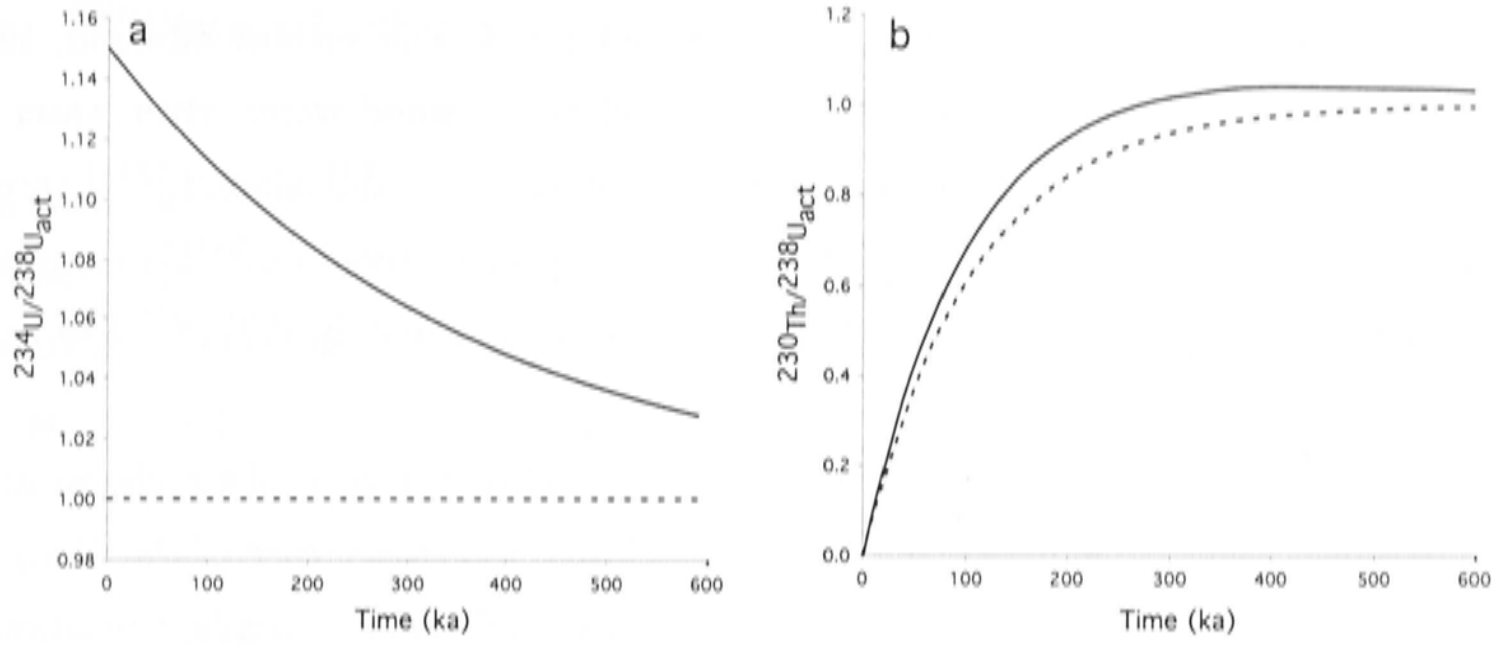

Figure 2.1: a) The $^{234}U/^{238}U$ activity ratio as a function of time for the case of initial disequilibrium, $[^{234}U/^{238}U]_{act}$ of 1.15 (solid) and initial equilibrium (dashed). b) The $^{230}U/^{238}U$ activity ratio as a function of time for the same two cases.

deposition of the coral skeleton to the U-Th isotopic composition of the coral as follows:

$$1 - \left[\frac{^{230}Th}{^{238}U}\right]_{act} = e^{-\lambda_{230}T} - \left[\frac{\delta^{234}U_m}{1000}\right]\left[\frac{\lambda_{230}}{\lambda_{230}-\lambda_{234}}\right]\left(1 - e^{(\lambda_{234}-\lambda_{230})T}\right) \tag{2.4}$$

where $\left[^{230}Th/^{238}U\right]_{act}$ is the measured activity ratio of ^{230}Th and ^{238}U. The quantity $\delta^{234}U_m$ is a conventional expression of the present day $^{234}U/^{238}U$ activity ratio:

$$\delta^{234}U_m = \left\{\left[\frac{^{234}U}{^{238}U}\right]_{act} - 1\right\} \times 10^3 \quad (‰) \tag{2.5}$$

$$= \left\{\left[\frac{\lambda_{234}N_{234}}{\lambda_{238}N_{238}}\right] - 1\right\} \times 10^3 \quad (‰) \tag{2.6}$$

River water (and consequently ocean water) contains an excess of ^{234}U with respect to ^{238}U.[2] The decay of ^{238}U produces ^{234}U via the emission of an alpha particle and short-lived intermediate daughters, ^{234}Th and ^{234}Pa. The daughter ^{234}U recoils as a result of this decay, which can damage its lattice site and allow for more efficient leaching and removal from the host material compared to the lattice bound ^{238}U. (Cherdyntsev, 1971; Osmond and Ivanovich, 1992). This alpha recoil may also lead to ejection of the ^{234}U daughter directly from the surface of the host material and into surrounding pore-water (Fleischer, 1982). The dislocation of ^{234}U and the damage of its lattice site may also encourage oxidation to the more soluble uranyl (U^{6+}) ion (Ku *et al.*, 1992). As a result, there is enhanced leaching of ^{234}U compared to ^{238}U during continental weathering, particularly from

[2] An excess of ^{234}U with respect to ^{238}U means the activity of ^{234}U is greater than that of ^{238}U i.e. $\lambda_{234}N_{234} > \lambda_{238}N_{238}$; $\left[^{234}U/^{238}U\right]_{act}$ is greater than unity and δ^{234}U is greater than 0‰. In ocean water, δ^{234}U is around 148‰.

limestones, uraniferous black shales and sedimentary rocks (Palmer and Edmond, 1993). Hence, an enhanced δ^{234}U may be present in percolating ground water, river water and seawater. Another source of ^{234}U-enriched seawater may be the diffusion of ^{234}U through pore water in ocean sediments (Ku, 1965). As a result of these processes, ^{234}U in ocean water is maintained in excess over secular equilibrium by approximately 15% (δ^{234}U$\approx$ 148‰)

The uranium isotopic composition of seawater is recorded in the coral's skeleton at the time of growth. Over time, decay of the excess ^{234}U leads to a decrease of the ^{234}U/^{238}U activity ratio, represented by δ^{234}U. Hence at some time (T) after a coral's deposition, its δ^{234}U is related to the initial value ($\delta^{234}U_i$) by the following expression:

$$\delta^{234}U_m = \delta^{234}U_i e^{-\lambda_{234}T} \tag{2.7}$$

δ^{234}U of the ocean is generally assumed to have remained constant during the late Pleistocene due to the long residence time of uranium in the ocean (Chen *et al.*, 1986). Therefore, a comparison of the calculated $\delta^{234}U_i$ with the present day δ^{234}U of the ocean is regarded as the most useful quantitative test of the reliability of the measured U-Th age of a coral.[3] However, there is a growing body of evidence suggesting that δ^{234}U of the ocean has changed measurably during the last glacial cycle (see chapter 3). The δ^{234}U reliability criterion will be addressed further in section 2.3.3 and in chapter 3.

[3]This expression, instead of equation 2.4, could be used to calculate the age of a fossil coral if i) the initial δ^{234}U of the sample is known and, ii) the coral has remained a closed system with respect to the uranium isotopes. However, the effects of diagenetic alteration on the U-Th system in fossil corals are still not well understood. For this reason, the age of the coral is generally calculated from equation 2.4, with equation 2.7 then used to calculate the initial $\delta^{234}U_i$ of the sample.

2.2 ^{230}Th and ^{234}U half-lives

Until recently, the half-lives of ^{230}Th and ^{234}U generally used in the calculation of U-Th ages were 75.38±0.59 ka (Meadows *et al.*, 1980) and 244.5±0.7 ka (weighted average of 244.6±0.73 ka from De Biever *et al.*, 1971, and 244.4±1.2 ka from Lounsbury and Durham, 1971, see table 2.1).

Authors	^{234}U half-life	^{230}Th half-life
Meadows *et al.*, 1980	-	75.38±0.59
De Biever *et al.*, 1971	244.4±1.2	-
Lounsbury and Durham *et al.*, 1971	244.6±1.2	-
Ludwig *et al.*, 1992	245.29±0.14	-
Cheng *et al.*, 2000	245.25±0.49	75.69±0.59
Bernal*et al.*, 2002	244.29±0.12	-

Table 2.1: Summary of ^{230}Th and ^{234}U half-life determinations. The half-lives used in the calculation of U-Th age in this study are given by Meadows *et al.* (1980) $\tau_{230} = 75.38 \pm 0.59$ ka) and De Biever *et al.* (1971) and Lounsbury and Durham *et al.* (1971) (weighted average $\tau_{230} = 244.5 \pm 0.7$ ka). The decay half-life ($\tau_{1/2}$) is related to the decay constant (λ) by the following relationship: $\tau_{1/2} = ln(2)/\lambda$.

Cheng *et al.* (2000) recently revised the estimates of half-lives of ^{230}Th and ^{234}U by TIMS analysis, using electron multipliers for the low intensity beams. The measured half-lives were τ_{230} =75.69±0.59 ka and τ_{234} =245.25±0.49 ka respectively. Both of these revised values are higher than those determined in previous studies but are within the quoted error. Bernal *et al.* (2002) measured the half-life of ^{234}U to be 244.29±0.12 ka by simultaneously measuring high intensity uranium beams of a secular equilibrium uraninite standard in a Faraday cup array. The value determined by Bernal *et al.* (2002) is more consistent with the earlier measurements of ^{234}U half-life, but has a smaller quoted uncertainty. Bernal *et al.* (2002) suggest that the half-life determinations of Cheng *et al.* (2000) may have been biased by instrumental artefacts such as dead-time corrections for the non-linear response of the electron multiplier and/or the uncertainty in the transmission to the multiplier through the RPQ. Because of the possible uncertainties in the measurements of Cheng *et al.* (2000) and the apparent conflict with the results of Bernal *et al.* (2002), in this study I use the earlier determinations from Meadows *et al.* (1980), De Biever *et al.* (1971) and Lounsbury and Durham (1971). A brief discussion of the analytical uncertainties in the calculated U-Th ages is given in section 2.6.

2.3 Reliability criteria

The processes of leaching and/or recrystallisation of the primary aragonite skeleton of a coral can lead to the mobilisation of uranium and thorium isotopes, thus potentially changing the apparent U-Th age. The possible effects of alteration on the U-Th system include the following: i) loss of uranium and thorium isotopes by leaching and dissolution via freshwater or seawater percolating through the coral skeleton; ii) uranium and thorium in ground water fluids may be incorporated into the coral during recrystallisation; iii) extraneous uranium and thorium may be added to the coral skeleton from the surrounding seawater or percolating ground water in the form of pore cements or detrital contamination. In addition, the different chemical behaviour of uranium and thorium may lead to the preferential removal or addition of one element relative to the other.

Assessing the reliability of a coral's measured U-Th age relies on a number of isotopic criteria, as well as thin section microscopy and X-ray diffraction analysis to look for evidence of physical alteration such as leaching or re-crystallisation of the primary aragonite skeleton to calcite or secondary aragonite. These reliability criteria are discussed in more detail in the following sections.

2.3.1 Sample collection

The effects of diagenetic alteration on the U-Th system are not well understood (Gallup *et al.*, 1994; Bar-Matthews *et al.*, 1993; and Hamelin *et al.*, 1991). For this reason, isolated age measurements of samples that may have undergone subtle alteration have the potential to produce misleading results. Therefore, it is desirable to extensively sample each site of interest to obtain multiple ages for a given horizon. For calculating paleo-sea levels, it is also necessary to take into account the stratigraphic context of each coral sample. Using these guidelines minimises the assignment of erroneous ages. We believe this approach to be as important as other physical, chemical and isotopic criteria in determining the reliability of dating results.

2.3.2 Petrography

In nature, the two most common forms of calcium carbonate are aragonite, with an orthorhombic crystal structure and calcite, with a hexagonal structure. Under normal pressure and temperature conditions, aragonite is metastable (Deer et al. 1970). However, in a marine environment most organisms that have calcareous skeletons, including corals, precipitate them as aragonite. When a coral is removed from the marine environment and

exposed to sub-aerial weathering, it is susceptible to dissolution, and readily converts to calcite. In contrast, in a marine environemt, recrystallisation is more likely to be in the form of secondary aragonite (Bar-Matthews *et al.*, 1993).

The transformation of the coral skeleton through dissolution and/or reprecipitation occurs on a number of scales. In some cases, calcitic or aragonitic cements are precipitated in the pore spaces from percolating ground water or from sea water that is supersaturated with respect to calcium carbonate. This cementation can fill the pore spaces but leaves the bulk of the original skeleton untouched. In cases where large parts of the coral skeleton are dissolved and replaced, this process in obvious in thin section because the primary structure of the skeleton can be destroyed. In contrast, during neomorphic replacement, dissolution and replacement of primary aragonite occurs on a very fine scale while preserving the original structure of the skeleton (Marshall, 1983; Bar-Matthews *et al.*, 1993; and James, 1974). Under these conditions, dissolution of primary material is often initiated in the centres of the trabeculae, well within the skeletal walls, along the centres of calcification (Marshall, 1983). Fine scale dissolution can result in the formation of micropores in the crystal structure. These regions can be identified in thin section as dark patches where the primary aragonite fibrous bundles are obscured (Bar-Matthews *et al.*, 1993).

The presence of secondary calcite within a coral skeleton can be identified using X-ray diffraction analysis. This technique uses a collimated beam of monochromatic X-rays to measure the spacing between crystallographic planes to identify different crystalline structures. It can be used to determine the relative proportions of calcite and aragonite within a sample with a detection limit of 1-2% calcite. Generally, samples with non-negligible calcite fractions (>1-2%) are considered unsuitable for dating.

Secondary aragonite cannot be distinguished from the primary material using X-ray diffraction. Instead, secondary aragonite and dissolution textures must be assessed qualitatively in thin section. As discussed previously, the textures arising from alteration include regions of fine dissolution micropores in which the characteristic fibrous bundles of aragonite crystals are obscured in thin section. Bar-Matthews *et al.* (1993) have shown that these micropores are sometimes filled with micron-sized aragonite crystals. In some cases, on a larger scale, micron-sized equant-tabular aragonite crystals replace the primary radial-fibrous texture. The precipitation of aragonite needle cements in the pore spaces of the coral skeleton are also identifiable in thin section. The micro-dissolution textures discussed above are also evident in modern corals. For this reason samples are not disregarded on

the basis of these textures.

In this study, samples were generally found to contain negligible calcite. However, in a number of samples there is some evidence for the dissolution textures described by Bar-Matthews *et al.* (1993) where the primary fibrous bundle textures of the skeleton are partially obscured. There is also evidence for precipitation of aragonite needles in the pore spaces in some samples. All of the corals in this study were exposed to sub-aerial weathering shortly after growth due to uplift and falling sea level, therefore any precipitation of secondary aragonite probably occurred shortly after growth in a marine environment. If this is the case then these aragonite cements should have a minimal effect on the U-Th age (Hamelin *et al.*, 1991). Figure 2.2 illustrates of a range of petrographic textures in thin sections that have been observed in the samples collected for the present study. Bar-Matthews *et al.* (1993) were not able to establish a correlation between the observed petrographic textures and the results of the U-Th measurements and this is also the case in this study. Therefore, samples showing subtle petrographic indicators of alteration were not disregarded *a priori*.

2.3.3 Isotopic and chemical reliability criteria

Uranium content

The uranium concentration of modern coral ranges between 2 and 3.5 ppm (Edwards *et al.*, 1987a; Szabo *et al.*, 1994; Shen and Dunbar, 1995; Gallup *et al.*, 1994; Hamelin, *et al.*, 1991). A distinct offset between the uranium concentrations of different species is evident in both modern and fossil corals (see results in chapter 3 and Min *et al.*, 1995; Chen *et al.*, 1991), which is probably due to biological effects. In addition, Min *et al.* (1995) and Shen and Dunbar (1995) have shown that the U/Ca ratio of a coral is also a function of water temperature and can vary by up to 3-4% per °C.

It is expected that the uranium concentration of a pristine fossil coral will fall within the range observed in modern samples, assuming the uranium concentration in the ocean has not changed significantly during the last several hundred thousand years. Alteration processes such as leaching, dissolution and re-precipitation of secondary calcite and aragonite may lead to the addition of extraneous uranium to the skeleton or the mobilisation and loss of uranium from the coral, both of which may affect the apparent U-Th age of the sample.

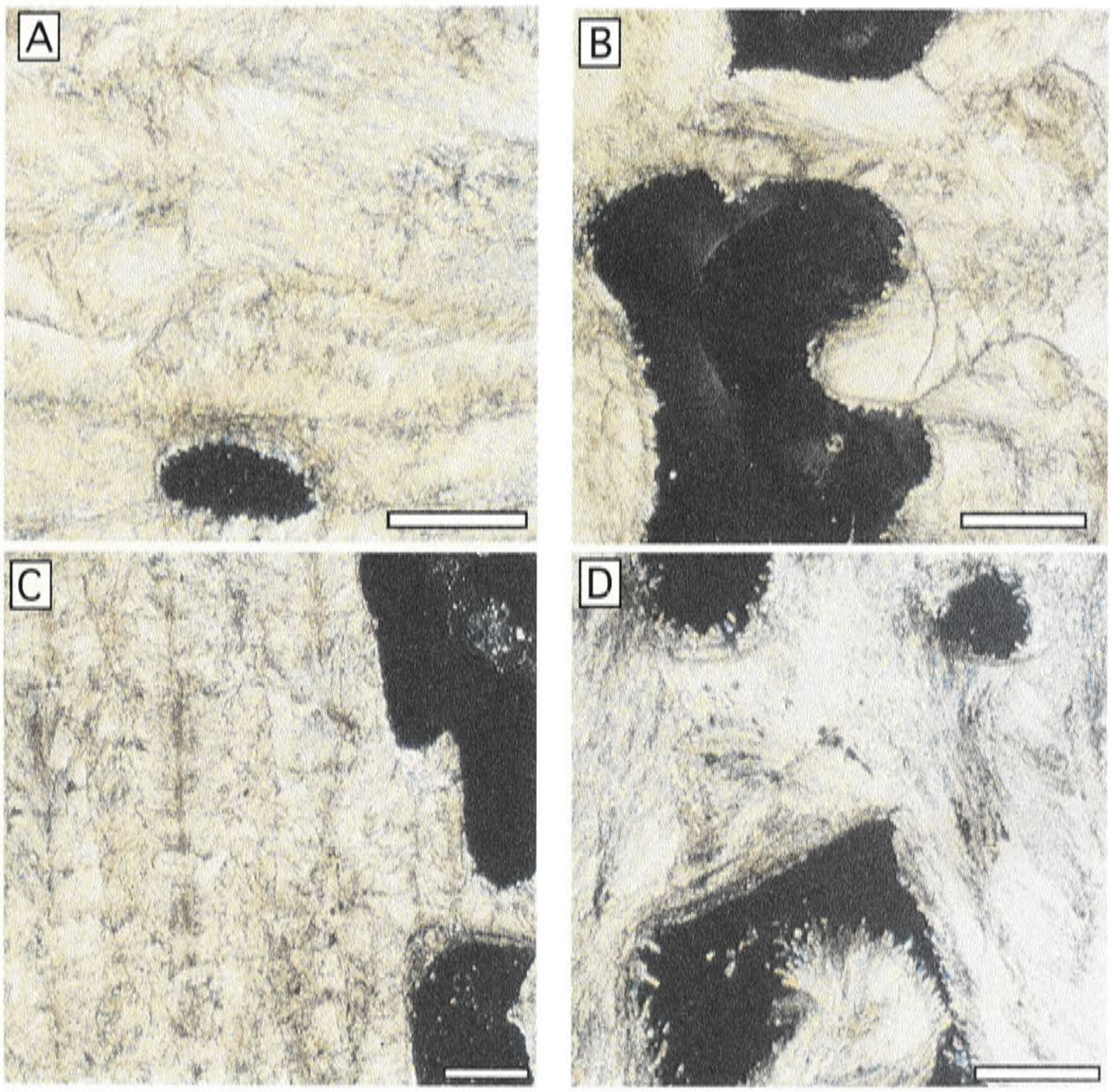

Figure 2.2: Examples of alteration textures seen in corals collected during this study (length of scale in each case is 400μm) a) *Acropora palmata* - longitudinal section, generally well preserved bundles of aragonite fibres; some cements on void walls; b)*Acropora palmata*, longitudinal section, in cross polarised light - generally well preserved bundles of aragonite fibres; small, secondary aragonite cements in voids c) *Diploria sp.* - longitudinal section in cross polarised light, generally well preserved bundles of aragonite fibres; d) *Acropora palmata* longitudinal section in cross polarised light - fine aragonite cements on walls of voids.

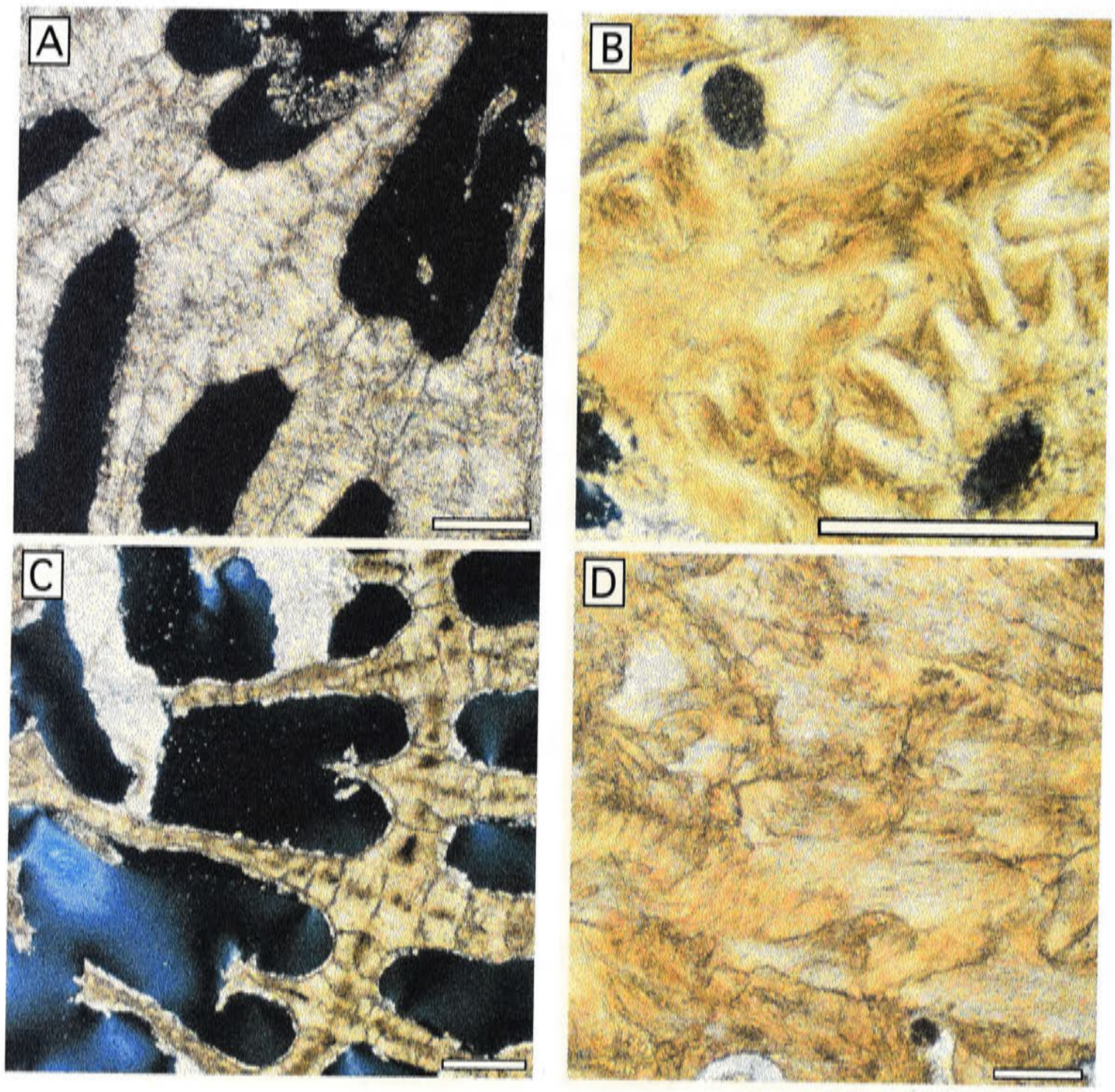

Figure 2.3: Further examples of alteration textures seen in corals collected during this study (length of scale in each case is 400μm). a) *Siderastrea sp.* - cross section in cross polarised light, well preserved bundles of aragonite fibres, some minor aragonite cements on walls; b) *Acropora palmata* - cross section in cross polarised light, possible infilling of voids, and aragonite fibres obscured, possibly an indicator of microscale dissolution processes; c) *Siderastrea sp.* - cross section in cross polarised light, possible infilling in septae, some cementation on walls; d) *Acropora palmata* - longitudinal section, generally well preserved bundles of aragonite fibres but possibly some dissolution textures.

^{232}Th concentrations

^{232}Th, like ^{230}Th, is highly insoluble and virtually absent from seawater. Consequently, a pristine coral skeleton initially contains negligible quantities of either isotope. Continental rocks and their particulate weathering products contain ^{232}Th in high concentrations (ppm to tens of ppm), as well as ^{238}U and its decay products ^{234}U and ^{230}Th. Therefore, if this detrital material is deposited in the pore voids of a coral via percolating fluids, it may affect the apparent U-Th age of the samples. The presence of ^{232}Th in a fossil coral sample is an indicator of this detrital contamination. Modern corals typically have a ^{232}Th concentration of less than 0.5 ppb (Edwards *et al.*, 1987a; Chen *et al.*, 1991). By assuming the composition of the contaminating material, a correction can be applied to the U-Th measured age to account for the detrital contamination (Chen *et al.*, 1991; Stein *et al.*, 1991; Eisenhauer *et al.*, 1993).

δ^{234}U

As discussed in section 2.1, the excess of ^{234}U with respect to ^{238}U in the ocean is mainly due to the preferential leaching of ^{234}U from uraniferous shales, sediments and limestone. This disequilibrium is also reflected in the initial isotopic composition of the coral skeleton. The decay of excess ^{234}U leads to a decrease of δ^{234}U in the coral with time (equation 2.7). By calculating the U-Th age of the sample, and measuring its present δ^{234}U, an initial $\delta^{234}U_i$ can be calculated. This initial value can be compared to that of modern corals to judge the reliability of a coral's measured U-Th age.

Published measurements of present day δ^{234}U of seawater give a mean value of ~144‰ (Chen *et al.*, 1986; Ku *et al.* 1977). New unpublished measurements suggest the value is around 148.5‰ (T. Esat, pers. comm.). δ^{234}U of modern corals has been measured to be around 148.5‰ (see figure 2.4, Stirling *et al.*, 1996; Chen *et al.*, 1991; Gallup *et al.* 1994; Edwards *et al.*, 1987a). The residence time of uranium in the ocean, based on steady state models and present day fluxes, is calculated to be around 200-400 ka (Ku *et al.*, 1977). Generally, if the initial δ^{234}U calculated for a fossil coral differs by more than 4-8‰ from the modern marine value, then the measured age is considered unreliable (Gallup *et al.*, 1994; Stirling *et al.*, 1998). However, there is growing evidence that ocean water δ^{234}U may have changed significantly during the last glacial cycle which would have profound implications for the interpretation of U-Th age measurements. This will be discussed further in chapter 3.

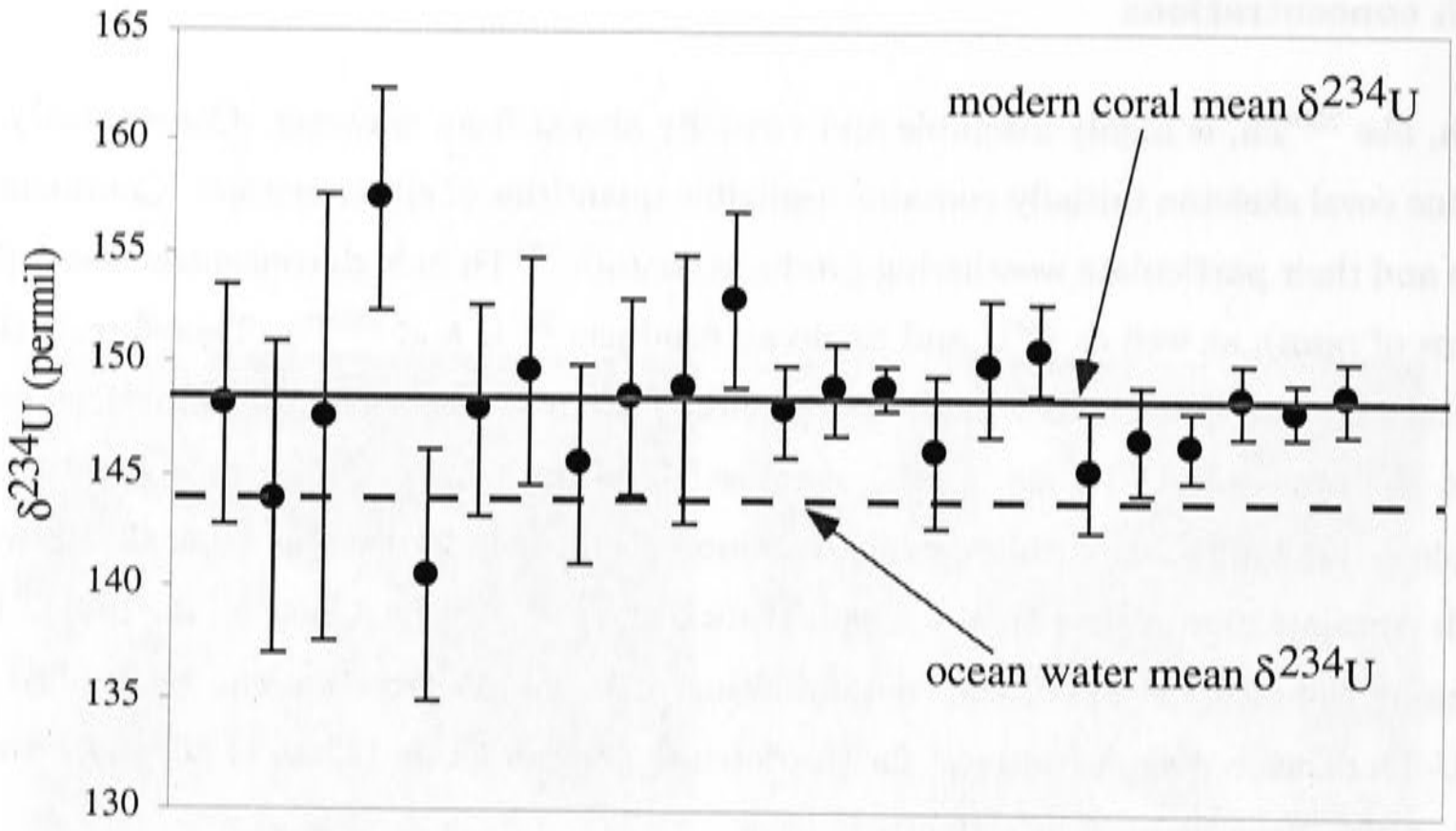

Figure 2.4: δ^{234}U measurements for modern corals (Gallup *et al.*, 1994; Stirling *et al.*, 1998; Chen *et al.*, 1991; Hamelin *et al.*, 1991; Edwards *et al.*, 1987a; Szabo *et al.*, 1994; Ludwig *et al.*, 1996; Edwards *et al.*, 1997). The mean value for modern corals is around 148.5‰. Measurements of δ^{234}U in the open ocean from Chen *et al.* (1986) have a mean value of around 144±2‰

Trace element composition

Many studies have attempted to examine the relationship between trace element and stable isotope composition of fossil corals and the effects of diagenetic alteration on the U-Th system (Chen *et al.*, 1991; Stein *et al.*, 1993; Bar-Matthews *et al.*, 1993). In a study of last interglacial age corals from the Bahamas, most of which contained negligible calcite, Bar-Matthews *et al.* (1993) demonstrated a rough correlation between Na, SO_3 and δ^{234}U which may be related to secondary aragonite emplacement. However, the timing of deposition of this secondary material and the effect of this on the apparent U-Th age of these corals is unclear.

For subtly altered corals, therefore, the trace element composition has not yet been established as a useful quantitative test for diagenesis. Trace element analysis was not performed on the samples in this work although it may prove useful for a future study of the effects of diagenesis.

2.4 Chemical preparation

Sample preparation and addition of ^{229}Th-^{233}U spike

Coral sub-samples are cut and mechanically cleaned, where possible, using a small diamond coated drill. Some coral types, such as *Diploria sp.* and *Siderastrea sp.*, have well defined wall and septa fractions. The walls are generally better preserved than the open, porous septa fraction which is more susceptible to alteration and secondary calcite cementation. Stirling (1996) showed that the removal of this septa fraction can reduce the calcite content in some samples and lead to an improvement of the U-Th results, such as a lowering of $\delta^{234}U_i$. Coral types such as *Porites sp.* and *Acropora sp.*, which have no well-defined, distinct wall structures, cannot be cleaned in this way. In these coral types, sub-samples are taken from the parts that appear to be the least altered.

Each sample is washed ultrasonically in water and acetone to remove surface contaminants, dried and then weighed. The samples are then covered in water and slowly dissolved by the step-wise addition of concentrated HNO_3. A known amount of a double spike, ^{233}U-^{229}Th, is added to each sample to enable the determination of the concentration of the naturally occurring isotopes by isotope dilution. Concentrated H_2O_2 is added to the dissolved sample to remove any remaining organic material and assist the equilibration of sample and spike.

Concentration of U and Th

Corals contain only ppm levels of uranium (~3 ppm) and less than ppb levels of thorium (20-40 ppt of ^{230}Th in 80-100 ka corals) so they must be pre-concentrated from the sample solution which is dominated by calcium. To do this the sample-spike mix residue is re-diluted in 1N HNO_3 and an Iron Chloride ($FeCl_3$) solution is added. By adding ammonium hydroxide to neutralise the acid solution, the Fe, U and Th are co-precipitated out of solution while Ca remains in solution. The precipitate, which contains Fe, U and Th and other trace elements is reserved and the supernate containing Ca is discarded. The precipitate is then washed and dissolved in 7N HNO_3.

Separation and purification of U and Th

The optimum configuration for TIMS measurement of uranium and thorium is different and these elements are chemically separated prior to analysis. This separation is achieved by using an anion exchange resin that exploits the different behaviour of various metal anion complexes that adsorb to the resin in acid solutions of varying pH. Each sample,

which is dissolved in 7N HNO_3 is loaded onto a pre-prepared anion exchange column. In concentrated HNO_3 both uranium and thorium anionic complexes are readily adsorbed onto the resin, whereas Fe passes through without adsorption. Thorium is then eluted by passing 8N HCl through the resin, whereas uranium remains adsorbed. A less concentrated HCl (0.5 N) is then used to elute the uranium from the column. The separated U and Th fractions are then loaded separately onto small anion exchange columns and purified. Any remaining Fe is eluted using HNO_3, and 0.5 N HCl is then used to elute the uranium and thorium. The purified fractions are then dried down in preparation for TIMS analysis.

2.5 TIMS analysis of uranium and thorium

The separated uranium fraction consists of the sample's naturally occurring ^{238}U, ^{235}U and ^{234}U, as well as the ^{233}U spike. The thorium fraction consists of ^{230}Th, which is the daughter product of the ^{238}U decay, as well as the naturally occurring ^{232}Th and the ^{229}Th spike component. The ^{233}U-^{229}Th spike also contains trace amounts of the naturally occurring uranium and thorium isotopes. This is taken into consideration when using the measured isotopic ratios to calculate a U-Th age. The optimum configuration for measuring uranium and thorium isotopes using TIMS is different and they were analysed in this study using different machines. An overview of the measurement techniques for each element is given below.

2.5.1 Uranium

The concentration of uranium (^{238}U) in corals is around 3ppm and ~1 μg of Uranium, or 0.3-0.5 g of coral, is required for analysis. The optimum ionisation efficiency for uranium on the Finnegan MAT 261 is achieved with a double filament configuration. In this set-up, the purified uranium fraction is loaded onto a rhenium 'evaporation' filament which is run at a temperature between 1000 and 1200°C. A much hotter (up to ~2000°C) rhenium 'ionisation' filament faces the evaporation filament. Both filaments have been pre-outgassed at ~2000°C. An ionisation efficiency of ~0.2% is achieved for a sample size of 1μg. The multi-collector system allows the simultaneous measurement of each of the isotopes ^{238}U, ^{235}U, ^{234}U and ^{233}U. The ^{238}U, ^{235}U and ^{233}U signals are measured on Faraday cups with a $10^{11}\Omega$ feedback resistor. The signal of the lower abundance isotope, ^{234}U, is measured with an electron multiplier.

Faraday cup and electron multiplier gain

The electronic gain of each Faraday cup is calibrated at the beginning of each sample run. The gain of the electron multiplier relative to that of the Faraday cups is measured regularly throughout a sample run. This is done by measuring the ^{235}U to ^{238}U ratio, first with both isotopes in Faraday cups and then with the ^{235}U in the electron multiplier. The ^{235}U to ^{238}U isotopic ratio measured for each of these configurations are then compared, giving a measure of the gain of the electron multiplier compared to the Faraday cups.

Isotopic fractionation correction

Isotopic fractionation of the uranium isotopes that occurs during the ionisation process, and which may vary during the course of a sample run, must be taken into account. This is done by comparing the measured $^{235}U/^{238}U$ ratio of the sample throughout the run, to that expected for a natural system (137.88) and adjusting the other isotopic ratios according to a power fractionation law.[4]

External reproducibility of uranium measurements

A uraninite standard, HU-1, was measured regularly to test the external reproducibility of the uranium analyses (figure 2.5). HU-1 is thought to be in secular equilibrium and the $\delta^{234}U$ should therefore equal 0‰. The small, mean offset may be attributed to intrinsic machine bias, rather than a non-equilibrium state of HU-1 (Stirling, 1996). To compensate for this offset, a correction is applied to the measured $^{234}U/^{238}U$ ratios.

2.5.2 Thorium

An optimum ionisation efficiency of 1-6% for thorium on the 61 cm TIMS at ANU is achieved by loading the purified thorium fraction between two layers of colloidal graphite on a single, pre-outgassed (2000°C) rhenium filament. The ^{230}Th concentration of corals analysed in this study was generally around 20-30 ppt and 2 g of prepared coral were used for analysis, equivalent to 40-60 pg of ^{230}Th. This produced a typical ion beam intensity of $1-5\times10^{-14}$ A. A standard multi-collector Faraday cup and feedback resistor configuration cannot produce the required sensitivity for high precision measurement of ion beams of this magnitude. The standard technique used in thorium analysis is peak hopping, where each of the isotopes is measured sequentially on an electron multiplier or Daley detector (Edwards *et al.*, 1987a; Bard *et al.*, 1990). The peak-hopping technique allows for the amplification of the each of the small isotope signals in turn. However, this

[4] $\left(\frac{N_X}{N+n_X}\right)_m = \left(\frac{N_X}{N+n_X}\right)_I (1+\alpha)^n$

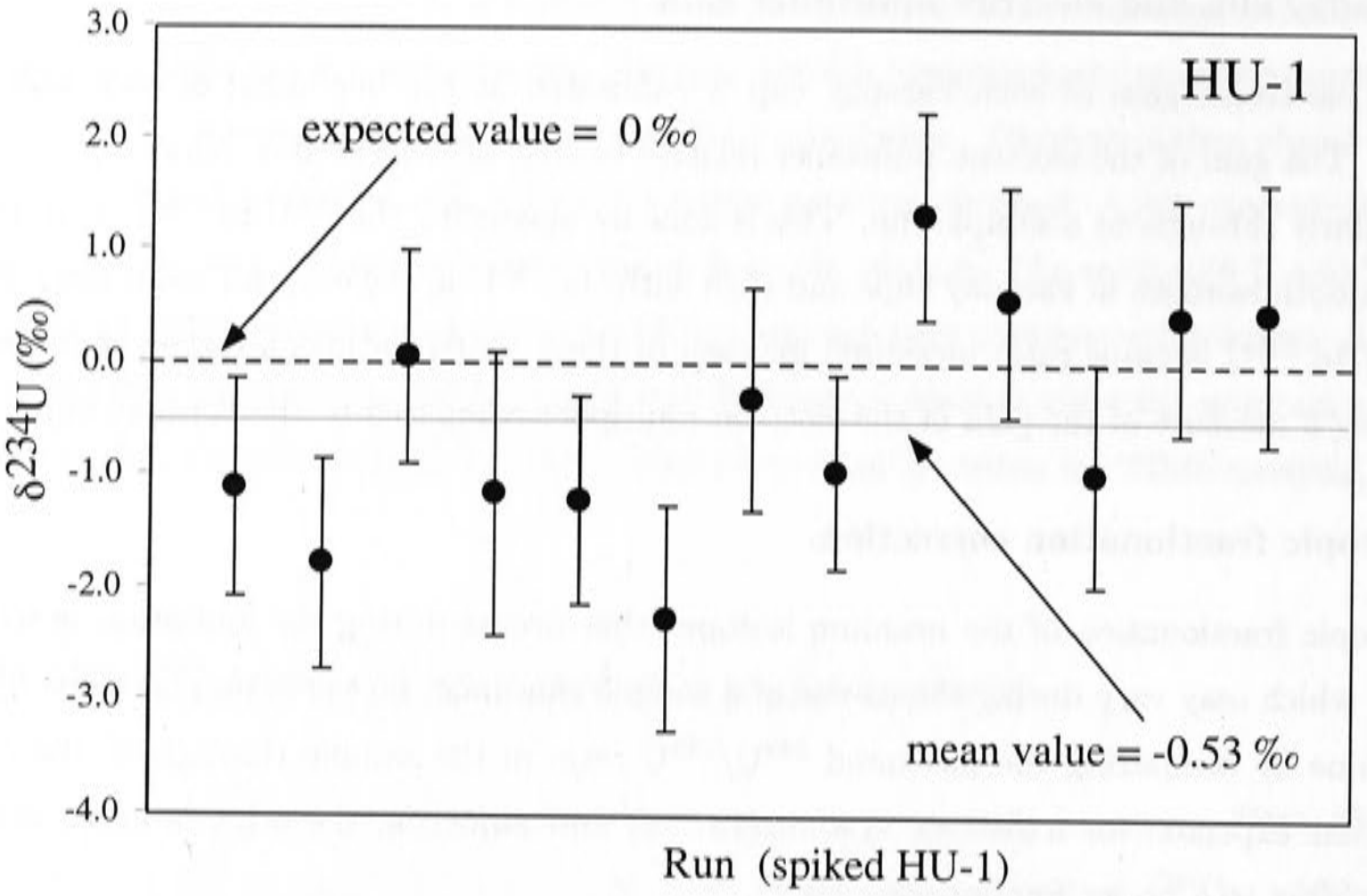

Figure 2.5: Repeat measurements of δ^{234}U of a standard (HU-1)-spike mix to test external reproducibility. As the HU-1 standard is thought to be in secular equilibrium, the expected δ^{234}U value is 0‰. The measured value (~0.5‰) is slightly offset from the expected value and can be attributed to machine bias. All measured ratios have been corrected for this. By normalising the measured isotopic ratios against those of the equilibrium standard, systematic error in decay constants and biases in the analytical procedure is largely eliminated (Ludwig *et al.*, 1992)

technique also reduces the effective analysis time and signal fluctuations can affect the measured ratios, so an alternative technique is used for thorium analysis in this work.

In this study, we use a charge collection technique to measure the isotope signals of ^{230}Th, ^{232}Th and ^{229}Th simultaneously on a multi-collector Faraday cup array. Instead of the signal of each isotope being measured across a feedback resistor, the system operates in 'charge mode' where the signal produces a build up of charge across a 20 pico-Farad air core capacitor (Esat, 1995). This charge collection technique, which is described in more detail below, enables high-precision analyses of low intensity ion beams.

For each isotope beam, the incoming ion current (I) results in a charge build-up across the capacitor (C). The rate of voltage accumulation across the capacitor is related to the ion current by: $I=C\frac{dV}{dt}$. Thus, for a stable ion signal, the charge build-up, or dV/dt, is linear with time and the slope of voltage versus time is proportional to the ion beam intensity. In practice, the measurement of charge accumulation is made in blocks of 60 voltage readings over an interval of ~1.5 minutes and a straight-line fit is made to the voltage signal as a

function of time. A background signal, which is measured for at least half an hour prior to each sample run, is subtracted from the measured signal. The ratio of the slopes of the straight line fit to each isotope signal is equal to the ratio of the isotope concentrations in the sample.

The uncertainty associated with each data block is based on the quality of the straight line fit to the voltage accumulation signal. If the intensity of the beam changes during the course of a block, the calculated isotope ratios are unchanged because each isotope beam is affected in the same way. However, in this case, because the charge accumulation is not linear, the goodness of fit of a straight line reflects both statistical variability and the effects of the intensity variation. For stable ion beams, statistical variation is the only contribution to the uncertainty and $C\frac{dV}{dt}$ is a good measure of the ion beam signal. Hence the quoted uncertainty for a variable beam is larger than for a stable beam of approximately the same mean intensity.

The typical isotope ratio uncertainty associated with each measurement block ranges upwards from 2‰. Early during each run, high intensity, stable ion beams produce relatively low uncertainties. As the run progresses, the signal degenerates, becoming unstable and eventually decays and block uncertainties increase. Generally, a sample run consists of 30-60 blocks of data (figure 2.6). A weighted average of all data blocks gives a typical isotope ratio uncertainty of ~0.5‰. This charge collection method, in conjunction with a high thorium ionisation efficiency, leads to more precise measurements than that of other researchers using the peak-hopping method, as shown in figure 2.7 (Edwards *et al.*, 1987a; Chen *et al.*, 1991; Gallup *et al.*, 1994). A series of $^{229}Th/^{230}Th$ ratios were measured of aliquots from a standard-spike mix as a test of external reproducibility of the thorium measurement technique. These, and previous measurements using this apparatus show that the reproducibility is within the calculated 1σ uncertainty (figure 2.7).

2.5.3 Spike calibration

A mixed spike (^{229}Th-^{233}U) is used to determine the concentrations of the naturally occurring isotopes in the coral samples by isotope dilution. The ratio of these spike isotopes must be known in order to calculate the ratios of uranium and thorium isotopes. The calibration of the spike $^{233}U/^{229}Th$ ratio is made using the HU-1 standard which is believed to be in secular equilibrium and therefore has a known $^{230}Th/^{235}U$ (or $^{230}Th/^{238}U$) ratio. The $^{229}Th/^{230}Th$ and $^{233}U/^{238}U$ isotope ratios for a particular HU-1 standard-spike mix

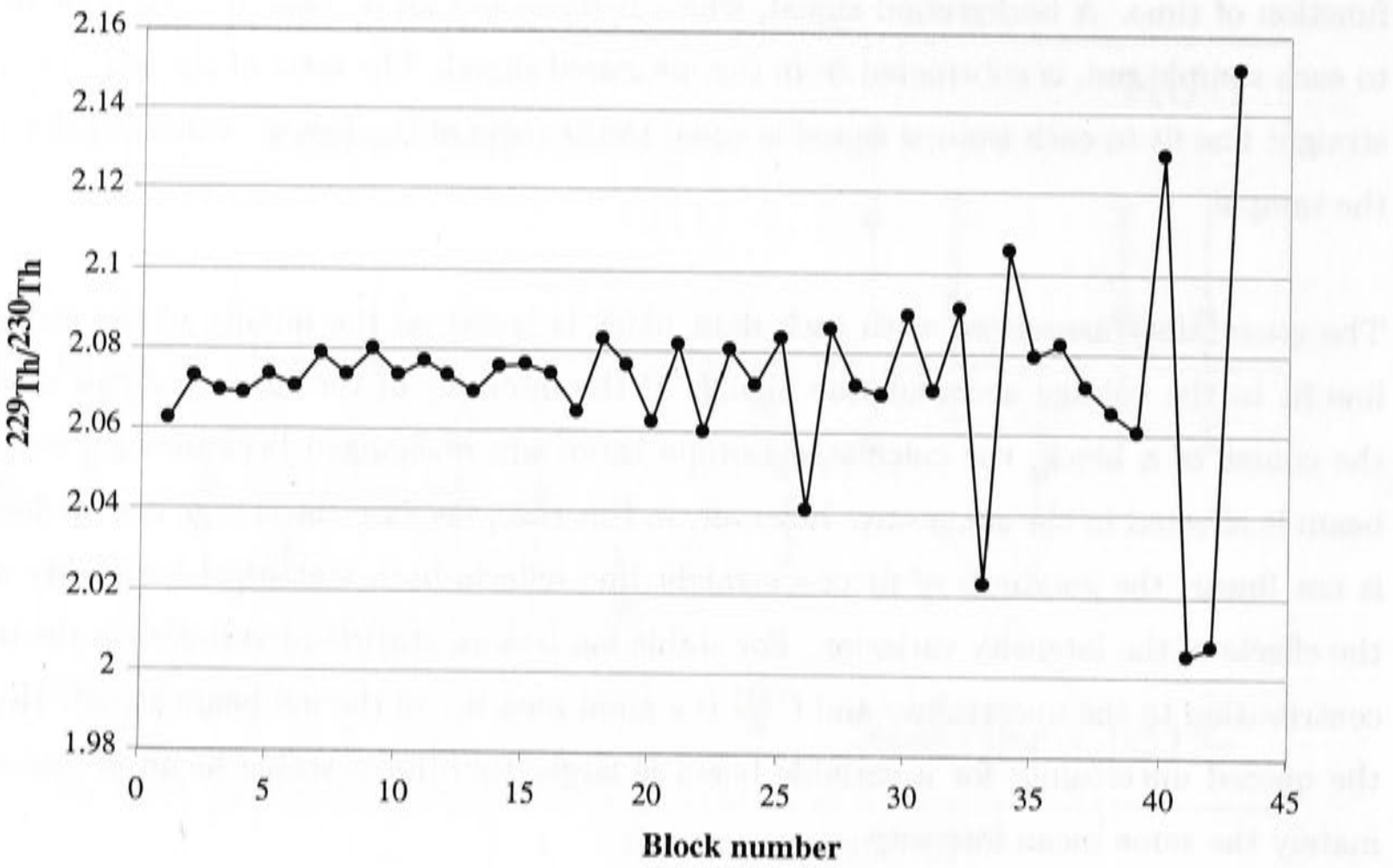

Figure 2.6: Example of $^{229}Th/^{230}Th$ ratios for each of the 43 blocks during one sample run. Note the increased scatter toward the end of the run as the signal decays. There is generally little evidence of a change in fractionation during the course of the run. This observation is in contrast to the observations of Edwards *et al.* (1987a), who observe a change in fractionation as the beam decays.

are measured and the $^{233}U/^{229}Th$ ratio calculated by:

$$\frac{^{233}U}{^{229}Th} = \frac{\lambda_{230}}{\lambda_{238}} \frac{^{233}U/^{238}U}{^{229}Th/^{230}Th} \tag{2.8}$$

Once this ratio is known, the thorium to uranium isotopic ratios can be calculated. For the particular mixture of spikes used in the present work, the spike $^{233}U/^{229}Th$ ratio was calculated to be 52.40. This calibration also accounts for any biases in the mass spectrometer systems that were used in this study.

2.5.4 Procedural blanks

Procedural blanks were analysed for most batches of chemical preparation. Both ^{238}U and ^{232}Th blank levels were generally less than 10 ppb and have a negligible effect on the calculated U-Th ages. (The assumption made is that ^{234}U blank levels are $\sim 10^{-4}$ times ^{238}U and ^{230}Th blank levels are negligible, $\sim 10^{-5}$ of ^{232}Th levels).

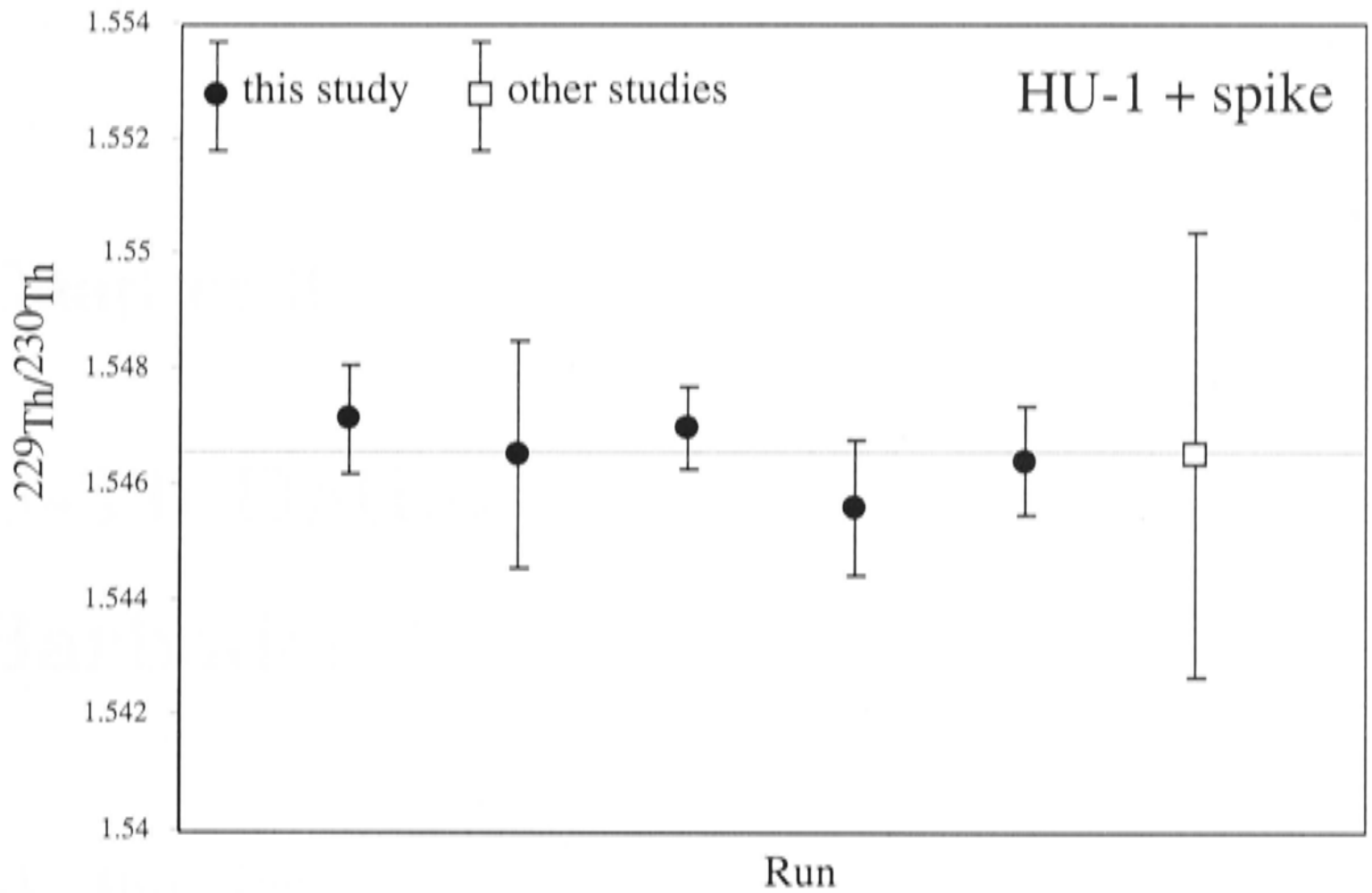

Figure 2.7: $^{229}Th/^{230}Th$ ratios of a standard (HU-1)-spike mix (closed circles) for spike calibration and as a test of external reproducibility. The reproducibility of measurements is better than the 1σ so only 1σ errors are propagated through the error calculation (Stirling *et al.*, 1995). The open square illustrates the best precision achieved by other laboratories (2σ).

2.6 Analytical age uncertainties

Typical analytical U-Th age uncertainties resulting from the procedures used in the present study (described above) are around 200-300 yr for ~80 ka samples and 300-400 yr for ~100 ka. These errors do not include uncertainties in the decay constants (half-lives). The uncertainties in the decay constants must be taken into account when comparing the U-Th ages with: (i) the age determinations from other dating methods, such as ^{231}Pa-^{235}U dating or ESR dating; and (ii) independent time-scales such as insolation calculations or layer counting of ice core records. This is not often considered in the comparison of different dating methods (e.g. Gallup *et al.*, 2002). The inclusion of the uncertainties of the decay constants from the studies of ^{230}Th and ^{234}U half-lives (described in section 2.2) increases the age uncertainties to ~600-800 yr for ~80 ka samples and ~900-1200 yr for ~100 ka samples.

Chapter 3

U-Th Dating Results from Barbados

3.1 Introduction

Barbados is a tectonically uplifting island located approximately 130 km east of the Lesser Antilles island chain (figure 3.1). The island is an exposed part of an uplifting submarine ridge associated with a subduction the North American plate under the Caribbean Plate (Jordan, 1975). Tertiary sedimentary rocks are exposed in the northwest of Barbados (Scotland district, see figure 3.2), however most of the island is capped by Pleistocene-age limestone terraces. The terraces, which are best developed on the southern and western coasts of Barbados, represent a series of emergent coral reefs that formed during sea-level transgressions in the late Pleistocene (Mesolella *et al.*, 1969). The island has experienced spatially variable uplift during the Pleistocene resulting in the warping of the reef tracts, however, there is very little evidence of faulting through the coral terrace cap. The rate of tectonic uplift is greatest in the southwest of the island (Clermont's Nose traverse, figure 3.2), and decreases in the north and the east.

The Barbados terraces are generally constructional features formed by coral reef building, but some erosional platforms have also been identified (Schellmann and Radtke, 2001). The youngest exposed terraces were formed late during marine isotope stage (MIS) 5. The age of the terraces generally increases with elevation, with some exceptions (discussed later in this chapter).

Figure 3.1: Location of Barbados in the context of the Caribbean region.

Figure 3.2: Barbados, West Indies. The island Barbados is capped by uplifted Pleistocene age coral reefs (except for the Tertiary age sedimentary rocks exposed in the Scotland district). The 'First High Cliff', is one of the most dominant terrace structures and represents coral growth during the Last Interglacial period (sub-stage 5e). In the southwest, the area of the Clermont's Nose traverse has experienced the highest rate of uplift on the island at over ~0.45 m/ka since the last interglacial period. The sites studied in this investigation are shown - Batt's Rock Bay (BRB1-4), Pepperpot (PEP), Maxwell terrace (MAX), Kendall Fort (KF), Inch Marlowe Point (IM), Paragon Point (U18), Salt Cave Point (U15), Foul Bay (U6), Animal Flower Cave (AC).

The purpose of this study is to constrain the timing of deposition of sub-stage 5a and 5c uplifted coral terraces at Barbados using U-Th dating. Combined with estimates of the rates of tectonic uplift, these ages can be used to calculate the paleo-sea level associated with each morphological feature. This chapter begins with a short review of the results of previous studies of the lower Barbados terraces. Corals collected during two field seasons in 1999 and 2000 have been analysed using U-Th dating techniques[1]. In this chapter, I summarise the results of the U-Th dating analysis and give a brief description of the facies and stratigraphy for each of the sites investigated in this study. At the end of this chapter, I will discuss the interpretation of U-Th results in the context of the δ^{234}U reliability criterion and include a discussion of the implications of ocean water δ^{234}U and the effect of diagenetic alteration on the U-Th system of fossil corals. In chapter 4, I will present the calculation of relative sea level for each of the sites investigated.

[1] 1999 field season - Tezer Esat, Malcolm McCulloch, Ulrich Radtke and Gerhard Schellmann. 2000 field season - Tezer Esat, Malcolm McCulloch, Ulrich Radtke, Gerhard Schellmann and Emma-Kate Potter

3.2 Previous sub-stage 5a and 5c Barbados analyses

The usefulness of Barbados coral terraces in the reconstruction of Pleistocene sea-level transgressions was recognised in the mid-1960s (Broecker *et al.*, 1968; and Mesolella *et al.*, 1969). Using U-Th α-spectrometry analytical techniques, these studies established approximate ages for the lowest Barbados terraces. Broecker *et al.* (1968) identified three MIS 5 terraces - the Rendezvous Hill (1^{st} High Cliff), Ventnor and Worthing terraces[2] with ages of ~122 ka, ~103 ka and ~82 ka respectively (with precision of ~2-4 ka). For the same features, Mesolella *et al.* (1969) quoted mean ages of ~125 ka, ~103 ka and ~82 ka respectively. Broecker *et al.* (1968) pointed out that the timing of these sea-level high-stands were consistent with the predictions of Milankovitch's orbital forcing model (Milankovtich 1941). The younger two deposits, with ages of ~82 ka and ~103 ka, correspond to the sub-stage 5a and 5c events identified in marine records. These will be referred to as the 'classic' sub-stage 5a and 5c events.

Dating of pre-last interglacial reefs on Barbados was conducted using He/U (Bender *et al.* 1973 and 1979), U-Th (Bender *et al.*, 1979) and ESR techniques (Radtke and Grün, 1988). Again, these studies demonstrated that the age of each of the major terraces can be correlated with the marine isotope interglacials identified in deep-sea core foraminiferal $\delta^{18}O$ records (Shackleton and Opdyke, 1973), to earlier than MIS 11.

The precision of U-Th dating was improved by the development of thermal ionisation mass spectrometry (TIMS) techniques for the analyses of uranium and thorium isotopes (Edwards *et al.*, 1987a). In a study of 29 Barbados coral samples, and comparison of α-spectrometry and TIMS techniques (Ku *et al.*, 1990; Edwards *et al.*, 1987b), three periods of reef growth were identified, corresponding to sub-stages 5a, 5c and 5e. Ages measured by Ku *et al.* (1990) for the sub-stage 5c terraces range between 101.5 and 110.5 ka. Sub-stage 5a ages quoted by Ku *et al.* range between 75.5 up to 87 ka. Edwards *et al.* (1997) dated sub-stage 5c deposits to be 103.1 to 105.5 ka and sub-stage 5a to be 82.9 to 86.1 ka.

Using high precision TIMS analyses, Bard *et al.* (1990) determined U-Th ages for a number of samples from the last glacial cycle. One sample gave an age of 88 ka (with the slightly higher than acceptable $\delta^{234}U$) and appears to represent the 'classic' sub-stage 5a sea-level high-stand. Also in that study, Bard *et al.* dated one sub-stage 5c sample with

[2]Rendezvous Hill, Ventnor and Worthing terraces also known as Barbados I, II and III and represent reef growth during sub-stages 5e, 5c and 5a respectively

	Sub-stage age estimates (ka)		
Author	5c	5a	Precision (ka)
Broecker *et al.* (1968)	103	82	±2 to ±4
Mesolella *et al.* (1969)	100-110	79-84	±2 to ±6
Ku *et al.* (1990)	101.5-110.5	75.5-87.5	±1 to ±2
Bard *et al.* (1990)	100.5	88	±0.6 to ±0.8
Gallup *et al.* (1994)	-	83.3-87.2	±0.3 to ±0.4
Edwards *et al.* (1997)	103.1-105.4	82.9-86.1	±0.4 to ±0.6

Table 3.1: Summary of reliable U-Th age measurements for the sub-stage 5a and 5c Barbados terraces which are discussed in the text. Results include both alpha spectrometric and TIMS analyses.

an age of 100.5 ka. Bard *et al.* (1990) measured U-Th ages of 70.8 ka and 77.8-79.8 ka for submerged samples collected at depths of 57 m and 46 m respectively. The latter ages can be considered unreliable due to their very high initial δ^{234}U values. Gallup *et al.* (1994) also measured the U-Th ages of 3 sub-stage 5a and 5c corals giving results of 83.3 ka, 87.2 ka and 104 ka (the latter having a very high δ^{234}U).

A recent study by Schellmann and Radtke (2001, 2002) has shown that the morphological structure of the lower Barbados reef terraces is more complex than previously thought (e.g. by Broecker *et al.*, 1968). They identified at least 6 morphologically distinct terrace platforms along the south coast of Barbados belonging to sub-stages 5a and 5c (shown in blue in figure 3.3). Based on the results of ESR dating of deposits on the south coast of Barbados, they suggest that there were multiple, distinct periods of reef growth during MIS 5, in addition to the 'classic' sub-stage 5a, 5c and 5e high-stands. However, the relatively low precision age measurements of the ESR dating technique (up to 10 ka for stage 5 corals) does not enable the timing of these events to be clearly constrained. The sub-stage 5a and 5c events identified by Schellmann and Radtke (2001) are summarised in table 3.2.

Schellmann and Radtke suggest there has been warping of the reef tracts in the region of the Christ Church traverse[3] (marked in figure 3.3). However they observed no evidence of warping in the region between the standard Christ Church traverse and South Point. Schellmann and Radtke suggest that the elevations of the reef platforms in this region, which I will refer to as the south coast traverse, should be used for sea-level calculations.

[3]The Christ Church traverse is the standard traverse defined by Bender *et al.* (1979) with elevations used for the calculation of sea level.

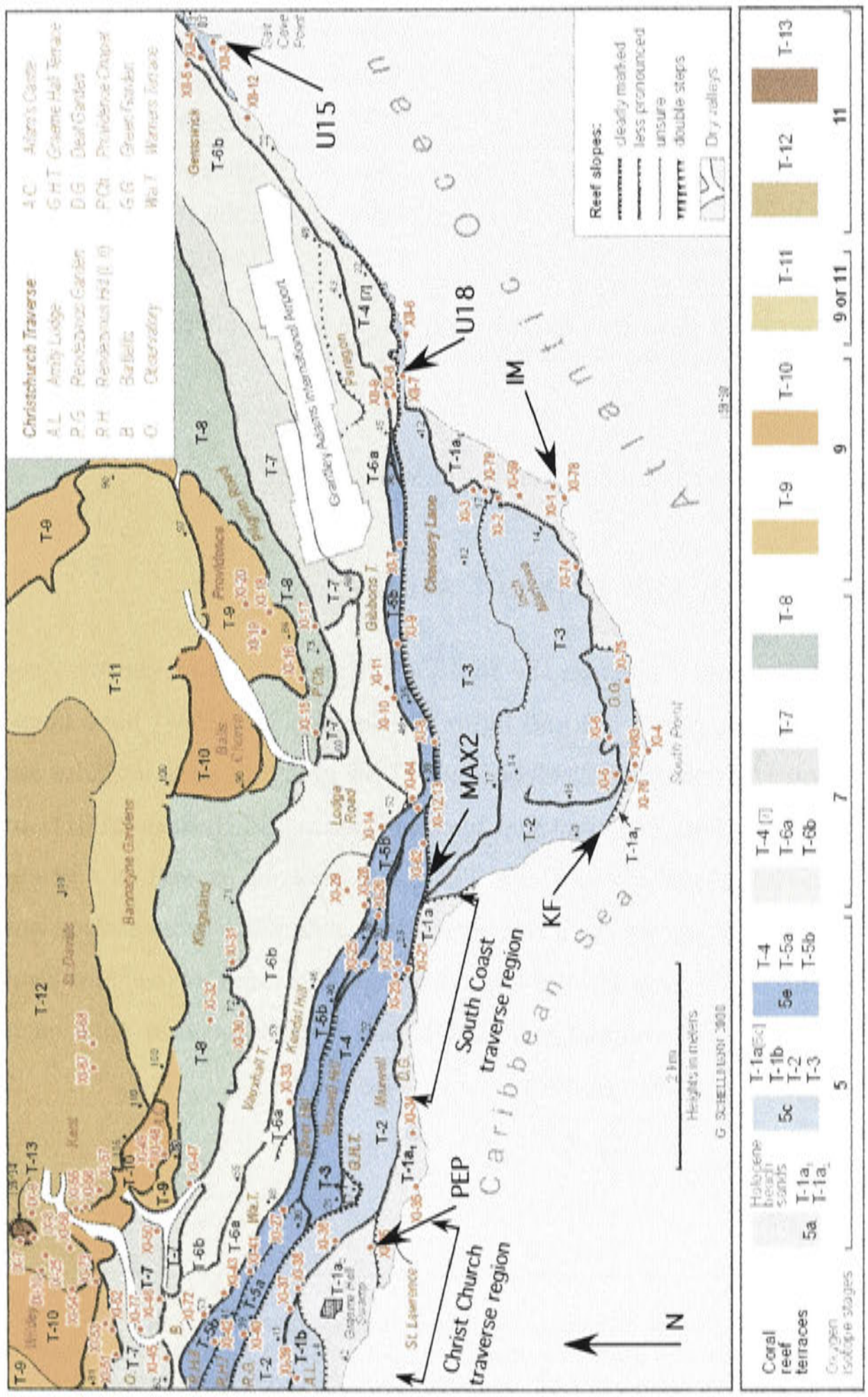

Pleistocene coral reef terraces in the southern part of Barbados with location of sample sites.

Figure 3.3: Pleistocene coral reef terraces on the southern coast of Barbados (from G. Schellmann). Elevations of MIS 5 platforms T-1a to T-5b (in blue) are given in table 3.2. Sample sites for this study are marked with black arrows (see also figure 3.2). Other annotations indicate samples sites used in ESR analysis by Schellmann and Radtke (2001). The region of the Christ Church (Bender *et al.*, 1979) traverse is shown in the left of the map.

MIS	Present elevation (m)	Platform	ESR Age (ka)
5a-1	2	T-1a$_1$	72±6
5a-2	3	T-1a$_1$	85±8
5c-1	4	T-1b	99±11
5c-2	9	T-2	104±11
5c-3	16	T-3	102±8
5e-1	22	T-4	120±14
5e-2	36	T-5a	130±16
5e-3	39	T-5b	134±15

Table 3.2: ESR ages and elevations for sub-stage 5a, 5c and 5e platforms on the south coast traverse of Barbados from Schellmann and Radtke (2001, 2002).

The elevations of these terraces are given in table 3.2.

3.3 Results from the present study

In this study, samples from 7 sites on the south coast and 4 sites on the west coast (Clermont's Nose traverse, see figure 3.2 and figure 3.3 for site locations) have been analysed using high precision U-Th analytical techniques. This group of sites includes some of the morphologically distinct features identified by Schellmann and Radtke (2001). In this section, I will present the results of the U-Th TIMS age analysis as well as a brief summary of the facies and stratigraphy for each site studied. A schematic cross section summary of the sub-stage 5a and 5c terraces for the two traverses (Clermont's Nose and South Coast) is shown in figure 3.4. The calculation of paleo-sea level associated with each of these features is presented in the next chapter.

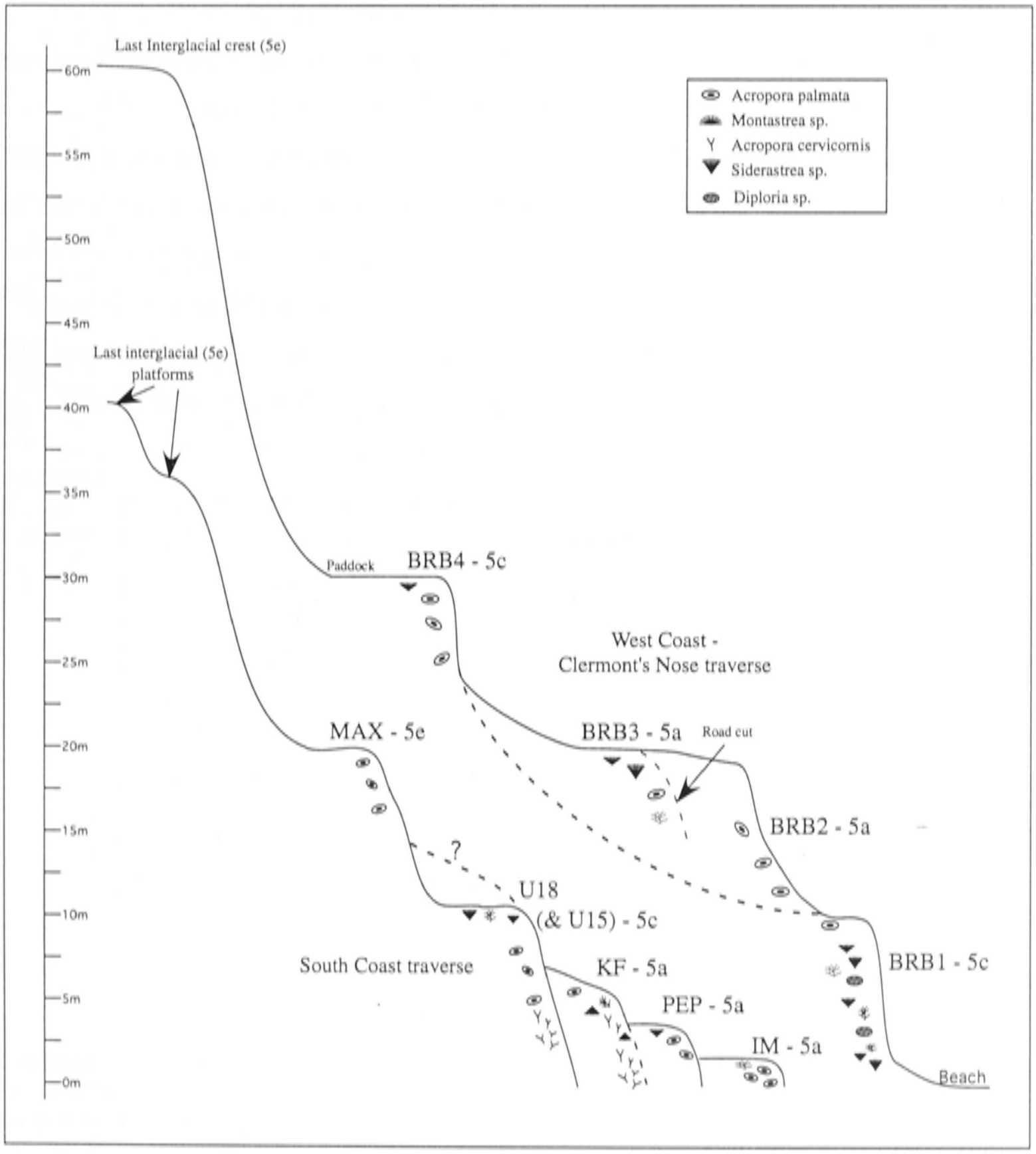

Figure 3.4: Schematic representation of the sites sampled in this study on the south and west coasts of Barbados (South coast traverse and the Clermont's Nose traverse). Elevations and general indications of facies and coral types are also included. Site name abbreviations - Batt's Rock Bay (BRB1-4), Pepperpot (PEP), Maxwell terrace (MAX), Kendall Fort (KF), Inch Marlowe Point (IM), Paragon Point (U18), Salt Cave Point (U15). See figure 3.2 and figure 3.3 for site locations.

3.3.1 South Coast

Inch Marlowe Point (IM)

Only 1.5-2 m of the deposit at Inch Marlowe Point (figure 3.5) is exposed above present sea level and its total thickness is unknown. This terrace corresponds to platform T-1a identified by Schellmann and Radtke (2001, 2002) (figure 3.3). It consists predominantly of shallow water facies *Acropora Palmata* with some characteristic 'rear zone' head corals including *Siderastrea sp.* and *Montastrea sp.* (facies types described by Mesolella, 1967).[4] The well-defined platform extends for several hundred metres along the coast in the Inch Marlowe Point region. In this study, 13 samples were selected for U-Th analysis (results shown in table 3.3). Measured U-Th ages range between 74 ka and 82 ka with initial δ^{234}U values of between 141‰ (well below the modern coral δ^{234}U value of 148.5‰) and 167‰ (well above the modern value). The age of this deposit corresponds to reef growth during sub-stage 5a.

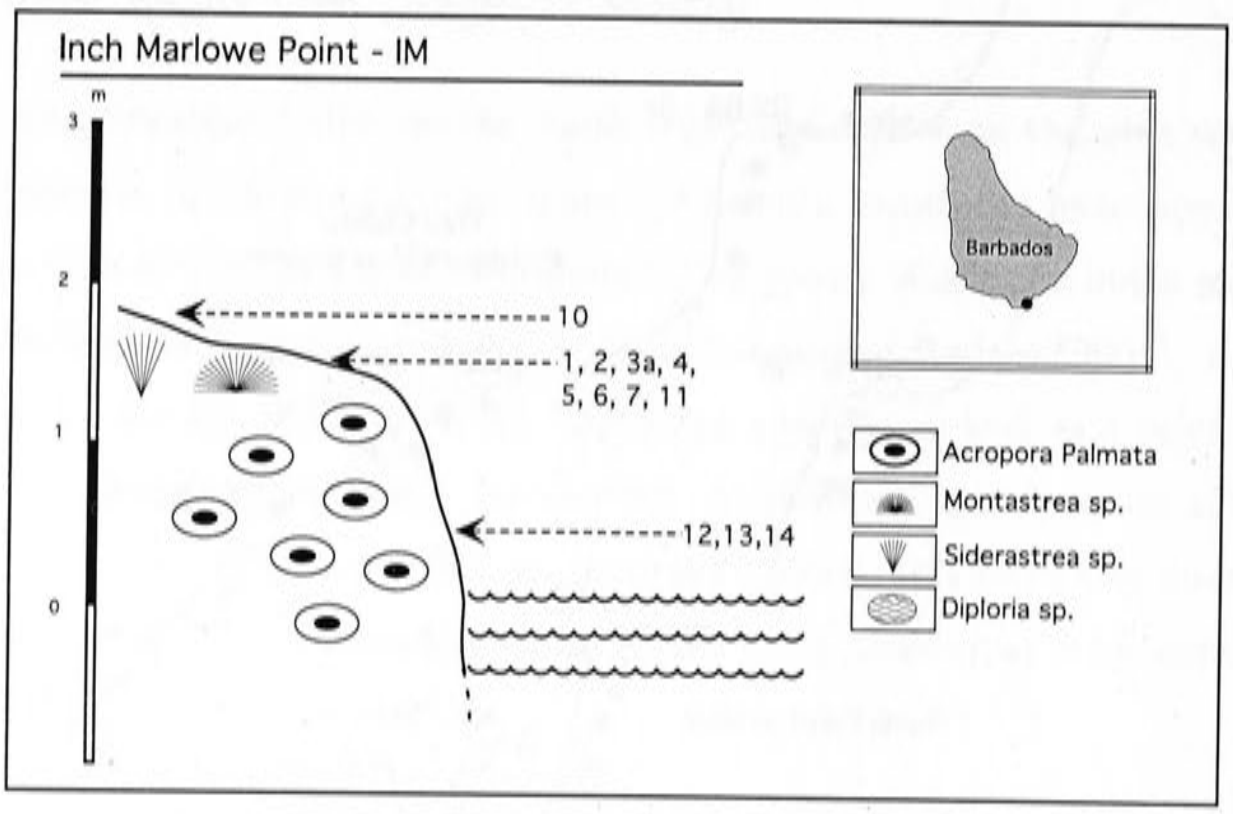

Figure 3.5: Inch Marlowe Point, South Coast. The platform at Inch Marlowe Point reaches 1.5-2 m above present sea level and consists predominantly of shallow water facies *Acropora palmata*. It is topped by mixed head corals including *Siderastrea sp.* and *Montastrea sp.*. In this setting, the head corals represent growth in the 'rear zone' of the coral reef, in shallow water (described by Mesolella, 1967).

[4]Zonation of Barbados coral reef facies is described by Mesolella (1967). At depths of >15 m, characteristic reef facies consists mainly of large head corals. This typically grades into an *Acropora cervicornis* zone (5-15 m water depth). The reef crest is dominated by *Acropora palmata* zone (growth depths of 0-5 m). A 'rear zone', which is protected by surf action by the reef crest also contains a mix of head corals. Although *Acropora palmata* is characteristic of shallow water growth, head corals that are collected from obviously 'rear zone' facies, judged from the context of the deposit, are often better preserved and were also used in dating.

Sample No.*	XRD	H† (m)	^{238}U (ppm)	^{232}Th (ppb)	$\delta^{234}U_m$‡ (‰)	$^{230}Th/^{238}U_{act}$	Age§ (ka)	$\delta^{234}U_i$¶ ‰
IM1-1 ^{S}	< 1%	1.5	2.20	0.23	121.5± 1.9	0.5861± 0.0013	79.1± 0.3	152.0± 2.3
IM1-2 ^{S}	< 1%	1.5	2.29	0.28	122.7± 1.1	0.5852± 0.0008	78.8± 0.2	153.4± 1.3
IM1-3a ^{S}	-	1.5	2.19	0.18	119.6± 1.1	0.5726± 0.0007	76.7± 0.2	148.7± 1.3
IM1-4 ^{S}	< 1%	1.5	2.02	0.04	122.6± 1.0	0.5725± 0.0006	76.3± 0.2	152.2± 1.2
IM1-5 ^{S}	< 1%	1.5	2.17	0.31	120.1± 1.1	0.5742± 0.0008	76.9± 0.2	149.3± 1.3
IM1-6 ^{S}	< 2%	1.5	2.26	0.26	118.3± 1.1	0.5581± 0.0007	74.1± 0.2	146.0± 1.3
IM1-7 ^{S}	< 1%	1.5	2.19	0.18	128.5± 1.0	0.5825± 0.0007	77.6± 0.2	160.2± 1.2
IM1-8 ^{Ap}	-	1.5	2.81	0.02	114.5± 1.0	0.5560± 0.0008	74.0± 0.2	141.3± 1.1
IM1-10 ^{S}	< 1%	2.0	1.99	0.15	115.9± 1.2	0.5723± 0.0007	77.0± 0.2	144.2± 1.4
IM1-11 ^{Ap}	-	1.5	3.47	0.06	132.5± 1.0	0.6060± 0.0008	81.7± 0.2	167.0± 1.2
IM1-12 ^{Ap}	-	0.2	2.92	0.03	117.1± 1.1	0.5715± 0.0012	76.7± 0.3	145.6± 1.3
IM1-13 ^{Ap}	< 1%	0.2	2.97	0.04	116.4± 1.0	0.5640± 0.0009	75.4± 0.2	144.1± 1.2
IM1-14 ^{Ap}	< 1%	0.2	3.14	0.04	119.8± 1.1	0.5783± 0.0012	77.7± 0.3	149.4± 1.3

Table 3.3: Inch Marlowe Point: Isotope ratios and U-Th age measurements. *Coral type given as: ^{Ap}*Acropora palmata*, ^{S}*Siderastrea sp.*, ^{M}*Montastrea sp.*, ^{D}*Diploria sp.*, ^{Ac}*Acropora cervicornis*; XRD - % calcite of sample, where measured; †Elevation above present sea level (m); ‡Measured $\delta^{234}U$, see equation 2.5; §Sample age, see equation 2.4; ¶Initial $\delta^{234}U$, see equation 2.7. Quoted uncertainties reflect analytical precision only and do not take into account uncertainties in decay half-lives of ^{234}U or ^{230}Th or uncertainties introduced by diagenetic mobilisation of U and Th. Decay constants used in calculations are $\lambda_{238} = 1.551 \times 10^{-10}$, $\lambda_{234} = 2.835 \times 10^{-6}$, $\lambda_{230} = 9.195 \times 10^{-6}$ (Meadows *et al.* (1980), De Biever *et al.* (1971) and Lounsbury and Durham (1971); see discussion of decay half-lives in section 2.2 of chapter 2)

Kendall Fort (KF)

The Kendall Fort deposit (figure 3.6) reaches an elevation of ~6-8 m at its crest. The top of this terrace appears to correspond to platform T-2 identified by Schellmann and Radtke (2001) (figure 3.3). The base of the deposit is dominated by *Acropora cervicornis*, which is typical of coral growth at 5-15 m below the reef crest (Mesolella, 1967). Overlying the *Acropora cervicornis* unit is a mix of *Siderastrea sp.*, *Montastrea sp.* head corals and some *Acropora palmata.* Eight corals were chosen for U-series analysis and measured ages range between ~82 ka and ~92 ka with initial δ^{234}U values between 143‰ and 195‰ (table 3.4). The age of corals in this deposit corresponds to sub-stage 5a. Further examination of this deposit (November 2002) reveals that the mixed zone of this deposit contains reworked corals that are obviously not in growth position (overturned head corals). The KF deposit may therefore be the result of storm emplacement and should not be used in the calculation of relative sea level.

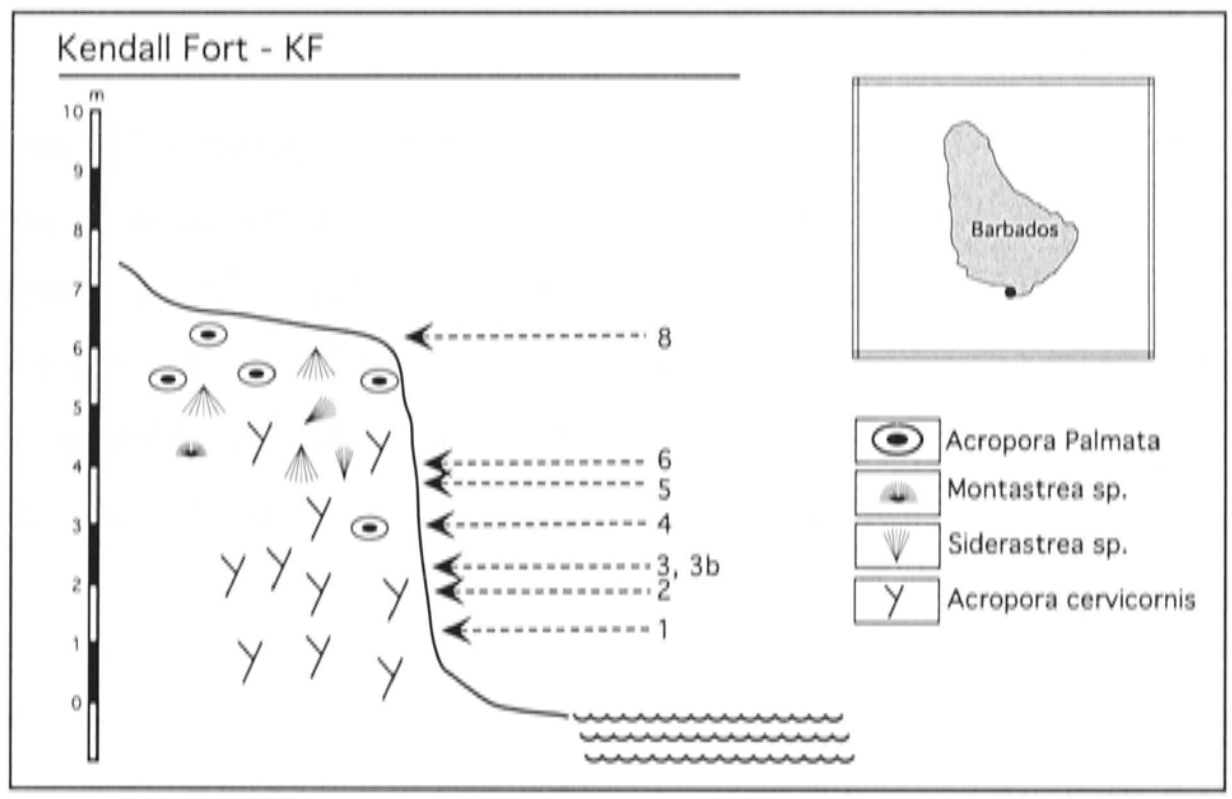

Figure 3.6: Kendall Fort, South Coast. This feature reaches 6-8 m above present sea level and predominantly consists of *Acropora cervicornis* with a mix of *Acropora palmata*, *Siderastrea sp.* and *Montastrea sp.*. The head corals overlying the *Acropora cervicornis* have been reworked (some are upside-down) indicating this deposit is not *in situ* and is probably the result of storm emplacement.

Sample No.*	XRD	H† (m)	^{238}U (ppm)	^{232}Th (ppb)	$\delta^{234}U_m$‡ (‰)	$^{230}Th/^{238}U_{act}$	Age§ (ka)	$\delta^{234}U_i$¶ ‰
KF-1 ^{Ap}	-	1.1	3.719	0.05	132.6± 1.0	0.6113± 0.0010	82.8± 0.2	167.7± 1.2
KF-2 ^{Ap}	-	1.6	3.20	0.06	130.5± 1.1	0.6481± 0.0013	90.6± 0.3	168.7± 1.4
KF-3 ^{S}	-	2.0	2.51	0.36	123.0± 1.3	0.6223± 0.0011	86.2± 0.3	157.0± 1.5
KF-3b ^{Ap}	-	2.0	3.94	0.03	150.7± 1.2	0.6661± 0.0015	91.7± 0.4	195.4± 1.5
KF-4 ^{S}	-	3.0	2.12	0.01	122.8± 1.1	0.6189± 0.0009	85.5± 0.2	156.4± 1.3
KF-5	-	3.5	2.19	0.03	113.0± 1.8	0.6024± 0.0013	83.3± 0.3	143.2± 2.2
KF-6 ^{S}	< 2%	4.0	2.42	0.03	117.9± 1.1	0.6037± 0.0009	83.0± 0.2	149.1± 1.3
KF-8 ^{S}	-	7.0	2.36	0.13	114.2± 1.0	0.5985± 0.0008	82.4± 0.2	144.2± 1.2

Table 3.4: Kendall Fort: Isotope Ratios and U-Th age calculations. See table 3.3 caption for explanation of symbols.

'Pepperpot' (PEP)

The 'Pepperpot' site is a bench at an elevation of 3-4 m asl (figure 3.7), landward of an uplifted paleo-lagoon (Graeme Hall Swamp). This terrace corresponds to platform T-1b identified by Schellmann and Radtke (2001) (figure 3.3). Shallow water *Acropora palmata* forms the bulk of this deposit and *Siderastrea sp.* is also present. Six samples from this site were analysed and the U-Th results are shown in table 3.5. Measured ages range between 81.5 ka and 87 ka with initial δ^{234}U values of between 140‰ and 156‰. The age of this deposit corresponds to reef growth during sub-stage 5a.

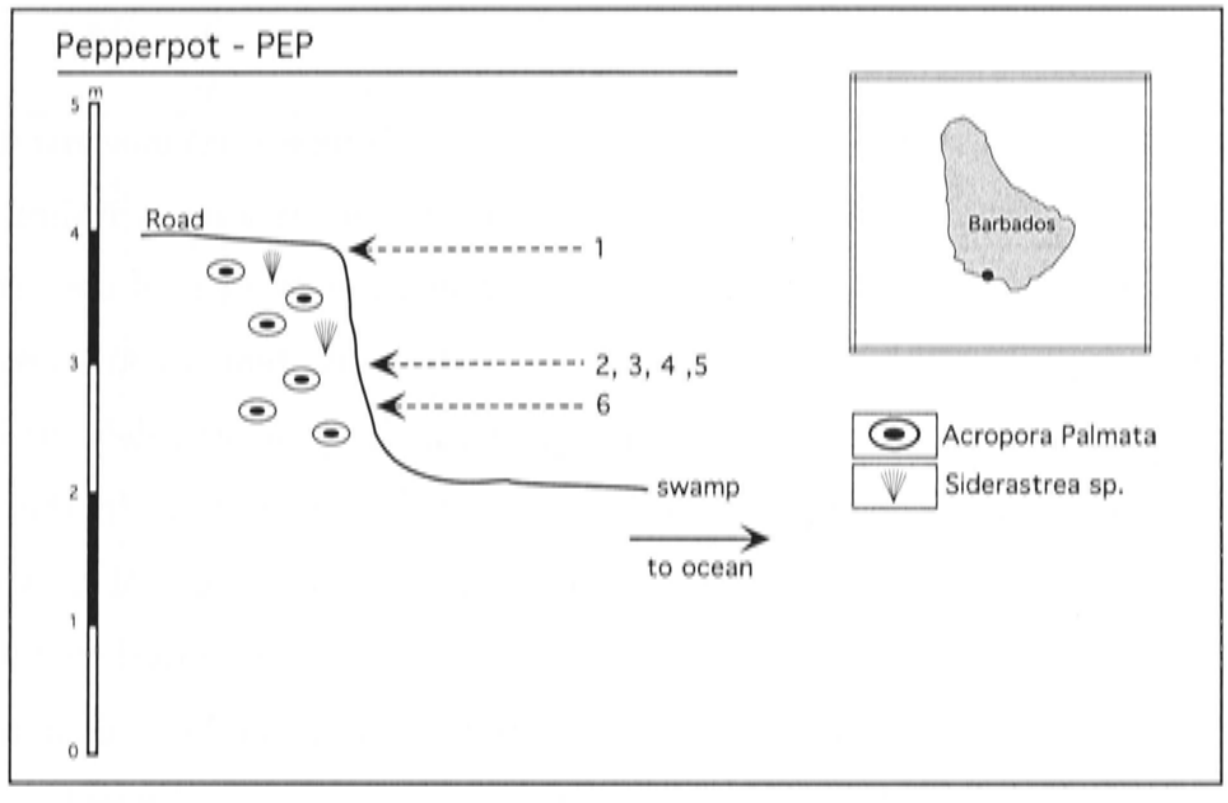

Figure 3.7: "Pepperpot" locality, South Coast. The crest of this deposit is 3-4 m above present sea level, and contains *Acropora palmata* and some *Siderastrea sp.*

Sample No.*	XRD	H† (m)	^{238}U (ppm)	^{232}Th (ppb)	$\delta^{234}U_m$‡ (‰)	$^{230}Th/^{238}U_{act}$	Age§ (ka)	$\delta^{234}U_i$¶ ‰
PEP1-1 ^{S}	-	2.5	2.2202	0.04	111.2± 1.1	0.5924± 0.0006	81.5± 0.2	140.1± 1.4
PEP1-2 ^{Ap}	-	2.5	3.17	0.08	122.7± 1.2	0.6169± 0.0013	85.1± 0.3	156.1± 1.4
PEP1-3 ^{Ap}	< 1%	2.5	2.46	0.03	117.0± 1.1	0.6075± 0.0009	83.9± 0.2	148.4± 1.3
PEP1-4 ^{S}	-	2.5	2.34	0.04	115.4± 1.4	0.6047± 0.0012	83.5± 0.3	146.2± 1.7
PEP1-5 ^{S}	-	2.5	2.35	0.06	116.9± 1.2	0.6101± 0.0007	84.4± 0.2	148.4± 1.5
PEP1-6 ^{S}	-	3.0	3.27	0.03	120.1± 1.1	0.6245± 0.0012	87.0± 0.3	153.7± 1.3

Table 3.5: Pepperpot locality: Isotope Ratios and U-Th age calculations. See table 3.3 caption for explanation of symbols.

Paragon Point (U18)

The sea cliff at Paragon Point (figure 3.8) has a distinct *Acropora cervicornis* unit overlain by a > 6m *Acropora palmata* zone and topped with a thin mixed zone including *Montastrea sp.* and *Siderastrea sp.* head corals. This facies structure is typical of the reef crest and 'rear zone' type described by Mesolella (1967). The terrace reaches an elevation of 11-12 m asl. Schellmann and Radtke (2001) suggest that the platform defined by the crest of this deposit corresponds to the T-3 platform further to the west (in the south coast transect), which has an elevation of up to 4 m higher than the crest of U18 (figure 3.3). G. Schellmann (pers. comm.) suggests the back reef deposits associated with the U18 reef crest reach an elevation of up to 15 m asl. Three erosional notches occur at elevations of ~1.3 m, ~4.8 m and ~7.8 m above present sea level, which suggests that three sea level still stands at these levels followed the deposition of this reefs. Twelve samples from the *Acropora palmata* unit and the overlying mixed coral head unit (*Montastrea sp.* and *Siderastrea sp.*) were selected for analysis (table 3.6). Measured ages ranges between 98 ka and 107 ka and have initial δ^{234}U values of between 138‰ and 161‰. Samples U18-5 and U18-9 may not have been collected from an *in situ* position. The age of this deposit corresponds to reef growth during sub-stage 5c.

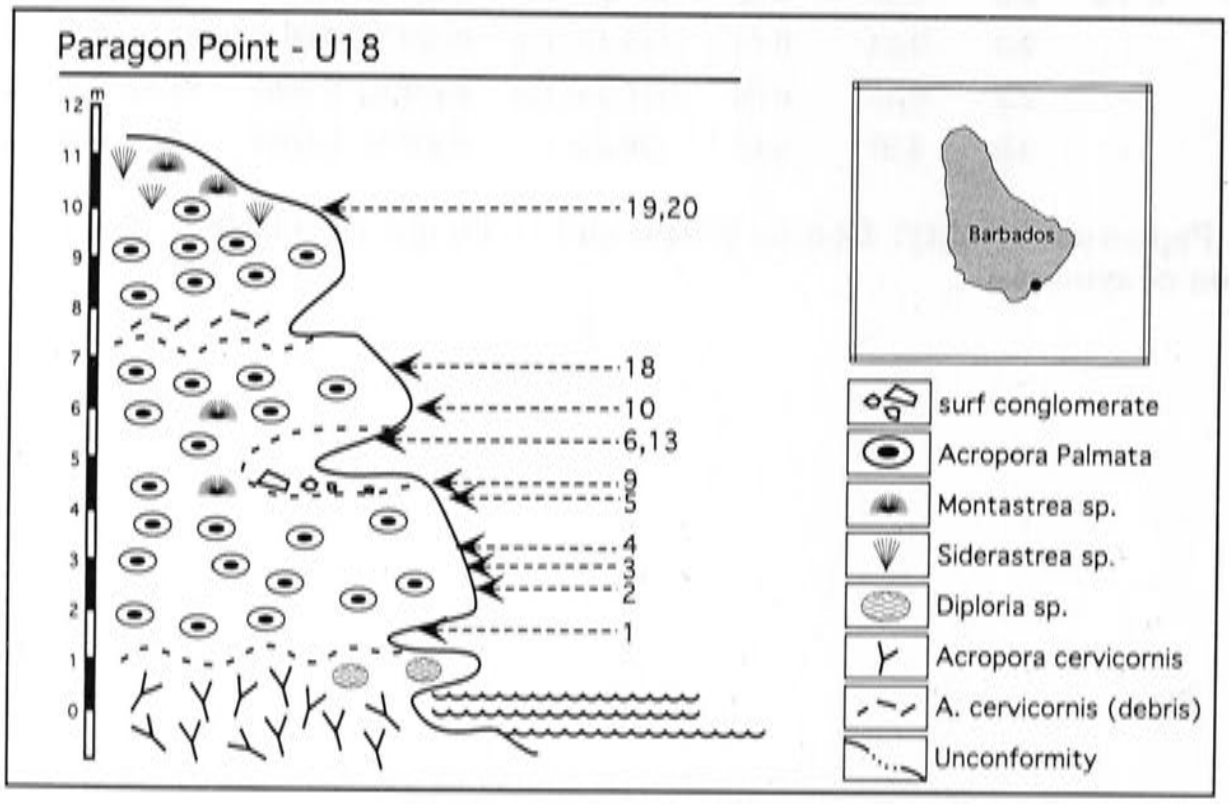

Figure 3.8: Paragon Point, South Coast. A 10-12 m high feature with a distinct *Acropora cervicornis* unit overlain by a thick *Acropora palmata* layer and topped by *Montastrea sp.* and *Siderastrea sp.*. Erosional notches at 1.3, 4.8 and 7.8 m asl indicate at least 3 sea-level still-stands following the formation of this terrace.

Sample No.*	XRD	H† (m)	^{238}U (ppm)	^{232}Th (ppb)	$\delta^{234}U_m$‡ (‰)	$^{230}Th/^{238}U_{act}$	Age§ (ka)	$\delta^{234}U_i$¶ ‰
U18-1 ^{Ap}	< 1%	1.3	3.0344	0.11	113.2± 1.0	0.6838± 0.0012	101.2± 0.3	150.8± 1.3
U18-2 ^{Ap}	< 1%	2.3	3.14	0.12	119.5± 1.0	0.6917± 0.0013	102.0± 0.4	159.6± 1.2
U18-3 ^{Ap}	< 1%	2.8	3.06	0.11	106.3± 1.0	0.6667± 0.0013	98.3± 0.3	140.4± 1.3
U18-4 ^{S}	< 1%	3.2	2.49	0.11	123.1± 1.2	0.7071± 0.0009	105.3± 0.3	165.9± 1.5
U18-5 ^{Ap}	< 1%	4.3	3.43	0.14	106.3± 1.1	0.6772± 0.0011	100.7± 0.3	141.4± 1.3
U18-6 ^{Ap}	< 1%	4.9	3.27	0.10	110.8± 1.0	0.6861± 0.0011	102.1± 0.3	148.0± 1.3
U18-9 ^{Ap}	< 1%	4.5	2.92	0.08	104.2± 1.0	0.6658± 0.0008	98.4± 0.3	137.7± 1.3
U18-10	< 2%	5.8	3.27	0.10	112.7± 1.0	0.6784± 0.0012	100.0± 0.3	149.6± 1.3
U18-13 ^{S}	< 1%	4.9	2.22	0.14	119.0± 1.1	0.7129± 0.0010	107.4± 0.3	161.3± 1.4
U18-18 ^{Ap}	< 1%	6.7	3.34	0.10	121.3± 1.0	0.6880± 0.0009	100.8± 0.3	161.4± 1.2
U18-19 ^{Ap}	-	9.6	2.98	0.16	111.9± 1.1	0.6890± 0.0011	102.6± 0.3	149.7± 1.3
U18-20 ^{M}	-	9.6	2.44	0.13	108.9± 1.0	0.6875± 0.0009	102.8± 0.3	145.7± 1.3

Table 3.6: Paragon Point: Isotope Ratios and U-Th age calculations. See table 3.3 caption for explanation of symbols.

Salt Cave Point (U15)

At this site, two *Acropora palmata* units are separated by an unconformity and rubble layer at ~4-5 m asl. The upper *Acropora palmata* unit is capped by a mixed-layer including *Montastrea sp.* and *Siderastrea sp.* head corals. Schellmann and Radtke (2001) suggest this deposit also corresponds to the T-3 platform further to the west, which has a peak elevation of 16 m asl (figure 3.3). Seven samples from the upper units were analysed. Measured ages range between 98 ka and 113 ka and initial δ^{234}U of between 149‰ and 181‰. Samples U15-2, U15-3 and U15-6, which were collected from the rubble layer are not *in situ* and are not used in the calculation of the mean age of this deposit. A sample from the lower unit, U15-10 has a measured age of ~168 ka and δ^{234}U of 154‰. The age of the upper deposit corresponds to reef growth during sub-stage 5c and the lower unit corresponds to MIS 6.

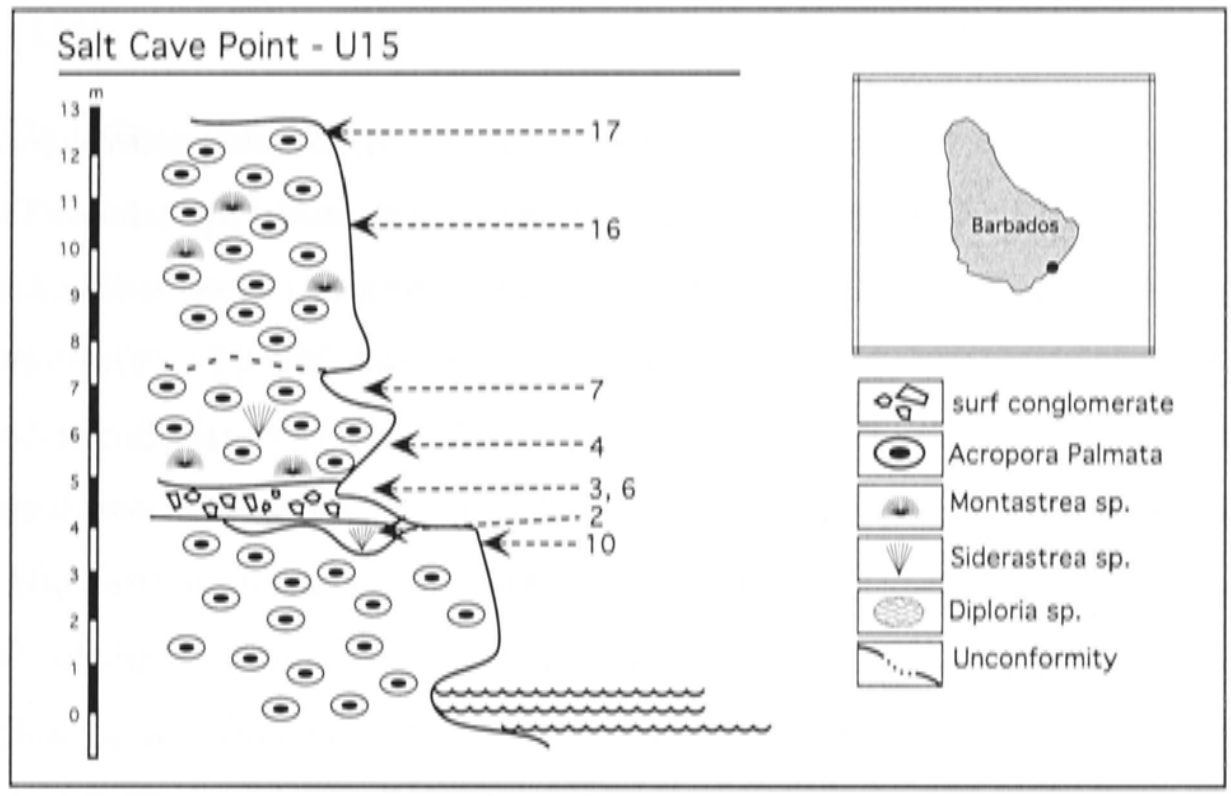

Figure 3.9: Salt Cave Point, South Coast. This 12-13 m high feature is dominated by *Acropora Palmata* in two units separated by an unconformity and rubble layer and topped by mixed coral heads including *Montastrea sp.* and *Siderastrea sp.*.

Sample No.*	XRD	H† (m)	^{238}U (ppm)	^{232}Th (ppb)	$\delta^{234}U_m$‡ (‰)	$^{230}Th/^{238}U_{act}$	Age§ (ka)	$\delta^{234}U_i$¶ ‰
U15-2 ^{D}	-	4.2	2.4396	0.22	113.7± 1.0	0.7311± 0.0012	113.2± 0.4	156.6± 1.3
U15-3 ^{Ap}	-	5.2	3.20	0.10	128.2± 1.1	0.7407± 0.0014	112.9± 0.4	176.6± 1.4
U15-4 ^{Ap}	-	5.4	3.50	0.12	113.2± 1.1	0.6699± 0.0015	97.9± 0.4	149.4± 1.4
U15-6 ^{Ap}	-	5.2	3.37	0.12	133.2± 1.1	0.7256± 0.0014	108.1± 0.4	180.9± 1.4
U15-7 ^{Ap}	-	6.7	3.56	0.12	116.4± 1.0	0.6793± 0.0013	99.6± 0.3	154.3± 1.3
U15-10 ^{Ap}	-	4.0	3.26	0.06	95.7± 1.1	0.8781± 0.0026	168.2± 2.4	154.2± 1.9
U15-16 ^{Ap}	-	10.3	3.10	0.11	117.8± 1.1	0.6961± 0.0011	103.3± 0.3	157.9± 1.3
U15-17 ^{Ap}	-	12.5	3.23	0.15	113.5± 1.1	0.7010± 0.0008	105.2± 0.3	153.0± 1.3

Table 3.7: Salt Cave Point: Isotope Ratios and U-Th age calculations. See table 3.3 caption for explanation of symbols.

Maxwell Terrace (MAX1,2)

The Maxwell terrace is a platform at an elevation of ~20 m above sea level (~20 m below the last interglacial reef, see figure 3.3). This terrace corresponds to platform T-4 identified by Schellmann and Radtke (2001) (figure 3.3). Two separate sites associated with this terrace were sampled for U-Th analysis (sites MAX1 and MAX2). Only two samples, one from each of the sites, were analysed. At the MAX1 site, the facies is dominated by large *Montastrea sp.* head corals that are indicative of relatively deep-water (~15 m) facies. The associated platform at this site is, therefore, probably an erosional bench that formed some time after the deposition of the corals that form the bulk of the deposit. The measured age of a sample from this site (MAX1-5), is 120 ka and has an initial δ^{234}U of 149‰, indicating it grew late in sub-stage 5e. Therefore, the erosional bench at site MAX1 may have formed some time following the last interglacial sea-level high-stand. The MAX2 deposit is dominated by large *Acropora palmata* trunks that are characteristic of shallow water growth (0-5 m) The measured age of the single sample that was analysed (MAX2-4) is 123 ka but has a very high initial δ^{234}U of 173‰. The deposit is not considered further in the interpretation of the U-Th ages in section 3.5 or sea-level calculations in chapter 4.

Sample No.*	XRD	H† (m)	^{238}U (ppm)	^{232}Th (ppb)	$\delta^{234}U_m$‡ (‰)	$^{230}Th/^{238}U_{act}$	Age§ (ka)	$\delta^{234}U_i$¶ ‰
MAX1-5 ^{S}	-	13.0	2.3811	0.08	106.4± 1.0	0.7514± 0.0009	120.3± 0.3	149.6± 1.3
MAX2-4 ^{Ap}	-	20.0	2.77	0.04	122.2± 1.0	0.7717± 0.0013	122.6± 0.4	172.9± 1.3

Table 3.8: Maxwell Terrace: Isotope Ratios and U-Th age calculations. See table 3.3 caption for explanation of symbols.

Foul Bay (U6)

The site at Foul Bay, (figure 3.10) reaches a maximum elevation of 22 m asl. It consists of a lower unit with a mixture of head corals, perhaps indicative of deep water growth (10-30 m). The bulk of the upper part of the deposit is *Acropora palmata*, which is characteristic of shallow water growth (0-5 m depth). Only two corals (both *Acropora palmata*) from this section were analysed. These samples, U6-2 and U6-11, were collected at elevations of ~6 m and 10 m asl respectively. Four sub-samples of U6-11 were analysed (results in table 3.9). Measured ages range between 165 ka and 253 ka and initial δ^{234}U values range between 143‰ and 249‰ (table 3.9). This deposit appears to corresponds to reef growth during stage 6.

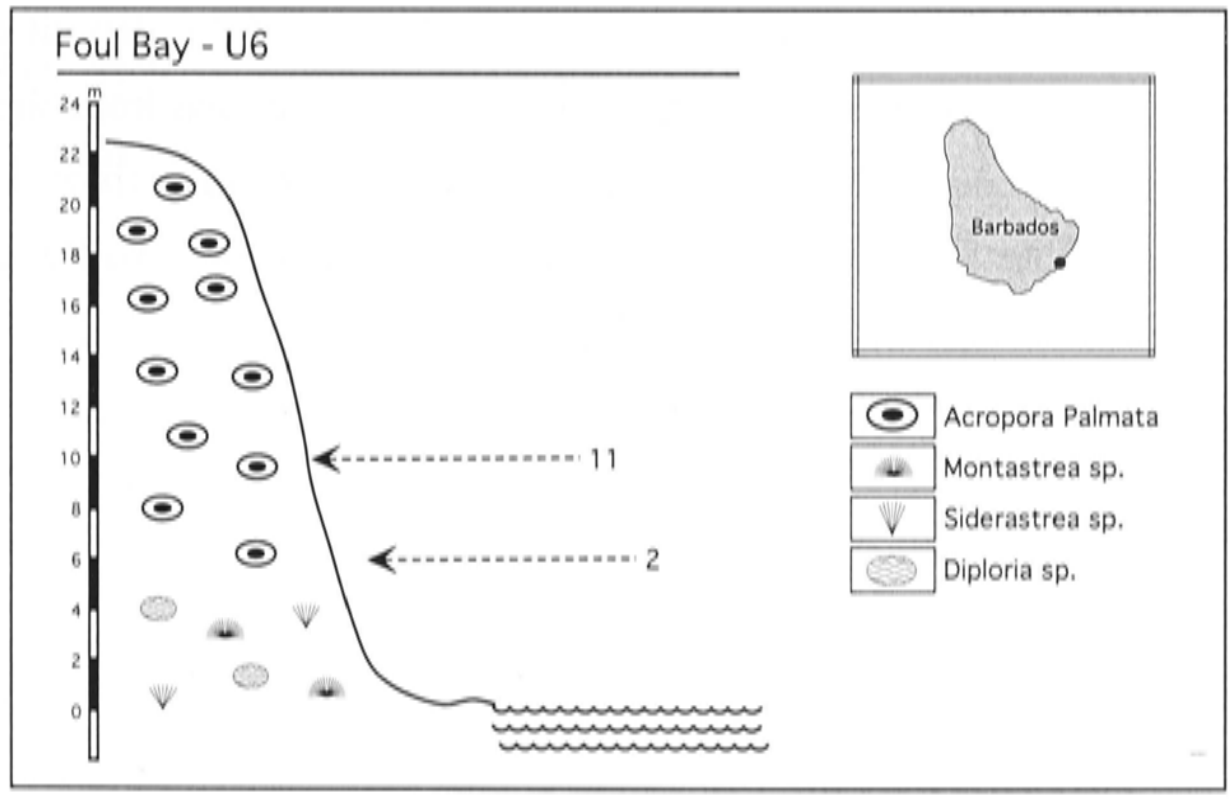

Figure 3.10: Foul Bay, South Coast. The crest of this feature is at ~22-23 m above present sea level. It predominantly consists of *Acropora palmata* with a lower unit of mixed head corals (perhaps deep water growth).

Sample No.*	XRD	H† (m)	^{238}U (ppm)	^{232}Th (ppb)	$\delta^{234}U_m$‡ (‰)	$^{230}Th/^{238}U_{act}$	Age§ (ka)	$\delta^{234}U_i$¶ ‰
U6-2 *Ap*	-	5.9	2.78	0.09	115.1± 1.2	1.0019± 0.0059	225.6± 4.3	218.2± 3.1
U6-11A *Ap*	-	9.8	2.81	0.21	121.6± 1.2	1.0434± 0.0045	253.3± 4.2	249.4± 3.3
U6-11B *Ap*	-	9.8	2.91	0.04	121.8± 1.0	1.0024± 0.0012	220.9± 1.1	227.8± 1.5
U6-11D *Ap*	-	9.8	3.22	0.03	89.8± 1.0	0.8646± 0.0016	164.8± 0.8	143.3± 1.4
U6-11E *Ap*	-	9.8	3.25	0.06	93.8± 1.0	0.8876± 0.0080	173.3± 3.7	153.4± 2.2

Table 3.9: Foul Bay: Isotope Ratios and U-Th age calculations. See table 3.3 caption for explanation of symbols.

3.3.2 West Coast

The west coast deposits sampled for this study are located along the classic Clermont's Nose traverse, which experiences Barbados' greatest rate of uplift.

Batts Rock Bay (BRB1, Beach)

The lowest 'Batts Rock Bay' deposit of this study (BRB1, figure 3.11) is a ~10 m high cliff of well preserved, large, *in situ* head corals such as *Montastrea sp.*, *Siderastrea sp.* and *Diploria sp.*. A collection of these coral types in this framework is indicative of deeper water growth (>15 m, according to Mesolella, 1967). The ages measured for the 9 samples collected from this deposit are summarised in table 3.10 and range between 103-108 ka with initial δ^{234}U values of between 144‰ and 158‰. The age of this deposit corresponds to reef growth during sub-stage 5c. One sample (BRB1-16) collected from the top of this deposit may not have been *in situ* and its measured age is 85 ka with an initial δ^{234}U of 139‰, corresponding to sub-stage 5a. The platform associated with the crest of this deposit is probably wave cut during sub-stage 5a.

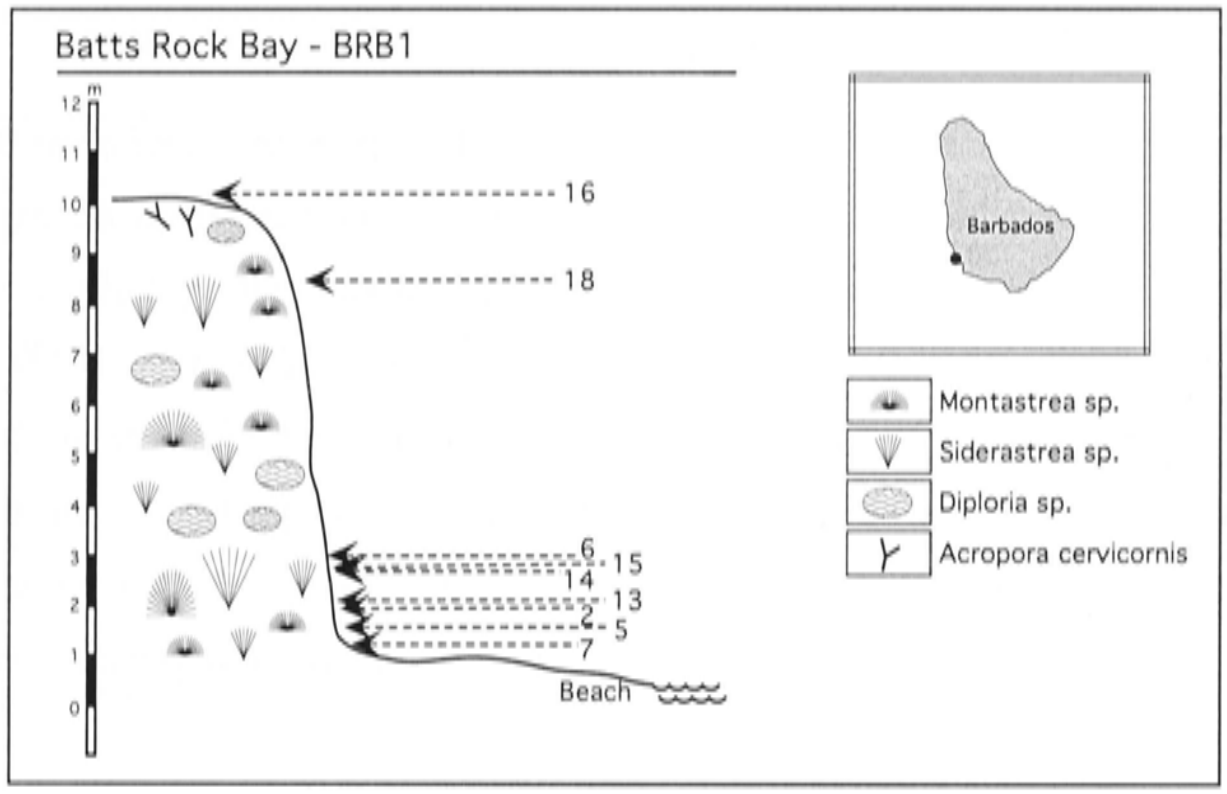

Figure 3.11: Batts Rock Bay, Clermont's Nose transect, West Coast. This 10 m feature is dominated by head corals *Montastrea sp.*, *Siderastrea sp.*, *Diploria sp.*, indicative of deeper water facies (>15 m below sea level).

Sample No.*	XRD	H† (m)	^{238}U (ppm)	^{232}Th (ppb)	$\delta^{234}U_m$‡ (‰)	$^{230}Th/^{238}U_{act}$	Age§ (ka)	$\delta^{234}U_i$¶ ‰
BRB1-2 ^{S}	-	2.1	2.08	0.16	113.5± 1.4	0.7000± 0.0008	105.0± 0.3	152.9± 1.7
BRB1-5 ^{D}	-	1.8	2.25	0.26	108.7± 1.1	0.7068± 0.0007	107.8± 0.3	147.5± 1.4
BRB1-6 ^{M}	< 1%	3.4	2.21	0.09	109.8± 1.0	0.6922± 0.0011	103.7± 0.3	147.3± 1.3
BRB1-7 ^{M}	< 2%	1.4	2.45	0.24	108.0± 1.1	0.7077± 0.0013	108.1± 0.4	146.7± 1.4
BRB1-13 ^{S}	-	2.4	2.00	0.02	114.1± 1.1	0.7038± 0.0009	106.0± 0.3	154.2± 1.4
BRB1-14 ^{S}	-	3.1	2.34	0.10	116.9± 1.1	0.7037± 0.0009	105.5± 0.3	157.7± 1.4
BRB1-15	< 1%	3.3	2.25	0.07	113.4± 1.0	0.6941± 0.0010	103.6± 0.3	152.1± 1.3
BRB1-16 ^{D}	-	10.0	2.27	0.51	109.6± 1.2	0.6077± 0.0007	84.8± 0.2	139.3± 1.4
BRB1-18 ^{M}	-	8.5	2.57	0.83	107.8± 1.0	0.6861± 0.0010	102.6± 0.3	144.2± 1.3

Table 3.10: Batts Rock Bay (1): Isotope Ratios and U-Th age calculations. See table 3.3 caption for explanation of symbols.

Batts Rock Bay (BRB2 and BRB3)

The two sites BRB2 and BRB3 (figure 3.12) appear to represent a reef crest and forereef slope. The BRB2 samples were collected (probably not *in situ*) from an exposed slope rising from 10.5 to 13.5 m asl, inland of the BRB1 site. Measured ages of the three BRB2 samples range between 72 and 81 ka with initial δ^{234}U values of between 141‰ and 147‰. Site BRB3, a reef crest exposed in a road cut, is at an elevation of 19-20 m above present sea level and contains a mix of *Acropora palmata* and other species. U-Th analyses of 6 samples from this deposit (table 3.11), give measured ages of between 85 ka and 93 ka with initial δ^{234}U of between 152‰ and 178‰. This age of these deposits corresponds to reef growth during sub-stage 5a.

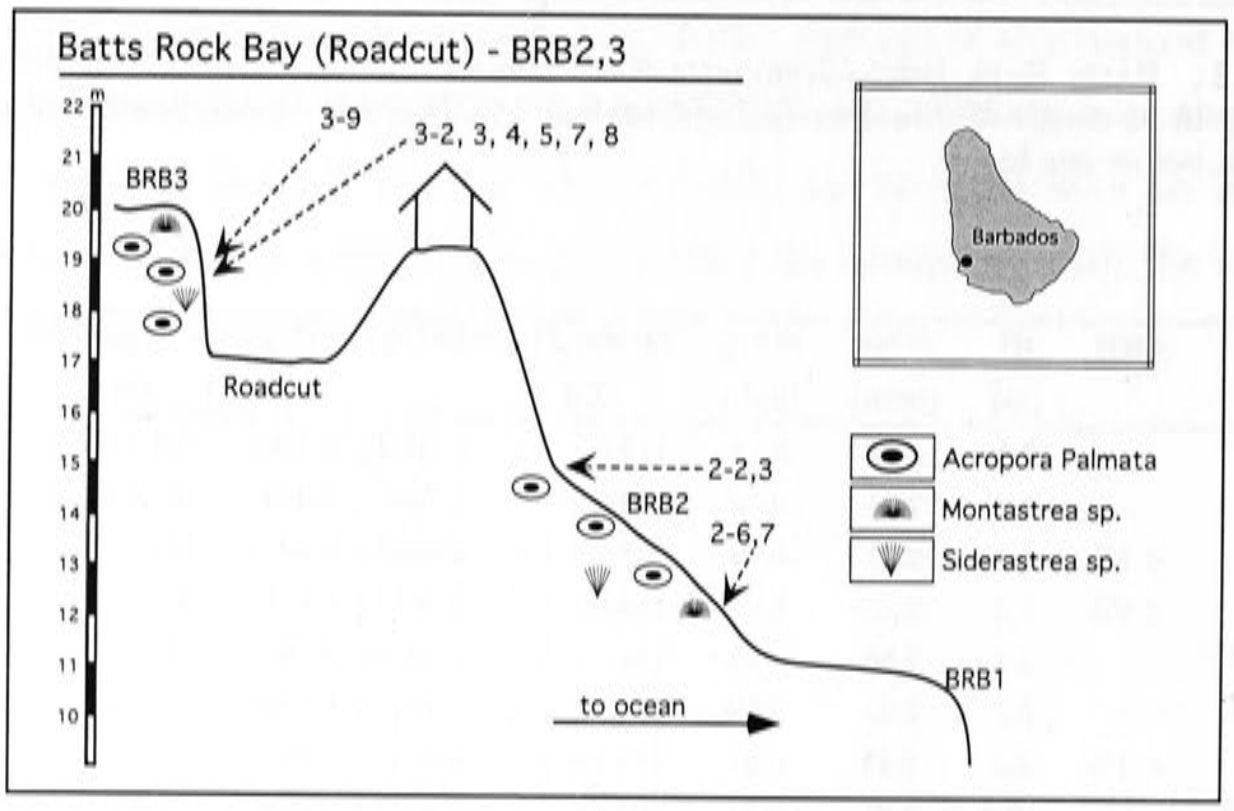

Figure 3.12: Batts Rock Bay, Clermont's Nose transect, West Coast. Site BRB3 and BRB2 represent a reef crest (at 19-20 m above present sea level) and fore-reef slope respectively. The reef crest contains a mix of *Acropora palmata* and some head corals.

Sample No.*	XRD	H† (m)	^{238}U (ppm)	^{232}Th (ppb)	$\delta^{234}U_m$‡ (‰)	$^{230}Th/^{238}U_{act}$	Age§ (ka)	$\delta^{234}U_i$¶ ‰
BRB2-2 ^{Ap}	-	14.3	2.8495	0.12	116.1± 1.1	0.5945± 0.0011	81.3± 0.3	146.2± 1.3
BRB2-3 ^{S}	-	14.3	1.78	0.16	119.6± 1.0	0.5476± 0.0008	72.0± 0.2	146.7± 1.2
BRB2-6 ^{S}	-	12.5	2.27	0.19	114.5± 1.0	0.5883± 0.0008	80.3± 0.2	143.8± 1.2
BRB2-7 ^{S}	< 1%	12.5	1.97	0.04	112.9± 1.0	0.5803± 0.0008	78.9± 0.2	141.2± 1.2
BRB3-1 ^{Ap}	-	18.5	3.35	0.03	130.3± 1.1	0.6422± 0.0013	89.4± 0.3	167.9± 1.3
BRB3-2 ^{Ap}	-	18.5	2.75	0.05	119.9± 1.5	0.6124± 0.0015	84.5± 0.4	152.3± 1.8
BRB3-3 ^{Ap}	-	18.5	3.25	0.04	137.7± 1.3	0.6556± 0.0015	91.2± 0.4	178.4± 1.6
BRB3-5 ^{Ap}	-	18.5	3.24	0.03	136.5± 1.1	0.6617± 0.0013	92.7± 0.3	177.6± 1.4
BRB3-8 ^{Ap}	-	18.5	3.63	0.03	119.5± 0.9	0.6186± 0.0014	85.8± 0.3	152.5± 1.1
BRB3-9 ^{S}	-	19.0	2.34	0.03	134.0± 1.1	0.6506± 0.0008	90.7± 0.2	173.3± 1.3

Table 3.11: Batts Rock Bay (2,3): Isotope Ratios and U-Th age calculations. See table 3.3 caption for explanation of symbols.

Batts Rock Bay 4 (BRB4, Paddock)

This reef crest, at an elevation of 30 m above present sea level (figure 3.13) predominantly consists of *Acropora palmata* with some *Siderastrea sp.* and *Montastrea sp.* head corals. The U-Th results from a set of 6 samples analysed (table 3.12) give measured ages of between 102 ka and 122 ka. Initial $\delta^{234}U$ for these samples range between 159‰ and 172‰. The age of this deposit appears to correspond to reef growth during sub-stage 5c.

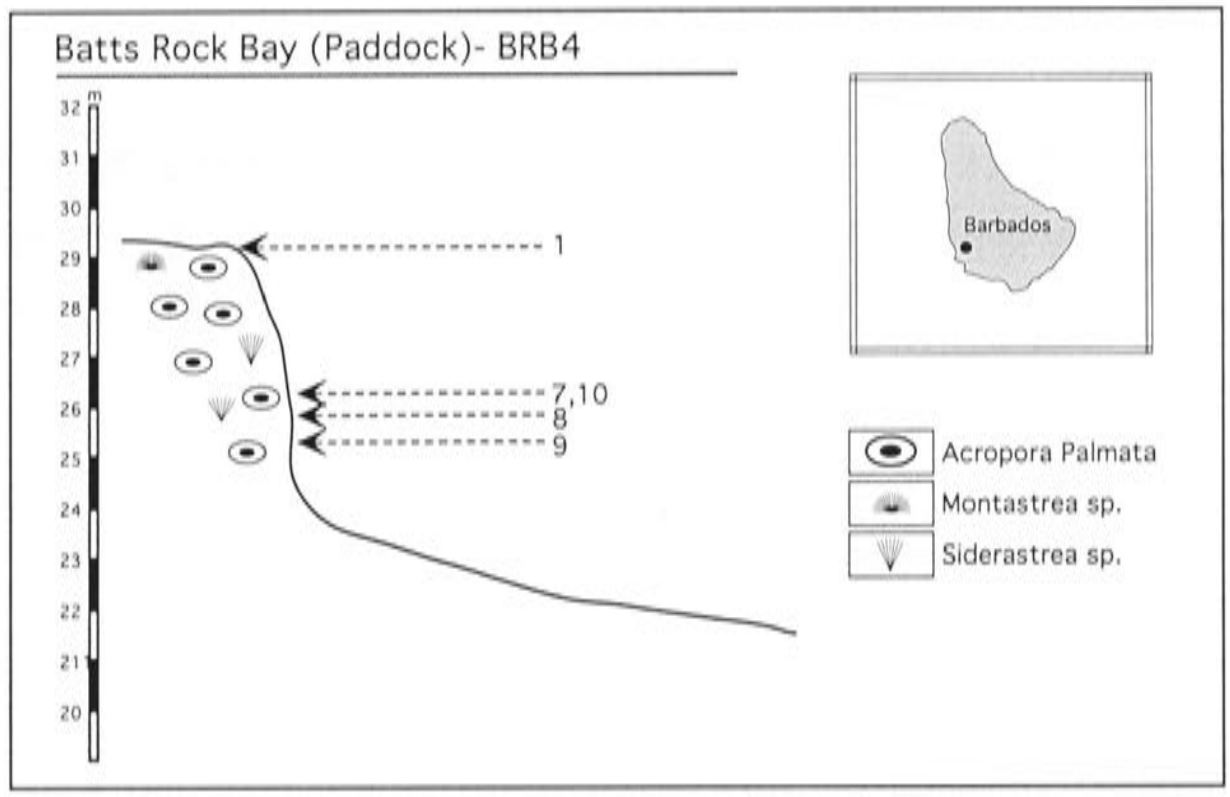

Figure 3.13: Batts Rock Bay, Clermont's Nose Transect, West Coast. The reef crest at 29-30 m above present sea level containing a mix of *Acropora palmata* with some *Siderastrea sp.* and *Montastrea sp.*.

Sample No.*	XRD	H† (m)	^{238}U (ppm)	^{232}Th (ppb)	$\delta^{234}U_m$‡ (‰)	$^{230}Th/^{238}U_{act}$	Age§ (ka)	$\delta^{234}U_i$¶ ‰
BRB4-1 ^{Ap}	-	29.0	3.1015	0.12	130.6± 1.4	0.7516± 0.0023	115.3± 0.7	181.1± 1.8
BRB4-4	-	28.9	3.17	0.19	113.7± 1.1	0.7647± 0.0015	122.4± 0.9	160.8± 1.5
BRB4-7 ^{Ap}	-	27.1	2.80	0.07	121.2± 1.1	0.7316± 0.0011	111.8± 0.4	166.4± 1.4
BRB4-8 ^{S}	-	27.5	2.38	0.07	116.9± 1.1	0.7107± 0.0011	107.3± 0.3	158.5± 1.3
BRB4-9 ^{Ap}	-	28.1	2.87	0.03	125.1± 1.1	0.7291± 0.0011	110.4± 0.3	171.1± 1.4
BRB4-10 ^{Ap}	-	27.0	3.20	0.32	128.6± 1.0	0.6985± 0.0013	102.1± 0.3	171.8± 1.3

Table 3.12: Batts Rock Bay (4): Isotope Ratios and U-Th age calculations. See table 3.3 caption for explanation of symbols.

Animal Flower Cave (AC)

A thick *Acropora palmata* unit reaches an elevation of 23 m above present sea level on the north coast of Barbados. One sample from this deposit has a measured age of 145 ka and an initial δ^{234}U of 218‰. It is unclear what marine isotope stage corresponds to this deposit. This is not considered further in the following chapters.

3.3.3 Reliability criteria

As discussed in chapter 2, there are several indicators that can be used to judge the reliability of a coral's measured U-Th age: (i) the uranium concentration of the sample should be consistent with the range observed in modern corals; (ii) the ^{232}Th of the sample should be lower than or equal to that measured in modern corals ($\leq$0.5 ppb); (iii) the sample should have experienced minimal diagenetic alteration as indicated by calcite content and petrographic textures; and (iv) the calculated initial δ^{234}U of the samples should be in agreement with that observed in modern corals.

Uranium concentration

The samples analysed in this study have uranium concentrations ranging between 2 and 4 ppm which is consistent with the modern range of 2 to 3.5 ppm. There is a distinct offset between species (shown in Figure 3.14) with *Acropora palmata* generally having higher uranium concentration than other coral species such as *Montastrea sp.*, *Diploria sp.* and *Siderastrea sp.*. This supports the results of other studies which suggest there is a species dependent uranium concentration of corals (Stirling *et al.*, 1996; Chen *et al.*, 1991). Min *et al.* (1995), Shen and Dunbar (1995) and Sinclair *et al.* (1998) also showed that there can be spatial variability of U/Ca within coral skeletons, which appear to be related to seasonal variations in temperature. No age measurements have been discounted on the basis of uranium concentration considerations.

^{232}Th concentration

Most of the samples analysed have ^{232}Th concentrations well within modern upper limit of 0.5 ppb (with only a few above this value, up to 0.8 ppb). The effect of detrital contamination on the calculated ages for all samples in this study is likely to be smaller than the analytical age precision if the composition of the detrital material is similar to that of silicate (Chen *et al.*, 1991).

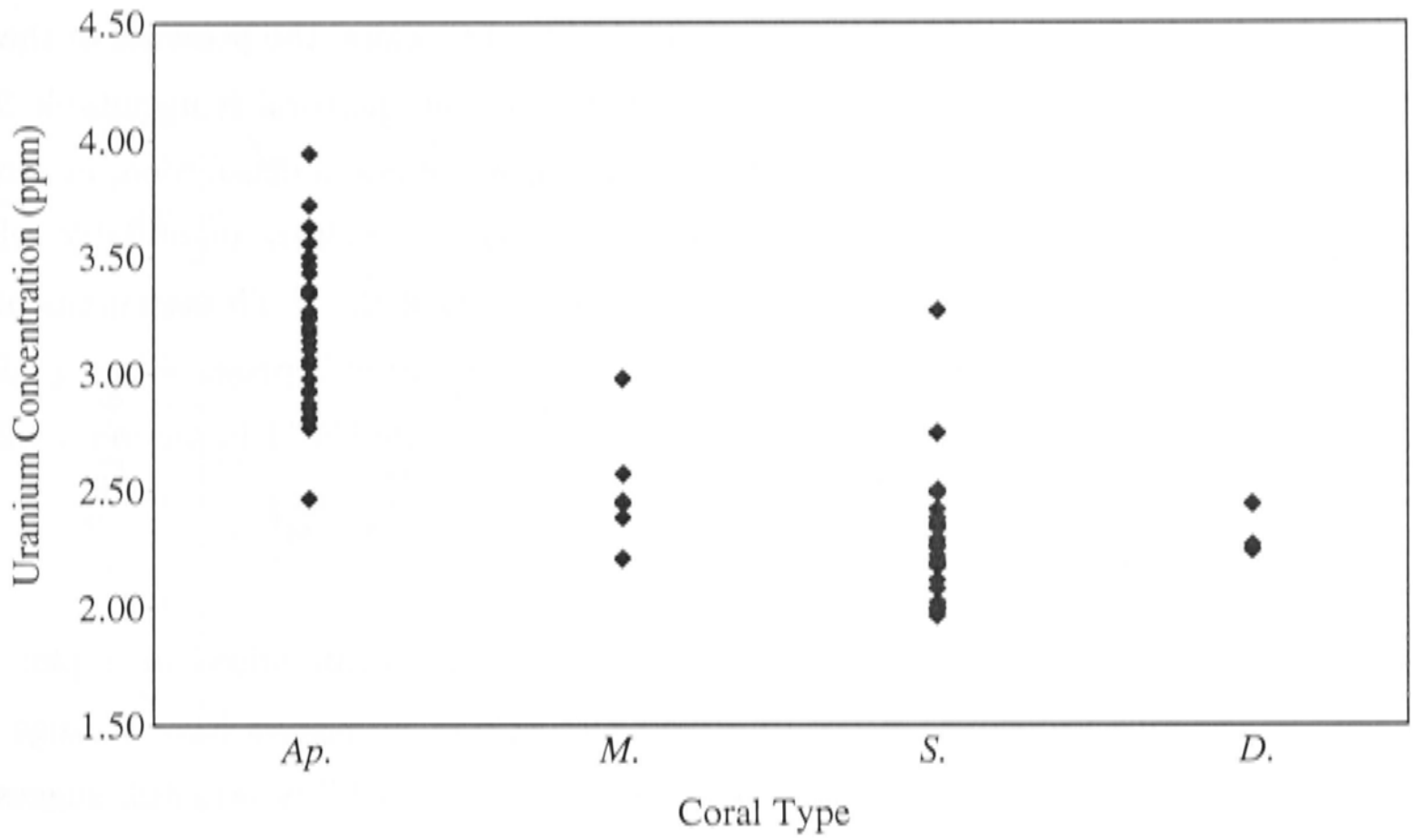

Figure 3.14: Summary of uranium concentrations measured for the samples in this study. There is a distinct offset in uranium concentration between species (Ap - *Acropora palmata*; M - *Montastrea sp.*; D - *Diploria sp.*; S - *Siderastrea sp.*)

XRD

A sub-set of the corals dated in this study (around 1/3) was analysed with XRD to check for the presence of calcite. All of the samples analysed were found to have a calcite content less than the detection limit of 1-2%.

Petrographic criteria

A subset of the corals dated in this study was examined in thin section. Some samples have been subjected to minor alteration in the form of: i) secondary aragonite cements on pore walls (figure 2.2d) and ii) micro-dissolution textures in the main aragonite matrix where the primary aragonite bundles are obscured (figure 2.3b).

The precipitation of secondary aragonite is characteristic of alteration in the marine environment (Bar-Matthews *et al.*, 1993). The deposits in this study have generally been exposed to sub-aerial weathering shortly after deposition due to uplift and sea-level fall. Therefore the precipitation of aragonite would have occurred early and thus should not have had a significant effect on the apparent age or $\delta^{234}U$ of the coral (Bar-Matthews *et al.*, 1993; Lazar *et al.*, 2002).

Micro-dissolution textures are also found in recent and modern corals (Fruijtier *et al.*,

2000; Bar-Matthews *et al.*, 1993 and Lazar *et al.*, 2002). Therefore, the presence of these textures in fossil corals is not an *a priori* indication that that the coral is unsuitable for U-Th dating. The corals in this study have varying degrees of micro-dissolution, in some cases equivalent to more than 10% of the total coral. There is no clear, quantifiable relationship between these petrographic textures and the results of the U-Th measurements, although samples with very high δ^{234}U values tend to have less well preserved aragonite fibrous structure, eg. U6-11 (see further discussion of the sample U6-11 in section 3.4.2).

Initial δ^{234}U

The results of the U-Th isotope analyses in this study are summarised in a plot of $^{230}Th/^{238}U_{act}$ vs $\delta^{234}U_m$ (figure 3.15). For each site, the U-Th results have a range of apparent ages and initial δ^{234}U values. The standard δ^{234}U reliability criterion suggests that those samples with initial δ^{234}U values within error of that of modern corals (148.5‰) have reliable U-Th ages. In the following sections, I discuss the validity of the δ^{234}U reliability criterion in the context of possible variations in ocean water δ^{234}U (section 3.4.1) and the effects of diagenetic alteration on the U-Th system of corals (section 3.4.2). Finally, in section 3.5, I present the interpretation of the U-Th results for each of the features investigated in this study that will then be used for the calculation of sea level in the next chapter.

3.4 Initial δ^{234}U

The range of initial δ^{234}U values observed for samples in this study are not all consistent with the expected modern value of ~148.5‰. In addition, the U-Th data for most of the sites in this study display a well defined correlation between apparent U-Th age and initial δ^{234}U (or $^{230}Th/^{238}U_{act}$ vs $\delta^{234}U_m$) (figure 3.15). This general trend of increasing initial δ^{234}U with apparent age has also been seen in other studies of fossil coral deposits from around the world (references in figure 3.16). Previous studies suggest that the uranium concentration and isotopic composition of ocean water has remained approximately constant during successive interglacial periods for at least the last several hundred thousand years (Henderson, 2002). Based on an assumption of steady state, combined with estimates of present day uranium fluxes, the residence time of uranium in the ocean can be calculated to be around 200-400 ka (Ku *et al.*, 1977). Therefore, it is generally accepted that the samples with $\delta^{234}U_i$ equal to the modern value of 148.5‰ have reliable ages and that other values are the result of diagenetic effects.

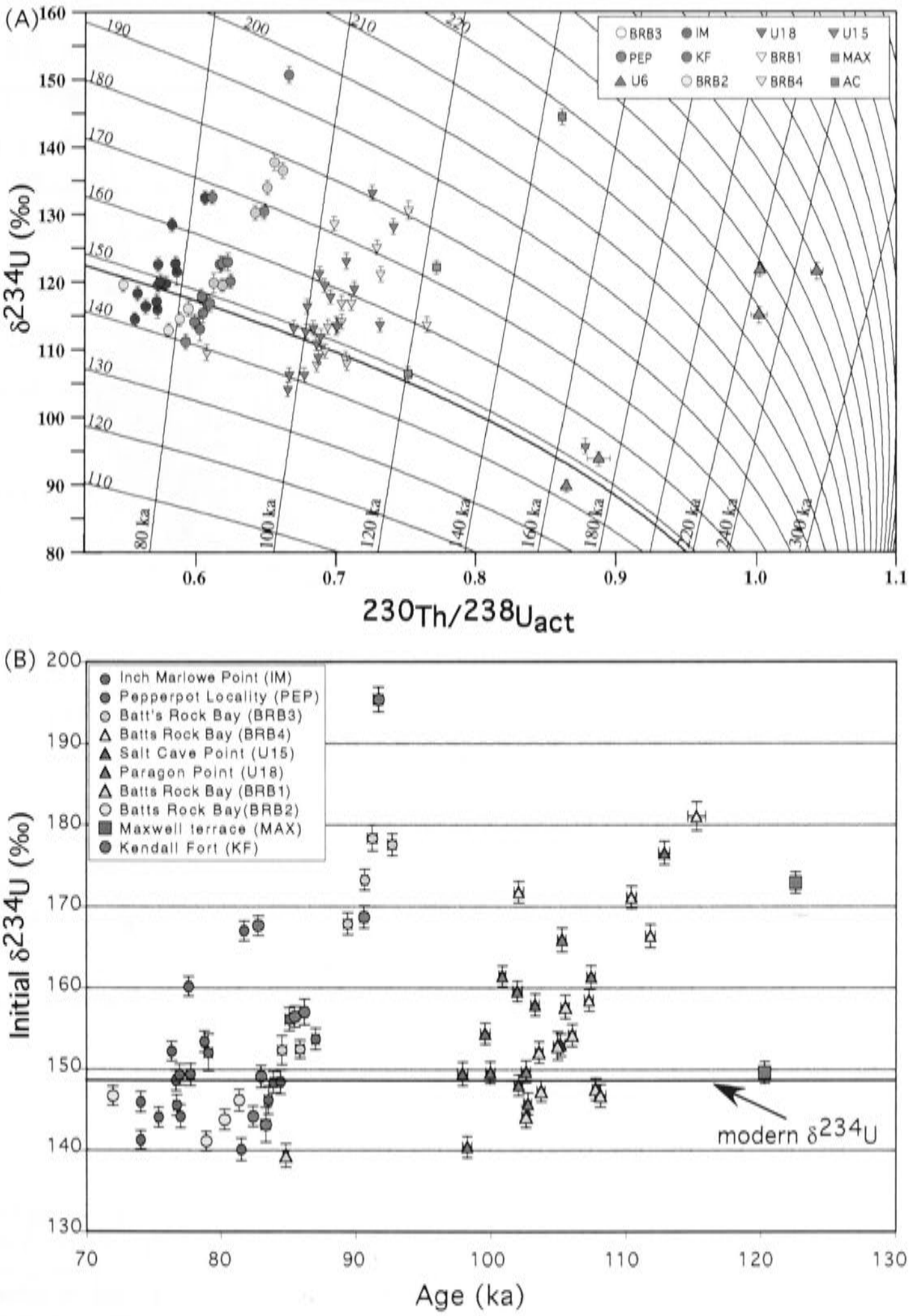

Figure 3.15: Top Panel (A) - Summary of U-Th isotopic analyses for samples investigated in this study ($^{230}Th/^{238}U_{act}$ vs $\delta^{234}U_m$). The sub-vertical lines are isochrons, and are labelled from 80 ka to 300 ka. The lines of evolution from initial $\delta^{234}U$ of 110 to 220 are also labelled. The dark line represents the line of evolution that a closed system coral would follow if the coral's initial $\delta^{234}U$ was equal to that measured in modern corals (148.5‰). Bottom Panel (B) - Summary of MIS 5 U-Th Age vs initial $\delta^{234}U$ for the Barbados sites analysed in this study. The dark line represents the modern day $\delta^{234}U$ value.

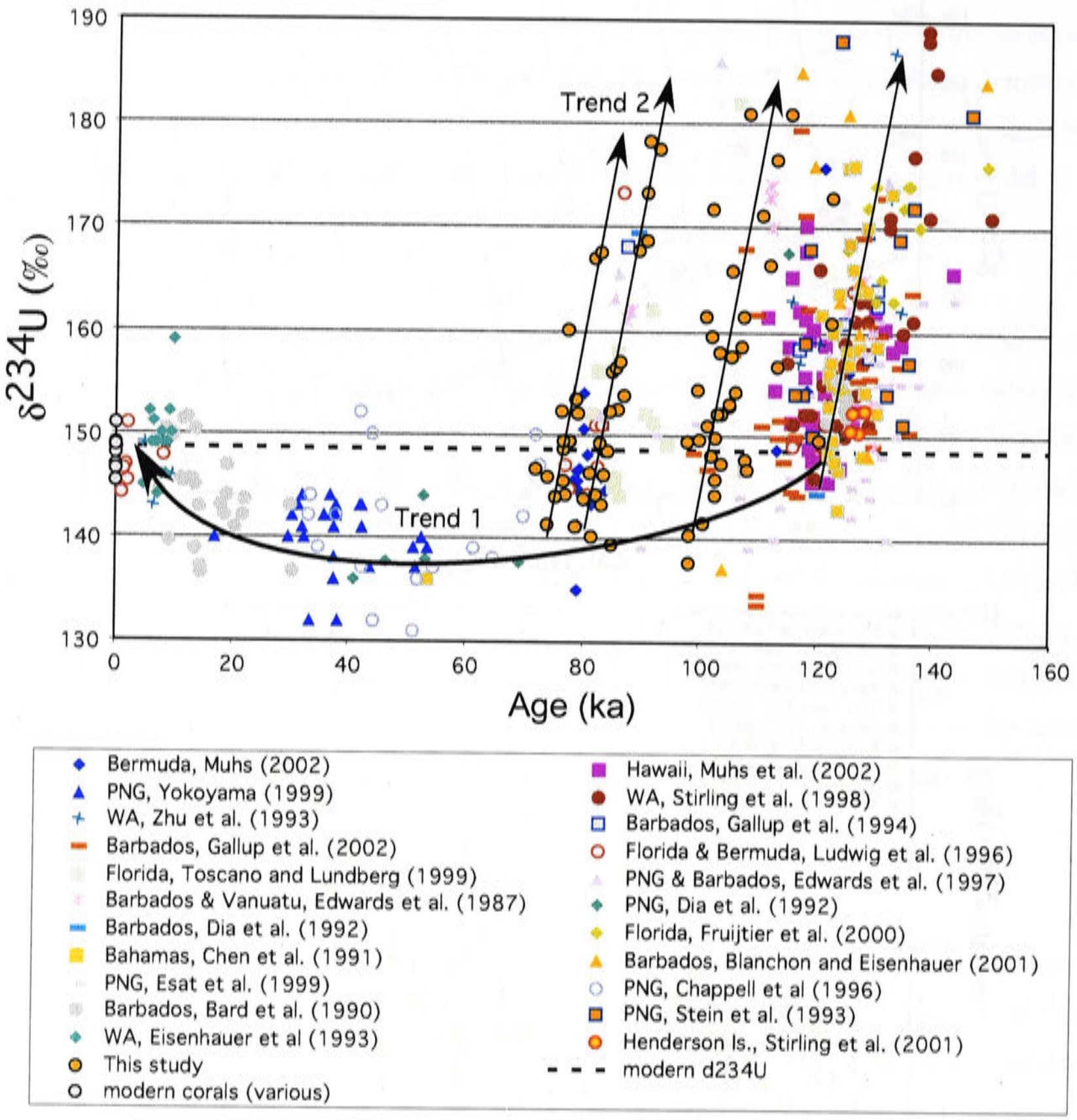

Figure 3.16: Summary of age vs $\delta^{234}U_i$ from a number of studies. In general, corals from the last interglacial period (5e) have initial $\delta^{234}U$ values equal to or higher than modern. Sub-stage 5a and 5c corals from the present study and others have $\delta^{234}U$ values ranging from a value of ~140‰, which is lower than the modern value of 148.5‰, to well above the modern value. The initial $\delta^{234}U$ of MIS 3 corals are generally 10-15‰ lower than modern and there appears to be a rise of initial $\delta^{234}U$ during the last deglaciation. There are two apparent 'trends' in this data. The first, trend 1, is an apparent gradual lowering of the minimum values of $\delta^{234}U_i$ throughout much of the glacial cycle, before rising again to modern values during the last deglaciation. The other, trend 2, is a steep correlation between apparent age and $\delta^{234}U$ within deposits of the same age.

Figure 3.16 summarises the results of calculated initial δ^{234}U values from a number of different studies of fossil corals from various locations around the world (since the last interglacial period). Although there increased scatter to higher δ^{234}U for older deposits, there appears to be some systematic behaviour in the variability of initial δ^{234}U throughout the last glacial cycle. Samples from last interglacial deposits (eg, WA - Stirling *et al.*, 1998; Barbados - Gallup *et al.*, 1994; PNG - Stein *et al.*, 1993) and deposits from previous interglacials (Barbados - Gallup *et al.*, 2002, Henderson Island - Stirling *et al.*, 2001) have initial δ^{234}U values which are generally equal to or higher than modern values.[5] MIS 3 corals from Huon Peninsula (Yokoyama, 1999; Chappell *et al.*, 1996a; Dia *et al.*, 1992) and Barbados (Bard *et al.* 1990) systematically have lower $\delta^{234}U_i$ than modern corals (up to 10-15‰).[6] A recent unpublished study by Linda Ayliffe also shows an apparent rise in initial δ^{234}U of ~10‰ during the last deglaciation (not shown in figure 3.16). Studies of sub-stage 5a and 5c corals (this study; Muhs *et al.*, 2002; and to a lesser extent Ludwig *et al.*, 1996; Toscano and Lundberg, 1999) include $\delta^{234}U_i$ below present day ocean water as well as those at higher values.

There are two systematic trends in the data in figure 3.16, one which suggests there has been a gradual lowering of minimum initial δ^{234}U values throughout the last glacial cycle followed by a rise to modern levels (trend 1) and the other which shows a steep correlation between age and δ^{234}U for corals from deposits of the same age (trend 2). Variations in the initial δ^{234}U values observed in fossil corals must be due to one of two processes, either: i) mobilisation of U and Th isotopes during diagenetic alteration; or ii) variations in ocean water δ^{234}U. Next, I consider what mechanisms may be responsible for the systematic 'trend 1' of changes of δ^{234}U in the ocean throughout the last glacial cycle. If δ^{234}U of the ocean has varied on glacial to interglacial time-scales, this has profound implications for the interpretation of U-Th coral ages.

3.4.1 δ^{234}U in the ocean

Sources of uranium

There are several sources of uranium to the ocean. Firstly, continental weathering and riverine transport provides a major contribution of enriched ^{234}U uranium to the ocean

[5]Henderson *et al.*'s (1993) study of corals from Hateruma Atoll, Japan, includes samples with anomalously low $\delta^{234}U_i$ values. The value changes depending of the mechanical cleaning methods applied so it is clear this variability is due to alteration.

[6]Yokoyama (1999) also suggests that there are also rapid variations in δ^{234}U during MIS 3, which appear to correlate with rapid oscillations in sea level during that period.

(Palmer and Edmond, 1993). Based on a study of the dissolved uranium content of waters from the Orinoco, Amazon and Ganges basins, Palmer and Edmond (1993) estimate the global riverine uranium flux to the ocean is $3 - 6 \times 10^7$ mol/yr. Studies indicate that present day river water δ^{234}U lies between 200‰ and 300‰ (Cochran, 1982). However, geographical and seasonal changes in total uranium content and isotopic composition of river water make estimating global averages of these parameters difficult. Based on these estimates of uranium concentration and isotopic composition approximately $2 - 4 \times 10^3$ mol/yr of ^{234}U enters the ocean via river input.

Secondly, the α-recoil of ^{234}U from ocean sediments into surrounding pore-water and its subsequent diffusion into the ocean is another potential source for enriching ocean δ^{234}U (Ku, 1965, 1977). However the magnitude of this source's contribution to ocean water excess δ^{234}U is uncertain. By considering a simple, steady state ^{234}U budget for the ocean, Henderson (2002) estimates the contribution of sediment pore-water ^{234}U flux to be on the order of 10% of the input via rivers (or 2×10^2 mol/yr).

The dissolution of marine carbonates is another potential source of uranium to the ocean. Russell *et al.* (1996) estimate the uranium flux from this source to be 1×10^7 mol/yr in a glacial ocean, based on estimates of carbonate dissolution from Opdyke and Walker (1992). If these carbonates are at or near secular equilibrium, this provides a source of low δ^{234}U.

Sinks of uranium

Uranium is removed from the ocean through a number of different processes including uptake by plankton and organic matter, precipitation of organic and inorganic carbonates and removal from solution by adsorption or precipitation of insoluble minerals in a reducing environment (in suboxic and anoxic sediments). Global removal rates of uranium from the ocean are not well constrained and estimates range between 81 and 261% of the riverine input rates (Barnes and Cochran, 1990; Russell *et al.*, 1996; Morford and Emerson, 1999; Klinkhammer and Palmer, 1991). Fractionation of uranium isotopes is not expected to occur during these removal processes.

Mechanisms for changing ocean water δ^{234}U

The range of estimates of modern day sources and sinks of uranium to the ocean are consistent with the conditions required for a steady state. Variations in ocean water δ^{234}U on long timescales may be a good indicator of the balance between physical and chemical

continental weathering (Henderson, 2002), as riverine input is thought to be the most important source of uranium to the ocean. Weathering processes should not change significantly on the time-scales of interest to this study, so an alternative mechanism must be sought to explain the variability of δ^{234}U in the ocean implied by trend 1 in figure 3.16. This mechanism(s) would need to act as a perturbation to the steady-state balance of uranium sources and sinks to the ocean.

The following is a brief discussion of some alternative mechanisms which may lead to rapid changes in ocean water δ^{234}U. Because there is very poor quantitative constraint on the magnitude and source and sinks of ^{234}U and uranium in the ocean, the mechanisms discussed below are necessarily speculative.

1. Riverine influx and glacial melt

There is an apparent rise in δ^{234}U between MIS 3 and the present day (figure 3.16, trend 1). If an increase in river water discharge volume or uranium concentration is responsible for this change in δ^{234}U (~10‰ increase) then the uranium discharge would need to be increased by more than a factor of 3 on a very short time-scale. However, it is unlikely that the discharge or uranium content of rivers would change by more that 50% between glacial and interglacial times (Henderson, 2002). The melting rate of the ice sheets over the period of the last deglaciation is approximately an order of magnitude smaller than the present annual river discharge rate[7]. Therefore it is unlikely that the increased weathering associated with the glacial melt would be sufficient to increase the global δ^{234}U ocean value by the observed amount unless the melt-water was extremely enriched in ^{234}U (possibly because of enhanced leaching of ^{234}U from fine glacial sediment).

2. Storage of ^{234}U in suboxic sediments

The data in figure 3.16 suggest there may have been a gradual lowering of oceanic δ^{234}U following the last interglacial period. Using the lowest estimates of present day uranium influx and isotopic composition from river water, a lowering of ~6‰ in 20 ka could be achieved by the decay of excess ^{234}U. If the removal of high δ^{234}U uranium from river water occurs before isotopic equilibration with the rest of the ocean, then the lowering of δ^{234}U of the global ocean could occur even more quickly (limited to ~8‰ in 20 ka by the decay of excess ^{234}U). In anoxic and suboxic conditions, uranium is readily reduced to its

[7]The ice sheets of the last glacial maximum were ~3-4% of the total ocean volume. If the melting occurred over ~10 ka, this would produce a melting rate of approximately ~5×10^{15} l/yr compared with the current global river discharge rate estimates of ~3.5×10^{16} l/yr.

+IV state and is therefore easily removed from solution (Klinkhammer and Palmer, 1991; Cochran *et al.*, 1986; Rosenthal *et al.*, 1995). This is a particularly important process in organic rich estuarine continental shelf sediments (Cochran *et al.*, 1986). The proportion of uranium that undergoes burial in near shore sediments is dependent on river discharge and sediment disturbance (Cochran, 1992; Cochran *et al.*, 1986). Estimates of the removal rate of uranium from the ocean into organic rich continental margin sediments range between $1 - 3 \times 10^7$ mol/yr (Morford and Emerson, 1999; Klinkhammer and Palmer, 1991), making them a major sink of oceanic uranium. Because this sink of uranium occurs near river sources of high δ^{234}U uranium, this may provide a mechanism for the removal of high δ^{234}U input before it mixes with the global ocean. A lowering of 8-10‰ in 20 ka is required to explain the low δ^{234}U measured in some sub-stage 5c samples in this study. If this observed value is real, it represents a near complete removal of high δ^{234}U sources to the ocean. Lowering of ocean water δ^{234}U to 135‰ by MIS 3 (Yokoyama, 1999) are possible, simply by using the lower estimates of present day uranium influx. Lowering of oceanic δ^{234}U could be achieved with the addition of a low δ^{234}U uranium source such as the dissolution of marine carbonate, but current estimates suggest this would not be sufficient to lower oceanic δ^{234}U by the observed magnitude (Russell *et al.*, 1996).

To explain rapid rises in ocean water δ^{234}U such as that during the last deglaciation, Esat and Yokoyama (1999) suggest the following scenario. Consider the enriched ^{234}U stored in suboxic continental shelf sediments that would immediately oxidise when exposed after a fall in sea level. Upon a subsequent sea-level rise, this oxidised uranium is immediately dissolved and disperses into the ocean, creating a source of high δ^{234}U. Esat and Yokoyama suggest that the amount of enriched uranium accumulated during a 10 ka interglacial on the continental shelves which are then exposed during a glacial period may be sufficient to raise the ocean δ^{234}U by the observed magnitude. Further studies into the uranium content and isotopic composition of these continental shelf sediments are needed to be able to judge the magnitude of this contribution to changes in global ocean δ^{234}U.

Changes in the distribution of reducing or oxidising conditions in deep oceanic sediments could result in changes in the net uranium budget of the ocean and influence the uranium isotope balance. Rosenthal *et al.* (1995) suggested that due to increased productivity in glacial oceans, there was a twofold increase in the aerial extent of suboxic sediment conditions at that time, from 8% to 16% of the total ocean floor area. This increase may change the magnitude of the potential uranium sink of the oceans during glacial periods. The magnitude of the contribution of α-recoiled ^{234}U from oceanic sediments to the total

ocean's ^{234}U budget is uncertain (Ku, 1965; Henderson, 2002) but may be around 2×10^2 mol/year (Henderson, 2002). In anoxic conditions, the α-recoiled ^{234}U in the sediment may not be immediately released into the ocean water. Let us consider the amount of α-recoiled ^{234}U that may be trapped in suboxic sediments in that 8% of the ocean floor during a 100 ka glacial period. 8% of 2×10^2 mol/year production of ^{234}U over 100 ka suggests there may be a total accumulation of 1.5×10^6 mol of ^{234}U (also accounting for the decay of ^{234}U). This accumulated excess ^{234}U may be released during the transition from glacial to interglacial conditions, as the aerial extent of suboxic sediments is reduced. However, the amount of accumulated ^{234}U is equivalent to only 1‰ of excess ^{234}U the total ocean (1.1×10^9 mol of ^{234}U) and cannot account for the total apparent rise of ~10‰ in δ^{234}U during the last deglaciation (trend 1).

3. Spatial variability of $\delta^{234}U$ within the ocean

Chen *et al.* (1986) estimated ocean water δ^{234}U to be 144±2‰ from 9 uranium isotopic analyses of waters from the Atlantic and Pacific oceans. The uncertainties of individual measurements in that study were ~4-8‰ and there is some scatter even outside the range of quoted uncertainties (in the Pacific samples), so spatial variability and depth dependence of δ^{234}U cannot be ruled out.[8] Uranium concentration in ocean water (measured by Chen *et al.*, 1986) has a range of values that is an order of magnitude larger than is predicted by steady state models. Based on this observation, Chen *et al.* (1986) suggest either i) previous estimates of uranium residence time in the ocean are too long and/or ii) the mechanisms for the distribution of uranium in the ocean is not well understood. If the uranium isotopic composition of the ocean is also not uniform then this has implications for the expected rates of change of δ^{234}U compared to estimates based on a single layer box model.

In Yokoyama's (1999) study of MIS 3 corals at Huon Peninsula there appears to be a succession of rapid oscillations in δ^{234}U of up to 10‰ around a mean value that is lower than that of modern corals. Esat and Yokoyama (1999) suggest that these variations correlate with sea-level oscillations. If real, these rapid variations during MIS 3 must reflect only local variability in δ^{234}U. Perhaps enriched ^{234}U uranium released from local estuarine or continental shelf sediments in that region during each sea-level rise was the source of these rapid increases. The observed rapid decrease of δ^{234}U would then reflect a dispersal of the high δ^{234}U plume into the global ocean. In this scenario, the amount of excess ^{234}U

[8] Recent unpublished measurements from a number of different sites give a value of ~148.5±1‰ which is also more consistent with observations of δ^{234}U in modern corals, T. Esat pers. comm.

may have appeared very high locally but would not have been sufficient to significantly increase the global $\delta^{234}U$ once it dispersed.

To test these hypotheses, a comprehensive study of $\delta^{234}U$ using high precision measurement techniques for open ocean and coastal environment waters and modern corals should be conducted for both uranium concentration and isotopic composition. This is beyond the scope of this thesis.

4. Fractionation of uranium isotopes

The mechanism for incorporation of uranium into the coral skeleton is not well understood. Studies suggest that the U/Ca ratio of a coral is dependent on temperature (Min *et al.*, 1995; Shen and Dunbar 1995; Sinclair *et al.*, 1998), but this has not been shown to affect the coral's U-Th isotopic composition. An alternative, but perhaps less likely, explanation for the observed variation of initial $\delta^{234}U$ in corals may be the fractionation of uranium isotopes during the deposition of the coral skeleton as is observed for oxygen isotopes as a function of temperature (McConnaughey, 1989) or biological effects (Smith *et al.*, 2000). However a fractionation of the magnitude required to explain the observations seems unlikely due to the small difference in uranium isotopic mass numbers relative to the total mass of uranium. To investigate this possibility, a systematic comparison of $\delta^{234}U$ in modern corals with that of water at the same sites should be made for a number of regions but this is also beyond the scope of this thesis.

Ocean $\delta^{234}U$ conclusions

Several potential mechanisms exist that may lead to systematic changes in isotopic composition of ocean water over a glacial cycle (trend 1, figure 3.16). These include (i) variations in riverine uranium content or isotopic composition, (ii) storage and release of ^{234}U from suboxic sediments and/or(iii) spatial variability of oceanic $\delta^{234}U$.

However, not all of the observed variability in $\delta^{234}U_i$, (that is, the highly elevated values described by trend 2 in figure 3.16) can be explained by variations in ocean water $\delta^{234}U$ because:

1. There are a number of instances where different corals with a similar apparent age show distinctly different $\delta^{234}U_i$. (e.g. the data from the present study, figure 3.15)

2. Very high values of $\delta^{234}U_i$, and the distinctive steep trend (trend 2 in figure 3.16) between $\delta^{234}U$ and apparent age that are observed in fossil corals cannot easily be

explained by variations in ocean water δ^{234}U.

3. Corals from the same site and stratigraphic horizon have a large range of ages (e.g. site BRB3).

Therefore diagenetic alteration must also be considered to explain the large range of observed δ^{234}U and the trend of increasing δ^{234}U with apparent age.

3.4.2 Modelling open system behaviour

Alteration, whether in the form of dissolution, recrystallisation or the addition of calcite or aragonite cements, can result in the mobilisation of uranium and thorium isotopes. However, the effects of these alteration processes on a coral's apparent U-Th age and initial δ^{234}U are not well understood.

The U-Th analyses from the present study (figure 3.15) confirm the previously observed correlation between apparent U-Th age and initial δ^{234}U (or measured ^{230}Th/^{238}U and δ^{234}U) in fossil deposits from different locations (see references in figure 3.16). In the present study, there is a particularly tight correlation between ^{230}Th/^{238}U and δ^{234}U in the two sub-stage 5a features (figure 3.15). The trend is also seen in the sub-stage 5c data, but with more scatter. A trend of increasing ^{230}Th/^{238}U and δ^{234}U is also defined by the group of older samples (U6, U15), although the slope of this trend is less steep than for the younger deposits. The U-Th data from the other studies define similar trends with varying degrees of scatter. The general consistency of these trends from different time periods and locations around the world indicates that the process(es) responsible for the variations in each of these isotopic ratios may be related.

The sub-stage 5a and 5c deposits analysed in this study include samples with lower than modern δ^{234}U. As discussed previously, it is possible that δ^{234}U of the ocean changed on this kind of time-scale. Alternatively, if we assume that the full range of ^{230}Th/$^{238}U_{act}$ and δ^{234}U values is the result of alteration, then we must invoke two opposing diagenetic mechanisms of open system U-Th behaviour, one which increases both apparent age and initial δ^{234}U and another in which both decrease.

In this section, I discuss several alternative models of diagenetic alteration that have been proposed to explain the observed trends (trend 2 in figure 3.16) of elevated δ^{234}U and apparent age. An emphasis is placed on the trends defined by the younger features identified in this study.

Addition of ^{234}U and ^{230}Th

Gallup *et al.* (1994) presented the results of U-Th analysis on a set of MIS 5e and MIS 7 age corals from Barbados, in which they identified the correlation of apparent U-Th age and initial δ^{234}U (or measured ^{230}Th/^{238}U and $\delta^{234}U_m$). Gallup *et al.* (1994) proposed an 'addition' model in which this correlation is attributed to the continuous addition of ^{234}U and ^{230}Th to the coral system. The ratio of the rate of addition of these two isotopes was determined empirically from the observed trend (^{230}Th:^{234}U of ~0.7:1).

A comparison of Gallup *et al.*'s (1994) data and diagenesis model with the data from the current study is shown in figure 3.17 (dashed lines). Gallup *et al.*'s (1994) model reproduces the trend observed by the sub-stage 5a and 5c data in this study reasonably well. In contrast, the model predicts a much steeper slope than is observed for the MIS 6 feature (site U6, this study).

Gallup *et al.* (1994) acknowledge that it is surprising that their model requires the addition of almost equal amounts of ^{230}Th and ^{234}U. Generally thorium is much less abundant than uranium in percolating groundwater because of its lower solubility. Gallup *et al.* (1994) suggest that the ^{230}Th and ^{234}U nuclides may be transported, not in solution, but attached to suspended organic colloids. These colloids may have an enhanced affinity for thorium isotopes thus providing a mechanism for enhanced thorium transport (Osmond and Ivanovich, 1992). The addition model proposed by Gallup *et al.* (1994) requires that percolating groundwater is enriched in ^{234}U with respect to ^{238}U. However, in a study of the U-Th isotopic composition of ground-waters at Barbados, Banner *et al.* (1991) found that present day groundwater samples were not enhanced in ^{230}Th or ^{234}U. Furthermore, this addition model does not provide a mechanism to explain the lower than present day initial δ^{234}U values observed for the sub-stage 5a and 5c features.

Early diagenesis in the marine environment

Banner *et al.* (1991) suggested that addition of high δ^{234}U may have occurred shortly after growth while the coral was still influenced by marine pore-waters. In this marine environment, cements or recrystallised material would be in the form of aragonite (Bar-Matthews *et al.*, 1993). Lazar *et al.* (2002) suggested that early dissolution and precipitation of secondary aragonite in 5% volume of a 1000 yr old submerged coral can lead to a slight *reduction* in apparent age (up to ~7%) with but with very little change in apparent initial δ^{234}U. Prolonged submergence would presumably lead to a further reduction of age and

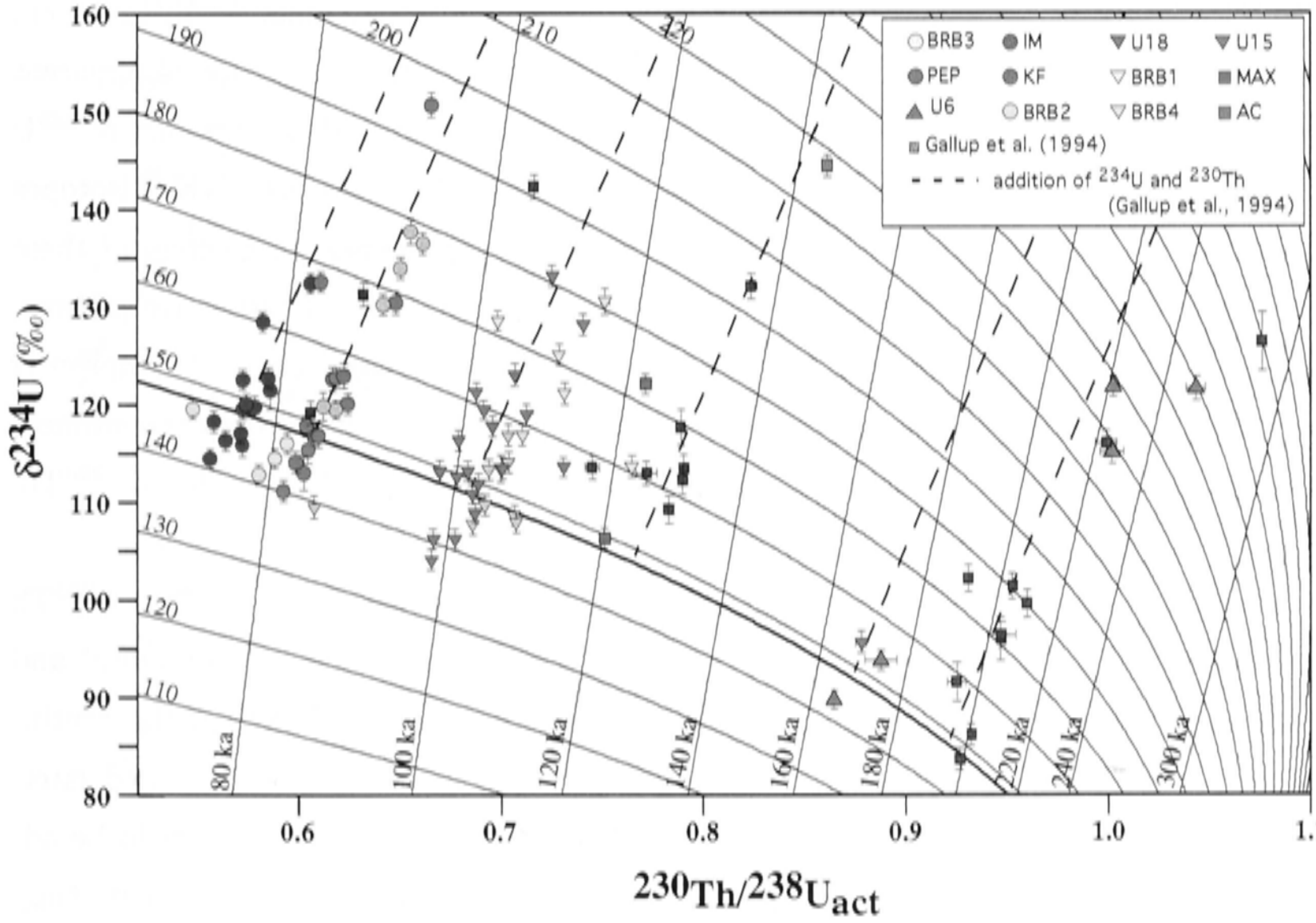

Figure 3.17: A comparison of Gallup *et al.*'s (1994) model of continuous ^{234}U and ^{230}Th addition (dashed lines) with the U-Th analyses from this study (coloured symbols) and from Gallup *et al.* (1994) (grey squares). The model reproduces the trend for the younger features but predicts a steeper slope than that defined by the older (MIS 6) feature identified in this study (red triangles).

an increase in δ^{234}U. Most of the exposed coral deposits at Barbados were removed from the marine environment shortly after their deposition because of tectonic emergence and sea-level fall. Therefore, the effect of this marine diagenesis on age is likely to be minimal. Marine environment diagenesis of this type cannot be responsible for the observed trend of increased apparent age and δ^{234}U.

Addition of ^{234}Th and ^{230}Th

The addition of ^{234}Th and ^{230}Th in approximately equimolar amounts (Fruijtier *et al.*, 2000; Thompson *et al.*, 2002)[9] has been proposed to explain the correlation of apparent age and initial δ^{234}U observed in fossil corals. ^{234}Th is the initial decay product of ^{238}U and unlike ^{234}U, both ^{234}Th and ^{230}Th are highly insoluble. The presence of these isotopes in percolating fluids in the fossil reef may be due to two processes: i) ejection of these isotopes via α-recoil from their host material following the decay of respective parents, ^{238}U and ^{234}U; or ii) the decay of dissolved uranium in percolating fluids (Thompson *et al.*, 2002). These daughter thorium isotopes may be quickly adsorbed onto the surfaces of corals, resulting in the enrichment of ^{234}U (from the rapidly decaying ^{234}Th) and ^{230}Th.

In a two-box model, Thompson *et al.* (2002) calculated the ratio of ^{234}Th to ^{230}Th lost from a carbonate 'source' (including α-recoil and decay of dissolved uranium) and the resulting change to the isotope ratios of the coral 'sink' resulting from the continuous addition of these isotopes.[10] With some assumptions, which are addressed later, they demonstrate that the decay-dependent ratio of ^{234}Th and ^{230}Th that would be adsorbed onto the coral 'sink' is consistent with the observed trends in the present study (see dashed lines in figure 3.18). The slope predicted by Thompson *et al.*'s model is in general agreement with the observed trends although the sub-stage 5a trends appear to be slightly steeper than predicted slopes. A variation of Thompson *et al.*'s model, in which the source of ^{234}Th and ^{230}Th is entirely from dissolved uranium, is shown as the dotted lines in figure 3.18. The best fitting model may be an intermediate between these two alternatives.

Thompson *et al.*'s (2002) model provides a physical process to explain the observed trends. However, there are still some uncertainties about the mechanisms involved (some of which

[9] Thompson *et al.*'s work has not yet been published but W. Thompson supplied a copy of the submitted paper and calculation spreadsheet.

[10] Thompson *et al.* suggest that non-continuous alteration does not necessarily affect the predicted trends but this will depend on the nature of the alteration history.

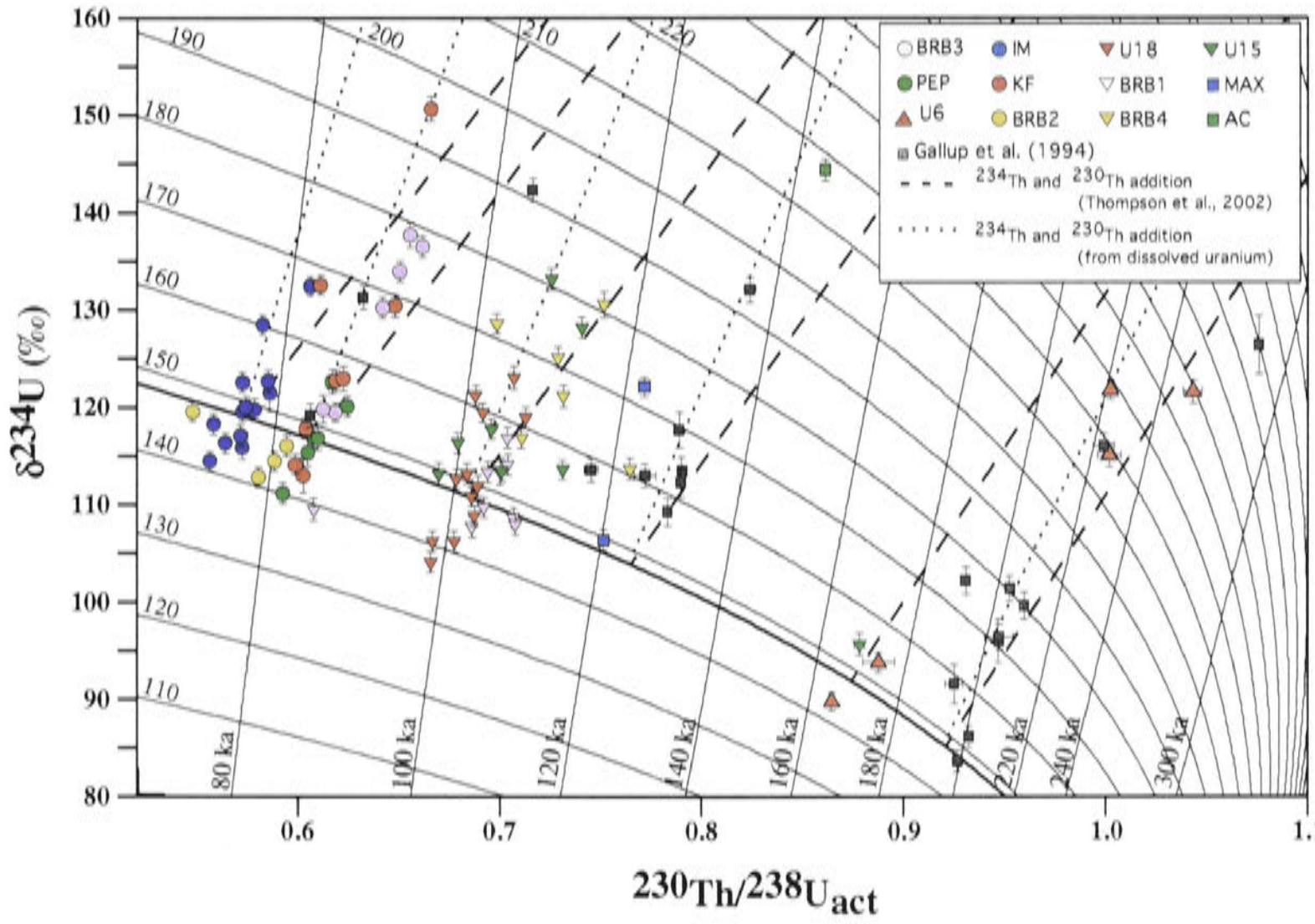

Figure 3.18: A comparison of the isotopic observations from the present study (coloured symbols) and Gallup *et al.*'s (1994) Barbados data (grey squares) with Thompson *et al.*'s (2002) preferred model of continuous ^{234}Th and ^{230}Th addition, which includes an α-recoil source and dissolved uranium (dashed lines) and continuous ^{234}Th and ^{230}Th addition from a dissolved uranium source only (dotted lines). The slope of the trends defined by the sub-stage 5a deposits lie between these two models.

are addressed by Thompson *et al.*):

1. The model proposed by Thompson *et al.* (2002) invokes the removal of ^{234}Th and ^{230}Th by α-recoil from some carbonate 'source'. If the source is other corals within the reef, then we may expect to observe depletions of ^{234}U and ^{230}Th in some corals. The sub-stage 5a and 5c corals analysed in this study include δ^{234}U values which are lower than present day, and these corals could be interpreted as the depleted source of these isotopes. One would expect this lowering of δ^{234}U to become more important with the age of the coral, but most last interglacial (and older) Barbados corals generally display higher than modern day δ^{234}U values, whereas MIS 3 corals consistently show a 10-15‰ depletion. Using Thompson's *et al.* (2002) estimates for the loss rate of ^{234}Th and ^{230}Th via α-recoil (approximately 2.5%), we would expect the minimum initial δ^{234}U of the source corals to decrease by ~25‰ (to ~125‰) by 200 ka BP, which is not observed. The limited number of corals displaying such depletions may be due to one of the following:

   (a) If ^{234}Th and ^{230}Th originates from the decay of dissolved uranium alone this would not influence the isotopic composition of the coral source.

   (b) The 'source' may not be other reef corals, but rather other carbonate material within the reef framework.

   (c) A sample bias may be introduced by sampling only the best corals from a largely altered reef. However, the low δ^{234}U samples in this study generally appear to be physically well preserved.

2. Thompson *et al.* (2002) point out that there are some unresolved problems with the uranium mass balance considerations in the model. If dissolved uranium is the source of the excess ^{234}Th and ^{230}Th then the concentration of uranium in the percolating water must be high (up to 5% of the corals' uranium concentration). This requires either a substantial volume of carbonate to be dissolved in order to maintain this uranium concentration (based on the estimated groundwater flow rates), or that the repeated dissolution and reprecipitation of mobilised uranium slows its transport through the reef and allows more time for the adsorption of decay products ^{234}Th and ^{230}Th onto the coral 'sink'. In contrast, studies of Barbados groundwater suggest that the uranium concentration is only on the order of 0.03% of that found in corals (Banner *et al.*, 1993).

3. There is no clear explanation for why the adsorbed ^{234}Th is not remobilised upon its decay to ^{234}U. Thompson *et al.* suggest that the adsorbed ^{234}Th does not remain

on the surfaces of the coral but rather migrates along crystal boundaries where it is more difficult to mobilise. In a discussion of a similar model, Fruijtier *et al.* (2002) suggested that the ^{234}U produced by the decay of ^{234}Th is in a reduced form and would, therefore, be more difficult to mobilise.

Assuming these uncertainties can be resolved, Thompson *et al.*'s model appears to provide a mechanism to describe the general trends observed in U-Th analyses of corals. However, the trend of $^{230}Th/^{238}U$ and $\delta^{234}U_m$ which is defined by the sub-samples of U6-11 is much less steep than that predicted by Thompson *et al.*'s model indicating that a process of addition of ^{234}Th and ^{230}Th is not the only one acting on these corals. A combination of Thompson *et al.*'s ^{234}Th and ^{230}Th addition model, together with a net loss of uranium for the more altered sub-samples would shift their isotope ratios in the observed direction.[11] Thompson *et al.* (2002) use their numerical open system model to correct apparent ages to find a 'true' age. This implicitly assumes that the mechanism they propose is the only one responsible for the mobilisation of U and Th isotopes. I suggest that although the addition of ^{234}Th and ^{230}Th may be a plausible mechanism to describe these trends, correcting ages based on this open system model should be avoided because it does not take into account other mobilisation processes that may be occurring, such as uranium loss.

Removal of uranium

In a study of last interglacial corals from the Bahamas, Bar Matthews *et al.* (1993) examined the relationship between U and Th isotopic composition and petrographic textures and chemical composition. The U-Th dating of those samples was discussed by Chen *et al.* (1991). Even though some samples displayed physical evidence of alteration, Bar-Matthews *et al.* (1993) concluded that "the textural criteria ...do not appear as a quantitative, even semi-quantitative, predictor of the trace element chemistry or of shifts in δ^{234}U". Bar-Matthews (1993) did identify an inverse relationship between δ^{234}U and changes in Na and SO_3 (and Mg to a lesser extent), although no clear relationship was identified between δ^{234}U and U concentration. Bar-Matthews *et al.* (1993) suggest that leaching of uranium would occur in preference to thorium, because the latter isotope is more difficult to mobilise. This mechanism may be consistent with the observed depletions of Na, S and Mg.

[11] An independent process of net uranium removal from the coral leads to an increase in $^{230}Th/^{238}U$ without changing the δ^{234}U.

A net removal of uranium can explain increases in the apparent age of the samples (by increasing $^{230}Th/^{238}U$) but cannot account for the magnitude of the observed increases in $\delta^{234}U$. To reproduce the observed elevated $\delta^{234}U$ values by invoking a process of uranium removal, there must be a fractionation of uranium isotopes during that removal, in which ^{238}U is removed in preference to ^{234}U. Fruijtier *et al.* (2000) speculated that the ^{234}U produced by the *in-situ* decay of ^{238}U may be in a reduced (+IV) state and therefore more difficult to mobilise than the primary ^{234}U that was incorporated into the coral skeleton during its formation (in +VI state). However, it is not clear why the decay process of ^{238}U to ^{234}U would trigger a change in oxidation state (discussed later).

Below, I present a numerical model that describes the open system behaviour of U-Th in a coral during the preferential leaching of uranium. This model allows for the arbitrary, time dependent addition or removal of U or Th isotopes (similar to the numerical model of Hamelin *et al.*, 1993). This formulation treats the ^{234}U that was originally incorporated into the coral ($^{234}U_{primary}$) independently to that formed by the decay of ^{238}U ($^{234}U_{secondary}$). Below are the differential equations that describe the rates of decay of each isotope (N_X) as a function of radioactive decay and time-dependent rate of removal or addition (R_X):

$$\begin{aligned}
\frac{dN_{238}}{dt} &= -\lambda_{238}N_{238} + R_{238}(t) \qquad (3.1)\\
\frac{dN^p_{234}}{dt} &= -\lambda_{234}N^p_{234} + R^p_{234}(t)\\
\frac{dN^s_{234}}{dt} &= \lambda_{238}N_{238} - \lambda_{234}N^s_{234} + R^s_{234}(t)\\
\frac{dN_{230}}{dt} &= \lambda_{234}N_{234} - \lambda_{230}N_{230} + R_{230}(t)
\end{aligned}$$

In this scenario discussed below, the value of R_{238} is an arbitrary function of time. The primary ^{234}U is not fractionated during leaching because it should be in the same oxidation state as the ^{238}U:

$$R^p_{234} = \frac{N^p_{234}}{N_{238}}R_{238} \qquad (3.2)$$

The ^{230}Th and secondary ^{234}U can be arbitrarily fractionated during removal, defined by the factors k^s_{234} and k_{230}:

$$\begin{aligned}
R^s_{234} &= k^s_{234}\frac{N^s_{234}}{N_{238}}R_{238}\\
R_{230} &= k_{230}\frac{N_{230}}{N_{238}}R_{238}
\end{aligned}$$

The set of linear, 1st order differential equations (3.1) are solved using a 5th order Runge-Kutta method.

First, an idealised situation is considered, where only ^{238}U and 'primary' ^{234}U are removed during leaching. In this case, k^s_{234} and k_{230} equal zero. A scenario with the *continuous* removal of ^{238}U and primary ^{234}U produces the trends shown in the dashed lines of figure 3.19. This model predicts a trend which agrees well with those defined by the 5a and 5c corals. It does not match the observed trend defined by the sub-samples of U6-11 (this study). The predicted trend becomes less steep when removal of the 'secondary' ^{234}U is introduced (the dotted line in figure 3.19) and may explain the observed trend for the U6 samples.

There are some significant problems with this model:

1. There is no consistent relationship between δ^{234}U and uranium concentration in the corals analysed in this study (with the exception of the stage 6 corals, discussed later), as might be expected if the preferential leaching of uranium were the cause of the observed trends. However, if the carbonate matrix is also dissolved and removed during this process then we may not expect a systematic lowering of uranium concentration.

2. The results shown in figure 3.19 are for a scenario with the continuous leaching of the coral since its deposition. However, to elevate the $\delta^{234}U_i$ values to the most extreme values observed for the sub-stage 5a corals (~180‰) would require a ~30% loss of the total uranium content. If the leaching occurred at a later time, ie during the last 20 ka, the same trend is predicted but the effect on the uranium concentration is smaller (10% for the extreme values). In general, low δ^{234}U corals appear to be better preserved (less extensive dissolution textures) than those with very high δ^{234}U values although this relationship is difficult to quantify. In the samples with the most extensive dissolution textures, the extent of this alteration is consistent with 10% dissolution (see discussion in section 3.3.3)

The slope in ^{230}Th/^{238}U vs $\delta^{234}U_m$ for the MIS 6 deposits at sites U15 and U6 (including four sub-samples of U6-11) is less than that for other features. For this group of samples, there is also a well-defined relationship between the δ^{234}U and uranium concentration in which the sub-samples with the highest δ^{234}U values have around 15% lower uranium concentration (see figure 3.20). This may indicate, in some cases, that uranium loss is a significant part of the alteration process. A distinct trend in other sample groups may be hidden by the natural range of uranium concentrations that exists in corals.

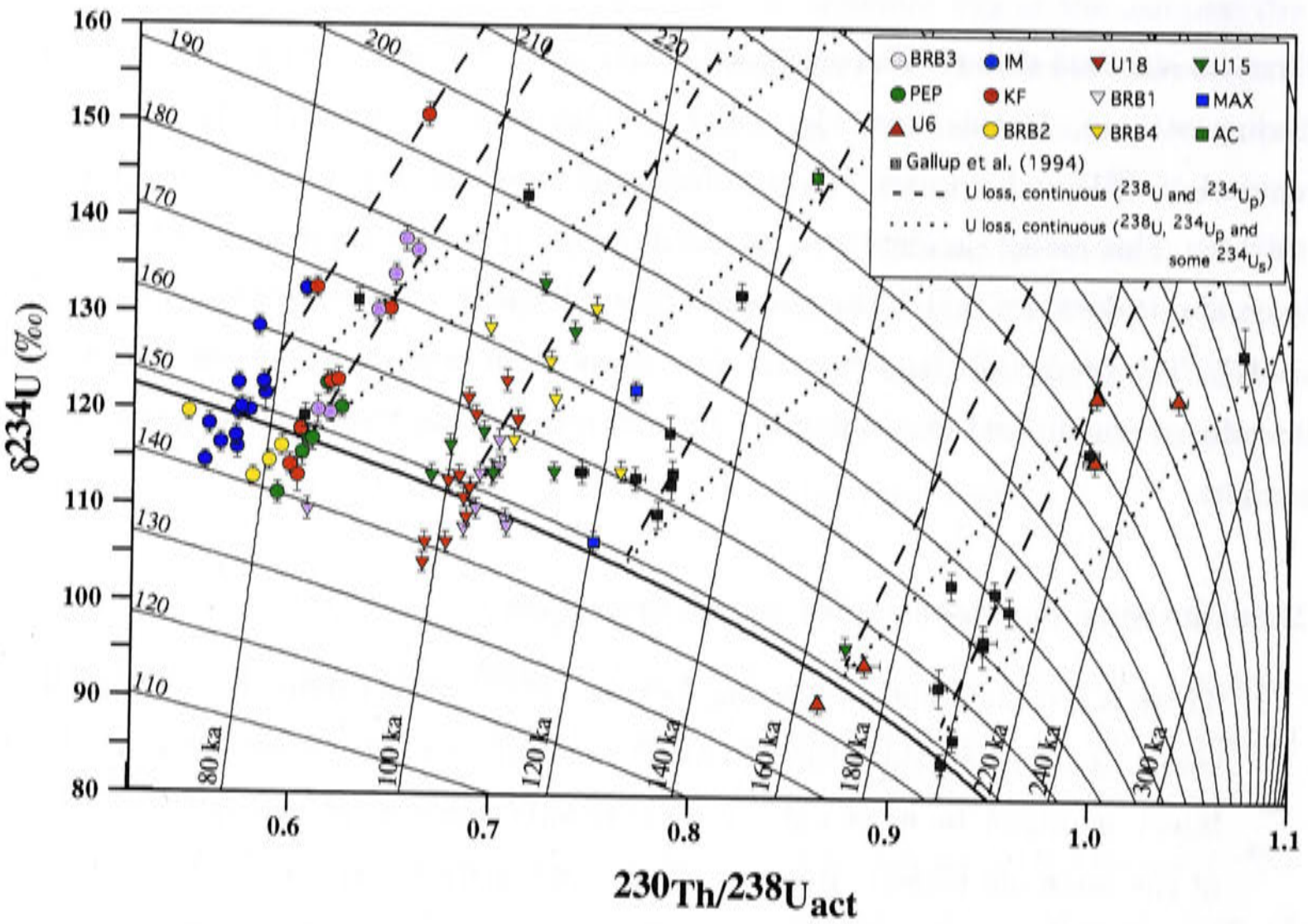

Figure 3.19: The trend of $^{230}Th/^{238}U$ vs $\delta^{234}U_m$ predicted by the continuous removal of ^{238}U and primary ^{234}U in preference to both ^{230}Th and secondary ^{234}U (dashed). The slopes predicted by this model for $^{230}Th/^{238}U$ vs $\delta^{234}U_m$ reproduce those observed for sub-stage 5a, 5c, 5e and MIS 7 corals from this study and Gallup *et al.* (1994). The shallower slope observed for MIS 6 is not reproduced by this model (see text for discussion). If 50% of secondary ^{234}U is also removed, the slope becomes less steep (dotted).

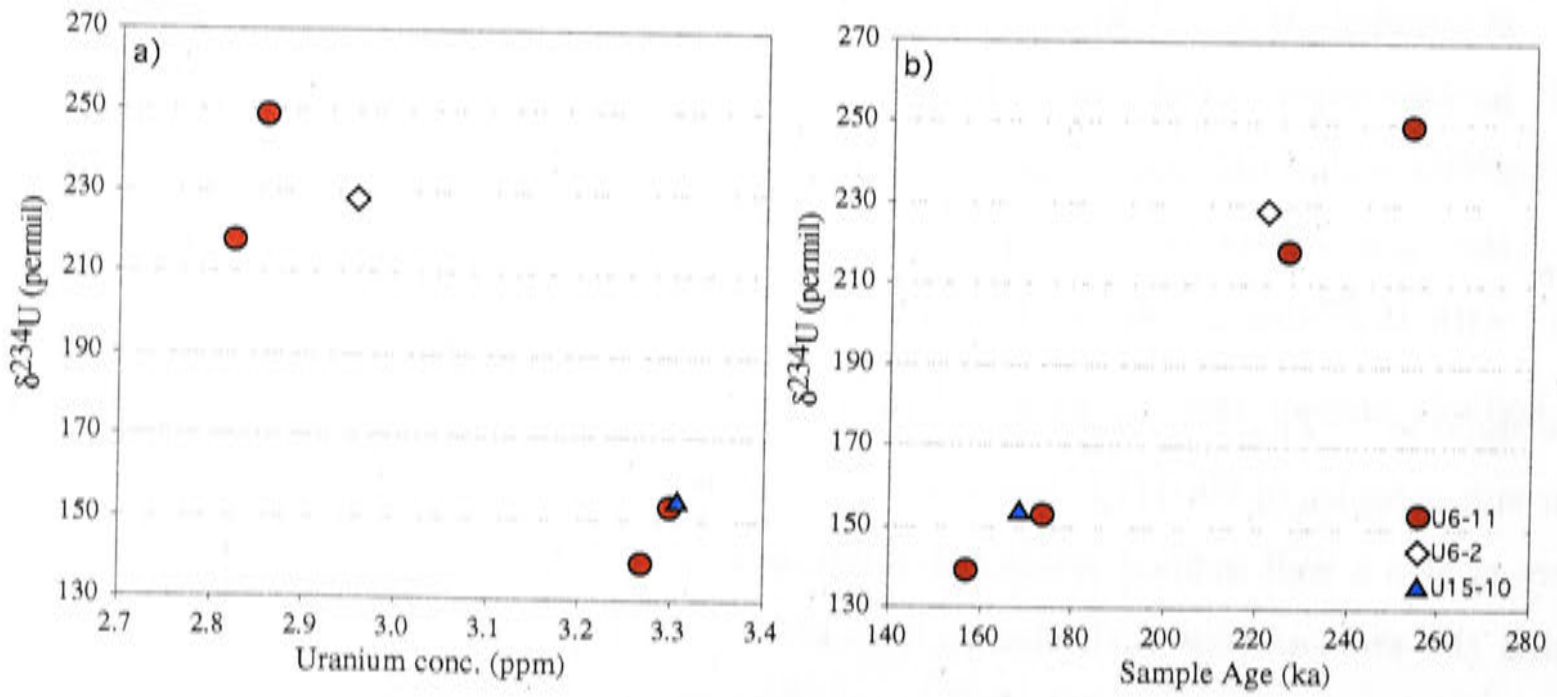

Figure 3.20: Correlation between apparent age, initial $\delta^{234}U$ and uranium concentration for the MIS 6 samples analysed in this study, including 4 subsamples from a single *Acropora palmata* trunk (U6-11). a) Uranium concentration *vs* $\delta^{234}U_i$ b) Apparent age *vs* $\delta^{234}U_i$

The uranium incorporated into corals from ocean water is in an oxidised, +VI state. The mechanism discussed in this section invokes the reduction of uranium to a more insoluble +IV state after the decay of ^{238}U to ^{234}U (postulated by Fruijtier *et al.*, 2000). A mechanism of this type is in direct contrast to the process leading to the preferential leaching of ^{234}U during continental weathering, which is responsible for the ^{234}U excess in the ocean. This mechanism is therefore speculative and further study of the isotopic composition of uranium in different oxidation states is required to establish the likelihood of these processes.[12]

Diagenetic alteration conclusions

A correlation between apparent age and $\delta^{234}U_i$ (or measured $^{230}Th/^{238}U$ and $\delta^{234}U$) is observed in the studies of corals from around the world. This trend is particularly well defined in the sub-stage 5a and 5c deposits in the present study 3.15. In this section, I have presented a number of alternative mechanisms that have been proposed to explain this trend. These include:

1. continuous addition of ^{234}U and ^{230}Th in a fixed ratio (Gallup *et al.*, 1994).

2. addition of ^{234}Th and ^{230}Th from a source via α-recoil and the decay of dissolved uranium (Thompson *et al.*, 2002; Fruijtier *et al.*, 2000).

3. net removal of uranium with a preference for ^{238}U and $^{234}U_p$ relative to $^{234}U_s$ due to secondary ^{234}U converting to a less mobile +IV state (Fruijtier,*et al.*, 2000).

Although each of these different models can explain the observed covariance of ^{230}Th and ^{234}U each is problematic and no single model can satisfactorily explain all of the observations. Possibly a combination of these processes is responsible for the correlation of $^{230}Th/^{238}U$ and measured $\delta^{234}U$. None of these diagenetic models has provided a satisfactory explanation for the lower than present day $\delta^{234}U$ values observed in the sub-stage 5a and 5c corals in this study and the MIS 3 corals from previous studies (see figure 3.16). I suggest that changing $\delta^{234}U$ of ocean water may be responsible for the lower than modern $\delta^{234}U$ values (as discussed in section 3.4.1) and that diagenetic processes (yet to be established) are responsible for the trend of increasing age and $\delta^{234}U$ from those minimum values.

The focus of this work has not been a comprehensive investigation of diagenetic processes leading to the observed elevations of measured age and $\delta^{234}U$. However, the sets of

[12]Separation of uranium of different oxidation states has been achieved in marine phosphates by cupferron precipitation (Kolodny and Kaplan, 1970; O'Brien *et al.*, 1987).

samples analysed in this study provide the opportunity for a future comprehensive study of physical, chemical and isotopic properties of these corals to investigate the effects of diagenesis on the corals U-Th system as well as the possibility of variable $\delta^{234}U$ in the ocean.

3.5 Interpretation of U-Th ages

The reliability of a coral sample's measured U-Th age is generally based on a comparison of its initial $\delta^{234}U$ value with that of modern corals. If the $\delta^{234}U$ is significantly different from this modern value (148.5‰, see section 2.3.3), the measured age is considered unreliable. However, the issues of variable ocean water $\delta^{234}U$ and the effects of diagenetic alteration complicates the interpretation of U-Th ages. In this section, I present the interpretation of U-Th ages for each deposit identified in this study, and give age estimates and uncertainties for use in the calculation of sea level in the next chapter.

If the $\delta^{234}U$ of the ocean at the time of deposition of these corals was equal to the present day, then the samples with $\delta^{234}U$ values within error of the modern value have reliable ages. However, if ocean water $\delta^{234}U$ was lower than the modern value at the time of these sub-stage 5a and 5c events (say, 140‰), the estimated ages of the deposits would be lower by more than 2 ka because of the distinct trend defined by each group of samples. It is not clear at this stage whether the lower $\delta^{234}U$ values observed in the 5a and 5c data sets (this study) are the result of diagenetic mobilisation of U and Th isotopes or changing ocean water $\delta^{234}U$, so both alternatives must be taken into account in assigning an age and uncertainty to each of the features.

The U-Th results for the sub-stage 5a and 5c features analysed in this study are shown in figure 3.21. Only samples that are regarded as *in situ* are included in the calculation of the mean age of the deposits. If we assume that the general trends are the result of diagenetic alteration, the scatter around the trendline may represent either noise (introduced by multiple diagenetic processes) and/or a true range of ages. There is very little scatter of data around the trendline for the feature 5a-2 compared to that of the 5c deposits. This may indicate either that the 5c deposits have been more extensively affected by a number of alteration processes or that a prolonged period of coral growth has been sampled for that event.

For the purpose of calculating sea level, I consider estimates of the 'mean age' of each deposit, rather than speculating about a true period of reef growth, with uncertainties

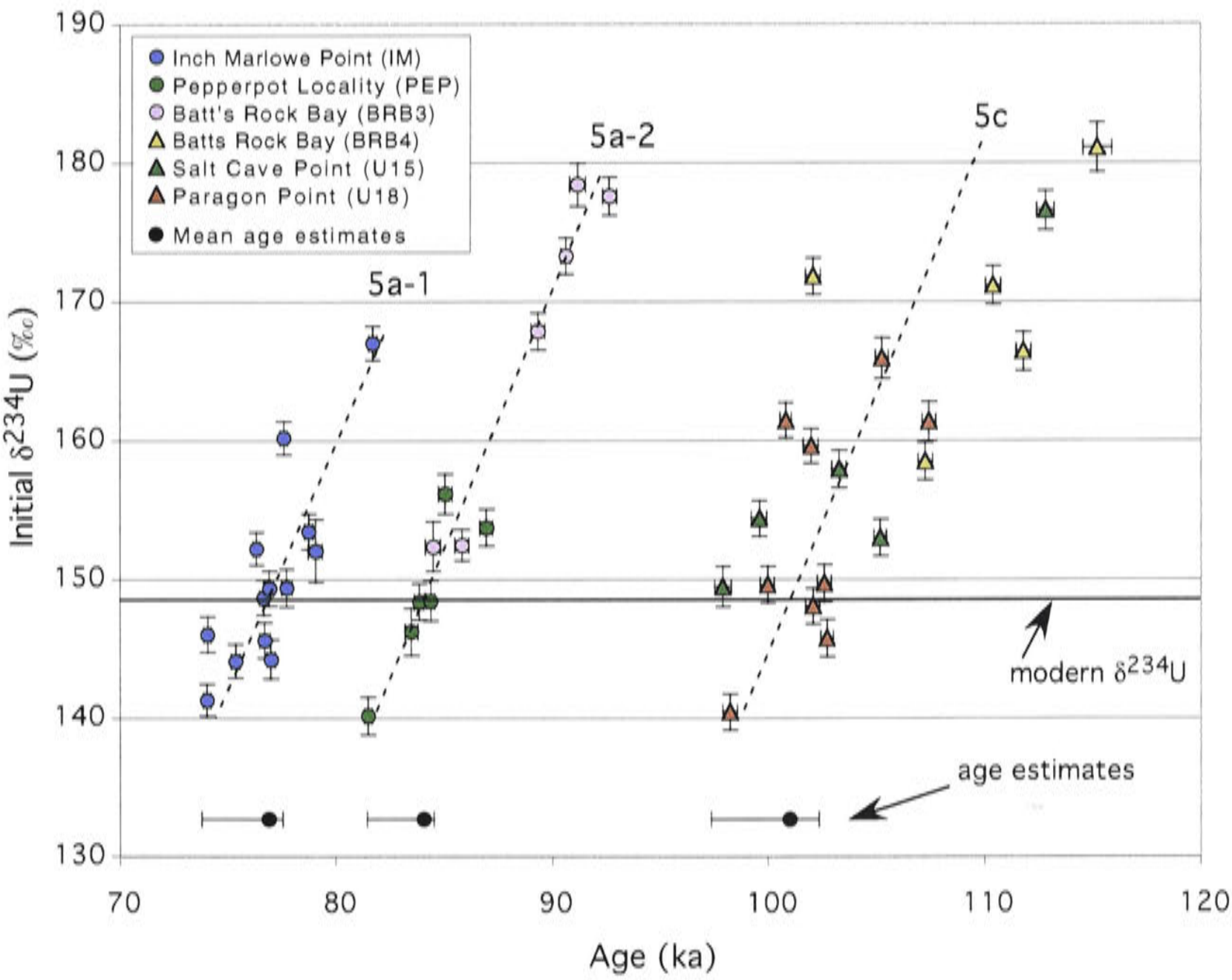

Figure 3.21: Summary of U-Th data for sub-stage 5a and 5c *in situ* corals analysed in the present study. The modern δ^{234}U value of 148.5‰ is marked. The trendline associated with each group of data is marked with a dashed line. More samples with δ^{234}U below the modern value were included in the original data set (compare with figure 3.15b), but these were from non-*in situ* deposits and were removed for the purposed of age calculation. Site BRB1, although being considered *in situ*, is not included in this plot because it represents deeper water growth during sub-stage 5c and is not included in the peak sub-stage 5c age calculation.

Feature	Age (ka) δ^{234}U=148‰	Age (ka) δ^{234}U=140‰	Age (ka)
5a-1	76.8±0.7	74.4±0.7	$76.8\pm^{0.7}_{3.1}$
5a-2	84.0±0.5	81.7±0.5	$84.0\pm^{0.4}_{2.7}$
5c	101.0 ±1.4	98.7±1.4	$101.0\pm^{1.4}_{3.7}$
6	168.3±3.7	166.0±3.7	$168.3\pm^{3.7}_{6.1}$

Table 3.13: Mean ages and uncertainties for each of the distinct periods of reef growth identified in the lower Barbados terraces. The final age estimate is based on the modern δ^{234}U criterion (148‰) but its quoted uncertainty range includes the ages defined by the lower δ^{234}U alternative (140‰) and is therefore asymmetric. Nomenclature of the sea-level features was defined by Schellmann and Radtke (2001). Separate ages are quoted assuming δ^{234}U at the time of growth was equal to the modern value of ~148.5‰ and equal to ~140‰. The uncertainties assigned to the ages of each of these events are much larger than the analytical precision of individual age determinations, even allowing for uncertainties in the decay constant (see sections 2.2 and 2.6 in chapter 2). For this reason, when comparing these ages with independent time-scales in the following chapter, the decay constant uncertainties are not considered further.

that allow for either of the above possibilities. The quoted mean age is defined by where the trend of the data passes through the modern δ^{234}U values (148.5‰). An alternative age is given for an assumed initial δ^{234}U of 140‰. Both of these alternatives are listed in table 3.13. The uncertainty assigned to each of these mean-age alternatives is based on the scatter of data around the trendline.[13] Because the true initial δ^{234}U of these deposits has not yet been established, the age used in the calculation of sea level for these deposits (quoted in the final column of table 3.13) is based on the standard modern day δ^{234}U criterion (148.5‰) but the uncertainty range is asymmetric because it is extended to include the ages associated with the lower δ^{234}U value of 140‰.

Deposits for which the data coincide, such as PEP and BRB3, are assumed to represent the same period of reef growth and the U-Th data is combined for the purpose of calculating a mean age and uncertainty estimate. If samples have been noted as non-*in situ* (section 3.3) they are not used in the calculation of age for that deposit. A more detailed discussion of the age interpretations for each of the features identified in this study follows:

[13] Each data point is projected onto the assumed initial δ^{234}U value along the slope defined by the trendline of that data set. The standard error of the mean of these 'projected ages' is used as the uncertainty of the age assigned to that feature for that δ^{234}U value. For the calculation of this scatter around the regression line, only samples with apparent initial δ^{234}U values less than 156‰ are used. This is an arbitrary value chosen to ensure the increased scatter at very high δ^{234}U values (particularly for the sub-stage 5c deposits) does not create an artificially large uncertainty estimate.

Sub-stage 5a-1

Site IM represents the youngest period of reef growth identified in this study. The age assigned to this deposit, for the purposes of calculating sea level, is $76.8\pm^{0.7}_{3.1}$ ka. This is the first time a distinct period of reef growth of this age has been precisely constrained.

Sub-stage 5a-2

The U-Th data from sites PEP, BRB3 and KF tightly coincide and therefore are assumed to represent the same period of reef growth. Only PEP and BRB3 samples were used in the calculation of the mean age of these deposits because the KF site has been identified as not *in situ*. The mean age assigned to these deposits is $84.0\pm^{0.4}_{2.7}$ ka. The uncertainty assigned to this age is less than that of the younger sub-stage 5a deposit because there is less scatter around the trendline. These deposits correspond to the 'classic' sub-stage 5a event identified in early studies (section 3.2).

Sub-stage 5c

The U-Th data of the sub-stage 5c sites (U15, U18 and BRB4) are more scattered than for the younger deposits. The broad scatter is maintained even if the data from each deposit is considered individually. The distribution of ages at high δ^{234}U values appears to be skewed to even higher apparent ages, which is either due to (i) an extended period of reef growth; (ii) the effects of multiple alteration processes; or (iii) a artefact of sampling. Because of this high scatter, I assume that the slope determined for the younger (sub-stage 5a deposits) can also be applied to this feature. Most proposed mechanisms of alteration predict small changes in the slope defined by the data as a function of the true age, however, this change is expected to be small between ~80 ka and ~100 ka relative to the scatter observed for the sub-stage 5c deposits.

These deposits have been assigned an age of $\sim 101\pm^{1.4}_{3.7}$ ka. The uncertainty is larger than that of the sub-stage 5a deposits because of the increased scatter of the data. At these sites, samples were taken from a range of heights within the reef exposures and so the scatter may represent a true prolonged period of reef growth, although there is no clear age-height stratigraphic relationship of the samples at these sites. If the scatter represents a true period of reef growth from 104 ka BP to 98 ka BP (based on the modern δ^{234}U), then the duration of this event was at least 6 ka, which is comparable to the duration of the last interglacial reef growth at Western Australia (Stirling *et al.*, 1998). This event corresponds to the 'classic' sub-stage 5c event identified in earlier studies.

The age of the corals of site BRB1 (not shown in figure 3.21) are grouped at a slightly older age than the other sub-stage 5c deposits. The large head corals of this deposit clearly represent deep-water facies (>15 m water depth). The U-Th data for this site do scatter around the modern δ^{234}U value. I do not combine the data from this site into a single age. Instead, I use the oldest age of ~108 ka to place a constraint on the sea level at that time (in the following chapter). It appears that this deposit formed early during sub-stage 5c, perhaps during the rise in sea level leading up to the peak of 5c defined by the other deposits (U15, U18 and BRB4).

Stage 6

Two deposits have been identified on the south coast that represent reef growth during MIS 6 (not shown in figure 3.21). The age assigned to these deposits is $168.3\pm^{3.7}_{6.1}$ ka. Further dating of these deposits is desirable to support this age determination.

Summary of age interpretations

The U-Th analysis of this study has identified a least 4 distinct periods of reef growth in the lower reef terrace at Barbados. These occur at $76.8\pm^{0.7}_{3.1}$ ka and $84.0\pm^{0.4}_{2.7}$ ka (sub-stage 5a), $\sim 101\pm^{1.4}_{3.7}$ ka (sub-stage 5c) and $168.3\pm^{3.7}_{6.1}$ ka (stage 6). This is the first time that a distinct period of reef growth at ~77 ka (in addition to the 'classic' feature at 84 ka) during sub-stage 5a has been clearly constrained. The sea level associated with each of these features, and a discussion of the Barbados sea-level record in the context of other sea level and proxy climate records is discussed in the next chapter.

Chapter 4

Relative Sea-Level Change during Marine Isotope Sub-stages 5a and 5c

4.1 Introduction

Evidence of paleo-shorelines associated with last glacial cycle sea-level transgressions is preserved at many localities around the world. At tectonically uplifting sites such as Barbados and Huon Peninsula, PNG, the emergence allows access to deposits that would otherwise be submerged or destroyed by subsequent sea-level oscillations. The relative sea level associated with those deposits can be calculated using the measured age and an estimate of the uplift experienced by that site. Sea-level estimates can then be compared to other proxy records to establish a coherent picture of global ice volumes and hence of climate.

In the study of the uplifted coral terraces at Barbados discussed in chapter 3, U-Th dating was used to establish the timing of the deposition of a number of reef terraces formed during marine isotope stages (MIS) 5 and 6. Deposits associated with the 'classic' sub-stage 5a and 5c sea-level high-stands were found to have mean ages of $84.0\pm^{0.4}_{2.7}$ ka and $101.0\pm^{1.4}_{3.7}$ ka respectively. A morphologically distinct reef was found to have a mean age of $76.8\pm^{0.7}_{3.1}$ ka and can be interpreted to represent a sea-level high-stand following the main sub-stage 5a peak. A $168.3\pm^{3.7}_{6.1}$ ka deposit is interpreted to represent a sea-level high-stand during MIS 6.

The first part of this chapter (section 4.2) presents the results of relative sea-level calculations at Barbados for each of the features identified in this study. In section 4.3, I summarise the survey results of a recent field expedition to the tectonically uplifted terraces of Huon Peninsula, PNG, discuss existing age measurements for those deposits and

present a preliminary sea-level curve for that location. Later in this chapter (section 4.4), the combined Barbados and Huon Peninsula MIS 5 sea-level records are interpreted in the context of climate change during that period. In section 4.5, I compare the sub-stage 5a and 5c Barbados relative sea-level estimates from this study with those from other locations throughout the Caribbean and surrounding region.

4.2 Sub-stage 5a, 5c and MIS 6 Barbados sea-level record

4.2.1 Sea-level calculations at Barbados.

The calculation of relative sea level (h_{sl}) associated with an uplifted coral terrace is based on the age of the reef (t), its present elevation (H), the growth depth of the samples or reef crest (h_{gd})[1], and the estimated rate of uplift (U) (assumed to be uniform) for that site:

$$h_{sl} = H + h_{gd} - Ut \tag{4.1}$$

The uplift rate (U) can be calculated from the present elevation of the last interglacial reef/shoreline (H_{LIG}), the assumed paleo-sea level of that high-stand (h_{LIG}), the age of the reef (t_{LIG}) and the growth depth of the reef crest (h_{gd}):

$$U = \frac{(H_{LIG} - h_{LIG} + h_{gd})}{t} \tag{4.2}$$

As a first order approximation, the uplift rate for each standard transect is assumed to have been uniform through time, at least since the last interglacial period (Bender *et al.*, 1979; Matthews, 1973). This assumption can be tested by the comparison of relative sea-level calculations for corresponding features at different transects with different uplift rates. This assumption will be discussed in more detail later.

Barbados has experienced spatially variable uplift along its coast (see overview in section 3.3 of chapter 3). The highest rate is evident at the 'Clermont's Nose' transect in the southwest of the island (Mesolella *et al.*, 1969; Bender *et al.*, 1979). At this location, the last interglacial reef reaches an elevation of ~61 m (Schellmann and Radtke, 2001). The rate of uplift decreases northward and eastward. Along the south coast, east of the classic 'Christ Church' transect (defined by Bender *et al.*, 1979), is a region that does not appear to have experienced any warping of the reef terraces (south coast transect in

[1]The inclusion of a possible growth depth of the reef crest allows for the possibility of erosion of the apparent crest of the deposit. If a dated coral reef deposit can be directly associated with another sea level marker, such as a notch, then this elevation should be used for the calculation of sea level and the growth depth estimate is not required.

Authors	Age range (ka)
Bard *et al.*, 1990	~125 ka
Blanchon and Eisenhauer, 2001	123-129 ka
Broecker *et al.*, 1968	120-128 ka
Edwards *et al.*, 1987b	122-129 ka
Edwards *et al.*, 1997	124-127 ka
Gallup *et al.*, 1994	117-130 ka
Ku *et al.*, 1990	118-123 ka

Table 4.1: Summary of previous age measurements for the last interglacial terraces at Barbados (both alpha spectrometry and TIMS analyses). Those samples considered unreliable because of very high δ^{234}U are excluded from this summary.

figure 3.3, Schellmann and Radtke, 2001). In this region, there are two distinct terraces of last interglacial age at elevations of 36 and 40 m (Schellmann and Radtke, 2001). Based on the results of the ESR dating, it is not clear which of these terraces represents the 'classic' last interglacial deposit that corresponds to the 61 m terrace on the west coast. I adopt a mean elevation of 38±3 m for the last interglacial terrace on the south coast transect to calculate uplift.

It is apparent that sea level during the last interglacial high-stand did not simply plateau, but may have undergone oscillations during the time period between 135 and 117 ka (Esat *et al.*, 1999; Gallup *et al.*, 2002; Blanchon and Eisenhauer, 2001; Chen *et al.*, 1991). The appropriate age to assign to the last interglacial reef crest at Barbados is therefore uncertain. Based on the range of age measurements from other studies (table 4.1), I adopt an age of 125±5 ka for the last interglacial reef crest. The paleo-sea level of the last interglacial high-stand at both far-field (Stirling *et al.*, 1998) and intermediate-field (Chen *et al.*, 1991) tectonically stable localities was ~ +4±2 m. The growth depth of the exposed reef crest is uncertain and approximated to be 1±1 m to allow for the possibility of erosion since the time of deposition.

Estimates of uplift rates for the Clermont's Nose and the Christ Church sections are shown in table 4.2.

4.2.2 Overview of previous Barbados sea-level estimates

Earlier studies of coral deposits at Barbados suggested that there were two main periods of reef growth corresponding to sub-stages 5a and 5c (see overview in section 3.2 of chapter

Transect	H_{LIG} (m)	Uplift rate (m/ka)
Clermont's Nose	61±2	0.46±0.03
Christ Church	38±3	0.28±0.03

Table 4.2: Last interglacial reef elevations above present sea level (Schellmann *et al.*, 2002) and uplift rates calculated for the west and south coast transects investigated in the present study (see equation 4.2). The assumed paleo-sea level of the last interglacial high-stand is 4±2 m above present sea level. A growth depth of 1±1 m is assigned to the reef crest. Uplift rates used in previous studies vary and are sometimes different from those calculated here, but are generally within the quoted uncertainty.

MIS	Present elevation (m)	Platform	ESR Age (ka)	Sea level (m)
5a-1	2	T-1a_1	72±6	-18
5a-2	3	T-1a_2	85±8	-20
5c-1	4	T-1b	99±11	-23
5c-2	9	T-2	104±11	-19
5c-3	16	T-3	102±8	-12

Table 4.3: ESR ages and approximate sea-level estimates from Schellmann and Radtke (2001). Sea-level estimates in this table are the average of the values quoted by Schellmann and Radtke (2001) for three uplift rates based on a last interglacial paleo-sea levels of 0 m, +2 m and +6 m. The effect of diagenetic alteration tends to decrease apparent ESR ages. Part of the aim of this study is to confirm the conclusions of Schellmann and Radtke (2001) by using higher precision dating techniques.

3) and that the timing of these correlate with periods of insolation maxima.[2] Sea-level estimates for these sub-stage 5a and 5c events range between −13 to −20 m and −12 to −17 m respectively (Broecker *et al.*, 1968; Bard *et al.*, 1990; Gallup *et al.*, 1994). Based on revised, comprehensive mapping of the morphostratigraphy and ESR dating of the southern Barbados terraces, Schellmann and Radtke (2001) infer a significantly more complex reef deposition history during MIS 5. The sea levels calculated by Schellmann and Radtke (2001) for each of the morphologically distinct features are displayed in table 4.3.

Bard *et al.* (1990) calculated a sea level of ∼70 m below present for a sample with an apparent age of 79 ka retrieved from a drill core at a depth of 46 m below present sea level. However, the age of this sample can be considered unreliable because it has a very high $\delta^{234}U$ (∼190‰). This sea level constraint is therefore disregarded.

Gallup *et al.* (2002) report a U-Th age of 168±1.3 ka for a deposit on the rapidly uplifting west coast of Barbados (Clermont's Nose traverse). Using an uplift rate of 0.44 m/ka the relative sea level associated with this deposit is calculated to be ∼38 m below present.

[2]Sub-stage 5a and 5c insolation maxima (July, 65°N) occur at approximately 82 and 103 ka respectively.

Using the higher uplift of 0.46 m/ka for that transect (calculated in the present study, table 4.2), this sea-level estimate is lowered to ~42 m below present. Deposition of this feature occurred in the middle of the glacial period MIS 6 and corresponds to event 6.5 in the Imbrie *et al.* (1984) stacked $\delta^{18}O$ record.

4.2.3 New sea-level estimates at Barbados

The paleo-sea levels calculated for the sub-stage 5a and 5c and MIS 6 deposits that were dated in this study (chapter 3) are presented here.

Sub-stage 5a

Two distinct periods of reef growth that occurred during sub-stage 5a have been constrained in this study. The reef crest deposits that correspond to the 'classic' sub-stage 5a peak are PEP, at a present elevation of 3 m above present sea level on the south coast, and BRB3, at a present elevation of 19 m on the west coast. The PEP deposit corresponds to the event 5a-2 (platform T-1a_2, figure 3.3), identified on the south coast by Schellmann and Radtke (2001). By assigning a mean age of 84.0 ka to both of these deposits, sea level associated with this event was calculated to be approximately -19±4 m (on both the south and west coasts, see table 4.4 and figure 4.1). The close agreement of the calculated sea level of these two deposits lend support to the assumed uniform uplift model.

A distinct period of reef growth at ~77 ka was identified in a morphologically distinct terrace, deposit IM, at a present elevation of 2 m above present sea level on the south coast (platform T-1a_1, figure 3.3). This deposit corresponds to the event 5a-1 discussed by Schellmann and Radtke (2001). The sea level associated with that reef crest deposit is calculated to be -19±4 m (see table 4.4).

The limited facies exposure of the Inch Marlowe Point (IM) deposit gives no indication of the magnitude of the sea level rise leading up to the ~77 ka feature. Therefore, the magnitude of global ice build-up between the ~84 ka and ~77 ka deposits is uncertain. It is possible that these two deposits both grew during a prolonged period of high sea level and only appear to be distinct morphological features because of a discrete uplift event between the two. However, because the deposits are morphologically distinct, and the scatter of U-Th data for each deposit is small compared to the separation of the ages (~7 ka) these features probably represent two distinct oscillations in sea level. This is the first time that two distinct sea level features during sub-stage 5a have been identified and precisely constrained. Ku *et al.* (1990) measured two ages which appear to correspond to this

MIS	Site	Platform	H (m)	Age (ka BP)	Sea Level (m) Site	Mean
5a-1	IM^s	T-1a	2^s	$76.8\pm^{0.7}_{3.1}$	-19±4	-19±4
5a-2	PEP^s	T-1b	3^s	$84.0\pm^{0.4}_{2.7}$	-19±4	
	BRB3^w		19^w	$84.0\pm^{0.4}_{2.7}$	-19±4	-19±4
5c	U18^s, U15^s	T-3	15^s	$101.0\pm^{1.4}_{3.7}$	-12±4	
	BRB4^w		29^w	$101.0\pm^{1.4}_{3.7}$	-17±4.	-15±4
5c$_{deep}$	BRB1^w		1-10^w	~108	$-48\pm^{30}_{4}$	$-48\pm^{30}_{4}$
6	U6^s, U15^s		10^s	$168.3\pm^{3.7}_{6.1}$	$-35\pm^{10}_{6}$	$-35\pm^{10}_{6}$

Table 4.4: Summary of relative sea-level calculations for the features identified in this study. H is the present elevation above sea level. Two additional sub-stage 5c features identified by Schellmann and Radtke (2002) were not identified in this study (figure 3.3). Sites on the south and west coasts are identified with a superscript (s) and (w) respectively. For the south coast sites, the platforms labelled by Schellmann and Radtke (2002) are also given. The representative age used for each sea-level feature is individual age measurements from each site as discussed at the end of chapter 3. The uncertainties in sea level (σ_h) are calculated from: $\sigma_h = \sqrt{\sigma_H^2 + \sigma_{gd}^2 + U^2\sigma_t^2 + t^2\sigma_U^2}$. A growth depth of 1±1 m is assigned in calculating these sea levels. The quoted uncertainty in sea level is based on the larger of the two quoted age errors. Using the smaller age error does not decrease the sea level uncertainty by a significant amount because most of the uncertainty is due to the uplift rate component.

younger sub-stage 5a feature, but it was not recognised as belonging to a morphologically distinct terrace.

Sub-stage 5c

Four deposits of sub-stage 5c age were analysed in this study, U15, U18, BRB4 and BRB1. A mean age of ~101 ka was determined for the first three of these deposits. An age of 108 ka is adopted for the site BRB1 (discussed later). On the south coast the crests of the deposits U15 and U18 are at 11-12 m above present sea level. Schellmann and Radtke (2001) suggest that these deposits correspond to the platform T-3 (figure 3.3 in chapter 3) which reaches an elevation of 16 m in the south coast transect used by those authors for sea level calculations. G. Schellmann (pers. comm.) suggests that the back reef of the U18 and U15 deposits do reach an elevation of 12-15 m above present sea level at those sites. Therefore, a present elevation of 15 m is used to calculate sea level for these deposits. Site BRB4, located on the west coast, produced no reliable U-Th analyses but it is clear that this deposit is of sub-stage 5c age and has therefore been assigned the same age as the U15 and U18 deposits. The elevation of this deposit is 29 m asl. The sea levels calculated for the south and west coast sub-stage 5c deposits are -12±4 m and -17±4 m respectively. The mean of these is -15±4 m. There is relatively poor agreement (but still within uncertainty) of the sea levels calculated for this event at each transect. Possible

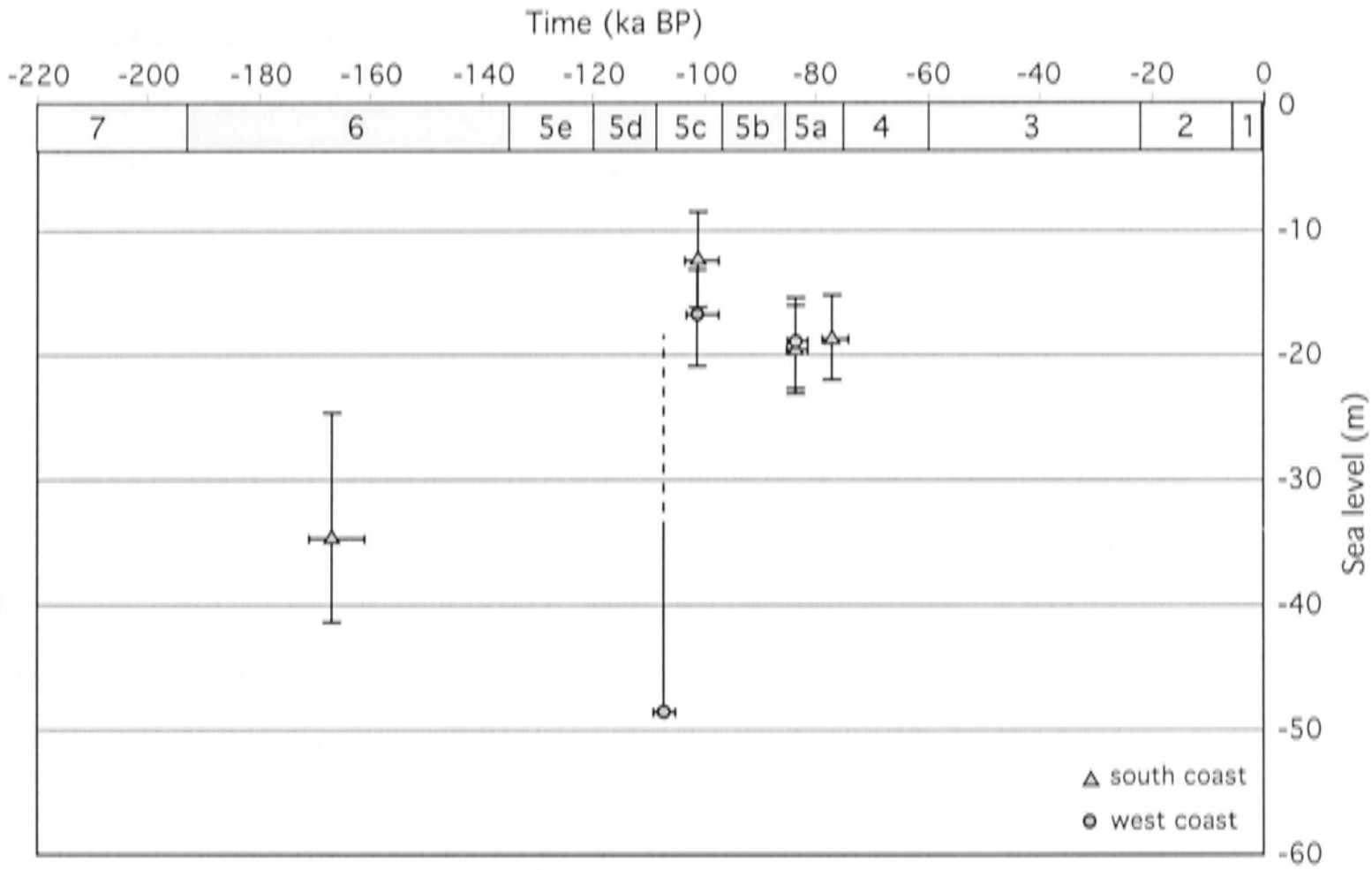

Figure 4.1: Barbados relative sea-level estimates from the west (circles) and south (triangles) coasts. The extended uncertainty range for the 108 ka feature is because this site contains deep water facies and could have been deposited in >15 m water depth.

reasons for this include (i) error in the age assigned to one or both deposits; (ii) error in the elevations assigned to one or both deposits (if the 10 m elevation of the U15 and U18 reef crests is used for the sea level calculation instead of the 15 m suggested by G. Schellmann, then the two sea level calculations would be in much better agreement); (iii) departure from uniform uplift at one or both transects. At this stage it is not possible to determine between these alternatives.

Measured ages of ~108-103 ka for the apparent deep water facies corals (growth depth of >15 m) at site BRB1 indicate that these corals grew at a time roughly corresponding to sub-stage 5c, but probably prior to the sub-stage 5c sea level maximum. The only constraint that can be placed on sea level based on this observation is that sea level was above -48 m by ~108 ka.

Sub-stage 6.5

Three samples from Foul Bay (U6) and Salt Cave Point (U15) have been analysed in this study and the mean age adopted for these deposits is ~168.3 ka. Further samples from these deposits should be dated to confirm this age. Based on the present day elevation of the upper-most sample U6-11 (at 10 m asl), and assuming the same uplift rate for this part of the south coast, the sea level associated with those deposits is calculated to be

~35 m below present.[3] This compares well with the estimate by Gallup *et al.* (1994) for the same event recorded on the west coast, at ~-37 m (or -42 m using a higher uplift rate). The deposits studied here are at a different location to that studied by Gallup *et al.* (1994) and therefore provide an independent confirmation of sea level for the MIS 6.5 event. The crest of the U6 deposit is ~10 m higher than the elevation of the sample that was analysed in this study (U6-11). Until further investigation of this deposit takes place, I assign an uncertainty of +10m to the calculated sea level (see table 4.4 and figure 4.1).

Summary

In this investigation, three distinct periods of reef growth represented by morphologically distinct reef deposits have been identified from dating the uplifted coral terraces at Barbados. The paleo-sea level of the two sub-stage 5a deposits is approximately the same, at ~19±4 m below present sea level, and the sub-stage 5c event may have reached a sea level of ~15±4 m below present. This is the first time that two distinct sea level events during sub-stage 5a have been precisely constrained and this supports the view of Schellmann and Radtke (2001) that the Barbados terraces record sub-orbital variations in sea level during MIS 5. In the following sections, I compare the sub-stage 5c and 5a Barbados sea levels with other sea level and climate records.

[3]The elevation of the last interglacial deposits on this part of the coast (figure 3.2) has not yet been established. The uplift rate may therefore vary outside the quoted uncertainty for the south coast transect.

4.3 MIS 5 Huon Peninsula sea-level record

Comparing sea-level records at different locations enables us to distinguish between a global ice volume signal and local effects such as tectonics. The raised coral terraces of Huon Peninsula in northeastern Papua New Guinea are one of the most spectacular records of Pleistocene sea-level variations in the world and provide a comparison for the sea-level record inferred from the Barbados terraces in the previous section. The Huon Peninsula terraces lie parallel to the coastline for approximately 80km and reach an elevation of ~1000m. They represent the sea-level oscillations of many glacial cycles (Veeh and Chappell, 1970; Chappell, 1974, Chappell and Shackleton, 1986). Huon Peninsula is a tectonically active region lying northeast of a zone of faults which reflect complex plate boundary interactions. Uplift rates range from approximately 0.5 m/ka in the northwest (Gitua) to over 3 m/ka in the southeast (Bobongara). During times of sea level rise, when the rate of sea level rise was greater than the rate of uplift, major coral reefs were formed. Figure 4.2 shows the location of Huon Peninsula (HP) and a map of the terraces between the Kwangam River and the village of Sialum.

Fairbridge (1960) first speculated about the geological significance of the terraced coastline, shown in aerial photographs from Allied Forces Wartime Intelligence documents in 1943. Corals and molluscs were dated and found to be of Quaternary age (Polach *et al.*, 1969; Veeh and Chappell, 1970; Chappell, 1974) with all of the major interstadial sea-level events of the last glacial cycle represented in the terraces. The Last Interglacial terrace is an easily identifiable barrier reef structure (reef VIIa,b) with a maximum elevation of just over 400 m at Bobongara. The succession of terraces below this last interglacial deposit, reefs VIa, VIb, Va-outer, Va-main, Vb and IV represent coral reef growth during the later part of MIS 5.[4] The complexity of the reef structure at Huon Peninsula implies a complex, sub-orbital period sea level variability during MIS 5 (Chappell and Shackleton, 1986; Lambeck and Chappell, 2001).

The Huon Peninsula terraces provide a wealth of information about late Pleistocene sea-level variations. However, inadequate sampling and poor sample quality has led to inconsistencies in the ages measured for the terraces and, therefore, the inferred sea-level record. In March, 2001, we conducted a field expedition to Huon Peninsula to conduct comprehensive sampling and a detailed field survey of three main transects at Bobongara, Kwambu

[4]The reef nomenclature is not related to the numbering scheme of the marine isotopes stages, but has evolved over a period of time as the sub-reefs were identified in transects of different uplift rates

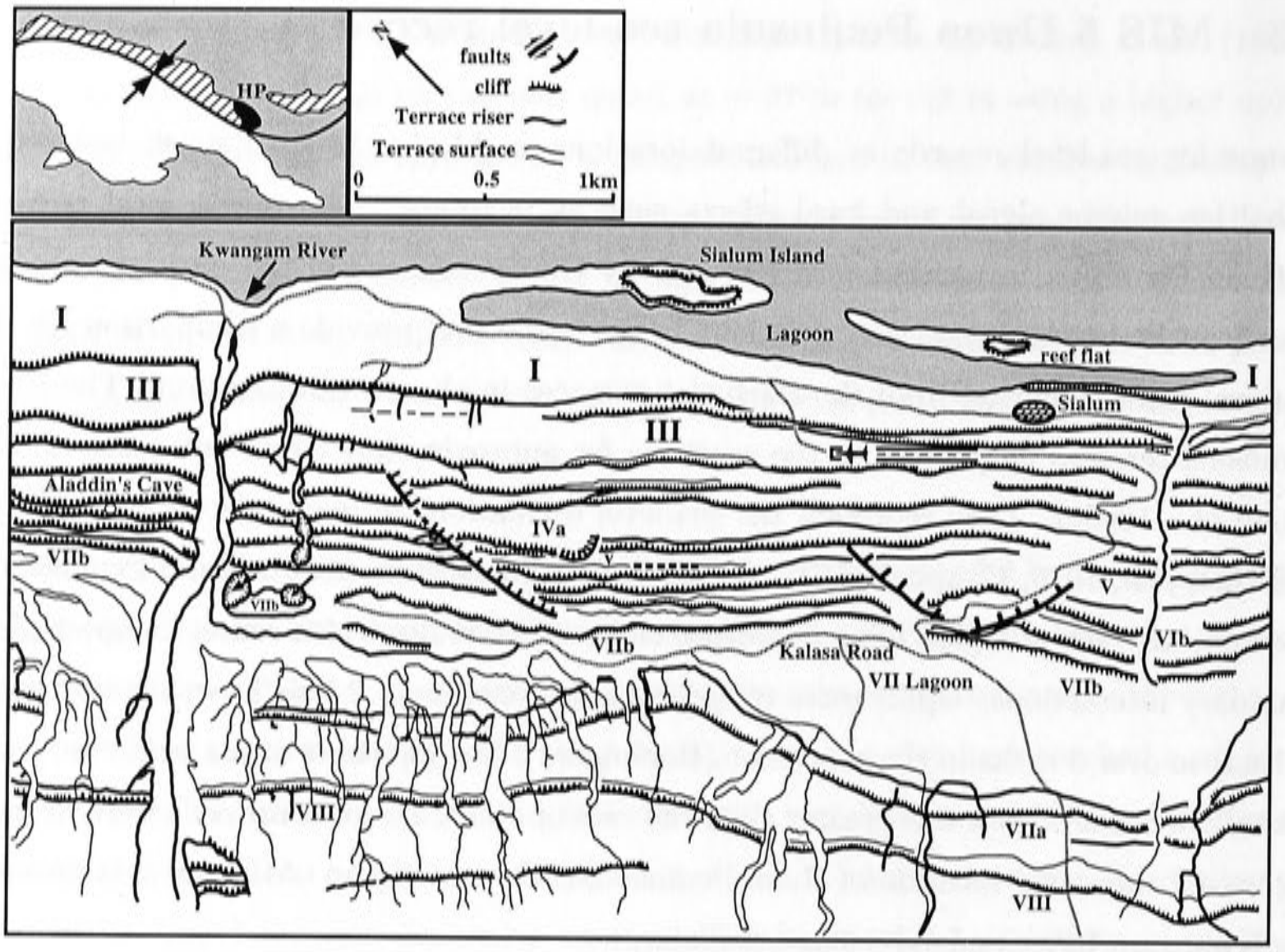

Figure 4.2: Location of Huon Peninsula in the north-east of New Guinea and map of uplifted coral terraces representing Holocene to MIS 7 sea level changes, between the Kwangam River and the village of Sialum.

and Kwangam.[5] Unfortunately, time constraints and the limited availability of a suitable mass spectrometer for thorium analysis restricted the number of Huon Peninsula samples that were investigated in this study. U-Th ages for three samples that were analysed in the present study are summarised in Appendix A, however these samples will not be referred to further. In this section, I will outline the results of previous studies of the sub-stage 5a and 5c deposits at Huon Peninsula, summarise the results of our recent reef elevation survey and discuss the calculations of the Huon Peninsula sea level. Facies descriptions are based on discussions with John Chappell during the 2001 field excursion. Appendix A contains a brief summary of field observations for each terrace and summarises previous age measurements and revised sea-level calculations for the Huon Peninsula terraces.

4.3.1 Terrace descriptions and existing age determinations

Reef VII

Reefs VIIa, VIIb and VIIc represent coral reef growth during sub-stage 5e, the last interglacial period. Here I do not discuss the structure of the reef VII complex in detail. Age

[5]Participants in March 2001 Huon Peninsula Field Expedition: Emma-Kate Potter, John Chappell, Tezer Esat, Eugene Wallensky, Nick Araho and Tim Denham.

data from Stein *et al.* (1993), Bloom *et al.* (1974), Chappell (1974) and Esat *et al.* (1999) (see table in Appendix A for a summary of age measurements) suggest that there are two clusters of ages for these deposits at around ~118 ka and ~136 ka, neither of which correspond to the period of last interglacial peak sea level defined by coral reef growth at Western Australia (between 128 and 122 ka, Stirling *et al.*, 1998) and in the Bahamas (between 132 and 120 ka, Chen *et al.*, 1991). Esat *et al.* (1999) suggest that the older age group represents the peak of a rapid sea-level oscillation prior to the last interglacial plateau. However, there is still debate about the detailed structure of sea-level variations during the last interglacial. The structure of the last interglacial back reef (VIIa) and barrier crest (VIIb) is similar to that of the Holocene reef deposit. By analogy, the back reef VIIa should correspond to reef growth early during the last interglacial highstand. Following this argument an age of 128±2 ka is adopted by Lambeck and Chappell (2001) to represent the timing of deposition of the last interglacial fringing reef (VIIa) for sea-level calculations. Stein *et al.* (1993) discuss an alternative scenario in which the fringing reef crest (VIIb) represents growth at a later time of ~119 ka. Both of these alternatives are considered later.

Reef VIa

Reef VIa is the first major reef structure below the Last Interglacial (Reef VII) complex. At the three transects studied (Bobongara, Kwambu and Kwangam), reef VIa contains a thick unit of shallow water reef crest facies (~12 m exposure at Bobongara).

Previous U-Th age measurements reported by Bloom *et al.* (1974), Esat *et al.* (1999) and Omura *et al.* (1994) are summarised in Appendix A. The scatter of the age measurements is large, ranging from 92.1 ka to 113.2 ka (samples noted as 'reef VI' are assumed to belong to reef VIa). However, some of those samples are noted as having been collected at or near the base of the reef VIa and therefore should not necessarily be considered for dating the peak sea level associated with that feature. Lambeck and Chappell (2001) use a mean age of 107±3 for this deposit based the previous age measurements.

Reef VIb

Reef VIb is not a well-developed structure and has a maximum of ~2 m of distinct shallow water facies at the study sites. At the Kwambu section, there is a clear discontinuity between the upper, shallow water (reef crest unit), and a lower coral limestone unit of mixed fore-reef corals and detritus.

Both Omura *et al.* (1994) and Esat *et al.* (1999) dated a number of samples from reef VIb with ages falling into two groups of ~126 ka to ~132 ka and ~90 ka to ~115 ka (see Appendix A). The older samples appear to have been deposited during the penultimate deglaciation, prior to the last interglacial peak (reef VII). None of the younger group of samples were collected from near the reef crest. Two of the three samples collected near the crest of this reef in the 2001 field expedition (see chapter 3) that have been dated in this study have ages of ~130 ka and the third has an age of ~106 ka. Based on the existing age measurements, it is difficult to establish the age of this deposit.

Perhaps the reef VIb platform does not represent a major high-stand during sub-stage 5c. Alternatively: (i) the VIb, platform may have formed during a sea-level event prior to the last interglacial high-stand and was then covered by a veneer of sub-stage 5c aged corals; (ii) it may represent a constructional feature that formed during the sub-stage 5d to 5c transition; or (iii) it may represent an erosional bench cut into the older deposits before or after the formation of the sub-stage 5c reef VIa deposition. Further comprehensive dating efforts are required to establish the true age of this reef. Lambeck and Chappell (2001) assume this deposit represents a secondary sub-stage 5a sea-level oscillation and adopt an age of ~100 ka, which roughly corresponds to the age of the sub-stage 5c deposit at Barbados analysed in the present study.

Reef Va

In the regions of higher uplift, reef Va is divided into two morphologically distinct units, Va_{outer} and Va_{main} and these two reefs may represent consecutive sea-level high-stands. Reef Va_{main} is best exposed at Bobongara, where it is clearly distinct from the overlying Va_{outer}. At that location Va_{main} contains more than 6 m of shallow-water reef-crest facies. At Kwambu and Kwangam, ~7-8 m of reef Va shallow-water facies are exposed.

Measured ages of these deposits are given by Bloom *et al.* (1974) and Omura *et al.* (1994). Bloom *et al.* (1974) reported ages of 61±4 ka, 84±4 ka and 86±4 ka for 'reef Va'. The age of the youngest sample (~61 ka) corresponds to the lower reef III ages measured by Yokoyama *et al.* (2001c) and Chappell *et al.* (1996a). If the older two are accepted, the mean age for this deposit is 85±4 ka, which is consistent, within age-measurement uncertainties, with other estimates of the 'classic' sub-stage 5a high-stand (e.g. ~84 ka, this study).

Two additional samples from reef 'Va' are slightly older, with a mean age of ~92.4±2

ka (Omura *et al.*, 1994). These were interpreted to correspond to the older reef Va_{main} deposit, although a distinction is not made in their field notes. This age is similar to that of samples at a submerged reef at Florida (Toscano and Lundberg, 1999) which underlie 'classic' sub-stage 5a (~84 ka) deposits. Lambeck and Chappell (2001) assign an age of 90.6±2 ka to this deposit.

Reef Vb

Reef Vb is a poorly developed structure, which at Bobongara has a sandy limestone cap of less than ~1 m and appears to be an erosional bench cut into the underlying Bobongara beds (defined by Pandolfi and Chappell, 1994). At Kwangam, this reef has a 2-3 m cap of rubbly grainstone. The age of this deposit has not been constrained directly as it contains very little material that is suitable for dating.

The two published ages given for reef Vb from Omura *et al.* (1994) (~94 and 106 ka) are inconsistent with each other and can be tentatively rejected as being too old for this deposit. Based on stratigraphic considerations, this reef Vb structure may correspond to the ~77 ka feature identified at Barbados (this study, chapter 3), and Lambeck and Chappell (2001) assigned an age of 77.8 ka to this reef calculated from the present elevation of two reefs (and an assumed age of the last interglacial deposit of ~119 ka). The age and the associated sea level estimate for this feature calculated by Lambeck and Chappell (2001) are open to revision based on future independent constraint on the timing of its formation.

Reef IV

At Bobongara, the reef IV structure is very broad and has several metres of shallow-water reef crest facies. The weighted mean of reliable reef IV ages from Chappell *et al.* (1996a) and Omura *et al.* (1994) is ~71.2±2 ka; however, there is some scatter in the ages. Reef IV is interpreted to represent a sea-level oscillation during the MIS 5-4 transition.

2001 field survey

A new, detailed field survey of the upper terraces (IV to VII) was conducted by trigonometric heighting using a total station (theodolite and EDM) during the 2001 field expedition to Huon Peninsula. The reef elevations are summarised in table 4.5 and figure 4.3.

Reef label	Reef elevation (m) BOBO	KWAM	KWANG	Age estimate (ka)
VIIa $_{rear}$	406†	240.4	204	
VIIb $_{crest}$	402†	227.6	197	
VIIc $_{rear}$	-	-	176	
VIIc $_{front}$	386†	207	163.3	(see caption)
VIa $_{rear}$	326	173.4	140.8	
VIa $_{front}$	317.8	170.8	139.9	107
VIb $_{upper,rear}$	302.4	-	-	
VIb $_{upper,front}$	291.5	-	-	
VIb $_{outer,rear}$	286.8	144.3	120.7	
VIb $_{outer,front}$	280.8	142.7	119	100
Va $_{main,rear}$	264	127.9	101.7	
Va $_{main,front}$	263.1	124.6	101.5	90.6
Va $_{outer,rear}$	250	123.6	100.9	
Va $_{outer,front}$	244.3	122.3	100.3	84
Vb $_{front}$	213.8	-	78.5	77.8
IV $_{rear}$	197	88†	-	
IV $_{front}$	190.6	82†	-	71.2

Table 4.5: Summary of Huon Peninsula reef elevation survey. Three transects were surveyed, in detail, during the 2001 field expedition: Bobongara (BOBO), Kwambu (KWAM) and Kwangam (KWANG). Elevations are in metres above present sea level. All elevations were measured in the 2001 survey except for those marked (†) which were measured by theodolite triangulation in previous expeditions in 1988 and 1992 (J. Chappell, pers. comm.). Ages are inferred from the existing information in the literature. There are two clusters of ages for the last interglacial reef deposit VIIb at around ~119 ka and ~136. The alternative ages for the last interglacial reefs used in the uplift calculation are 128 ka for deposit VIIa (by analogy with the Holocene reef) and 119 ka for the reef deposit VIIb. This is discussed in the text.

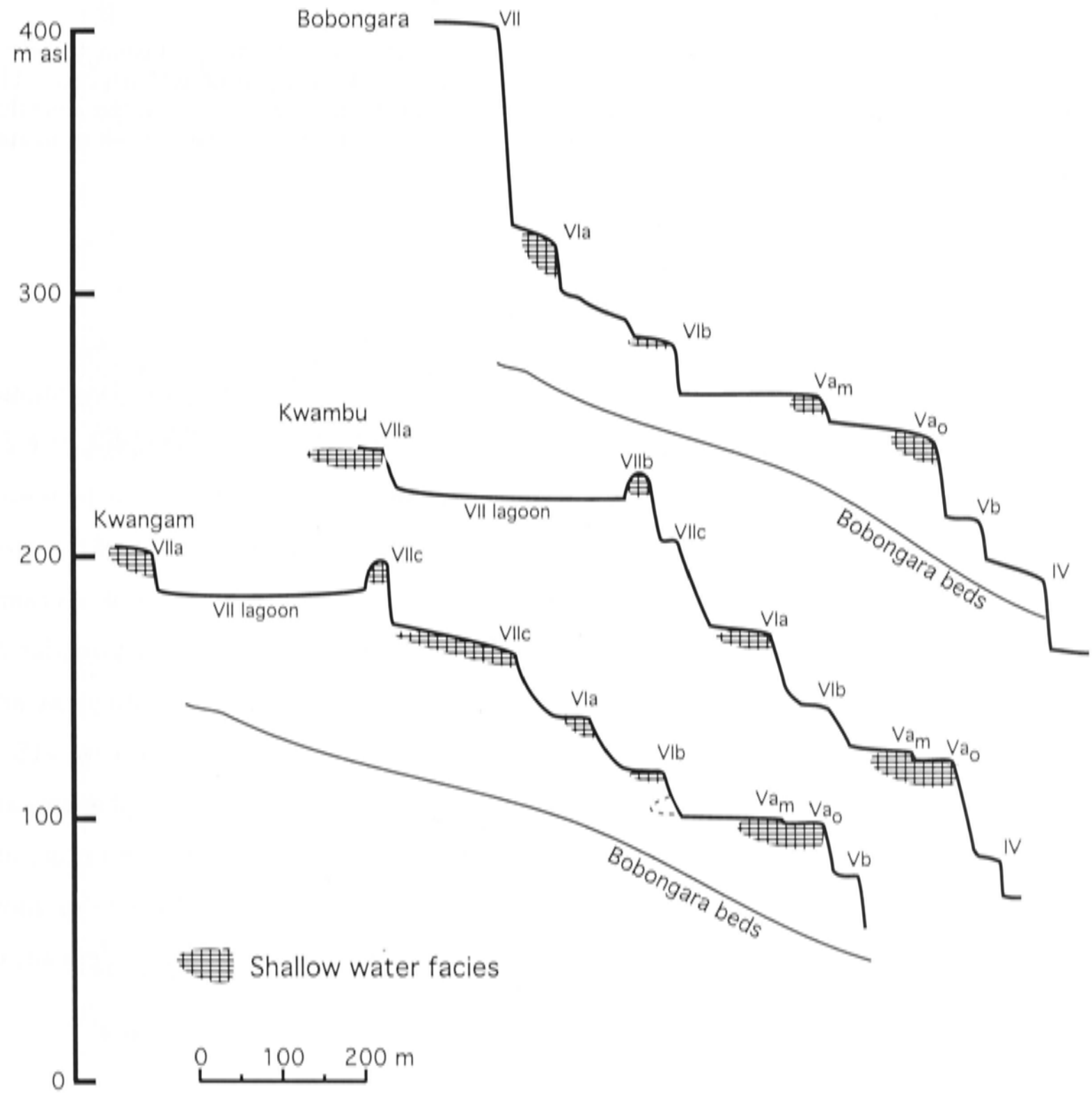

Figure 4.3: Reef profiles for Bobongara, Kwambu and Kwangam. Distance scale is approximate. Approximate shallow-water reef-crest facies are marked.

Transect	Deposit	Elevation (m)	Age (ka)	Paleo-sea level (m)	Uplift rate (m/ka)
Bobongara	VIIa	406	128±2	4±2	3.14±0.06
	VIIb	402	119±2	0±2	3.34±0.06
Kwambu	VIIa	240	128±2	4±2	1.84±0.04
	VIIb	227.6	119±2	0±2	1.88±0.04
Kwangam	VIIa	204	128±2	4±2	1.56±0.04
	VIIb	197	119±2	0±2	1.62±0.04

Table 4.6: Summary of alternative uplift calculations for the three Huon Peninsula transects studied. The uplift calculation does not take into account a growth depth of reef deposit. The quoted uncertainty includes uncertainty in the age of the deposit, the paleo-sea level, the elevation of the deposit and an allowance for the amplitude of discrete uplift events (mean of ~3 m during the Holocene).

4.3.2 Huon Peninsula sea-level calculations

Based on an analogy with the Holocene reefs, the last interglacial back reef (VIIa) should correspond to reef growth early during the last interglacial highstand. The uplift rate for each of the surveyed transects, based on an age of 128 ka for the reef VIIa at a paleo-sea level of 4±2 m are given in table 4.6. The sea level associated with each of the reef terraces, based on the interpretation of the existing age data in the literature (previous section), are shown in figure 4.4a. Details of the sea-level calculations are given in Appendix A. There is significant scatter in the calculated sea levels for each of the sub-stage 5a and 5c reefs. In particular, sea levels calculated at the Bobongara transect are up to ~15 m higher than estimates for corresponding features at the other transects. Possible reasons for discrepancies between the sea level calculated at different transects include uncertainties in the assigned ages of the reefs, error in the uplift rate estimated for one or more transects due to uncertainties in the formation history of the last interglacial deposit, or departure from uniform uplift at one or more transects.

As an alternative, the calculated sea levels for higher uplift rates, using an age of 119 ka for the last interglacial deposit VIIb (based on the age measurements of Stein *et al.*, 1993) and a paleo-sea level of 0±2 m are shown in figure 4.4b. Because the uplift rates are higher at each transect (compared to figure 4.4a), the estimates of sea level for each event are lowered. Furthermore, because the increase in uplift is proportionally larger at the higher uplift, Bobongara transect, this acts to bring the estimates for each of the features at individual transects into better agreement. This agreement would suggest that this choice of uplift rate is the preferred value. Hearty *et al.* (2001) suggested that there was a rapid sea-level excursion at the end of the last interglacial period in the Bahamas

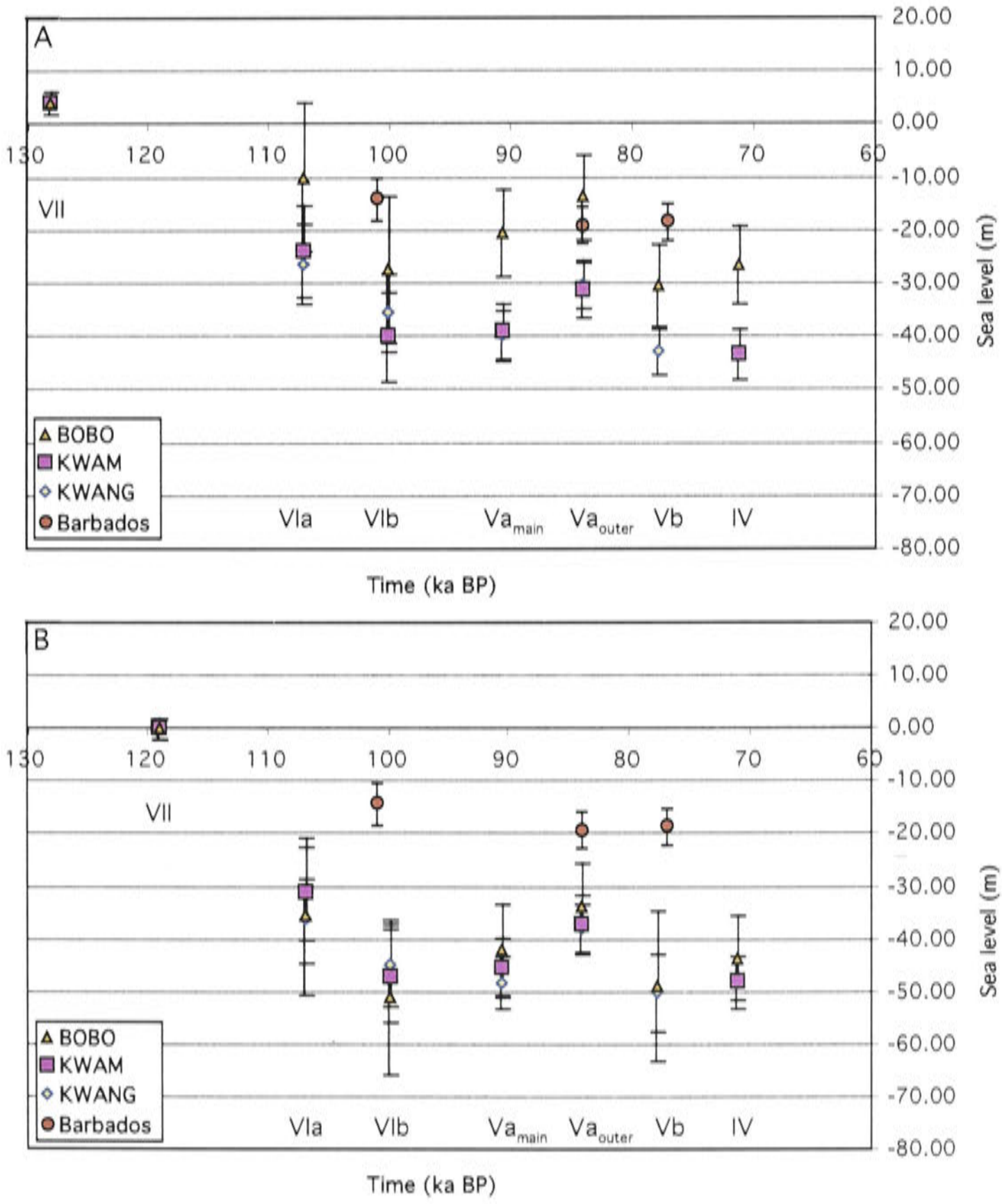

Figure 4.4: Sea levels calculated for the Huon Peninsula terraces at transects Bobongara, Kwambu and Kwangam for two assumed uplift rates. A) lower uplift rate calculated from assuming an age of 128 ka and sea level of 4±2 m for the last interglacial reef VIIa and B) higher uplift rate from assuming an age of 119 ka and sea level of 0±2 m for the last interglacial reef VIIb. See table 4.6 for details.

reaching up to 8 m above present sea level at that location, but the precise timing of this event has not been established. Assigning an age of 119 ka and a paleo-sea level of 8 m to the VIIb deposit increases the calculated Huon Peninsula sea levels by 4-7 m, but are these are still well below those sea levels calculated in figure 4.4a using an age of 128 ka for the last interglacial reef VIIa.

A graphical method of calculating relative sea level for features (for which the ages are not known) that are identified at multiple uplifted sites is outlined by Bloom *et al.* (1985, 1990). This method is equivalent to calculating the best estimate of sea level for each event numerically by using a least squares analysis if there is redundancy in the data, ie if there are multiple transects with terrace features of known ages. In this method, the present day elevation of each reef terrace is plotted against the elevation of the last interglacial terrace (corrected for the paleo-sea level of the last interglacial high-stand) for each transect. The y-axis is chosen to represent zero uplift, where the intercept of a line through the reef elevations of the last interglacial deposits is equal to the paleo-sea level associated with that high-stand (4±2 m at 128 ka or 0±2 m at 119 ka). The y-axis intercept of a line of best fit through the terrace elevations at each transect gives an estimate of sea level associated with that event. The slopes of the regression lines give a measure of the relative ages of each of the features represented.

Bloom *et al.* (1985) applied this method to the terrace elevations at Huon Peninsula and determined the sub-stage 5a and 5c paleo-sea levels to be at ~-7 m and ~0 m respectively. However, the reef-elevation data used by Bloom *et al.* (1985, 1990) are based on an early theodolite survey (with large quoted uncertainties ±5m) and appear to differ from the revised elevation data shown in table 4.5. Furthermore, the sub-structures evident in the reefs at Huon Peninsula are not noted by Bloom *et al.* (1985, 1990). Applying Bloom *et al.*'s method to the revised terrace elevations produces sea-level estimates for the sub-stage 5a and 5c events that range from -40 to below -60 m (see figure 4.5).

The relative ages of the deposits can be inferred from the slopes of the regression lines, assuming an appropriate age for the last interglacial reef. Assuming an age of 128 ka for the last interglacial deposit VIIa, the ages calculated for the rest of the MIS 5 reefs are consistently higher than those estimated independently (table 4.7). The ages inferred from the slopes of the regression lines agree better with the observed values if the age assigned to the last interglacial reef VIIb is ~119 ka (table 4.7). This is equivalent to the result shown figure 4.4, in which the calculated sea levels are more consistent between

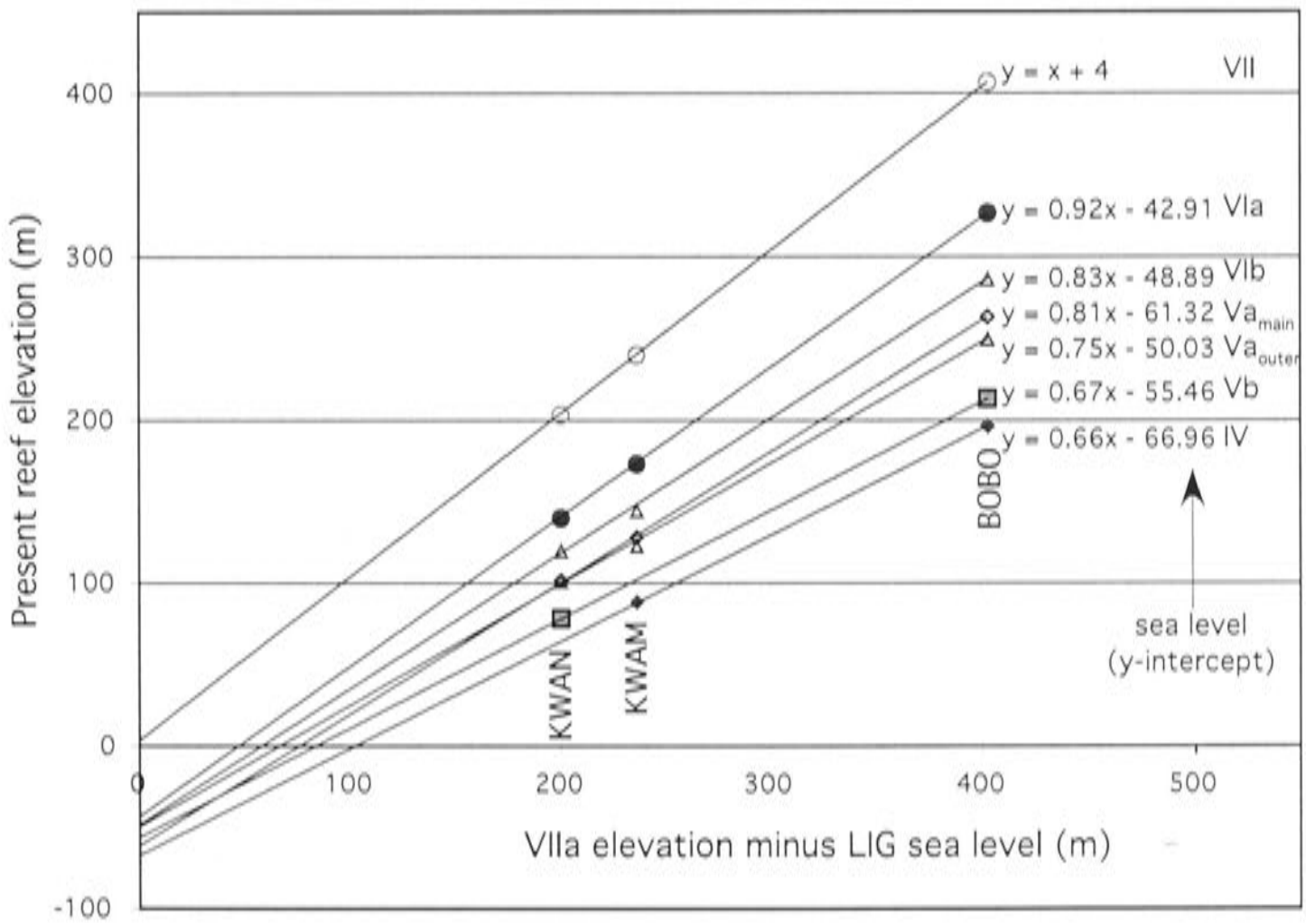

Figure 4.5: Example of the graphical 'intercept' method described by Bloom *et al.* (1985, 1990) applied to the MIS 5 terraces at Bobongara, Kwambu and Kwangam transects at Huon Peninsula. In this example, the terraces elevations are plotted against the elevation of the last interglacial reef VIIa (adjusted for a paleo-sea level of 4 m above present, or any other arbitrary value could be chosen). The y-axis intercept of each line of best fit through each set of terrace elevations is equal to the sea level associated with that feature. The ratios of the slopes of the lines are equal to the ratios of the ages of the associated features. See text for details.

Reef	Age (ka) estimated	Age (ka) $t_{LIG} = 128$ ka	Age (ka) $t_{LIG} = 119$ ka
VIa	107	118	106
VIb	100	107	96
Va,main	90.6	104	93
Va,outer	84	95	86
Vb	77.8	86	78

Table 4.7: Comparison of terraces age estimated in the previous section, based on existing age measurements (column 1), with ages inferred from the slope of the regression lines through the terrace elevations, assuming (i) an age of 128 ka for the last interglacial deposit VIIa (column 2) and (ii) an age of 119 ka for the last interglacial deposit VIIb (column 3).

the three transects if an age of 119 ka for reef VIIb is used to calculate uplift. Again, these comparisons suggest an age of 119 ka for the last interglacial reef VIIb is the most appropriate to use for the calculation of uplift for the Huon Peninsula terraces.

Although the age of 119 ka for the last interglacial terrace VIIb produces sea-level estimates that are more consistent between the different Huon transects, these values are now up to 30 m lower than the estimates for the corresponding events at Barbados (figure 4.4). As I will discuss in chapter 6, we do not expect the relative sea levels at Barbados and Huon Peninsula to be equal due to the effects of glacio-hydro-isostasy. However, based on isostatic considerations, the difference between the relative sea levels at the two locations is expected to be small ($<\sim$5 m). Therefore, in contrast to the above discussion, this comparison now suggests that the higher uplift rates (based on an age of 119 ka for the reef VIIb deposit) are not appropriate.

The reason for some of these inconsistencies is likely to be the result of uncertainty of uplift rate at Huon Peninsula because of: (i) uncertainties in deposition history of the last interglacial reef deposits at Huon Peninsula or (ii) non-uniform uplift since the last interglacial period at one or more sites. A more detailed discussion of uplift considerations follows.

Uplift considerations

The rate of uplift at Huon Peninsula has varied spatially as a function of distance along the coast. The minimum uplift rates occur in the northwest of the region and increases more than 3 m/ka in the southeast. The actual rates of uplift can be estimated from observations of reefs whose counterparts in tectonically stable areas have known elevations:

1. Most commonly, the elevation of the last interglacial reef is used for the calculation of uplift. At tectonically stable continental margins that lie far from the former ice sheets, the elevation of the last interglacial-age deposits are around 4±2 m above present sea level, depending on the period within the interglacial that the reef formed. Uncertainties in the estimation of uplift using this method arise because of uncertainties in the deposition history of the last interglacial deposits. More extensive dating of the last interglacial deposits at Huon Peninsula is required to establish the appropriate age to use for the calculation of uplift based on these deposits.

2. During the mid-Holocene, at around 7 ka BP, sea levels at tectonically stable continental margin sites reached a maximum of 1-2 m above present sea level. The Holocene back reef crest is well defined along the Huon coast and can be used for this calculation.

3. The paleo-sea levels and ages associated with interglacial sea-level high-stands prior to the last interglacial are generally less well constrained. (Gallup *et al.*, 2002; Stirling *et al.*, 2002). Estimates can also be made based on correlation with other proxy indicators of ice volume such as δ^{18}O records, which suggest sea levels during major interstadials were similar to present. However, because of the large uncertainties with this approach, it will not be considered further.

These different approaches determine average uplift rates over different time intervals. If the uplift rates estimated by each of these methods are similar, within the uncertainties of the calculation, then this suggests that there have been no long-term changes in the uplift rates.

Mean uplift since the last interglacial

The issues associated with calculating uplift since the last interglacial period at Huon Peninsula has been discussed in the previous sections. Uncertainties arise from the uncertainty in the deposition history of the last interglacial reefs deposits. A summary of the uplift rate calculations for two transects (Bobongara and Kwambu) is given in table 4.8. Although the analogy with the construction history of the Holocene reef suggests the back reef VIIa should represent growth early during the last interglacial period (~128 ka), this leads to inconsistent estimates of sea level for the same events at different transects. If the VIIa elevation at Bobongara is in error and the uplift at that site was higher than estimated here, then this may bring the estimates into better agreement. However, this seems unlikely because the back reef elevations are relatively well constrained. For the other uplift scenario an age of 119 ka was adopted for the reef VIIb deposit. However, the

VIIb barrier may represent an eroded surface at one or all of the sites and its elevation may not be appropriate for sea-level calculations. A correction for this (<10-15 m) would be insufficient to bring the Huon estimates into agreement with the Barbados observations.

Mean Holocene uplift

The uplift at Huon Peninsula has not been continuous throughout the late Pleistocene. Rather, it appears that uplift during the Holocene and MIS 3 occurred as metre-scale seismic events with mean amplitudes of ~2-3 m every 1-1.3 ka (Ota *et al.*, 1993; Chappell *et al.*, 1996b; Ota and Chappell, 1996). Small regressive features that formed after each co-seismic uplift event, in the form of surf benches, intertidal platforms, algal rimmed pools and shingle beaches, are cut into the transgressive Holocene reef (Ota and Chappell, 1996). Such regressive features are not observed in the older reefs (ie MIS 5), presumably because of prolonged exposure to erosion.

Ota *et al.* (1993) compared the mean uplift rate over the last glacial cycle (based on the estimated age and paleo-sea level of the last interglacial deposit) with uplift estimates for the Holocene period based on the age and elevation of the Holocene reef crest. Within the uncertainties quoted by Ota *et al.* (1993), these two uplift rate estimates are the same. If a +2 m Holocene highstand at Huon Peninsula is taken into account (based on isostatic considerations, Lambeck *et al.*, 2002c), this reduces the Holocene uplift estimates but the two estimates still agree within the uncertainties of the calculations, which are large in the case of the Holocene estimates (table 4.8).

Estimates of uplift at Huon Peninsula for the Holocene and the last glacial cycle agree, within the large uncertainties of the Holocene estimates, but small changes in uplift over the longer time period cannot be disproved. Because the sea levels calculated for the sub-stage 5a and 5c reefs using the two uplift scenarios are either inconsistent between the different Huon transects (i.e. if t_{LIG}=128 ka), or different from the Barbados estimates (i.e. if t_{LIG}=119 ka), this suggests that further consideration of the uplift rate over the last glacial cycle is required.

Additional uncertainties in uplift may arise from (i) the assumed deposition history of the last interglacial reef at one or more transects; or (ii) non-uniform uplift over the last glacial cycle at one or more transects. Consider a scenario in which the age of the last interglacial deposit, VIIa, is 128 ka (figure 4.4a). A decrease of uplift rate of 15% over the last glacial cycle at the two lower uplift transects (Kwambu and Kwangam) is within the

Kwambu

Time period	Elevation (m)	Age (ka)	Paleo-sea level (m)	Uplift rate (m/ka)
Holocene	13.2	6.9±0.2	2±1	1.62±0.33
LIG_{early}	240	128±2	4±2	1.84±0.04
LIG_{late}	227.6	119±2	4±2	1.88±0.04

Bobongara

Time period	Elevation (m)	Age (ka)	Paleo-sea level (m)	Uplift rate (m/ka)
Holocene	23	6.9±0.2	2±1	3.04±0.47
LIG_{early}	406	128±2	4±2	3.14±0.06
LIG_{late}	402	119±2	4±2	3.38±0.06

Table 4.8: Comparison of uplift estimates for the Holocene and since the last glacial cycle for two transects - Kwambu and Bobongara. Uncertainties include the mean co-seismic uplift magnitude of 2-3 m (Ota and Chappell, 1996). The paleo-sea level assumed for the last interglacial highstand is 4±2 m at 128 ka (or 0±2 m at 119 ka)

uncertainty range of the Holocene uplift estimate and would raise the sea-level estimates at those locations into better agreement with the Bobongara estimates. A change in uplift at Kwambu and Kwangam, but not at Bobongara, is consistent with the suggestion that the Huon coast is divided into several tectonic sub-regions with buried faults between the northwestern area near Kwambu and the southeastern regions of Hubegong and Bobongara (Chappell *et al.*, 1996b).[6] Any further discussion of the uplift history of the Huon Peninsula terraces requires further comprehensive study into the deposition history of the last interglacial terraces along the Huon coast and is beyond the scope of this investigation. However, this uncertainty must be kept in mind when using sea-level estimates from Huon Peninsula.

4.3.3 Conclusions

Emergent coral reef terraces at Huon Peninsula represent reef growth during interstadial events of the late Pleistocene. The paleo-sea levels associated with these features can be calculated by estimating the age associated with each reef and the uplift experienced by each site, however reef ages are sometimes uncertain due to inadequate sampling and poor sample quality (section 4.3.1). Although the high uplift at locations such as Huon Peninsula allow a more detailed and complex snap-shot of sea-level history than at tectonically stable sites, the sea-level estimates may be less precise.

[6]Based on the analysis of the ages and elevations of regressive terraces cut into the Holocene deposits, these authors suggest there is a decelerating uplift trend at the northern Kwangam-Kilasaro region during the Holocene, compared to the higher uplift locations in the southeast (Bobongara).

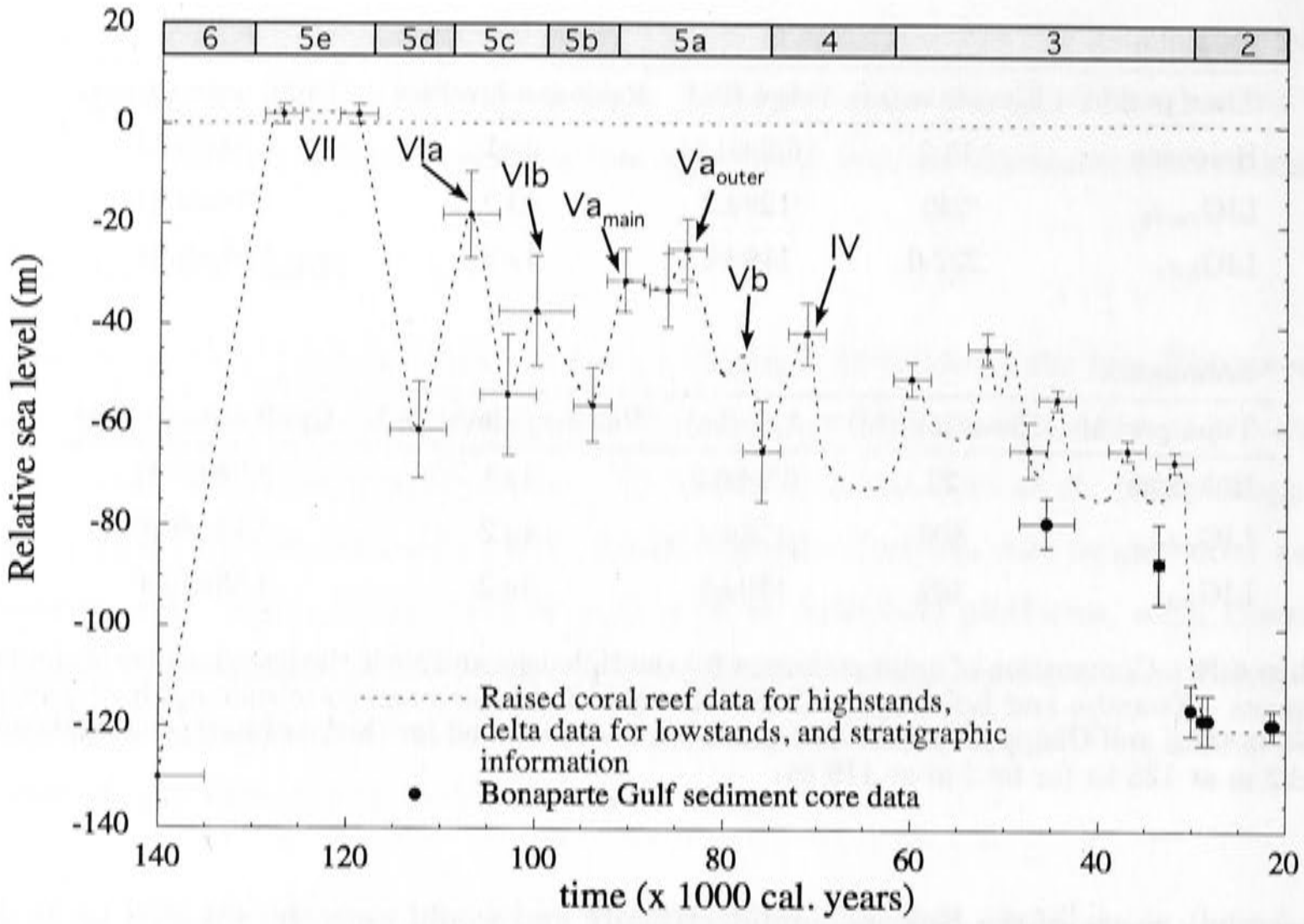

Figure 4.6: Composite sea level curve for Huon Peninsula (this section, Lambeck and Chappell, 2001; Chappell *et al.*, 1996a; Yokoyama *et al.* 2001c) and the Bonaparte Gulf (Yokoyama *et al.*, 2000b). The last interglacial period sea level history has been simplified in this model. The Huon Peninsula reef nomenclature (VII, VIa, VIb, etc) and the marine isotope stages (6, 5e, 5d, 5c, etc) are also shown on this plot. All of the MIS 5 sea levels, with the exception of reef Vb event were calculated assuming an age of 128 ka and sea level of 4±2 m for the last interglacial deposit VIIa.

The sea levels calculated using the lower uplift rates (based on an age of 128 ka for the reef VIIa deposit) are more consistent with the Barbados estimates (figure 4.4a). This is the assumption used by Lambeck and Chappell (2001) and so I use their sea level curve (figure 4.6) for the sea level calculations in chapter 6.[7] The Lambeck and Chappell (2001) calculations are in good agreement with the sea levels in figure 4.4a, with the exception of reef Vb. Lambeck and Chappell appear to have applied a different uplift rate to the calculation of sea level for the Vb deposit. The revised sea-level calculation in this chapter leads to an difference of ~10 m (from ~46 to ~37 m below present). For convenience, and despite this inconsistency, I use the Lambeck and Chappell (2001) curve for the sea-level calculations in chapter 6, allowing for the possibility of revision. Estimates of sea-level minima in this curve are based on the stratigraphy of uplifted gravel stream deltas (Chappell, 1983) and reef growth models (Lambeck and Chappell, 2001).

[7]The sea level for the reef Vb feature in the Lambeck and Chappell curve is ~10 m lower than estimated in the calculations in this section. This sea level is revised after closer comparison with other observations in chapter 6.

Both the Huon Peninsula and the new Barbados sea-level records show multiple events during MIS 5 (Chappell and Shackleton, 1986; Lambeck and Chappell, 2001; Schellmann and Radtke, 2001; and this study). The agreement of the two records in this respect suggests that the multiple features identified at both locations are not the result of discrete tectonic events but rather represent true sub-orbital oscillations in global ice-volume. The complexity of the inferred sea-level curve (figure 4.6) is in contrast to early studies at these locations which suggested there were only two sea-level high-stands during this period corresponding to the sub-stage 5a and 5c events in marine records (Bloom *et al.*, 1974; Broecker *et al.*, 1968). Further comprehensive dating analysis of the upper Huon Peninsula terraces, such as was conducted for the Barbados deposits in this study, is required for the confirming the direct correspondence of the features at these two locations. The remaining inconsistencies between the Huon Peninsula and Barbados records will be addressed in chapter 6.

4.4 Complexity of glaciation

A more complex view of MIS 5 sea-level change is emerging from the coral records at Barbados (this study; Schellmann and Radtke, 2001) and at Huon Peninsula (Lambeck and Chappell, 2001). In the following sections, I compare the MIS 5 sea-level records with other proxy climate records and discuss the interpretation of these in the context of the factors controlling climate change during this period.

4.4.1 Comparison of MIS 5 sea-level record with δ^{18}O records

The oxygen isotope composition of the ocean ($\delta^{18}O_{water}$)[8] reflects global variations in ice volume. During glacial periods, the oceans become enriched in ^{18}O (increase δ^{18}O) as the lighter ^{16}O is evaporated preferentially and precipitated to form ice sheets. The identification of interstadial (low δ^{18}O and low ice volume) and stadial (high δ^{18}O and high ice volume) in oxygen isotope records of deep sea cores forms the basis of the marine isotope stage nomenclature (Imbrie *et al.*, 1984; Martinson *et al.*, 1987).

The oxygen isotope signal recorded in the carbonate tests of foraminifera not only reflects the ocean water δ^{18}O, but also temperature changes of the water in which they are precipitated. This complicates the interpretation of global ice volume from these records. Deep water is expected to experience less temperature variability and so benthic foraminifera are often used in preference to their shallower, planktonic counterparts. However, comparison of independent sea-level estimates with individual and stacked benthic records show

[8] $\delta^{18}O_{water} = \frac{(^{18}O/^{16}O)_{water}}{(^{18}O/^{16}O)_{SMOW}} - 1$

that these records may still contain significant temperature effects (figure 4.7). Sea surface temperature in the Western Pacific warm pool is not expected to have changed significantly over the course of a glacial cycle, so planktonic $\delta^{18}O$ should only reflect changes in the $\delta^{18}O$ of the water (Shackleton, 1987; Linsley, 1996). However the planktonic record may not only reflect global ice volume variability but also millennial scale oceanographic changes in the Western Pacific warm pool. Indeed, the Sulu Sea record (Linsley, 1996) shows a glacial to interglacial change in ocean water $\delta^{18}O$ of 1.4‰, which is larger than the range for the global ocean suggested by studies of pore water in deep sea sediments ($\leq$ 1‰, Schrag and DePaolo, 1993; Schrag *et al.*, 2002).

High frequency variations in $\delta^{18}O$ may not be recorded in low sedimentation rate environments, or the signal can be smoothed out bioturbation. Furthermore, the uncertainties introduced by variations in sedimentation rate within a single core make assigning an accurate time-scale difficult. In order to minimise these types of uncertainties common to individual records, they are often stacked, or averaged together (Imbrie *et al.*, 1984; Martinson *et al.*, 1987; Prell *et al.*, 1986). The purpose of stacking is to enhance major variations in global ice volume that are common to the individual records, while smoothing out the 'noise' of individual cores. Generally, events that are common to each isotopic record are correlated graphically (Prell *et al.*, 1986). Assigning a time-scale to these records is based on (i) the independently constrained timing of major events (U-Th dating of sea-level high-stands, or the timing of magnetic reversal events) and/or (ii) tuning to insolation variations. Small or rapid events may not be recorded in all the $\delta^{18}O$ records, consequently they may not be recognised as distinct features and omitted from the graphical correlation procedure. This is evident in the Imbrie *et al.* (1984) stacked record where only two broad events corresponding to sub-stages 5a and 5c have been identified, whereas the high resolution Sulu Sea core (Linsley, 1996) records multiple oscillations in $\delta^{18}O$ during these interstadials that are superimposed on the broader signal.

A comparison of the peak sea levels calculated at Barbados (this study) and those estimated at Huon Peninsula (Lambeck and Chappell, 2001) is shown in figure 4.7. The $\delta^{18}O$ records have been scaled to a sea level of -135 m at the last glacial maximum (Yokoyama *et al.*, 2000b). No other scaling or temperature adjustments have been applied. The independent sea-level estimates at Barbados are consistently ~20 m higher than predicted by the $\delta^{18}O$ records[9] (with the exception of the sub-stage 5a Sulu sea record from Linsley,

[9]Isostatic corrections have not been made to the sea level observations for this comparison (see chapters 5 and 6) but this adjustment would be less than 10 m at these sites.

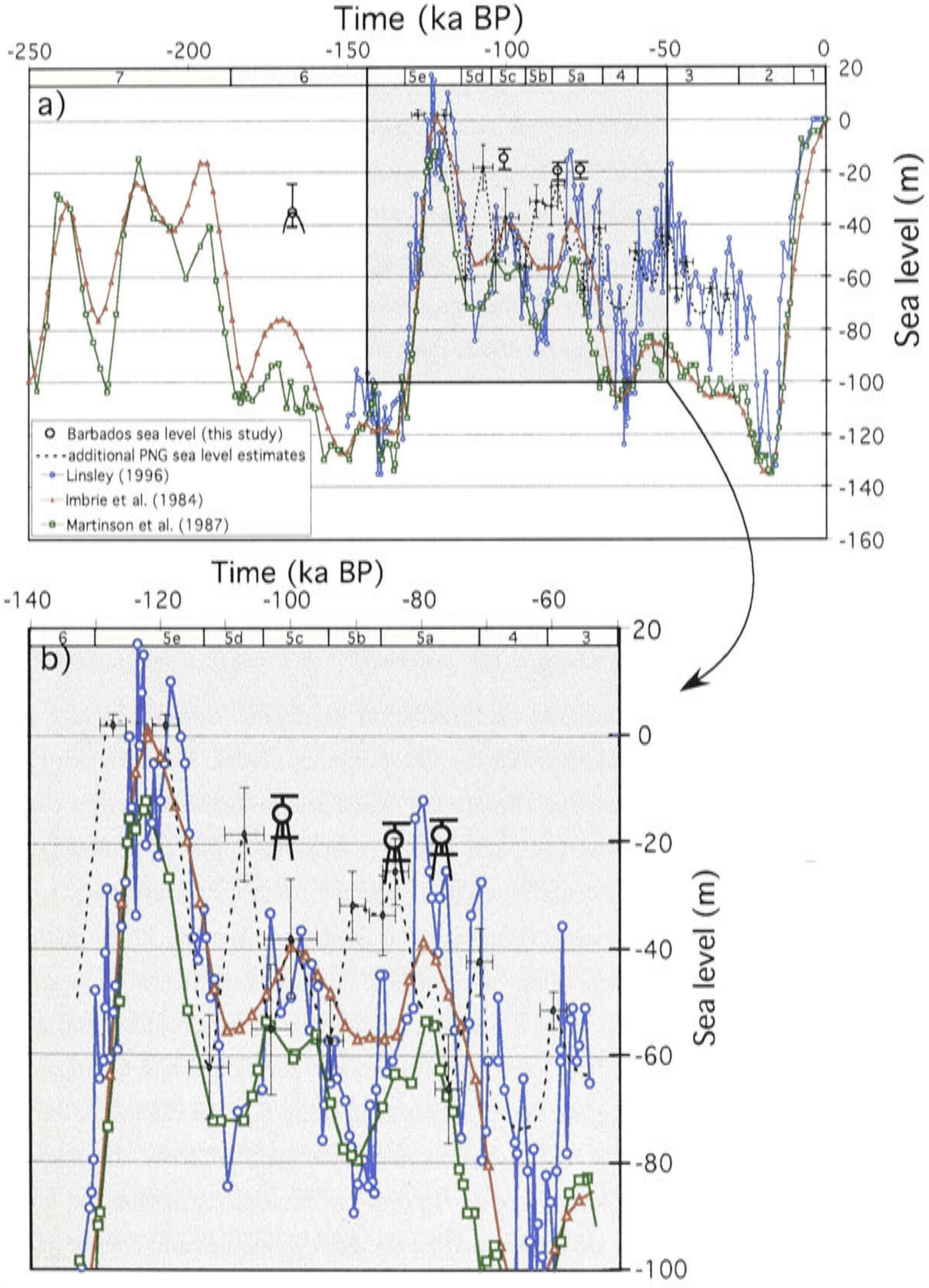

Figure 4.7: Comparison of relative sea-level observations at Barbados with stacked benthic foraminiferal $\delta^{18}O$ record (Imbrie *et al.* 1984, Martinson *et al.*, 1987) and the single core Sulu Sea record (Linsley *et al.*, 1996). The $\delta^{18}O$ records are linearly scaled for ice-equivalent sea level at the last glacial maximum (~135 m, Yokoyama 2000b) and are uncorrected for temperature. Benthic $\delta^{18}O$ records often underestimate sea-level during glacial periods due to the temperature effects.

1996). This implies that water temperatures during these interstadials were lower than at present. This temperature effect appears to be even more significant for the MIS 6 event.

A more detailed comparison of the $\delta^{18}O$ records and the calculated sea levels is shown in figure 4.7b. This illustrates that the combined sea-level record inferred from the Barbados and Huon Peninsula terraces is significantly more complex than the stacked records of Imbrie *et al.* (1984) and Martinson *et al.* (1987). The high resolution Sulu Sea record (Linsley *et al.*, 1996) contains more complexity during sub-stages 5a and 5c than the other $\delta^{18}O$ records and appears to contain oscillations similar to those identified in the independent sea-level records at Barbados and Huon Peninsula. This comparison suggests that global ice volume variations during sub-stages 5a and 5c were made up of two components: (i) large scale oscillations in ice volume that are consistent with an orbital forcing timescale (see below) and (ii) and a rapid sea-level oscillations superimposed on the broader signal.

4.4.2 Comparison of MIS 5 sea-level record with insolation forcing predictions

Comparison of the timing of sea level and insolation excursions during the late Pleistocene is a crucial test of the Milankovitch insolation-forcing model. Milankovitch (1941) postulated that global ice volume and climate are dependent on orbitally-driven changes in seasonal solar insolation received at high northern latitudes. The dominant periods of variability in the insolation calculations are at around 19-23 ka (precession), ~41 ka (obliquity), and ~100 ka (eccentricity) (Berger, 1978; Berger and Loutre, 1993). Although each of these main periods is also evident in records of climate variability such as stacked $\delta^{18}O$ records (Hays *et al.*, 1976), there are many inconsistencies in the phase and amplitude of the variations. In particular, ice volume variability during the late Quaternary is dominated by a 100 ka cycle, whereas this is only a weak component of the insolation forcing function (Imbrie *et al.*, 1993). This indicates that there are significant non-linearities in the climate's response to insolation forcing. In order to establish a mechanism for this non-linear response, researchers have examined (i) ice sheet dynamics and energy balance considerations (Weertman, 1976; Birchfield, 1977; Imbrie and Imbrie, 1980); (ii) multiple state models (Paillard, 1998; Manabe and Stouffer, 1988); (iii) changes in the inclination of the Earth's orbit (Muller and MacDonald, 1995); and (iv) the importance of seasonal and latitudinal gradients in insolation (Johnson, 1991; Schaffer *et al*, 1996). However, none of these models have yet been able to explain all of the observed characteristics in climate variability.

During the last deglaciation, global sea level reached modern values after the 65°N summer insolation maximum. However, the sea-level rise during the penultimate deglaciation appears to have preceded the associated insolation rise (Esat *et al.*, 1999; Stein *et al.*, 1993; Gallup *et al.*, 2002). Continental records and oceanic $\delta^{18}O$ also support a penultimate deglaciation climate shift prior to the insolation rise (Winograd *et al.*, 1992; Henderson *et al.*, 2000). Despite the uncertainties in constraining the precise timing of earlier interglacials (MIS 7 and 9), their occurrences generally correspond to the timing of 65°N summer insolation maxima (Stirling *et al.*, 2001; Bard *et al.*, 2002; Robinson *et al.*, 2002).

$\delta^{18}O$ records point towards large scale oscillations in ice volume which occur with a periodicity that it consistent with insolation forcing. However, the combined sea-level record from Barbados and Huon Peninsula indicate multiple sub-orbital period sea-level oscillations during MIS 5. The timing of the 'classic' sub-stage 5a and 5c sea-level high-stands at ~84 ka and ~101 ka BP, as determined in this study, roughly correspond (within uncertainty) to the timing of the 65°N summer insolation maxima in this period at 82 ka and 103 ka BP (see figure 4.8). Therefore, these peaks are roughly consistent with the predictions of the Milankovitch insolation-forcing model. Despite this, the timing of the ~77 ka BP sea-level feature identified here at Barbados and the additional events inferred from the Huon Peninsula terraces (section 4.3.2) cannot be simply reconciled with insolation forcing. The MIS 6 event at ~168±5 ka BP lags the associated insolation peak by ~5 ka but is consistent with insolation forcing, within the uncertainties of the dating.

The two Barbados sub-stage 5a features at ~84 ka and ~77 ka BP are both associated with a single insolation maximum at ~82 ka BP. If these two features represent only minor oscillations superimposed on a broad sea-level high-stand then this implies the duration of this broad event is at least 7 ka, which is comparable to the duration of the main period of last interglacial reef growth identified at Western Australia (Stirling *et al.*, 1998). Further investigation of the magnitude of the fall in sea level between these two events at Barbados, possibly by drilling into the reefs, is required.

4.4.3 Sub-orbital period climate variability

Although the main frequencies observed in Pleistocene proxy climate records (such as $\delta^{18}O$) are largely consistent with an insolation forcing model, many other records point

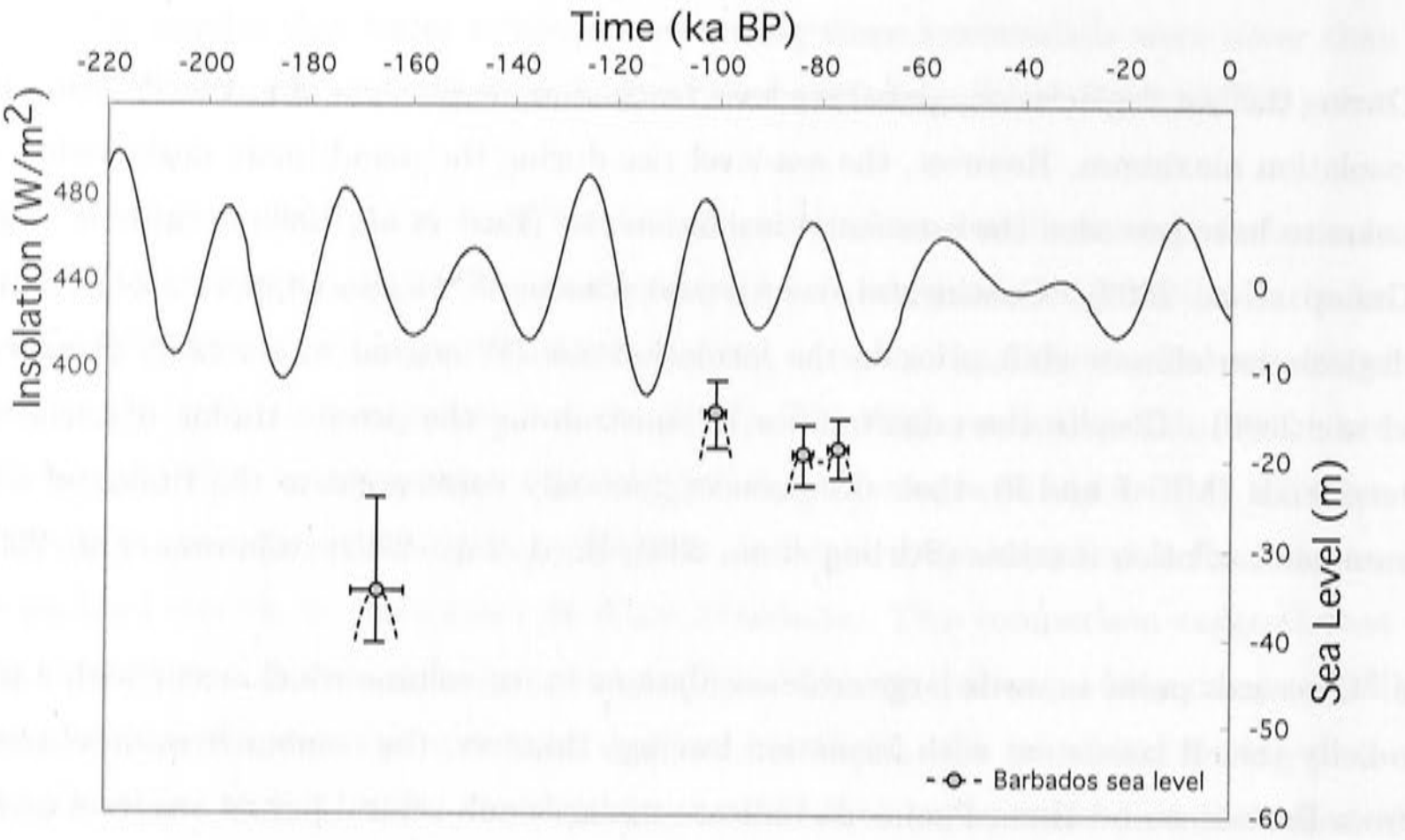

Figure 4.8: Comparison of Barbados sea-level observations with summer 65°N insolation.

towards sub-orbital climate variability during the last glacial cycle. Climate records from around the world, but particularly in the North Atlantic region contain periodicities of 1-2 ka and 5-10 ka during MIS 3 and the last deglaciation (Broecker and Hemming, 2001). Rapid changes in climate conditions during these times occurred on decade to century timescales. Recent studies of MIS 5 sea level (this study) and North Atlantic climate (McManus *et al.*, 1994; Chapman and Shackleton, 1999) now reveal comparable complexity. The mechanisms responsible for these rapid variations have not yet been clearly established, however a comparison of these records with the sea-level observations presented earlier in this chapter provide some hints on the processes of insolation, atmosphere, ocean and ice sheet interaction during these periods.

Marine isotope stage 3 and major deglaciations

Two main frequencies of variability are evident in the MIS 3 Greenland $\delta^{18}O$ temperature records (figure 4.9). Rapid millennial-scale oscillations known as Dansgaard-Oeschger (D-O) cycles are modulated by longer period (5-10 ka) Bond cycles (Dansgaard *et al.*, 1993; Bond *et al.*, 1993). Gradual cooling over a Bond cycle culminates in an extreme D-O cold period, which is then followed by a rapid warming (figure 4.10). The coldest part of the Bond cycles are correlated with episodes of decreased sea surface temperature (SST) in the North Atlantic inferred from increase in the abundance of *N. pachyderma (s.)* in North Atlantic sediment cores (Bond *et al.*, 1993). Distinctive layers of ice rafted debris

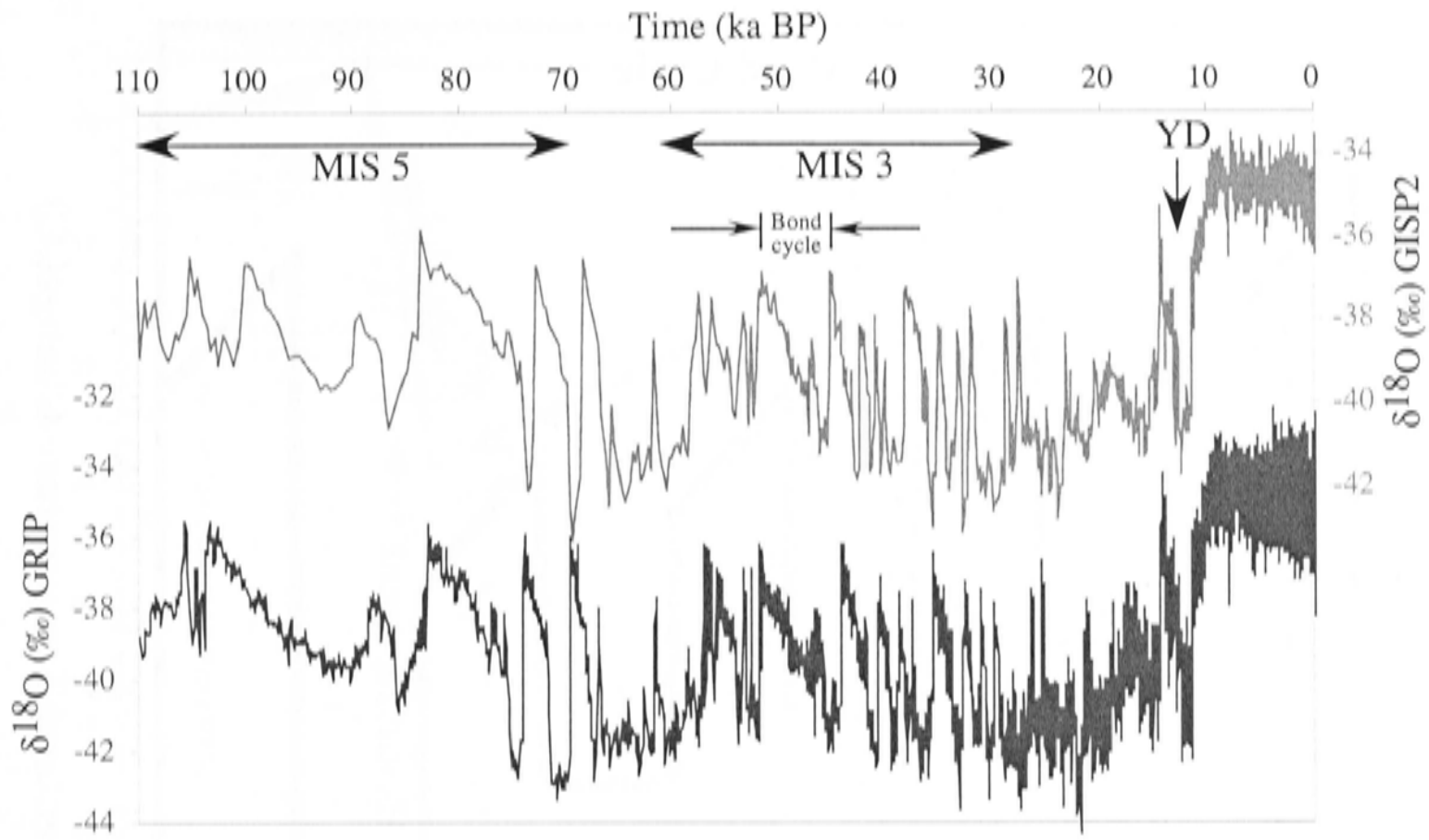

Figure 4.9: Greenland ice core δ^{18}O records, GRIP and GISP2. The rapid D-O oscillations can be seen during the later part of the record (stage 3) but not during stage 5.

(IRD) in the sediment cores are also associated with these extreme events (Heinrich, 1988; Bond *et al.*, 1993; Chapman *et al.*, 2000; Bond and Lotti, 1995; see figure 4.11). These IRD deposits, known as Heinrich layers, thicken towards the Hudson Bay area of northern Canada and predominantly consist of detrital carbonate-enriched material that is characteristic of that region. Heinrich layers also contain smaller amounts of material from other iceberg source areas around the North Atlantic (Bond and Lotti, 1995).

The Heinrich layers were deposited rapidly and have been interpreted to represent ice rafting during episodic, catastrophic partial decay of the Laurentide Ice Sheet over Hudson Bay. MacAyeal (1993a, b) proposed that the sudden collapse of the ice sheet may have occurred due to a build up of basal heat over the period of a Bond cycle, which triggered sliding and surging of ice. One hypothesis is that the influx of freshwater to the North Atlantic triggers an interruption of the thermohaline circulation (THC) and reduced North Atlantic Deep Water (NADW) formation (MacAyeal, 1993a). In that scenario, there is a reduction of northward heat transport via THC resulting in the discrete cold events in the observed North Atlantic SST and Greenland atmospheric temperature records, which correspond to the IRD layers. Accompanying changes in oceanic circulation and bottom water conditions during these events are recorded in δ^{13}C variations in the same North Atlantic sediment cores (Chapman and Shackleton, 1998). Sub-orbital period sea-level oscillations during MIS 3 have been constrained from the uplifted coral terraces

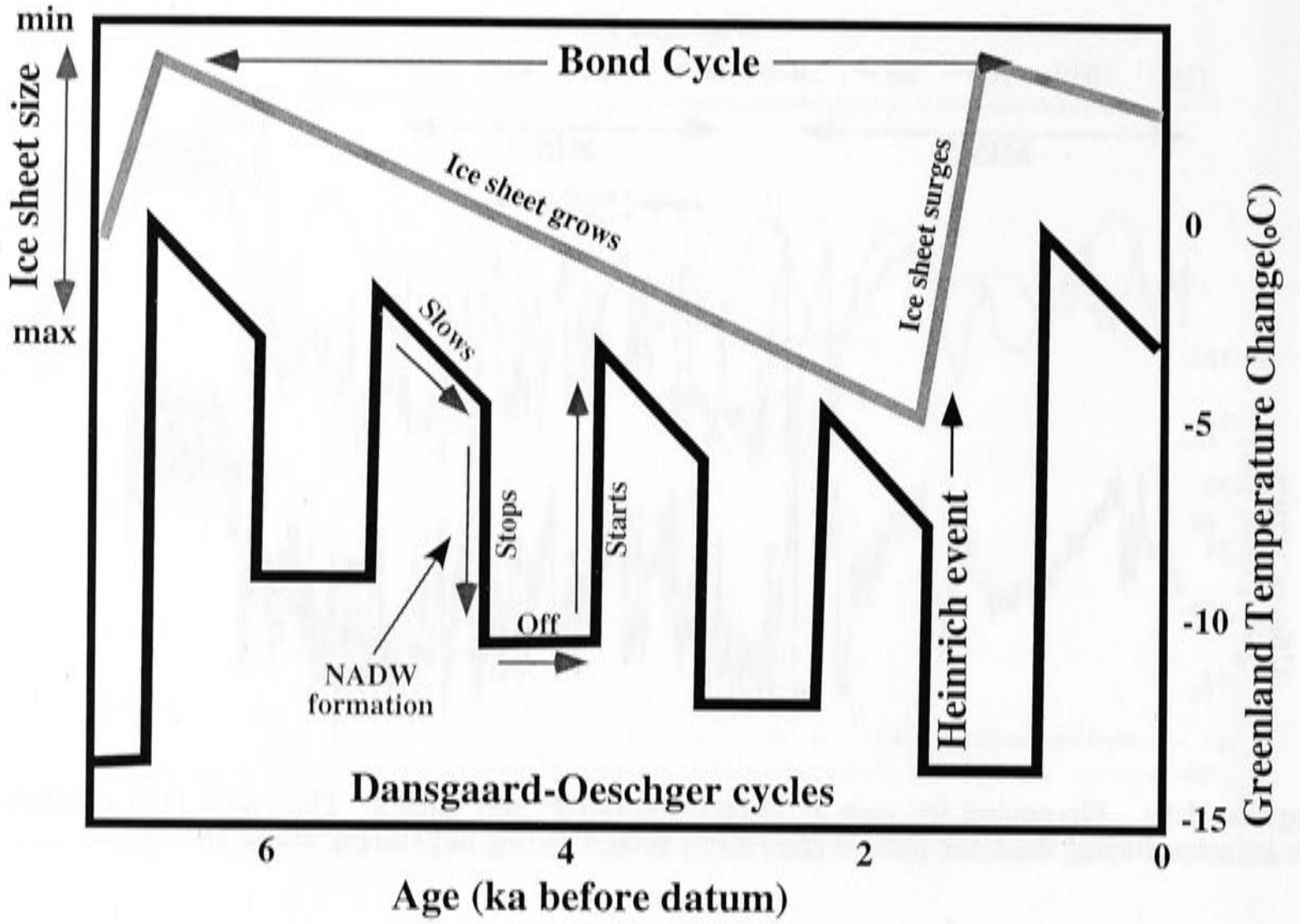

Figure 4.10: Schematic representation of Dansgaard-Oeschger cycles and Bond cycles (modified from Alley, 1998). Millennial-scale temperature variations (D-O cycles) are observed in the Greenland ice core $\delta^{18}O$ records. Average temperatures fall over several of these D-O cycles as ice builds up in the Laurentide ice sheet. The timing of minimum in temperature corresponds to the deposition of massive amounts of ice rafted debris (IRD) across the North Atlantic Ocean. This IRD is deposited by icebergs released during a partial collapse of the Laurentide ice sheet.

at Huon Peninsula, PNG (Yokoyama *et al.*, 2001b; Chappell, 2002) and are inferred to be a direct consequence of sudden massive ice and melt-water discharge during Heinrich events.

Smaller, intermediate IRD events, which occur on the shorter D-O period cyclicity, have also been identified in the Irminger Basin, the Norwegian Sea (Elliot *et al.*, 1998, 2001) and elsewhere in the North Atlantic (Bond and Lotti, 1995). These IRD layers consist of material from multiple iceberg source-regions in the North Atlantic. However, the trigger of these minor ice-rafting events has not yet been established. Nor is it clear by what mechanism these apparently small ice rafting events are sometimes amplified to appear as episodes of strong D-O cooling over Greenland. Elliot *et al.* (1998) suggest that episodic destabilisation of coastal ice sheets such as the Icelandic, Greenland and Fennoscandian ice sheets may be the origin of these 'D-O' ice rafting events. However, the apparent synchroneity of ice rafting from multiple source areas recorded in these events has prompted some researchers to suggest that an external forcing mechanism, such as an atmosphere-ocean interaction, triggered the ice sheet destabilisation (Bond and Lotti, 1995). The

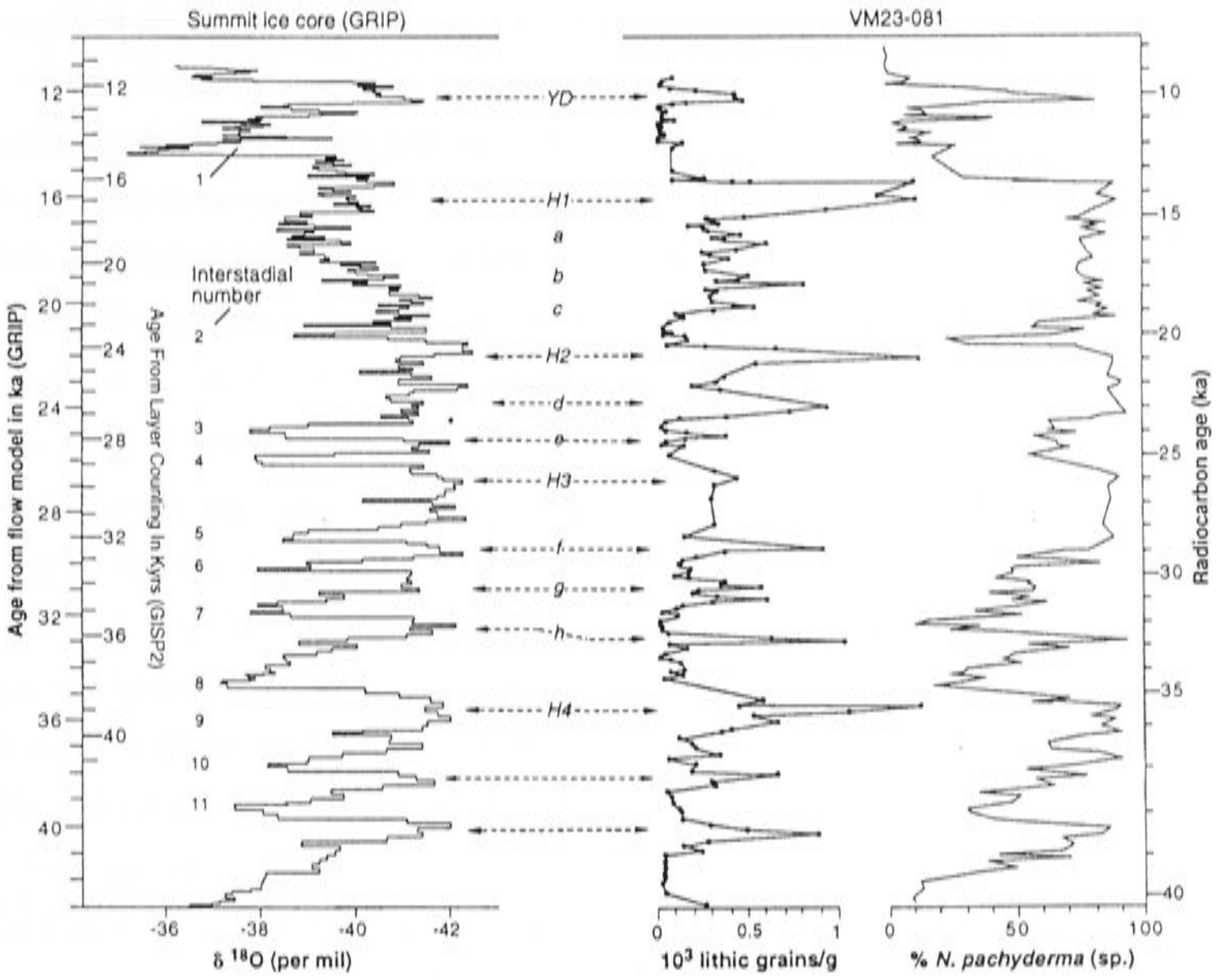

Figure 4.11: Correlation of extreme cooling events over Greenland during MIS 3 (from GRIP δ^{18}O record) with episodes of enhanced IRD deposition (lithics grains/g) and decreased sea surface temperature inferred from *N. pachyderma* abundance (from Bond and Lotti, 1995).

external forcing hypothesis is supported by evidence of a 1500 yr periodicity in the North Atlantic sediment record during the Holocene, at a time of minimal ice volume (Bond *et al.*, 1997). The presence of ice in the North Atlantic region during glacial times may simply act to amplify an inherent oscillation in the climate system. In summary, climate and ice volume during MIS 3 change with a much higher frequency than predicted by insolation forcing and occur at a time of low insolation variability.

During the last deglacial transition there was a major climate reversal, at ~11.5 ka, known as the Younger Dryas (YD) (figure 4.9). Oceanic and continental records indicate a strong cooling event during the YD which lasted for ~1 ka (review - Peteet, 1993). The timing of the sequence of events during the YD is much better than for the rapid oscillations during MIS 3 and is therefore useful for examining the processes associated with such rapid climate events. In North Atlantic Ocean sediment records, the YD period is accompanied by a small Heinrich event, H0. Two periods of rapid sea-level rise (exceeding 40 mm/year, Fairbanks, 1989; Bard *et al.*, 1990), known as melt-water pulses 1A and 1B (mwp-1A,B),

bracket the YD period. The source of the rapid rises are not well established. However, Clark *et al.* (2002a) suggest that the Antarctic Ice Sheet made a substantial contribution to mwp-1A. During the Younger Dryas period, the rate of global sea level rise is reduced (Lambeck *et al.*, 2002a). The last deglaciation and the YD event occur during a period of rapid insolation change and may better correspond to the insolation conditions during MIS 5, in contrast to the MIS 3 events. Two alternative scenarios that may explain the sequence of events surrounding the YD are discussed below:

1. Perhaps the sea-level rise associated with isolation-induced melt during the last deglaciation triggered a destabilisation of North Atlantic coastal ice sheets, leading to the H0 ice rafting event and subsequent interruption of THC and YD cooling. In this scenario, the cold-snap in the North Atlantic region temporarily dominates over the effects of rising insolation, hence leading to the reduced rate of sea-level rise during that period. This is in contrast to the sequence of events during MIS 3, where is it thought that the collapse of the LIS is the source of the sea level rise. The process leading to the YD climate oscillation may be different to those leading to the D-O cycle and Heinrich events during MIS 3.

2. Clark *et al.* (2001) propose a model in which re-routing of melt-water from southern drainage through the Mississippi River to eastern drainage through the St Lawrence Gulf is triggered by the retreat of the Laurentide Ice Sheet's southern margin out of the Lake Superior basin. It is suggested that melt-water drainage in the Gulf of Mexico acts to promote THC whereas a sudden drainage via the eastern route may have interrupted the THC. The rapid draining of pro-glacial Lake Agassiz via an eastern route may have contributed to the sudden interruption of North Atlantic Ocean circulation (Teller *et al.*, 2002). Oscillatory behaviour of the southern Laurentide ice margin, promoted by feedback effects from the resulting climate changes in the North Atlantic would occur when the ice margin was close to the eastern drainage outlet, at times of intermediate ice volume. Clark *et al.* (2001) propose that the interruption of the THC produced conditions favourable for readvance of the Laurentide Ice Sheet's southern margin hence setting up a feedback loop. In this scenario, the ice rafting events occur as a consequence of the North Atlantic cooling rather than being the trigger. This model provides a mechanism for why millennial scale oscillations occur during periods of intermediate ice volume, ie, last deglaciation and MIS 3. However, it does not explain the persistence of millennial scale variability during periods of low ice volume, such as the Holocene.

During MIS 3, insolation variability (65°N summer) was much lower than other periods during the last glacial cycle. The role of insolation forcing during the last and penultimate deglaciation is unclear. The penultimate deglaciation also appears to have been accompanied by a climate reversal, perhaps analogous to the YD. This event is recorded as an oscillation in sea level prior to the last interglacial high-stand (Esat *et al.*, 1999; Gallup *et al.*, 2002) and is also evident in other proxy climate records around the world (Bar-Matthews *et al.*, 2000; Chapman and Shackleton, 1998). A Heinrich-like ice rafting event, H11, and accompanying decrease in sea surface temperature occurred during the penultimate deglaciation (Chapman and Shackleton, 1998), however the timing of this event relative to the deglacial sea-level change is unclear. Perhaps insolation induced sea-level rise, either summer 65°N (or another insolation index), led to the destabilisation of coastal ice sheets, such as discussed in scenario (1) on the previous page, or modulated some kind of internal climate oscillation. Without further constraint on the relative timing of these events, the mechanism will remain unclear.

Marine isotope stage 5

North Atlantic sediment core records indicate episodic ice rafting events, accompanied by reduced SST during MIS 5 (Chapman and Shackleton, 1998; Chapman and Shackleton, 1999; McManus *et al.*, 1994; Oppo and Lehman, 1995, Oppo *et al.*, 2001). Chapman and Shackleton (1999) use a correlation of sediment lightness in core NEAP18K with GISP2 δ^{18}O variations to show that these events also correlate with cold episodes over Greenland. These MIS 5 events occur with a similar periodicity but are smaller in magnitude than the Heinrich events of MIS 3. The composition of the MIS 5 IRD material includes detrital carbonate, haematite-stained quartz and dark basaltic glass, which indicate multiple iceberg source regions (Chapman and Shackleton, 1999; Bond and Lotti, 1995). Records of MIS 5 sub-orbital climate variability are seen well into the sub-tropical North Atlantic (Oppo *et al.*, 2001). The more intense IRD events (C21 and C24) penetrate further south and east than the smaller ones (C19, C20, C22, C23 and C25) (figure 4.12f, labels by Chapman and Shackleton, 1999). Oppo *et al.* (2001) also identified shorter period variability (1-4 ka) during MIS 5 in a western subtropical Atlantic planktonic δ^{18}O record (site 1059). However, this D-O periodicity signal is not a dominant feature in the IRD and Greenland δ^{18}O records. Similarly, small-magnitude, short-period oscillations (~1500 years) are evident in some Holocene records, a time of minimal ice volume (Bond *et al.*, 1997).

The differences between the MIS 3 and MIS 5 records may be attributed to the dif-

ferent distribution of ice during those two periods. Global ice volume during MIS 5 was generally smaller than MIS 3 and coastal ice sheets surrounding the North Atlantic may have been less extensive during the earlier period and therefore less susceptible to collapse. The spatial distribution of ice in the Laurentide Ice Sheet during MIS 5 and MIS 3 and the last deglaciation was very different (Clark *et al.*, 1993; also see discussion in chapter 6). Clark *et al.* (1993) suggest that ice was more extensive in the north of the North American continent than at later times during the glacial cycle. The southern margin remained north of the St Lawrence Lowlands for much of MIS 5 and so the ice may not have reached far enough south to trigger changes in the southern/eastern drainage routes via the mechanism proposed by Clark *et al.* (1998) to explain the millennial scale interruptions to the THC during the last deglaciation and perhaps MIS 3. The fact that the composition of the MIS 5 IRD events is not predominantly Hudson Bay material is consistent with other observations that suggest the Laurentide Ice Sheet contained a smaller proportion of the global ice volume during MIS 5 than during MIS 3 or the LGM (Clark *et al.*, 1993; Kleman *et al.*, 2002; and the conclusions of chapter 6). Therefore, the Laurentide ice sheet may not have been susceptible to 'Heinrich-event' catastrophic collapse at that time. Svendsen *et al.* (1999) suggest that the ice cover over Arctic Russia, and into the Kara Sea, was much more extensive during the early period of MIS 5. Perhaps instability of this ice sheet is responsible for some of the MIS 5 sub-orbital climate variability.

The sub-stage 5a and 5c sub-orbital period sea-level excursions that have been identified at Barbados and Huon Peninsula and appear to be superimposed on the broad $\delta^{18}O$ signal cannot be explained by simple insolation forcing. Because of these time-scale uncertainties, linking variations in these records with the timing of sea-level excursions is difficult.[10] However, the number of sea-level events discussed in this chapter may be linked to the discrete events seen in the Greenland ice core and North Atlantic sediment records during MIS 5 (figure 4.12).

How are the MIS 5 sea-level excursions related to climatic events in the North Atlantic? Two speculative scenarios that link MIS 5 sea-level oscillations to the North Atlantic climate system are explored below:

1. In the first hypothetical scenario, internal ice sheet instability and collapse leads to a rise in sea level which is similar to the mechanism proposed for the Heinrich

[10]The time-scales of the Greenland ice core during MIS 5 are based on ice dynamical models and correlation with the marine oxygen isotope records (Meese *et al.*, 1994; Bender *et al.*, 1994) so absolute ages may be uncertain by up to several thousand years (see differences in the GISP2 and GRIP records in figure 4.9). MIS 5 events in the North Atlantic sediment cores cannot be dated directly but can be tied to the GISP2 record (Chapman and Shackleton, 1999).

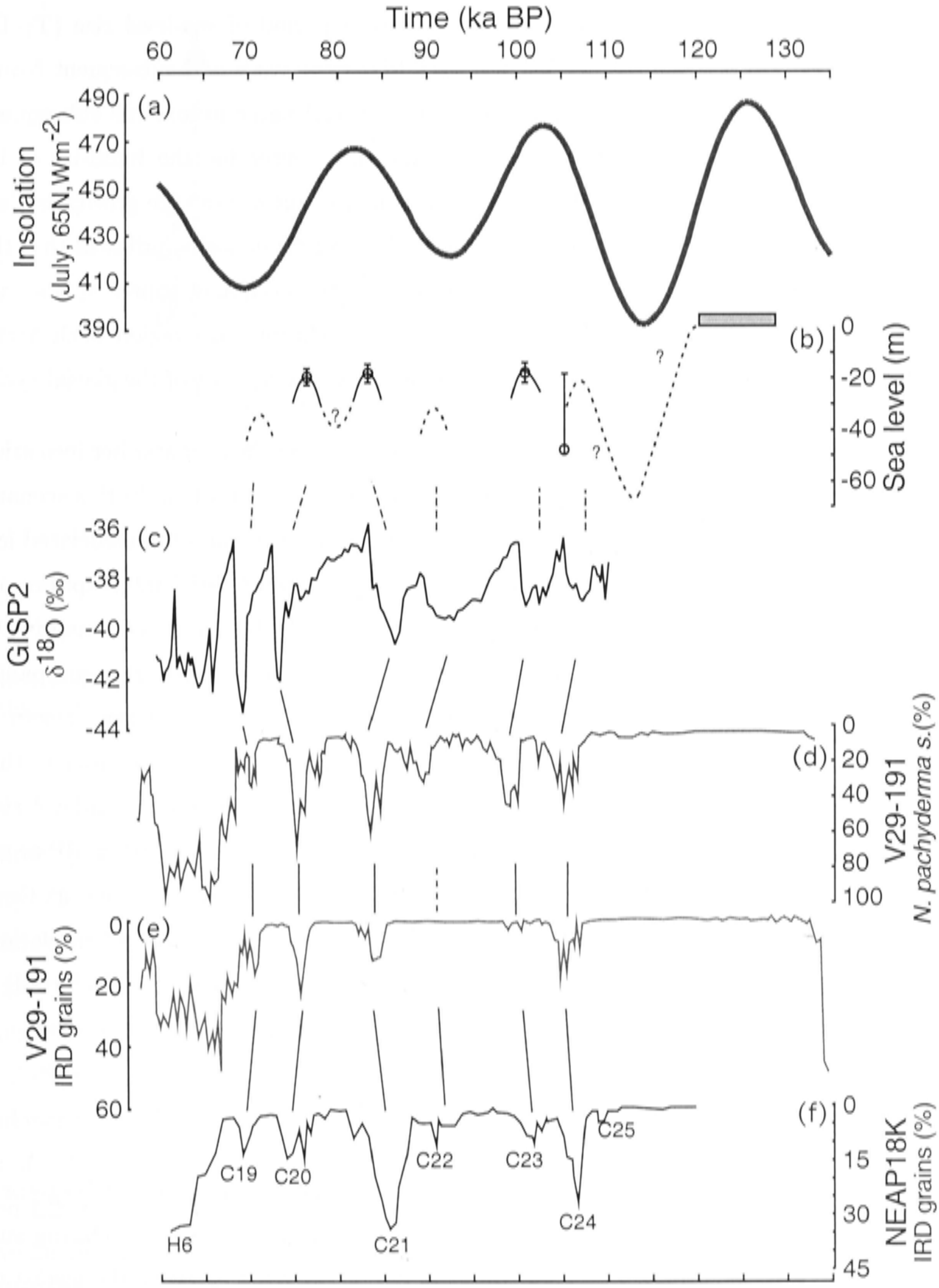

Figure 4.12: Comparison of timing of sea-level oscillations identified at Barbados (circles) and other locations (dashed curves) with a) 65°N summer insolation (Berger and Loutre, 1991); b) Composite Barbados and Huon Peninsula sea level record. The sea levels in the solid curves are the estimates of Barbados sea level from the present study and the dashed curves are the Huon Peninsula estimates of intermediate sea level events not identified at Barbados; c) GISP2 $\delta^{18}O$ record (Grootes *et al.*, 1993; Grootes and Stuiver, 1997) plotted on ice core timescale (Bender *et al.*, 1994); d) V29-191 *N. pachyderma (s.)* abundance - high values indicate low SST (from McManus *et al.*, 1994); e) V29-191 IRD % - ratio of total coarse particles to bulk sediment weight (from McManus *et al.*, 1994). Time scales of V29-191 records are approximate, but can be directly correlated with the NEAP18K record in panel (f); f) NEAP18K IRD %, time-scale tied to GISP2 using sediment core lightness (from Chapman and Shackleton, 1999).

events (MacAyeal, 1993a, b). In this scenario, a period of sea-level rise (T_1-T_2, in figure 4.13) corresponds to the timing of IRD deposition and subsequent North Atlantic cooling. After the reduction of ice and freshwater influx, the subsequent restart of the THC results in a renewed moisture source for the build-up of ice (T_2-T_3). The process of ice sheet destabilisation and subsequent ice growth is then repeated (T_3-T_4-T_5). The composition of the MIS 5 IRD deposits indicates that the large-scale collapse of the LIS was not necessarily the dominant source of sea-level rise during MIS 5. The source may lie with other ice sheets in the region, such Arctic Russia, where ice cover was more extensive during the early part of the glacial cycle.

2. Alternatively, insolation-induced melt associated with the 65°N or another insolation index may have been the cause of the initial sea-level rise (T_1-T_2). In this scenario sea-level rise triggers the destabilisation of coastal ice sheets and the associated ice-rafting events. In this case, the IRD event and associated THC interruption and North Atlantic cooling coincide with the peak sea level (T_2). The cold snap in the North Atlantic prevents further melting. Renewed moisture transport accompanies the restart of the THC leading to a sea level fall (T_2-T_3) as ice sheets began to grow, before insolation again dominates (T_3-T_4). This mechanism is similar to that discussed earlier for the YD climate reversal and associated pause in sea-level rise. This scenario cannot explain the early sub-stage 5a sea-level rise at ~91 ka BP or the additional sea-level oscillation at ~71 ka, both of which occurred during at times of low insolation (figure 4.12). It is most likely that a combination of insolation-induced melt and ice sheet destablisation (either internally or externally forced) is responsible for the observed sea-level record.

Conclusion

Broad variations in ice volume during the Pleistocene, inferred from stacked $\delta^{18}O$ records appear to correspond to the dominant frequencies of insolation variability. During sub-stages 5a and 5c, only two sea level high-stands would be expected based on the insolation forcing model. In contrast, at least five sea level events during this period have been recorded at Huon Peninsula, although the timing of these has not been well constrained. Three distinct periods of reef growth during sub-stages 5a and 5c have been constrained by U-Th dating at Barbados (this study). These include the 'classic' sub-stage 5a and 5c sea-level high-stands, at 84 ka and 101 ka BP, which roughly correspond to insolation maxima, and a secondary sub-stage 5a feature at ~77 ka. These additional sub-orbital period sea-level variations appear to be superimposed on an orbitally-forced signal.

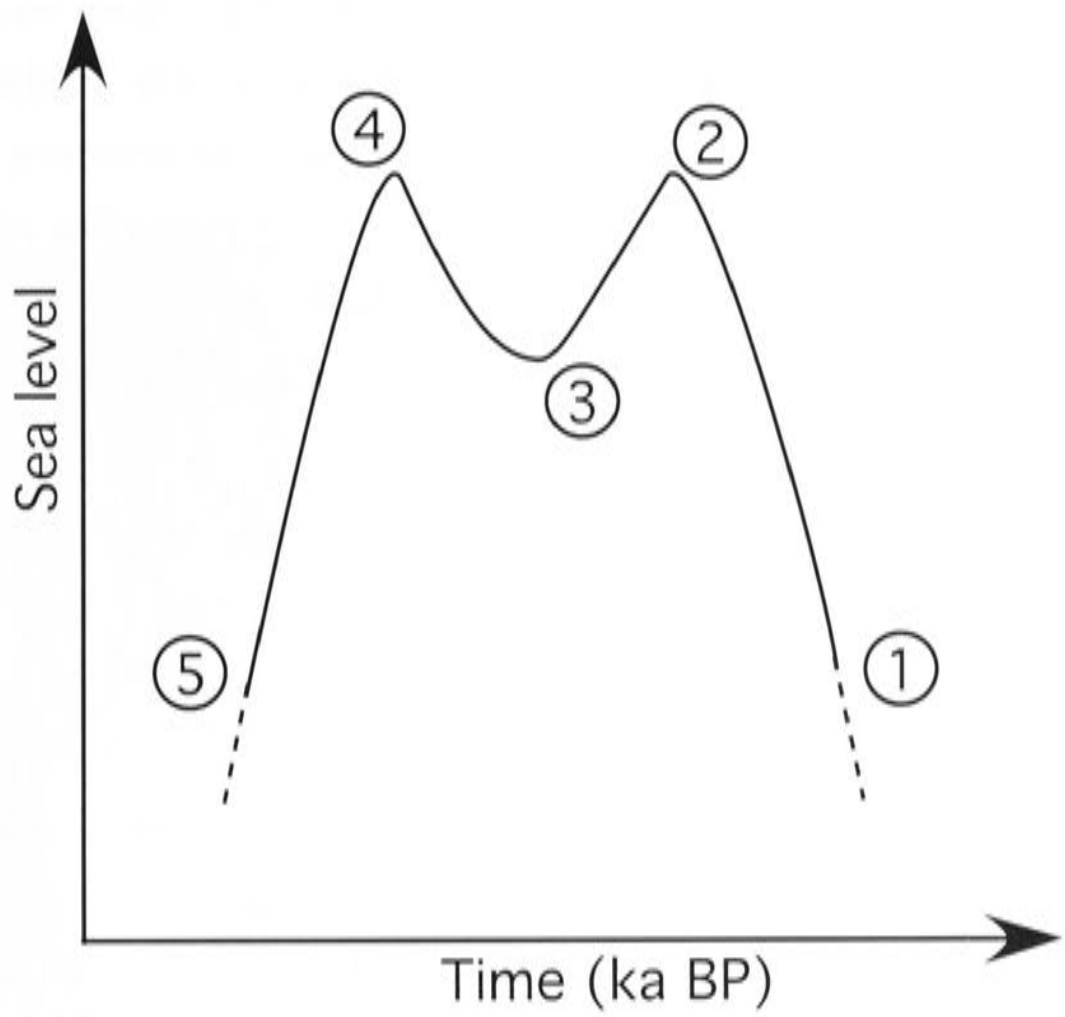

Figure 4.13: Schematic representation of multiple sea-level oscillations during sub-stage 5a. Referred to in text.

There appears to be a correspondence between MIS 5 sea-level oscillations and climate events in the North Atlantic, however the relative timing of these is yet to be established. The dominant periodicity of oscillations in the North Atlantic during MIS 5 is ~5-10 ka and is similar to the Bond cycles (and Heinrich events) of MIS 3. However there are some important differences in the records from these two periods which suggests that ice volume and distribution during MIS 5 was significantly different to MIS 3. This is supported by independent observations of ice distribution for those periods (Clark *et al.*, 1993; Svendsen *et al.*, 1999). The composition of these MIS 5 IRD layers, and their smaller size, suggests the LIS was not the dominant contributor to instabilities during that period. This is consistent with estimates of Laurentide ice volume and global ice distribution during that period (Clark *et al.*, 1993; and chapter 6). In conclusion, it appears that the ice volume and climate variability during MIS 5 reflect interplay between insolation forcing and North Atlantic climate instability.

4.5 Stage 5a sea level in the Caribbean region

Based on the measurements in this study, sea level at Barbados during sub-stage 5a reached a peak of -19±4 m. However, estimates of sub-stage 5a sea level from other

locations throughout the rest of the Caribbean and surrounding region vary by over 20 m, which is well outside the uncertainties of these individual estimates. In this section, I will review the observations of stage 5a (and 5c) relative sea-level observations for this region. Later, in chapter 6, I will demonstrate that these seemingly conflicting observations can be reconciled by taking into account the effects of glacio-hydro-isostatic deformation of the earth in this region in response to the growth and decay of the Laurentide Ice Sheet.

4.5.1 Haiti

Dodge *et al.* (1983) identified a series of uplifted coral terraces of late Pleistocene age on the Northwest Peninsula of Haiti, reaching an elevation of over 600 m. Most show well defined *Acropora palmata* reef crest facies but the older terraces are extensively weathered and most are unsuitable for dating (Mann *et al.*, 1995). Regardless, Dodge *et al.* (1983) used U-Th dating methods to define the approximate ages of the three lowest main reefs. The last interglacial formation, analogous to the "1^{st} High Cliff" at Barbados, reaches a height of 52 m above sea level and was found to have an age of 130±6 ka. The two lower reefs, at heights of 28 and 16 m, were dated at 108±5 and 81±3 ka (sub-stage 5c and 5a) respectively. The paleo-sea level calculated for the stage 5c and 5a high-stands at Haiti using the ages determined in the present study are -10±3 m and -12±3 m, assuming an age of 125±5 ka for the last interglacial reef and a sea level of 4±2 for the last interglacial high-stand (as in section 4.3). Neither Dodge *et al.* (1983) or Mann *et al.* (1995) note any further complexity in the structure of the MIS 5 reef deposits at this site.

4.5.2 Bahamas

At several sites on north Eleuthera, Hearty and Kaufmann (2000) report skeletal eolianites of 5a age overlying well developed oolites (of stage 5e age) . These two distinct deposits are separated by a moderately developed paleosol and karst surface. The age distinction between these two units has been established using amino acid racemization techniques. This is not a precise dating technique, but these results suggest a distinct separation in the time of deposition consistent with the ~40 ka separation between the stage 5e and 5a sea-level high-stands. Hearty and Kaufmann (2000) suggest that the younger eolinite deposits are the result of a sea-level high-stand of between -5 and 0 m at that time. Kindler and Hearty (1996) and Hearty and Kindler (1993) also describe morphologically similar deposits on the islands of Abaco, Bimini and San Salvador. In some locations the stage 5a unit is overlain by an upper paleosol that separates these deposits from the Holocene unit.

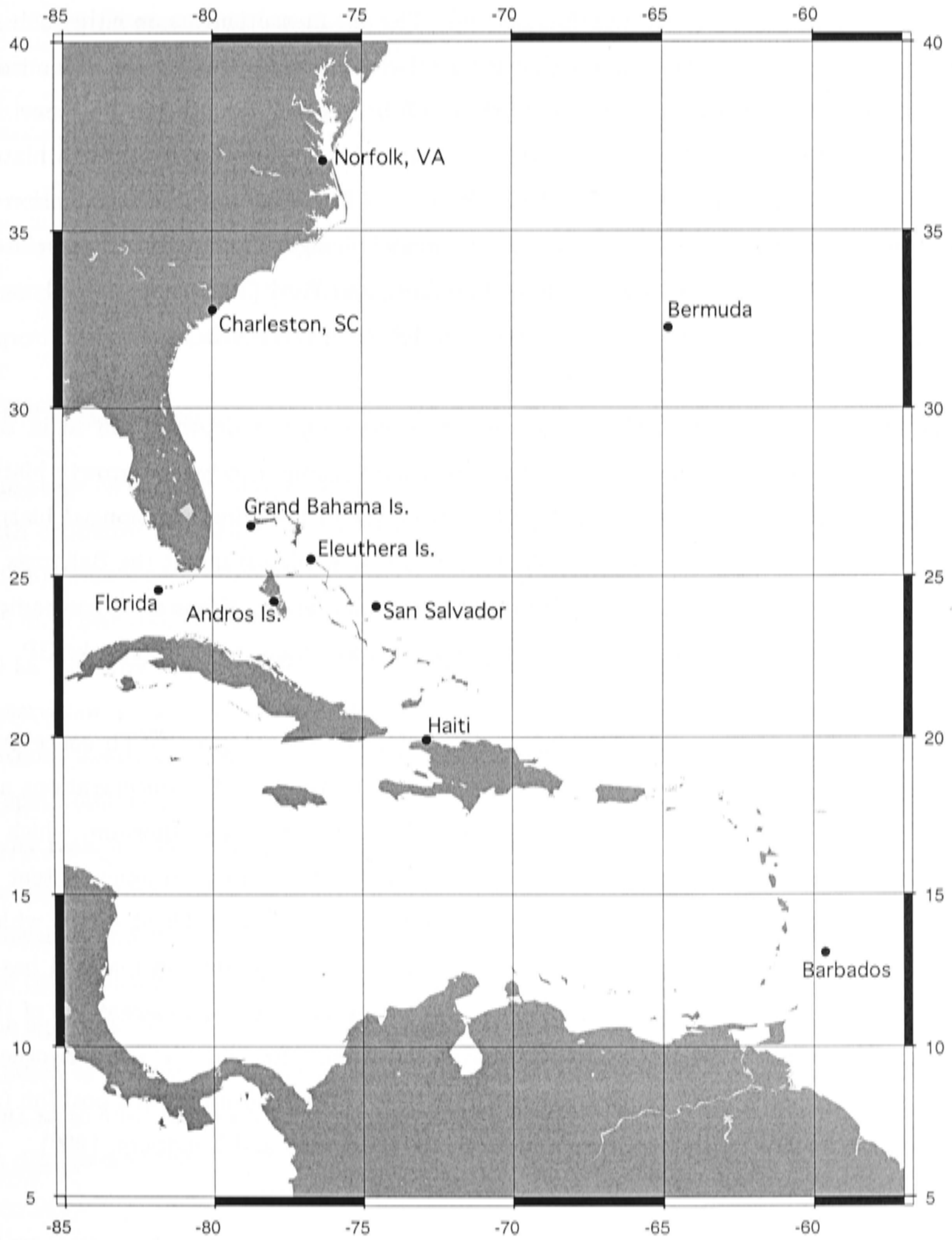

Figure 4.14: Map of the Caribbean area. Sub-stage 5a and 5c sea-level observations for the sites marked are discussed in the text and summarised in figure 3.1.

Lundberg and Ford (1994) presented the results of U-Th dating of a submerged flowstone, DWBAH, collected at a depth of 15 m. This depth estimate was recently revised to up to ~8.5 m (Toscano and Lundberg, 1999). The age measurements on either side of a growth hiatus of DWBAH suggest that sea level rose to above this level at some time between 108 ka and 93 ka but remained below -8.5 m from 93 ka until the Holocene. It is not clear whether sub-stage 5c sea level rose above this level during the growth hiatus between ~108 ka BP and ~93 ka BP. Richards *et al.* (1994) point out that termination of speleothem growth can also occur because of regional changes in climate and associated changes in groundwater recharge. Indeed, Lundberg and Ford (1994) note that there is no evidence of marine overgrowth in that growth hiatus of DWBAH.

Richards *et al.* (1994) studied a speleothem recovered from a depth of -18 m in Lucayen Caves, Grand Bahama Island. U-Th ages of sub-samples overlying a growth hiatus suggest that this speleothem resumed growth at ~79.4 ka following a prolonged hiatus. This observation is consistent with a sub-stage 5a sea-level high-stand at the Bahamas of higher than ~-16 m (after correction for Pleistocene subsidence). However, it contradicts the observation at Barbados that sea level at ~77 ka was similar to that at 84 ka BP.

The 79.4 ka sample analysed by Richards *et al.* (1994) has a higher ^{232}Th concentration than other sub-samples of the same speleothem. Elevated ^{232}Th concentrations are an indicator of detrital contamination or the initial incorporation of thorium, which is expected to increase the apparent age of a sample, depending on the isotopic content of the contaminating material.[11] The 79.4 ka sample has a ^{230}Th/^{232}Th of ~190, which is within the generally acceptable limits. However, if the contaminating material has a high ^{230}Th/^{232}Th, such as marine carbonate, this would increase the apparent age of the sample without producing an elevated ^{232}Th concentration. Alternatively, the speleothem analysed by Richards *et al.* (1994) may not have been collected from growth position (as was the case for DWBAH; Lundberg and Ford, 1994; Toscano and Lundberg, 1999).

4.5.3 Florida

Sub-stage 5a age deposits have been identified as submerged reefs 10-12 m below present sea level off the south-east Florida Keys (Toscano and Lundberg, 1999; Ludwig *et al.*,

[11] Following the same arguments as is used for the dating of coral samples, speleothems are assumed to have negligible thorium content at the time of formation. A low ^{230}Th/^{232}Th ratio indicates that the sample contains extraneous ^{232}Th and corresponding excess ^{230}Th. Generally, samples with a ^{230}Th/^{232}Th activity ratio higher than 100 are considered reliable however this criterion is highly dependent on the isotopic composition of the contaminant which may vary.

1996). Drilling of these reefs and subsequent U-Th TIMS dating reveal a thick deposit corresponding to the classic stage 5a sea-level maximum which is overlain by Holocene-age corals. The ages measured for the deposit range between 81-86 ka (Ludwig *et al.*, 1996) and 81-83 (Toscano and Lundberg, 1999). Taking into the minimum growth depth of the *Montastrea sp.* samples that were analysed and possible submergence of this site, these authors conclude that sea level was no lower than 6-10 m below present during stage 5a.

Several ages of between ~91-95 ka were measured for corals lying beneath the sub-stage 5a deposit (Toscano and Lundberg, 1999). It is possible that these corals were deposited during an older sea-level transgression prior to the main stage 5a high-stand. This older deposit may correspond to the reef Va_{main} at Huon Peninsula.

4.5.4 Bermuda

Sub-stage 5a age deposits at Bermuda have been the focus of controversy for some years, with estimates of stage 5a sea level ranging between <-15 m and +1 m. Harmon *et al.* (1983) present results of U-Th dating of submerged speleothems collected from a depth of -15 m. Their results suggest that the speleothem grew continuously between 111±9 ka and 10 ka BP, which restricts the sea-level high-stand during stage 5a to below -15 m. This observation is inconsistent with the well constrained -6 to -10 estimate at Florida (with or without isostatic considerations, see chapter 6). The upper age limit is based on a single α-spectrometry age measurement (typical sample size of 50-100g). The $^{230}Th/^{232}Th$ activity ratio is quoted as '>200', which is within acceptable limits. However, depending on the isotopic composition of any contaminating material (the sample was taken from near a growth boundary or hiatus) this apparent age could be higher than the true age. Again, if the contaminating material has a high $^{230}Th/^{232}Th$ ratio, such as older marine carbonate, the age could be affected without changing the ^{232}Th concentration. Another speleothem studied by Harmon *et al.* (1983) at a depth of 3 m suggests that it grew continuously from ~97 ka to after ~68 ka BP, but this constraint may also subject to the same uncertainties as discussed above.

U-Th dating of coral deposits at Fort St Catherine, Bermuda (Ludwig *et al.* 1996; Muhs *et al.*, 2002) give a range of ages (78-84 ka) which correspond to the timing of sub-stage 5a. Harmon *et al.* (1978, 1983) and Toscano and Lundberg (1999) attribute deposits of this age to storm (wave) deposition. Indeed, these corals do not seem to be in growth position (Muhs *et al.*, 2002). However, the deposit does not appear to contain samples of any other age which suggest that they are probably part of a cobble unit associated with the stage 5a

high-stand at that time. This conclusion is supported by a detailed stratigraphic study of a number of sites on the Bermuda coast by Vacher and Hearty (1989). Vacher and Hearty identified a number of locations where the stage 5e age deposits ("Devonshire Formation") are overlain by younger eolianites and some marine deposits. Aminostratigraphy of these younger deposits suggest a correlation with a stage 5a high-stand. Some of the sites are part of reasonably protected shorelines which suggests that they are not the result of storm deposits as argued by Harmon *et al.* (1978, 1983) and Toscano and Lundberg (1999).

At this stage, there is no reasonable explanation for the discrepancy of estimates of stage 5a sea level at Bermuda between the submerged speleothem (Harmon *et al.*, 1983) and eolinite and marine deposits (Vacher and Hearty, 1989; Ludwig *et al.*, 1996; and Muhs *et al.*, 2002). However, the constraint placed on the maximum sub-stage 5a sea level by Harmon *et al.* (1983) is based on two ages, which may be susceptible dating uncertainties. It would be useful to have more age measurements in those speleothem samples to check for stratigraphic consistency on shorter timescales.

Vollbrecht (1990) dated coraliferous deposits from submerged ridges off the Bermuda coast at a depth of -12 to -18 m. The ages, which range between ~94 ka and ~114 ka indicate deposition during sub-stage 5c.

4.5.5 US East Coast

Cronin *et al.* (1981) and Szabo (1985) investigated several marine fossil deposits above present sea level on the south-east US Coast which contain isolated corals in 'sediments of a detrital character'. At Charleston, South Carolina, the marine unit consists of shelly, clayey sand with faunal assemblages similar to that in regional modern coastal waters and reaches an elevation of 3-10 m above present sea level. The average U-Th age of 7 coral samples collected from this deposit is 89 ka (or 87±4 ka if corrected for detrital contamination), and is probably associated with the stage 5a sea-level high-stand. At Norfolk, Virginia the marine deposit reaches an elevation of 4-10 m above present sea level and contains fossils that are also consistent with modern faunal assemblages. The mean age of 9 samples is 71±5 ka, which suggests this deposit corresponds to the timing of the secondary stage 5a feature identified at Barbados in this study. The reliability of this age is supported by concordant ^{231}Pa ages measurements for the three of these samples (Szabo, 1985). More recent age analyses for these and other deposits along the US East Coast range between 72 and 84 ka (J. Wehmiller, pers. comm.).

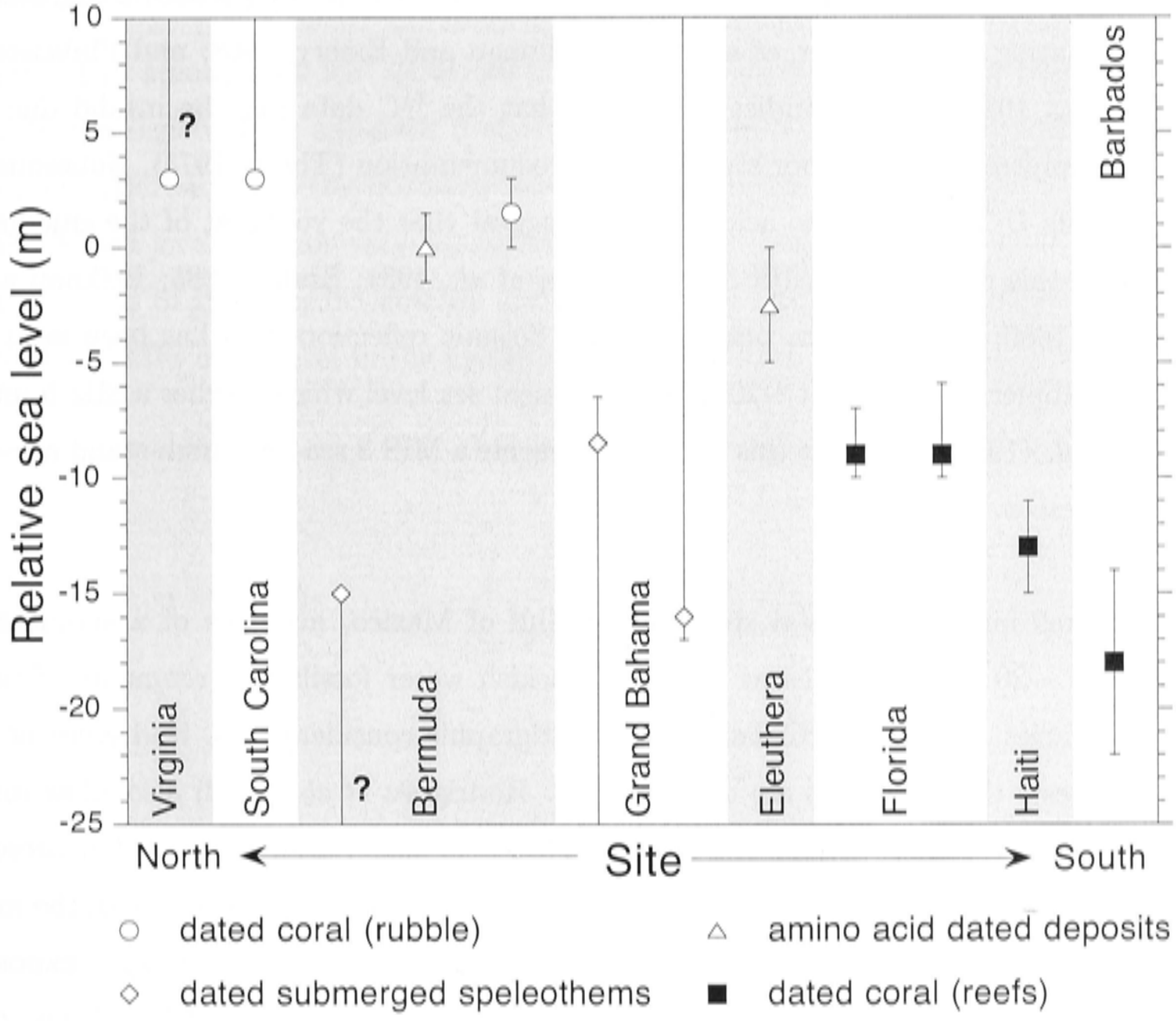

Figure 4.15: Summary of observations of stage 5a relative sea level in the Caribbean and surrounding region. Estimates based on dated coral reefs, submerged speleothems, coral rubble units and undated or amino acid racemisation dated stratigraphic units. US East Coast - Szabo (1985), Cronin *et al.* (1981); Bermuda - Harmon *et al.* (1978, 1983), Ludwig *et al.* (1996), Muhs *et al.* (2002), Vacher and Hearty (1989), Hearty and Vacher (1994); Bahamas - Lundberg and Ford (1994), Toscano and Lundberg (1999), Richards *et al.* (1994), Hearty and Kaufman (2000), Hearty and Kindler (1995), Kindler and Hearty (1996); Florida - Ludwig *et al.* (1996), Toscano and Lundberg (1999), Haiti - Dodge *et al.* (1983), Mann *et al.* (1995); Barbados - this study. The observation of sub-stage 5a sea level below -15 m at Bermuda is uncertain because of single age measurement used to constrain this constraint (see text for details). The observation at Norfolk, Virginia has an age of 71±5 ka and so may not correspond directly to the 'classic' sub-stage 5a peak.

Other time periods

MIS 3

In the Caribbean region, the maximum height reached by MIS 3 sea level has been the focus of controversy since the late 1960s. On the US Atlantic coast, marine deposits near present sea level were identified by early studies as representing a MIS 3 highstand using ^{14}C dating (Blackwelder *et al.*, 1979; Milliman and Emery, 1968; and Finkelstein and Kearney, 1988). Later studies concluded that the ^{14}C data may be invalid due to inadequate pretreating and poor stratigraphic documentation (Thom, 1973). Subsequent studies, using U-Th and amino-acid analysis, suggest that the youngest of the emergent deposits on this coast are of MIS 5 age (Cronin *et al.*, 1981; Szabo, 1985; Belknap and Wehmiller, 1980; J. Wehmiller, pers. comm.). Seismic reflection data has been used to identify a submerged barrier at ~20 m below present sea level which overlies a MIS 5 unit. Wellner *et al.* (1993) infer that this barrier represents a MIS 3 sea-level high-stand at ~20 m below present.

On the Texas inner continental shelf in the Gulf of Mexico, evidence of a submerged shoreline at ~20 m below present includes brackish water fossils and remnants of barrier island facies. Based on ^{14}C dating and stratigraphic considerations, Rodriguez *et al.* (2000) suggests these deposits are of MIS 3 age. Rodriguez *et al.* (2000) also allow for a subsidence rate of 1 mm/yr and infer that sea level may have reached 15 m below present during that period. However, this rate of subsidence is substantially greater than the long term subsidence rate of 0.01 mm/yr for this region inferred from the elevation of exposed last interglacial deposits (Paine, 1993). Therefore, if these deposits are of MIS 3 age, the sea level at that time was around ~20 m below present. These estimates contrast with the sea-level calculations for MIS 3 events at Huon Peninsula which reach no higher than 40 m below present (see figure 4.6).

Sub-stage 5e - the last interglacial period

In contrast to the sub-stage 5a and MIS 3 events discussed above, for which estimates of sea level vary across the Caribbean region, the maximum height reached during last interglacial does not vary significantly. At Bermuda, sea level rose to ~5±1 m above the present level based on the elevation of patch reefs and marine calcarenites (Harmon *et al.*, 1983) and other stratigraphic consideration and amino acid racemisation dating (Hearty and Vacher, 1994). At Florida, the Key Largo formation records a last interglacial sea-level highstand at ~5-6 m above present (Fruijtier *et al.*, 2000). At the southern Bahama island of Great Inagua and San Salvador, Chen *et al.* (1991) suggest sea level rose to

~4 m above present. This estimate is supported by other stratigraphic studies across the Bahamas (Hearty, 1998; Hearty and Kaufmann, 2000). The difference between the trends observed in the sub-stage 5a Caribbean deposits and the 5e evidence is addressed in chapter 6.

4.5.6 Summary

Figure 4.15 summarises the estimates of sub-stage 5a relative sea level throughout the Caribbean region. It is apparent that there is a gradient in sea-level estimates from the southern (Barbados) to the northern Caribbean (Bermuda, US East Coast) whereas sub-stage 5e sea levels do not vary significantly across the region. In chapter 5, I introduce the concepts of glacio-hydro-isostasy and in chapter 6, I apply these concepts in an investigation of MIS 5 sea level in the Caribbean region.

Part II

Glacio-Hydro-Isostasy

Chapter 5

Principles of Glacio-Hydro-Isostasy

5.1 Introduction

The rise in sea level associated with melting a volume of ice is not uniform across the oceans. Instead, local sea-level change reflects the superposition of changes in ice-equivalent sea level and the effects of glacio-hydro-isostasy through the deformation of the Earth and perturbation of the geoid in response to changing ice and water surface loads (Farrell and Clark, 1976). The Earth's response to surface loading is dependent on a number of factors including the size, distribution and melting history of the ice and water loads as well as Earth's rheology. Predicting the magnitude of this isostatic response is crucial for the interpretation of observed relative sea-level change. In this chapter, I will review some of the principles of glacio-hydro-isostasy and illustrate these using simplified axisymmetric earth and ice models.

5.2 The Earth's response to surface loads

Observations of the Earth's response to forcing on different time-scales suggest that the Earth behaves elastically in the short term and approaches fluid behaviour on longer time-scales. The timescale for the Earth's response to glacial loading lies between these two extremes. It is mathematically convenient to model the Earth as a spherically symmetric Maxwell body with a linear viscoelastic rheology (Cathles, 1975; Peltier, 1974).

The constitutive equation that describes the relationship between stress and strain of a material can be solved more easily for an elastic body than for a viscoelastic material. However, there is a useful mathematical technique, known as the *correspondence principle*, that makes solutions to viscoelastic problems achievable. A property of a generalised linear viscoelastic constitutive equation is that its Laplace transform takes the form of an

elastic constitutive equation, the solution to which is more easily calculated[1]. An inverse Laplace transform of this 'elastic' solution provides a solution to the original viscoelastic problem.

The response of a linear viscoelastic Earth to changes in surface loading can be described in terms of the following six independent variables:

1. radial and tangential components of deformation (u_r, v_θ)
2. radial and tangential components of stress (τ_{rr}, $\tau_{r\theta}$)
3. perturbation of potential (ψ)
4. gradient of potential (gravity perturbation, g)

Because we are dealing with a linear viscoelastic body, it is convenient to describe the surface loads using spherical harmonics. A load, L_n (of degree n) induces a response $\mathrm{R}_n\mathrm{L}_n$ and the total response is the sum of the spherical harmonic components: $\sum_n R_n L_n$. Each of the variables above can be expressed as a sum of spherical harmonic components with spherical harmonic coefficients u_n, v_n, T_{rn}, $T_{\theta n}$, ϕ_n, g_n. The equations governing the relationship between these variables are given by Longman (1962) and Johnston (1994). They form a set of linear differential equations that can be written in Runge-Kutta form and solved numerically:

$$\begin{aligned} \frac{dy_n}{dr} &= A^n(r)y_n \\ \text{where} \quad y_n &= (u_n, v_n, T_{rn}, T_{\theta n}, \phi_n, g_n)^T \end{aligned} \tag{5.1}$$

In the Laplace domain, the solutions, $\tilde{y}_n$, are a function of the Laplace parameter, s. By applying boundary conditions at the surface, the core mantle boundary and any internal density discontinuities, the solution can be found for an arbitrary, radially symmetric internal structure.

[1]The Lamé parameters in the Laplace domain elastic solution are dependent on the viscosities, $\eta(r)$, of the viscoelastic body.

To calculate a time dependent response for the viscoelastic Earth, the inverse Laplace transform of these solution must be found:

$$y(t) = \mathcal{L}^{-1}(\tilde{y}(s)) = \frac{1}{2\pi i} \lim_{n\to\infty} \int_{\gamma-iT}^{\gamma+iT} e^{st}\tilde{y}(s)ds \tag{5.2}$$

Using complex variable theory, the solution, $y(r,t)$, can be expressed as a linear superposition of an initial elastic response y^E and a summation of exponentially decaying viscous terms (Johnston, 1994; Peltier, 1985):

$$y(r,t) = y^E(r)\delta(t) + \sum_{j=1}^{N} R^j e^{s_j t} \tag{5.3}$$

The values of s_j (defined as the negative of the inverse relaxation time) and corresponding R^j are defined by the poles of the function $\tilde{y}(s)$ in complex space. For a very simple, single layer, viscous Earth, the complete set of s_j can be analytically determined and the coefficients, R_j, calculated. In the Laplace domain, rigidity ($\tilde{\mu}$) is a function of the rigidity (μ), viscosity (η) and Laplace parameter (s) (Johnston, 1994):

$$\tilde{\mu}(s) = \frac{\mu s}{s + \mu/\eta} \tag{5.4}$$

and numerical instabilities can occur when -s equals μ/η and $\tilde{\mu}(s) \to \infty$. For a continuously varying viscosity profile, the s_j values cannot be calculated explicitly. To overcome this problem, a 'pure collocation' method can be used in which an arbitrary set of s_j values is chosen to span the range of relaxation times of interest, in this case, the transition between elastic and viscous response.

In the long time (or fluid limit) of the response (s$\to$ 0), the Laplace domain rigidity ($\tilde{\mu}$) approaches the product of the viscosity (η) and Laplace parameter (s) ($\tilde{\mu} \approx \eta s$). Because the solution of equation 5.1 is dependent on $1/\mu$ (Johnston, 1994), in the limit of small 's' (or low viscosity), there is an increased risk of numerical instabilities.

Since the aim of this study is to investigate the response over glacial cycle time-scales, it is important to test the stability of the earth model calculation for long time-scale relaxation. The stability and accuracy of an earth model calculation is dependent on the complexity

of its rheological structure and the range and the choice of spacing of collocation points (s_j). Each earth model used in the calculations of sea level in this study has been tested for stability at the long time-scale limit. Figure 5.1 shows some examples of the time dependent response of the Earth to a Heaviside load for a number of rheological models and collocation point distributions. The calculations shown in figure 5.1 are expressed in terms of the deformation Love number spherical harmonic coefficient, h_n, which are defined below.

Love numbers

Love numbers are a normalised and dimensionless representation of the displacement and gravitational potential field and are a convenient way of describing the Earth's response to forcing (Lambeck, 1988). Love numbers can be expressed in terms of the spherical harmonic coefficients determined previously. The deformation Love numbers (h_n and l_n), which describe the vertical and tangential deformation respectively, and the gravitational Love number (k_n) are defined as:

$$\begin{pmatrix} h_n(r) \\ l_n(r) \\ 1 + k_n(r) \end{pmatrix} = \frac{2n+1}{4\pi a G} \begin{pmatrix} g^{(0)}(r) u_n(r) \\ g^{(0)}(r) v_n(r) \\ \phi_n(r) \end{pmatrix} \tag{5.5}$$

where the 1 in the gravitational term describes the gravitational attraction to the load itself. In these calculations, the Love numbers are calculated up to degree (n) 256, producing a spatial resolution of better than 1°.

5.3 Rheological structure of the Earth

The earth models used in the calculations of isostatic rebound are spherically symmetric, compressible Maxwell viscoelastic bodies. The models in this study consist of four layers including: (i) an elastic lithosphere of thickness, H; (ii) an upper mantle, with a uniform viscosity, η_{um}, but depth-dependent density and Lamé parameters, which extends from the base of the lithosphere to the 670 km seismic discontinuity; (iii) a lower mantle, with a viscosity of η_{lm}, and depth-dependent density and elastic structure, which extends from the 670 km discontinuity to the core mantle boundary at a depth of 2891 km; and (iv) an inviscid, fluid core. The depth dependence of mantle viscosity may in fact be more complex, as indicated by studies of isostatic rebound (Kaufmann and Lambeck, 2002). However, the effective viscosities of a two layer mantle are sufficient for the purposes of this study. The elastic moduli and density structure are based on the PREM model (Dziewonski and Anderson, 1981), derived from seismic studies.

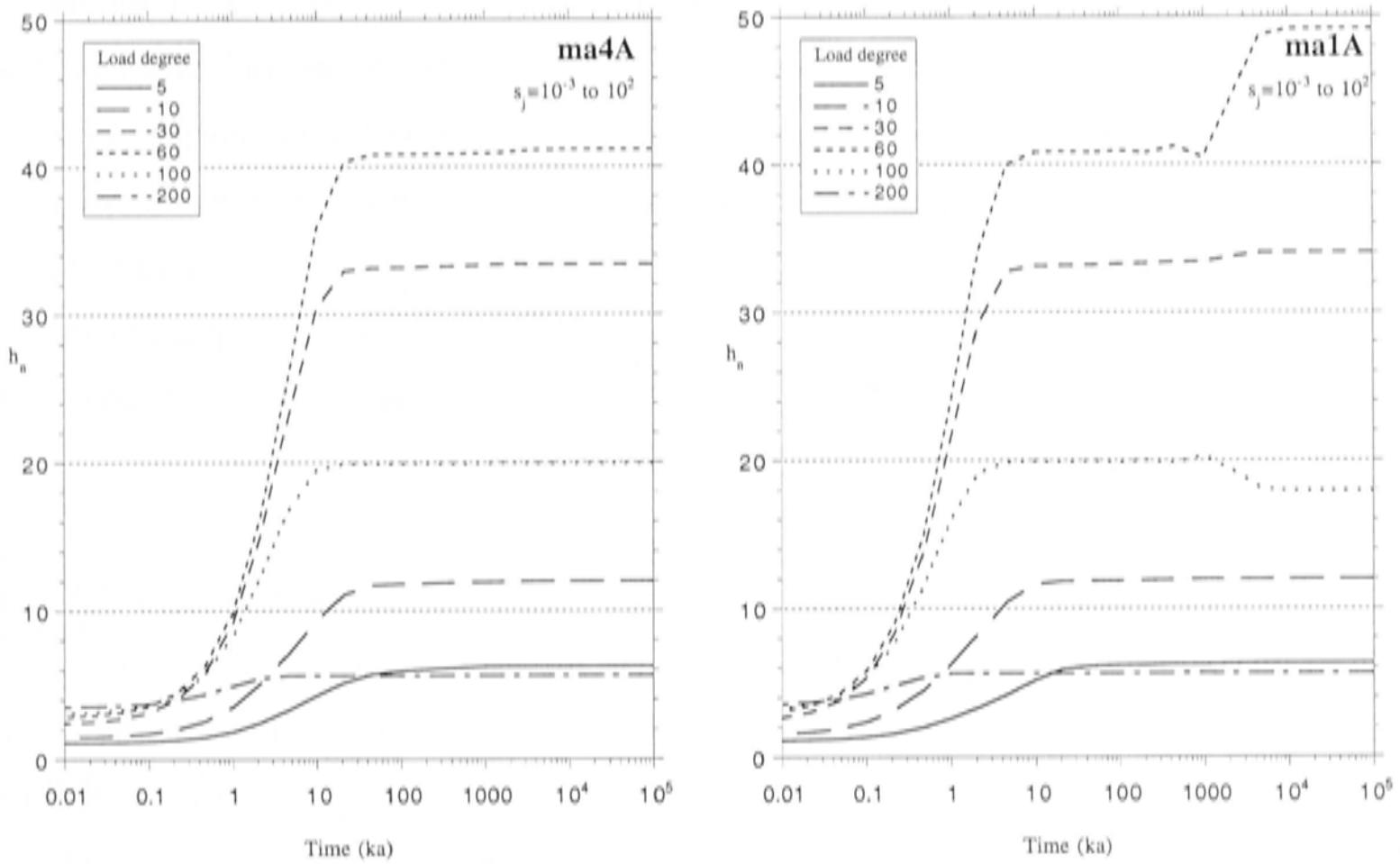

Figure 5.1: Time dependent vertical deformation Love number (h_n) for a Heaviside load history for three earth model calculations between 10 yr and 10^8 years (approaching the fluid limit). The reference model ma4A (top left) (see later discussion and table 5.1 for definition of rheology) is calculated for collocation points (3 per log decade) ranging from 10^{-3} to 10^2 (corresponding to inverse relaxation times of 1 Ma to 10 yr). The resulting earth model is stable in the fluid limit (t>10^3 yrs in this case). If the upper mantle viscosity is lowered (ma1A, top right) then the numerical solution becomes unstable in the fluid limit for the same collocation point distribution, as seen in the second plot for the wavenumbers 30-100. If the range of collocation points for the ma1A model is reduced to between 10^{-2} to 10^2 (100 ka to 10 yr) (bottom), the calculation becomes more stable and approaches the same fluid limit as the ma4A calculation.

Of course, the Earth is more complex than this simple spherically symmetric model. Observations of elastic wave velocity anomalies and lateral attenuation indicate that there are large-scale temperature imhomogeneities within the mantle (Romanowicz, 1998) and because viscosity is strongly temperature dependent, we can expect lateral viscosity variability within the mantle. In addition, the thickness of the lithosphere is known to vary between ocean and continental regions. For these reasons, the rheological parameters used in this study should only be considered effective parameters, and may not represent the true rheology of the Earth.

In a recent study, Kaufmann and Lambeck (2002) used inverse modelling to define the radial viscosity profile of the Earth based on a large data set of near-, intermediate- and far-field site observations of relative sea-level change during the last deglaciation. Typical viscosity profiles are characterised by an increase in viscosity of up to two orders of magnitude between the upper and lower mantle. The viscosity of the upper mantle was estimated to be 2-10$\times 10^{20}$ Pa s and that of the lower mantle to be $> 10^{22}$ Pa s. Kaufmann and Lambeck (2002) found that existing sea-level observations could not be used to distinguish between a gradual or abrupt increase in viscosity between the upper and lower mantle. Their models also suggest that there may be a decrease of viscosity in the deep lower mantle. Kaufmann and Lambeck's (2002) generalised model differs from other rheological models such as i) Forte and Mitrovica (1996) and Simons and Hager (1997), both of which have a lower viscosity in the transition zone between the upper and lower mantle and ii) Peltier (1998), which has a significantly lower viscosity in the lower mantle and less contrast between the upper and lower mantle viscosities. Fjeldskaar (1994) proposed that an Earth with a thin lithosphere (<50 km) overlying a low viscosity channel, or asthenosphere (10^{19} Pa s, 75 km) and single viscosity mantle was consistent with observations. However, Lambeck *et al.* (1996) demonstrated that the observations could be reproduced satisfactorily without the need for a low viscosity channel. These studies demonstrate the trade-off between rheological parameters such as lithospheric thickness and upper mantle viscosity.

Based on the calculations of Kaufmann and Lambeck (2002), I consider a simplified, 3 layer rheological model with a wide range of possible parameter values: an elastic lithosphere (50-80 km), low viscosity upper mantle (2×10^{20} to 10^{21} Pa s) and higher viscosity lower mantle (10^{21} to 5×10^{22} Pa s). The model (ma4A), with a lithospheric thickness of 65 km, upper mantle viscosity of 4×10^{20} Pa s and lower mantle viscosity of 1×10^{22}

Model	H_L (km)	η_{um} (Pa s)	η_{lm} (Pa s)
ma4A	65	4×10^{20}	1×10^{22}
mb4A	50	4×10^{20}	1×10^{22}
mc4A	80	4×10^{20}	1×10^{22}
ma2A	65	2×10^{20}	1×10^{22}
ma6A	65	6×10^{20}	1×10^{22}
maAA	65	1×10^{21}	1×10^{22}
ma41	65	4×10^{20}	1×10^{21}
ma45	65	4×10^{20}	5×10^{21}
ma4E	65	4×10^{20}	5×10^{22}

Table 5.1: Rheological parameters for the earth models used in this study. Lithosphere, with infinite viscosity and thickness H_L (km); Upper mantle with effective viscosity of η_{um}; Lower mantle with effective viscosity of η_{lm}.

Pa s is found appropriate for most rebound studies and is used in this study for reference purposes. Table 5.1 summarises the rheological parameters for a series of earth models used in this study.

5.4 Sea-level calculations

The loading of the Earth's surface deforms the planet through flexure of the elastic lithosphere and the flow of mantle material from beneath the load to surrounding regions (figure 5.2). The deformation of the surface is greatest under the centre of an ice load. In the regions beyond the ice sheet margin, displaced mantle material and lithospheric flexure produce a 'peripheral bulge' of deformation in the Earth's surface. As the ice sheet melts, the surface beneath the load rebounds in response to the reduced surface load, causing a redistribution of mantle material and subsidence of the associated peripheral bulge. In addition, the water released by the glacial melt increases the water load on the oceanic lithosphere and produces a further redistribution of mantle material and results in a change in the profile of the ocean floor. In the absence of other effects such as winds and currents etc, the ocean surface represents an equipotential surface, or geoid, the shape of which is a function of the ice, ocean and solid earth at a given time, including the redistribution of mantle material in response to the changing surface ice and water loads.

Collectively, these effects are termed 'glacio-hydro-isostasy' and an understanding of them is crucial to the interpretation of relative sea-level observations. The magnitude and rate of the Earth's response to changes in surface loading is dependent on the Earth's rheology. The precise nature of the isostatic response at a given site is dependent on the site's

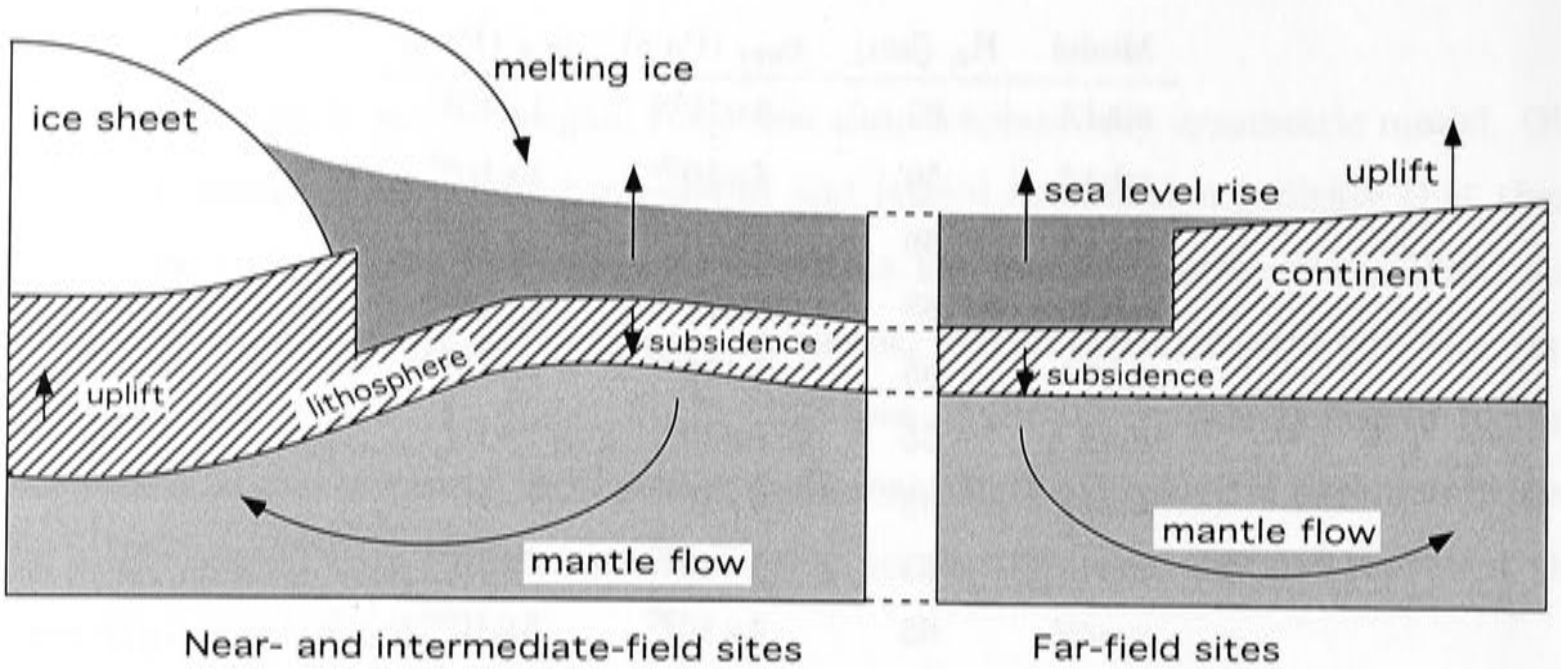

Figure 5.2: Summary of the Earth's response to glacial unloading including - redistribution of mantle material; rebound of lithosphere underneath ice sheet; subsidence of peripheral bulge; gravitational attraction of water to ice sheet (see section 5.5 for details)

proximity to the ice load and continental shelf edge.

Ice-equivalent sea-level change ($\Delta\zeta_{esl}(t)$) is defined as the ocean averaged change in sea level from the change in ice volume (dV_i):

$$\Delta\zeta_{esl}(t) = -\frac{\rho_I}{\rho_W}\int_t \frac{1}{A_O(t)}\frac{dV_I}{dt}dt \tag{5.6}$$

where $A_O(t)$ describes the ocean area as a function of time, V_I is the grounded ice volume and ρ_I and ρ_W are the densities of ice and water respectively. 'Ice-equivalent' or ' equivalent sea-level change' is defined in the same way as 'eustatic sea-level change' if no other factors contribute to the change in ocean volume, such as thermal expansion.

Relative sea-level change ($\Delta\zeta_{rsl}(\phi, t)$), as a function of time (t) and location (ϕ) can be defined as the sum of:

1. the ocean averaged change in sea level, or equivalent sea-level component ($\Delta\zeta_{esl}(t)$)

2. an isostatic component, which accounts for the deformation of the Earth and perturbation of the geoid in response to the changing ice and water surface loads ($\Delta\zeta_{iso}(\phi, t)$)

3. any tectonic component, which accounts for tectonic uplift or subsidence of a site ($\Delta\zeta_{tect}(\phi, t)$)

$$\Delta\zeta_{rsl}(t,\phi) = \Delta\zeta_{esl}(t) + \Delta\zeta_{iso}(t,\phi) + \Delta\zeta_{tect}(t,\phi) \tag{5.7}$$

The isostatic component, $\Delta\zeta_{iso}(t)$, can be expressed as the sum of the glacio-isostatic and hydro-isostatic components:

$$\Delta\zeta_{iso}(\phi,t) = \Delta\zeta_{iso,i}(\phi,t) + \Delta\zeta_{iso,w}(\phi,t) \tag{5.8}$$

The magnitude and rate of change of $\Delta\zeta_{iso}(\phi,t)$ in response to a surface load is determined by the rheological structure of the Earth. The isostatic contribution to relative sea-level change ($\Delta\zeta_{iso}(\phi,t)$) includes the effect of deformation and the perturbation of the geoid, described by the Love numbers, h_n and k_n (defined in equation 5.5) which define the vertical deformation and gravitational components of the Earth's response to surface loading. The ocean-ice mass is conserved at all times.

In these calculations, relative sea-level change is defined on land as the change in the height difference between the Earth's surface and the geoid. This accounts for both gravitational effects and deformation of the Earth's surface and provides a generalisation over the rest of the Earth that is consistent with sea-level change and is continuous across evolving coastlines.

The effect of ice loading through time is based on the prescribed ice melting history. The water surface loading at a given site is a function of the change in ocean water depth at that site which is, in turn, a function of the change in grounded ice volume (equation 5.6), deformation and gravitational changes due to both the ice and water loads. Thus, the water loading term is calculated iteratively, with an initial estimate of the change in sea level equal to the equivalent sea-level term. Successive iterations include the effect of the deformation due to the water load and migrating coastlines. Formally, grounded ice that is lifted from the sea floor as sea-level rise occurs should be treated as floating ice and also included in the term dV_I (equation 5.6) in successive iterations of the calculation (Lambeck *et al.*, 2002b). However, in the version of the program used for relative sea-level calculations in this investigation, the contribution of floating ice is not included to dV_I, although this effect is not significant for these calculations.

5.5 Components of isostasy

In the absence of tectonic effects, the nature of relative sea-level change at a given site is a function of the coupled change in equivalent sea level and the effects of isostasy. The magnitude of glacio-hydro-isostatic effects varies depending on a site's location relative to an ice load and/or continental margin. For sites within the former ice sheet margins (interior and near-field sites) the glacio-isostatic rebound of the crust and the gravitational influence of the ice sheet dominate the change in relative sea level. For sites far from the ice margins (far-field), the glacio-isostatic contribution is smaller and varies more gradually with distance. At such locations, the relative sea-level change is dominated by a combination of equivalent sea-level change and the hydro-isostatic adjustment of the crust in response to the change in water load. In this section I will discuss each of the components (gravitational and total ice and water) that contribute to glacio-hydro-isostasy and overview how these components vary spatially.

5.5.1 Gravitational component

The redistribution of ice and water on the Earth's surface during a glacial cycle leads to perturbations in the Earth's gravitational field. A large ice sheet exerts a gravitational attraction on the ocean water. For a hypothetical rigid Earth, which experiences no deformation in response to changing surface loads this effect produces a gradient in sea level between sites near the ice sheet and those further away (see figure 5.3). In this rigid model, the gravitational attraction of the ice sheet at near- and intermediate-field sites produces relative sea levels that are higher than mean sea level. At far-field locations, relative sea level is lower than mean sea level because of the extra water attracted towards the ice sheet. As the ice sheet melts, the gravitational attraction decreases and the water retreats from regions close to the ice sheet.

Of course, the Earth is not a rigid body and so the surface displacement and internal redistribution of mantle material also affect the shape of the geoid. This internal mass redistribution of material from beneath the ice sheet to intermediate-field regions partly counters the effect of the gravitational attraction of the ice sheet.

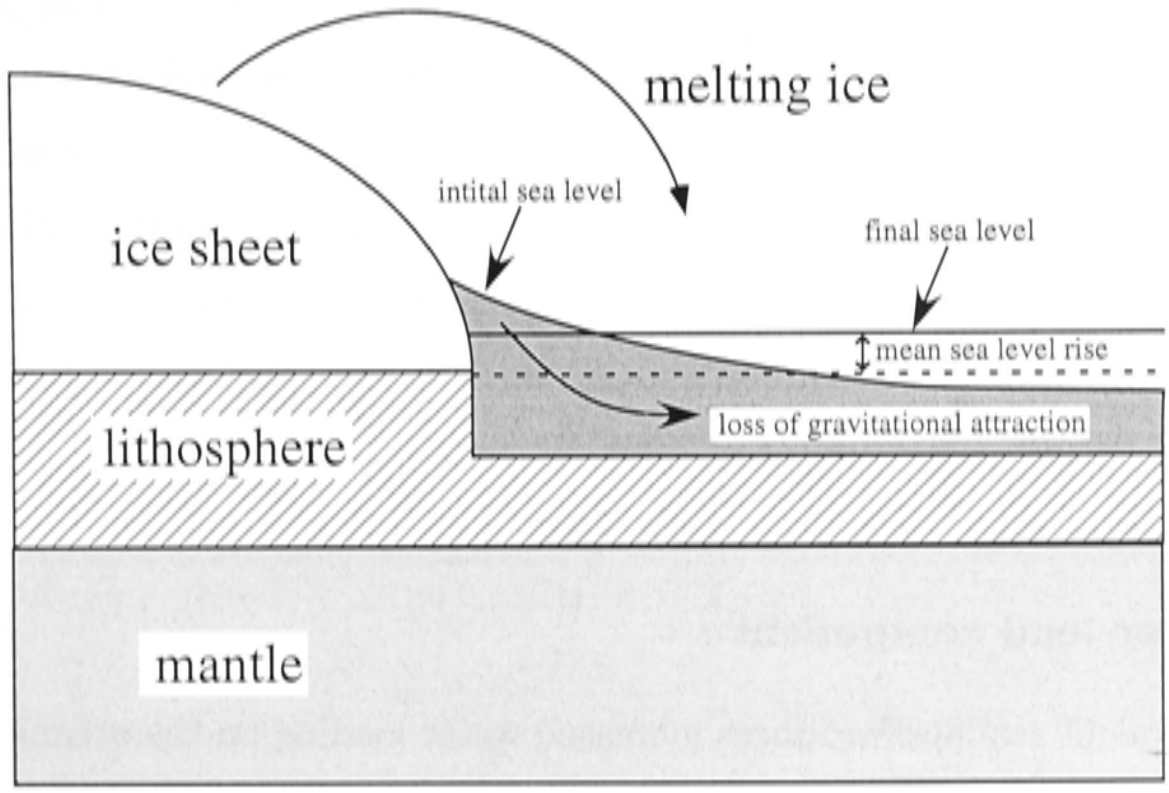

Figure 5.3: Rigid Earth gravitational component of sea-level change. An ice sheet mass attracts ocean water, producing a gradient in sea level. At sites near the ice sheet, sea level is higher than mean sea level and at sites far from the ice sheet sea level is lower than mean sea level. This gravitational component decreases instantaneously as the ice sheet decays.

5.5.2 Ice load component

The deformation of the Earth's surface under an ice load leads to a redistribution of mantle material from directly under the load to regions outside the ice sheet margins. The deformation of the surface is greatest directly underneath the centre of the ice load and a large ice sheet, such as the Laurentide, can depress the crust by several hundreds of metres.[2] The lithospheric flexure and flow of mantle material to the regions surrounding the ice sheet produces a 'peripheral bulge' of deformation in the Earth's surface (see figure 5.4). When the ice sheet melts, the crust beneath the ice loads rebounds and mantle material flows back to the region beneath the former load, and the peripheral bulge subsides. At sites directly under an ice sheet, relative sea level is dominated by isostatic rebound leading to a fall in relative sea level. The subsidence of the peripheral bulge in response to deglaciation produces a component of sea-level rise superimposed on the ice-equivalent sea-level rise for those intermediate field sites. A consequence of the time-dependent collapse of the peripheral bulge is that the shape of the entire ocean basin changes as a function of time. As the bulge subsides, the size of the ocean basin increases, introducing a component of sea-level fall at far-field sites (known as ocean syphoning; Mitrovica and Peltier, 1991; Johnston, 1993).

5.5.3 Water load component

A rise in equivalent sea level produces increased water loading on the oceanic crust, which then subsides relative to the unloaded continental regions. The differential response across the continental margin produces a spatially variable component of relative sea-level fall that is superimposed on equivalent sea-level rise and continues long after melting ceases (figure 5.5).

[2] In the isostatic limit the deformation of the crust (δr) is controlled by the height of the load (h_I) and the relative densities of the ice load (ρ_I) and the mantle (ρ_M), where ($\rho_I/\rho_M \approx 1/3$: $\delta r = \rho_I/\rho_M h_I$). For a 3 km ice load, the deformation in the isostatic limit would be approximately 1 km.

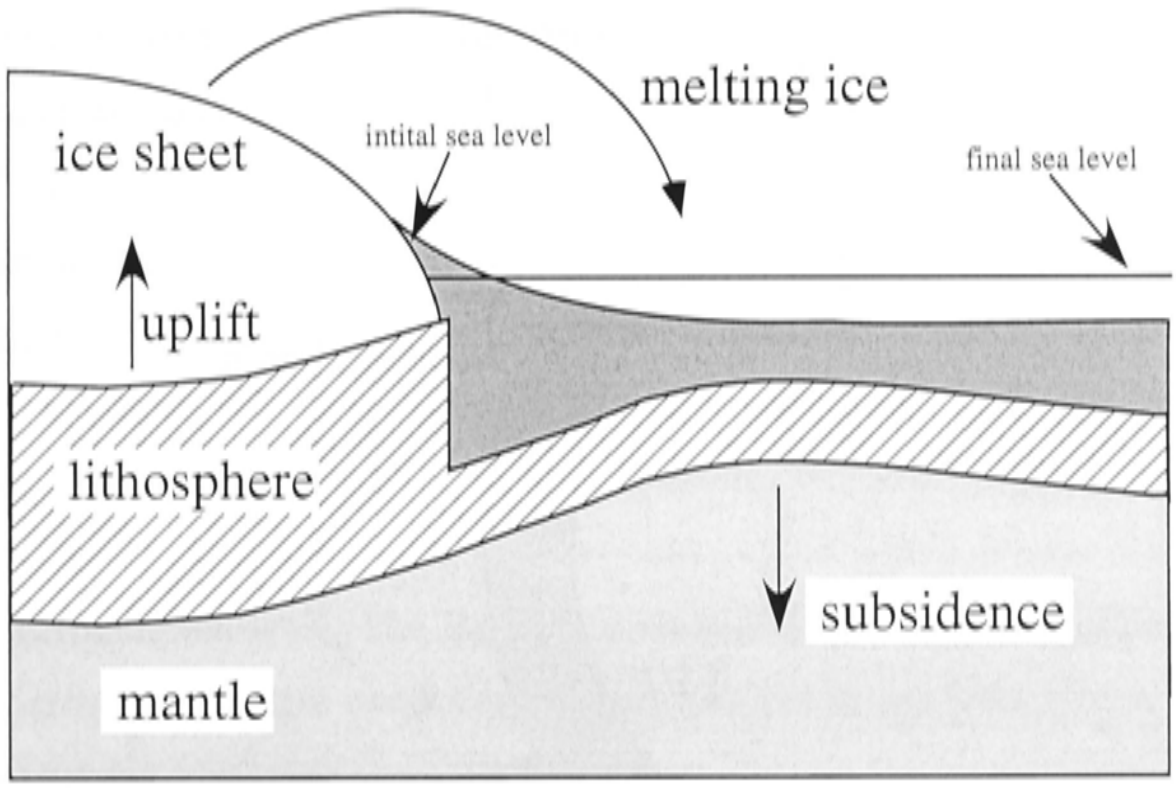

Figure 5.4: Glacio-isostatic component of sea-level change. The mass of large ice sheet weighs down the crust and produces flexure of the elastic lithosphere and redistribution of mantle material. This redistribution produces a 'peripheral bulge' of deformation of the Earth's surface. Upon melting of the ice sheet, the peripheral bulge collapses and the crust directly beneath the load rebounds, influencing relative sea-level change in those regions. Changes in the shape of the ocean basin due to the collapse of the peripheral bulge also influences sea level at far-field sites.

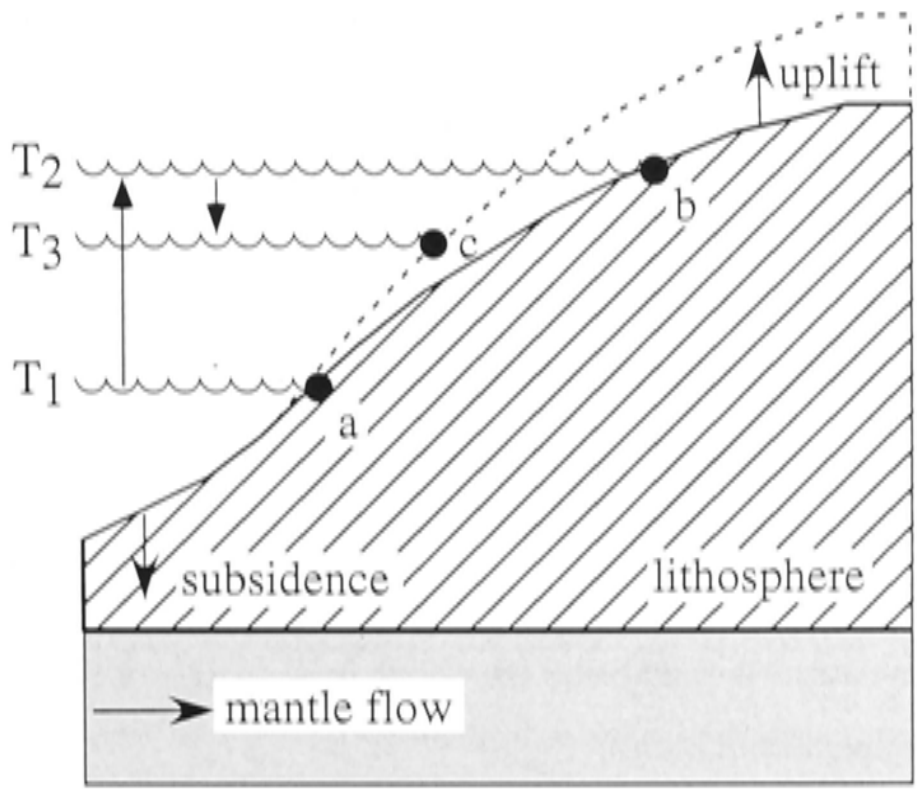

Figure 5.5: Hydro-isostatic component of sea-level change at a far-field continental site in response to a rise in equivalent sea level. The increased water loading in response to a deglaciation (T_1-T_2) produces a subsidence of the oceanic crust (T_2-T_3) and uplift of the unloaded, continental crust. So at continental sites, the initial rise in equivalent sea level (a to b) is followed by a fall (b to c) after the as the Earth responds to the increased water load.

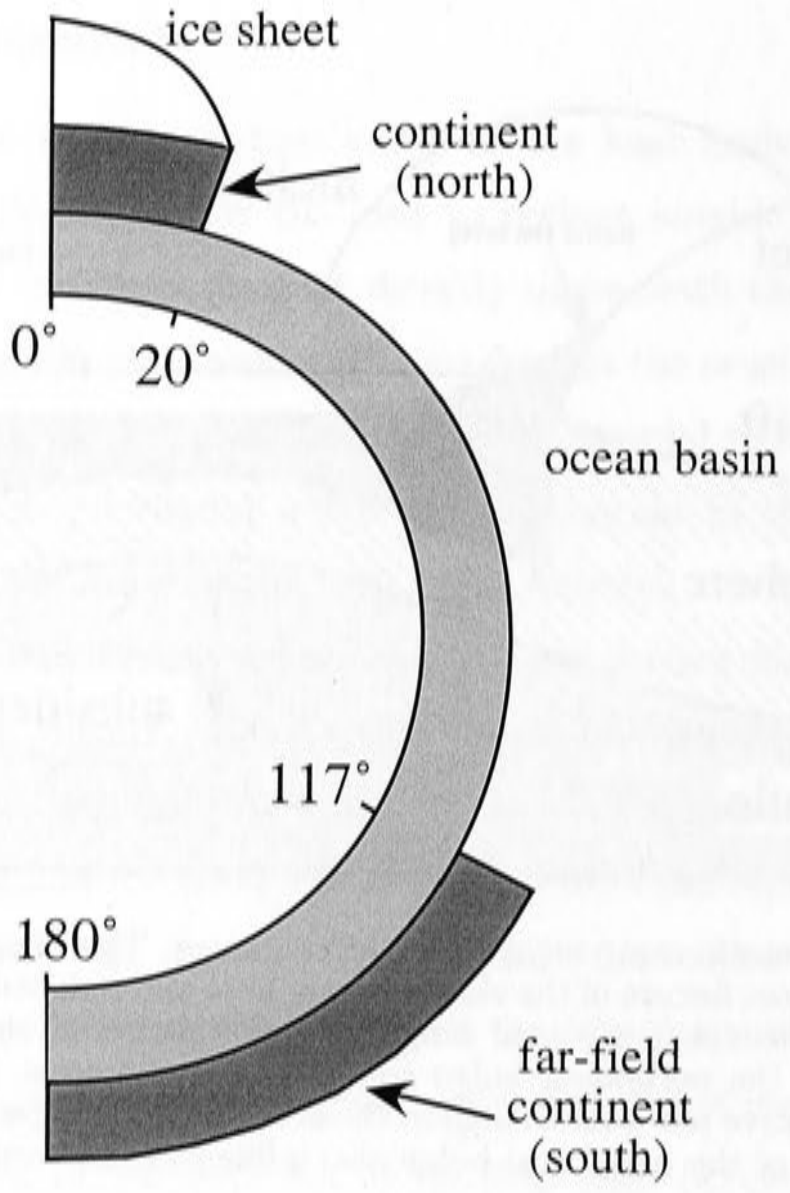

Figure 5.6: An axisymmetric Earth, with a parabolic ice sheet on the north continent used for the simple calculations in this chapter. An ocean basin between 20° and 117° is equivalent to the extent of the ocean basin on a realistic Earth (~70% of total surface area).

5.6 Spatial and temporal variations

In the following sections, I demonstrate some of the effects of glacio-hydro-isostasy on the observed relative sea-level records and discuss the importance of factors such as location, time of observation, earth rheology and ice sheet size and distribution and rate of melting. To demonstrate the effects of these parameters, I use a spherical axisymmetric earth model with two continents (north and south) separated by an ocean reaching from a colatitude of 20° to 117° (see figure 5.6). A parabolic ice sheet load of Laurentide ice sheet dimensions is located on the northern continent.

The sites of interest in this study in the Caribbean and surrounding regions (see section 4.5) span the intermediate field range of the Laurentide Ice sheet. For this reason, the following discussion concentrates mainly on the comparison of relative sea-level response at intermediate- and far-field sites to a glacial unloading of a Laurentide-sized ice sheet.

Spatial variability

Figure 5.7 summarises the characteristic relative sea-level curves associated with a hypothetical deglaciation that is completed a several thousand years before the present day at interior, near-, intermediate- and far-field sites. For a site directly under the ice sheet (A), radial displacement of the surface dominates the response during and after unloading, and there is an apparent drop in relative sea level. For sites very close to the ice margins (B), the change in sea level can be a more complicated superposition of the crustal rebound and equivalent sea-level rise. At intermediate-field sites (C), the collapse of the 'peripheral bulge' leads to a rise in sea level for sites in that region which is also superimposed on the rise in equivalent sea level. For far-field continental sites (D), the differential surface deformation across the margin produces an apparent fall in sea level that is superimposed on the equivalent sea-level rise.

5.6.1 Relative magnitude of ice and water components

Figure 5.8 shows the separate glacio- and hydro-isostatic components of sea-level change in response to the deglaciation of a Laurentide-sized ice sheet for the axisymmetric Earth and the reference earth model (ma4A, table 5.1). The calculations are for a linear deglaciation between 18 ka and 6 ka BP of an ice sheet of thickness 3.8 km at its centre and which contributes ~80 m to ice-equivalent sea-level change. The glacio- and hydro-isostatic components are measured relative to present day (6 ka after the cessation of melting). At interior, near and intermediate-field sites, the glacio-isostatic response is the dominant contribution to the isostatic component of sea-level change. Beneath the centre of the ice sheet glacio-isostasy contributes >700 m to a fall in sea level during the deglaciation. At far-field continental sites, the glacio-isostatic component is smaller and hydro-isostatic adjustment becomes more important.

5.6.2 Time of observation

For the examples discussed above, relative sea level is calculated relative to the present day. However, at the present day, the Earth has still not relaxed fully since the last deglaciation. Figure 5.9a and b show a comparison of the relative sea level as a function of time for a set of intermediate and far-field sites with reference to the present day (5.9a) and an equilibrium state (5.9b). The glacio-isostatic component of sea-level change as a function of colatitude from the centre of the load is shown in figure 5.10. During the Pleistocene, the waxing and waning of the ice sheets on 20-100 ka time-scales has meant that the Earth has been continually readjusting and has never reached an equilibrium state. However,

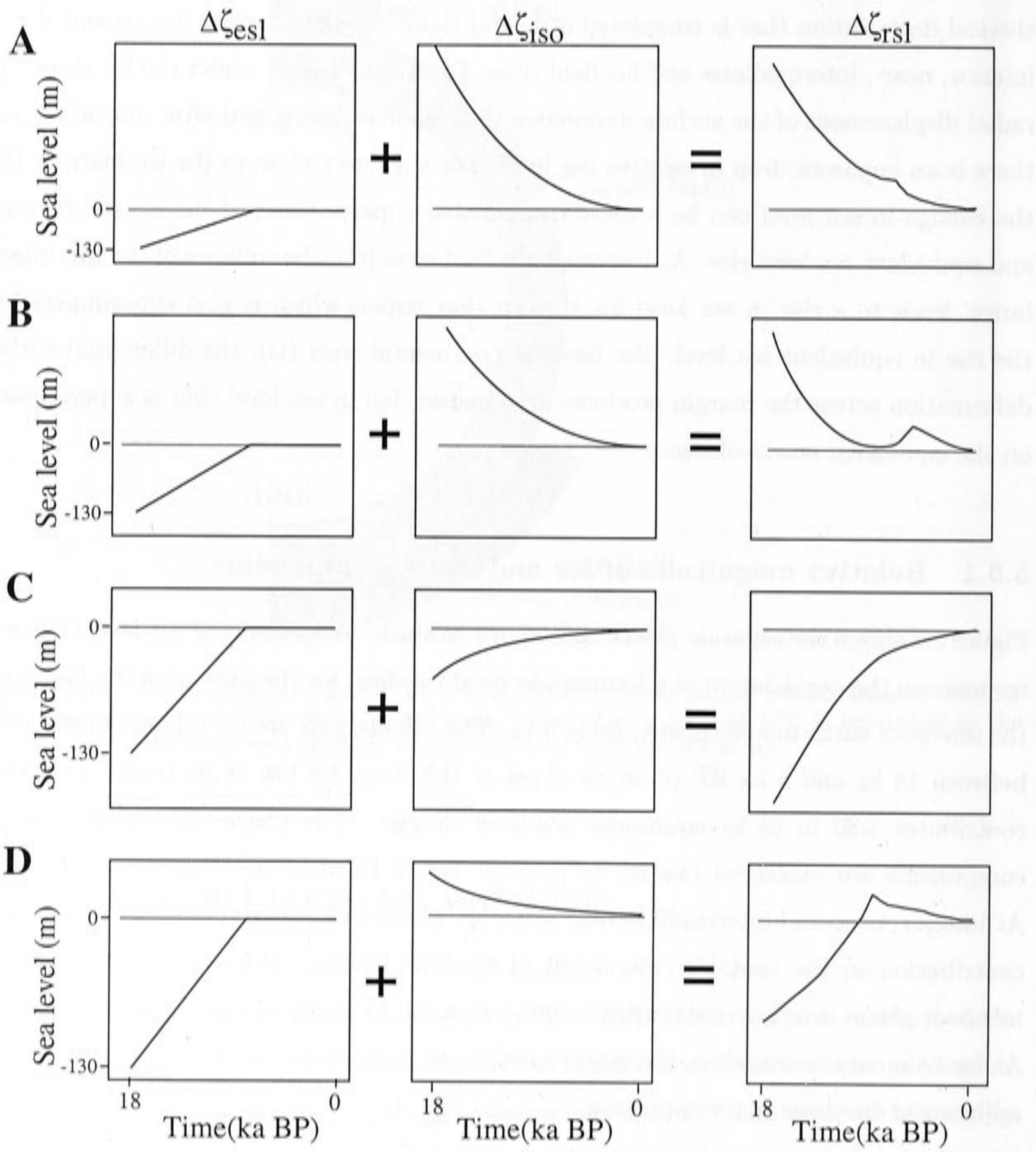

Figure 5.7: Characteristic sea-level curves for interior- near-, intermediate- and far-field sites associated with the last deglaciation as a function of equivalent sea-level change and isostatic components (after Yokoyama, 1999). A) Interior - Well inside the margins of the ice sheet, the response is dominated by the glacio-isostatic rebound of the crust leading to a dramatic fall in relative sea level at those sites. B) Near-field - The equivalent sea level and isostatic rebound components are of similar magnitude, and relative sea level change is a complex superposition of these. C) Intermediate-field - The collapse of the glacial bulge leads to an isostatic component of sea-level rise that is superimposed on the equivalent sea-level rise. D) Far-field continental - The uplift of the continental crust in response to the increased water loading of the oceanic crust produces an isostatic component of sea-level fall superimposed on the equivalent sea-level rise.

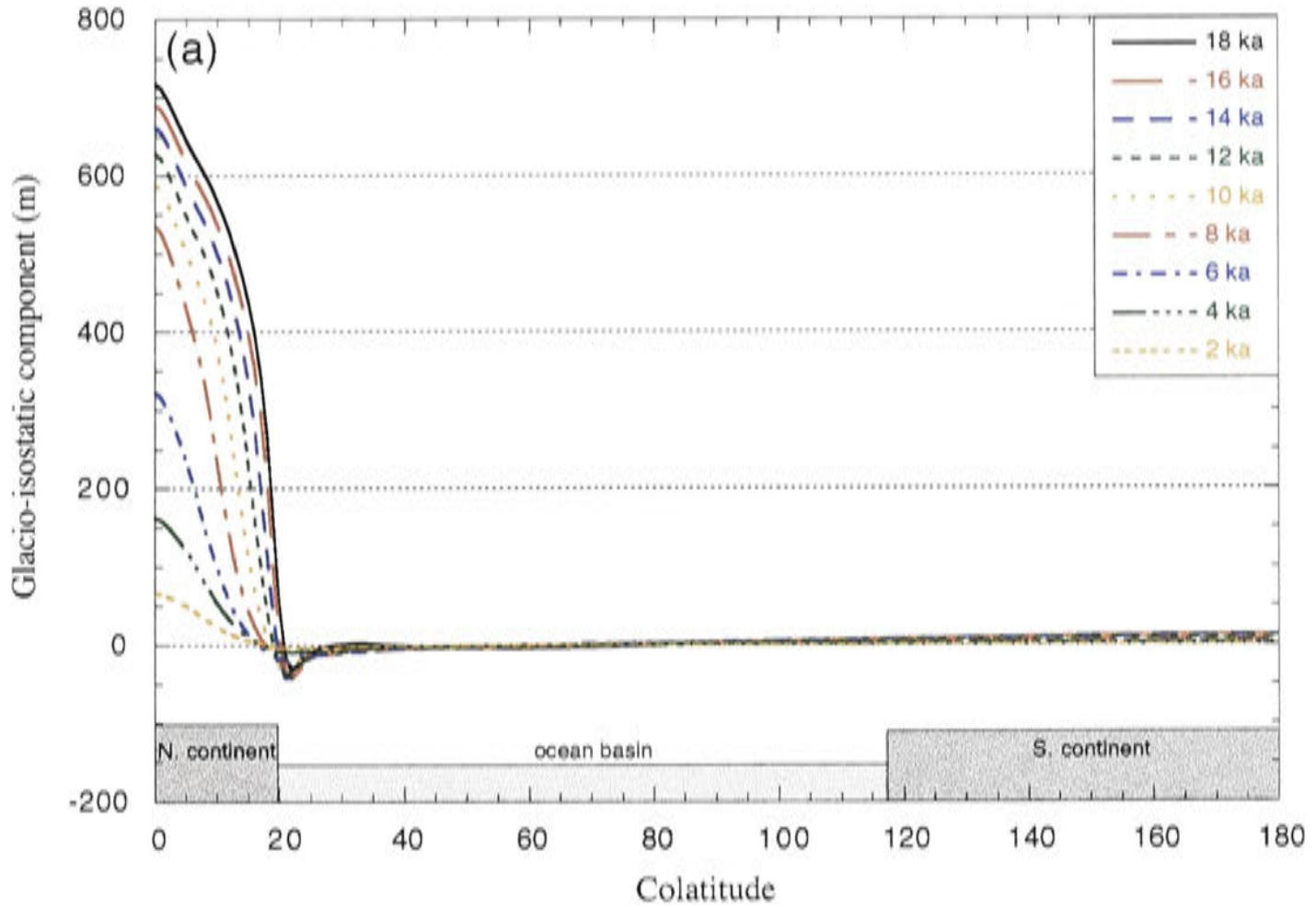

Figure 5.8: Glacio- and hydro-isostatic components of sea-level change associated with the melting of a Laurentide sized ice sheet between 18 ka and 6 ka BP. The ice sheet is located on the northern continent, with a radius of 20°. The southern continent extends to a colatitude of ~117°. a) relative sea-level change and interior and near-field sites is dominated by glacio-isostasy. b) The continental hydro-isostatic component is the result of increased loading on the oceanic crust from the increased ocean depth and corresponding uplift of continental crust. For sites near the margin of the northern continent, the water load also depends on the glacio-isostatic effects due to the nearby ice sheet.

for the purpose of studying the nature of the Earth's response to changing surface loads, displaying the isostatic response of the Earth with respect to an equilibrium state enables glacio-hydro-isostatic effects to be more easily demonstrated.

The internal deformation of the Earth associated with a surface load attenuates with depth, and higher degree (shorter wavelength) deformation attenuates more rapidly with depth. Therefore, the vertical deformation of the boundary between the upper and lower mantle is smaller and is broader (longer wavelength) than at the surface (figure 5.11). Because the viscosity of the upper mantle is much lower than that of the lower mantle, it responds more rapidly to changes in surface load. As a result of this viscosity contrast, during a deglaciation, the peripheral glacial bulge broadens as it collapses reflecting the broader deformation at depth (figure 5.12). Because of this broadening, at intermediate field sites near the ice sheet margin (e.g. 67°N in figure 5.9) the sea-level after a deglaciation (measured relative to an equilibrium state) would overshoot its equilibrium level before then returning to it from above.

The total rise in sea level during a deglaciation differs between intermediate and far-field sites. Intermediate-field sites, which lie on the peripheral bulge, subside in response to a deglaciation. Consequently, the total rise in sea level (measured at an equilibrium state) is generally larger than the equivalent sea-level rise (sites 67 N and 56 N in figure 5.9b). In contrast, at far-field continental margin sites, which are uplifted in response to deglacial water load increase, the total rise in sea level is less than the equivalent sea-level rise. If sea level is not measured relative to equilibrium, the total rise in sea level is dependent on time of observation. In the case of intermediate field sites, where the peripheral bulge is still collapsing at the present day, the total rise in relative sea level relative to present day can be less than the rise in equivalent sea level (site 56N in figure 5.9a).

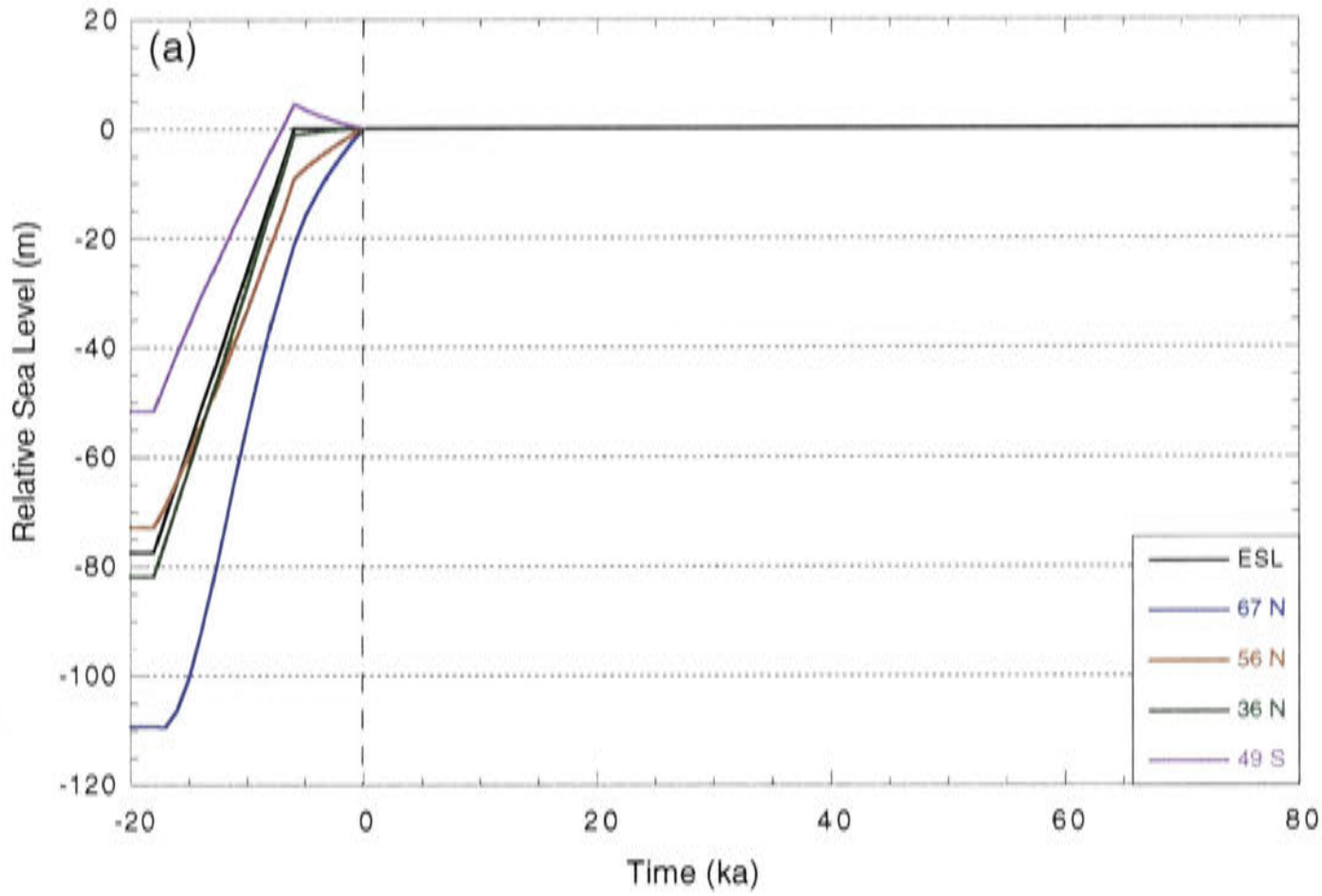

Figure 5.9: The apparent change in relative sea level is dependent on the time of observation. For a deglaciation between 18 and 6 ka BP, the relative sea level for a number of intermediate and far field sites would appear as in the panel (a) of this figure. Panel (b) shows relative sea-level curves for the same deglaciation, measured relative to equilibrium. The position of the intermediate field sites relative to the ice sheet margin are shown in figure 5.10.

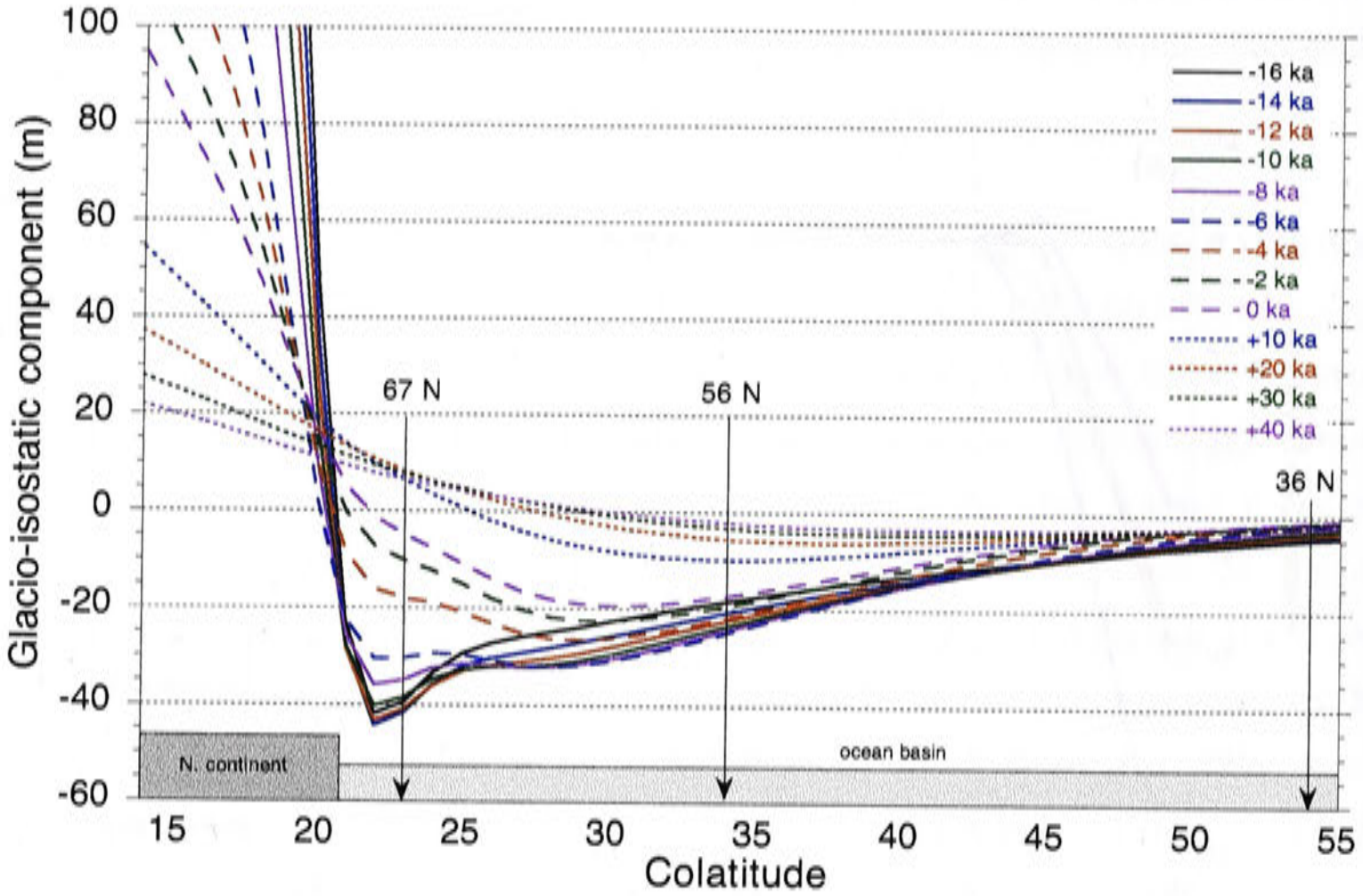

Figure 5.10: Glacio-isostatic component of sea-level change relative to equilibrium during and after a deglaciation in the near and intermediate field region. Location of intermediate field sites for which relative sea-level curves are calculated in figure 5.9 relative to the ice sheet margin and northern continent in the axisymmetric model.

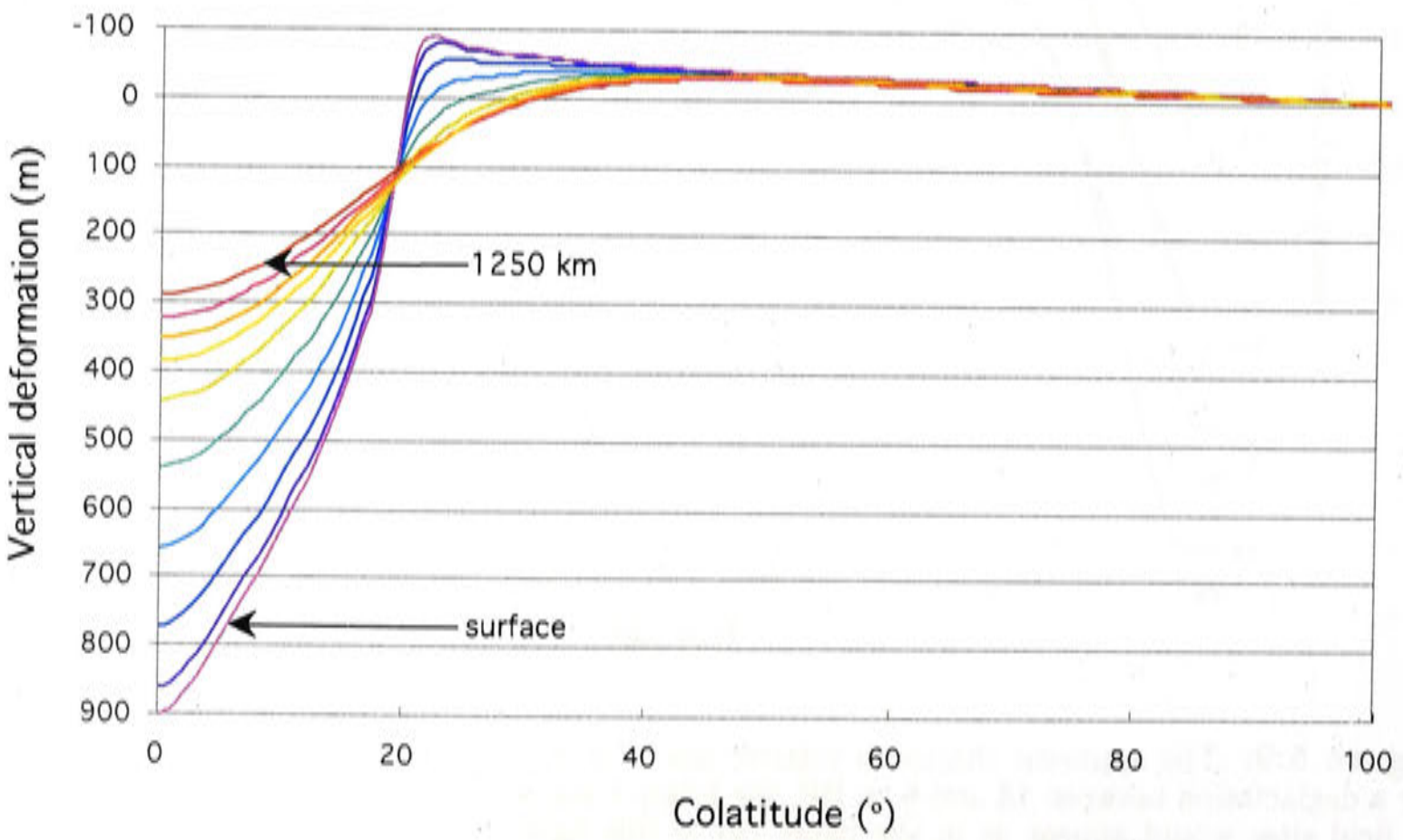

Figure 5.11: Vertical deformation at a range of depths resulting from a Laurentide sized ice load. Deformation attenuates and broadens with depth.

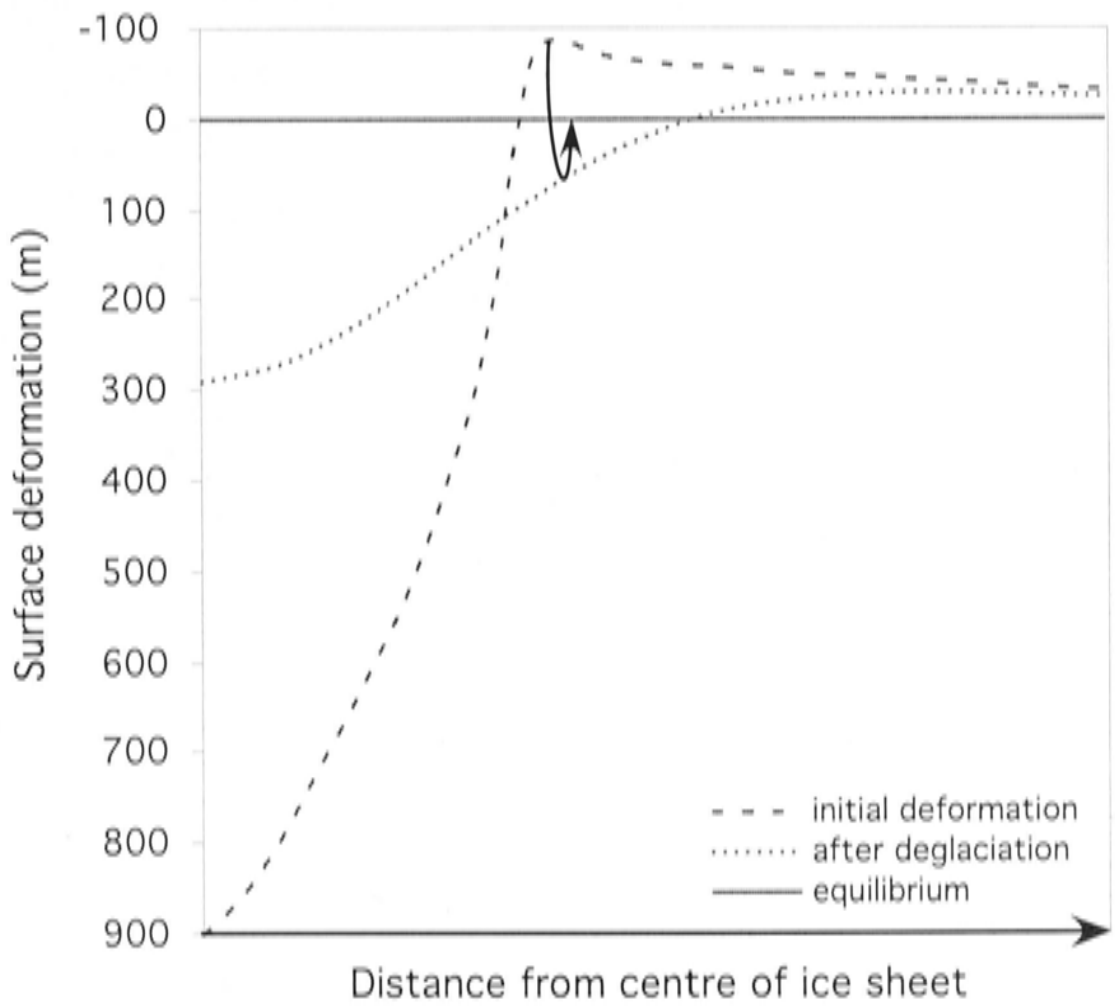

Figure 5.12: Collapse and broadening of the surface deformation peripheral bulge in response to a deglaciation.

5.6.3 Dependence on rheology

Lithospheric thickness

The lithosphere partially supports a surface load through its rigidity and elastic flexure. For a load of a given size, a reduction in the thickness of the lithosphere will mean that the load is supported less by the lithosphere and more by the buoyancy forces from the mantle. In the case of a load of the size of the Laurentide Ice Sheet, the lithospheric thickness (~50-80 km) is much less than the size of the load (in this model, ~2000 km radius) and so the support of this load is dominated by buoyancy from the mantle. In this case, changing the lithospheric thickness will not significantly affect the isostatic response or the resulting relative sea level (figure 5.13), except possibly very near the ice sheet margins where lithospheric flexure is important. A smaller load would be supported more by the elastic lithosphere and the isostatic response to such a load would therefore be more sensitive to the lithospheric thickness.

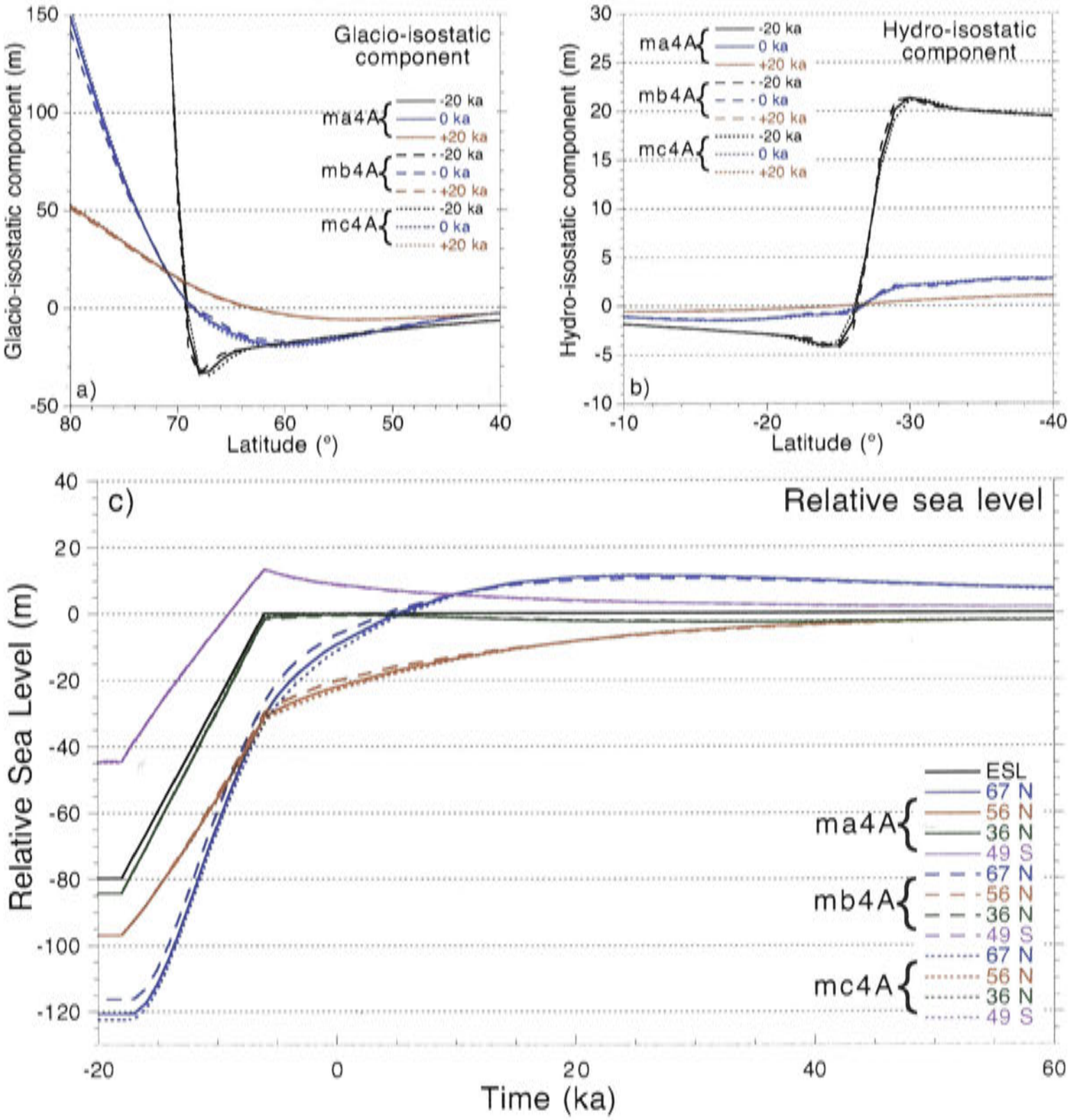

Figure 5.13: Changes in lithospheric thickness from 65 km (ma4A), 50 km (mb4A), 80 km (mc4A) - sensitivity of glacio-hydro-isostatic components and relative sea-level change in response to a Laurentide Ice Sheet sized deglaciation measured relative to equilibrium. a) Near and intermediate field glacio-isostatic component; b) Far-field hydro-isostatic component; c) Relative sea level for intermediate-field (67°N, 56°N), far-field oceanic (36°N) and far-field continental (49°S) sites.

Upper mantle viscosity

Changing the upper mantle viscosity affects the rate of the Earth's response to glacial unloading (figure 5.14). The viscosity contrast between the upper and lower mantle in these models is responsible for the 'overshoot' of relative sea level past the equilibrium level at intermediate-field sites that are very close to the ice sheet margin. If the viscosities of the upper and lower mantle are closer, lower mantle readjustment keeps better pace with the upper mantle and, as a consequence, the surface deformation does not broaden as quickly or by the same magnitude (dotted lines in figure 5.14a). Therefore, an increase in upper mantle viscosity produces a smaller 'overshoot' of relative sea level at the intermediate field sites following a deglaciation (blue dotted line in figure 5.14c). If the upper mantle viscosity is decreased then the initial rate of relaxation is faster, the peripheral bulge collapses and broadens more rapidly (dashed lines in figure 5.14a) and the overshoot at sites near the ice sheet margin is larger (blue dashed line in figure 5.14c). Relative sea level at far-field sites are relatively insensitive to changes in upper mantle viscosity (site 49 S, purple lines in figure 5.14c) because the of the very wide water load (see following discussion of lower mantle viscosity).

The total change in sea level between the glaciated and ice-free equilibrium states is insensitive to changes in mantle viscosity because earth models that have the same elastic structure but varying viscosity will approach the same fluid limit (demonstrated in figure 5.1).

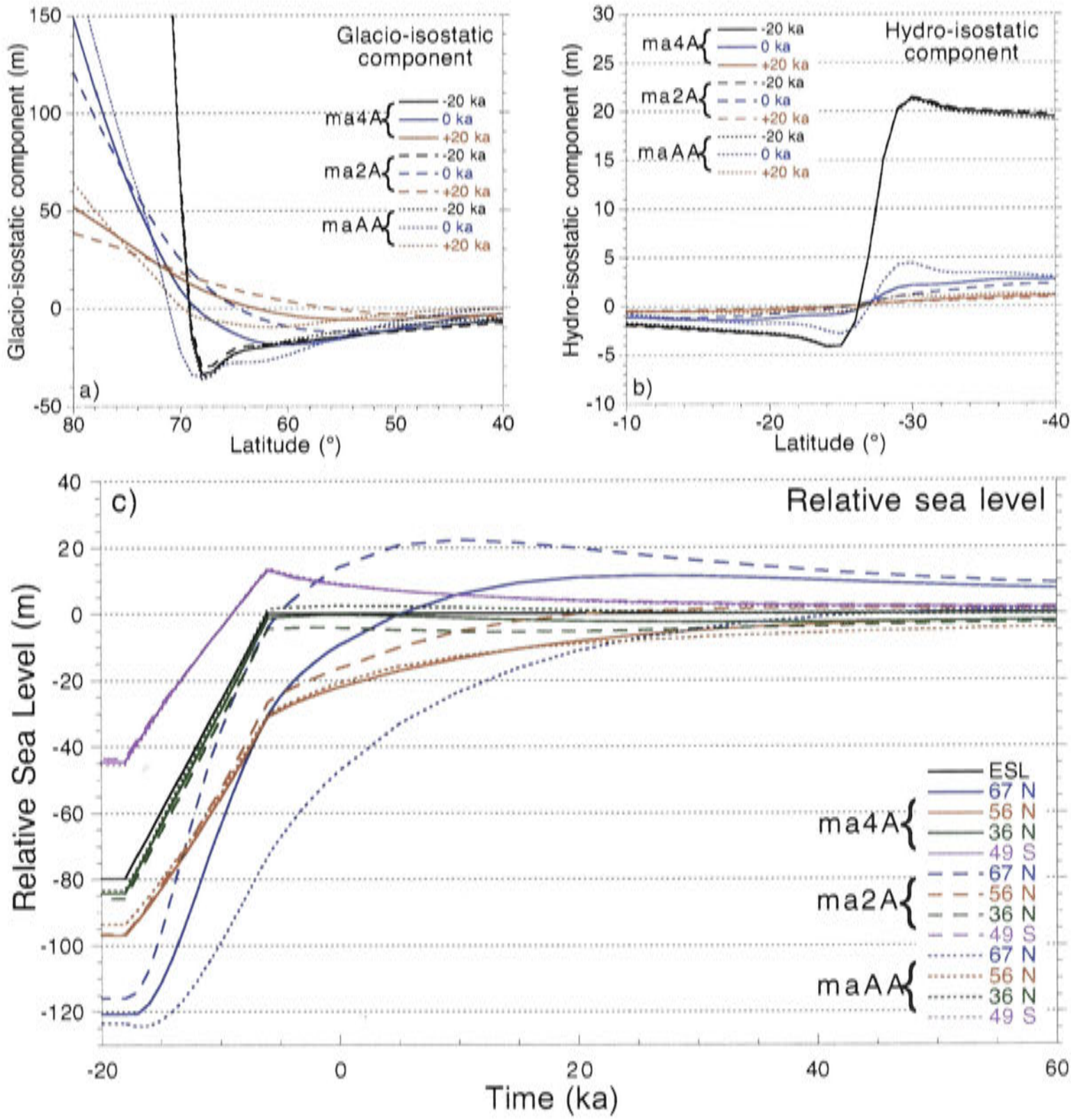

Figure 5.14: Changes in upper mantle viscosity from 4×10^{20} Pa s (ma4A) to 2×10^{20} Pa s (ma2A) and 1×10^{21} Pa s (maAA) - sensitivity of glacio-hydro-isostatic components and relative sea-level change in response to a Laurentide Ice Sheet sized deglaciation measured relative to equilibrium. a) Near and intermediate field glacio-isostatic component; b) Far-field hydro-isostatic component; c) Relative sea level for intermediate-field (67°N, 56°N), far-field oceanic (36°N) and far-field continental (49°S) sites.

Lower mantle viscosity

If the lower mantle viscosity is increased, while maintaining the same upper mantle viscosity, the initial rate of response in the intermediate-field remains approximately the same but the broadening and final collapse of the peripheral bulge is delayed because of the slower response of the lower mantle (compare dotted line in figure 5.15a). This also leads to a more obvious overshoot in sea level at sites near the margin of the former ice sheet (site 67 N, blue lines in figure 5.15c). The far-field hydro-isostatic component (site 49 S, purple lines in figure 5.15c) is more sensitive to variations in lower mantle viscosity because the deformation caused by the broad water load penetrates deep into the mantle.

Earth rheology - summary

The response of the Earth to surface loading is dependent on the rheological parameters such as lithospheric thickness, and mantle viscosity. The horizontal dimensions of a load determines its sensitivity to changes in mantle rheology. A load of small radius, relative to the flexural wavelength of the lithosphere, is supported to a greater degree by the elastic strength of the lithosphere the response of the Earth to such a load is highly sensitive to the thickness of the elastic lithosphere. For a broad load, such as the Laurentide Ice Sheet or the oceanic water load, the isostatic response is insensitive to lithospheric thickness and is more dependent on mantle viscosity. Wider loads penetrate deeper into the mantle.

If the history of the surface loading is known, then this enables us to place constraints on these rheological parameters. The viscoelastic structure of the Earth is more complex than the simple three-layer model used in these calculations. For example, the radial viscosity profile of the mantle is more complex than a simple upper and lower mantle contrast (Kaufmann and Lambeck, 2002). In addition, lateral variability of viscosity can be inferred from the results of seismic studies but this cannot yet be included in these isostatic models. Therefore, rheological parameters in these models are effective parameters only and describe the regional behaviour of the Earth.

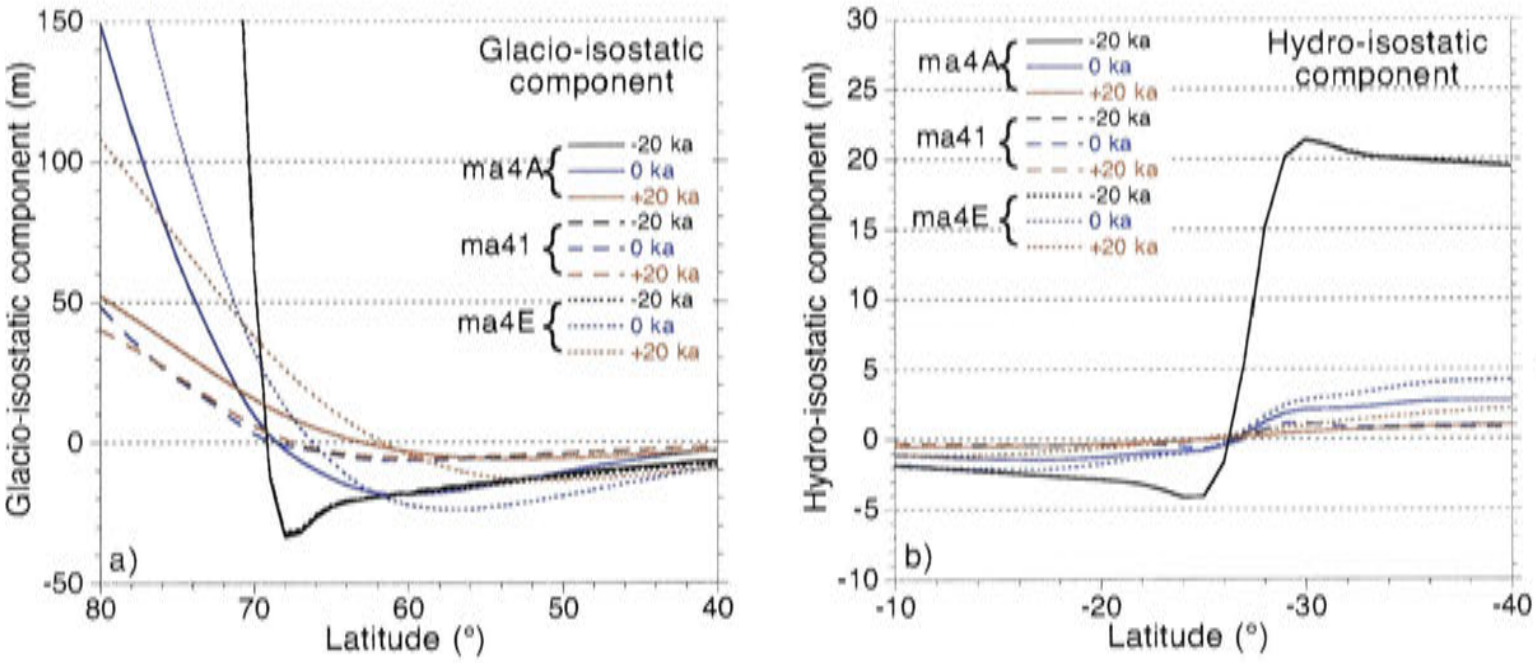

Figure 5.15: Changes in lower mantle viscosity from 1×10^{22} Pa s (ma4A) to 1×10^{22} Pa s (ma41) and 5×10^{22} Pa s (ma4E)- sensitivity of glacio-hydro-isostatic components and relative sea-level change in response to a Laurentide Ice Sheet sized deglaciation measured relative to equilibrium. a) Near and intermediate field glacio-isostatic component; b) Far-field hydro-isostatic component; c) Relative sea level for intermediate-field (67°N, 56°N), far-field oceanic (36°N) and far-field continental (49°S) sites.

5.6.4 Dependence on ice load

Ice load melting history

Distribution

In regions near the margins of an ice sheet, the relative sea-level history is very sensitive to the position of the margin through time. Figures 5.16a and b show the glacio-isostatic response to a deglaciation between 18 and 6 ka BP (relative to equilibrium) for two ice sheets with the same initial dimensions. In the upper panel, the ice sheet simply thinned with time while the ice extent was kept constant. In the second scenario (lower panel), the ice sheet's margins migrated inwards while the ice sheet thinned. These models demonstrate that for sites very close to the ice sheet margin, a complex relative sea-level history can be expected. For the second scenario (figure 5.16b) there is competition between the collapse of the peripheral bulge and its migration inwards as the ice sheet shrinks. Because of this complexity, the detailed reconstruction of an ice sheet's melting history requires observations of relative sea level which are both spatially and temporally distributed.

Rate of melting

The glacio-isostatic response of the Earth to a deglaciation is dependent on the rate of the melting (figure 5.17). For an instantaneous melting of the ice load (figure 5.17a) the entire isostatic readjustment occurs after the end of the deglaciation which 'enhances' the observed isostatic effects after the deglaciation. For example, there is a larger high-stand at far-field continental sites and an apparent further delay in the sea-level rise at intermediate field sites following the a rapid deglaciation. For a slowly melting ice sheet (figure 5.17c), the Earth's response begins during the deglaciation and is partially complete by the end of the deglaciation. In this case, the magnitude of the far-field high-stand is reduced and the intermediate field response occurs sooner (relative to the end of the deglaciation). Therefore, the relative sea level at the present day (t=0 ka) is closer to the equilibrium value following a slow deglaciation, compared to a rapid melt.

Ice load history - Summary

The isostatic component of sea-level change is ice model dependent. If the Earth's rheological structure is known then observations of relative sea-level change can be used to establish constraints on the ice melting history. In reality, both the Earth and ice models will be partly known, at best. One approach is to use periods of well constrained sea level such as the post-LGM, to solve for the earth model appropriate for a given region, then assume that the same earth model is appropriate for earlier periods to make inference about the earlier ice history.

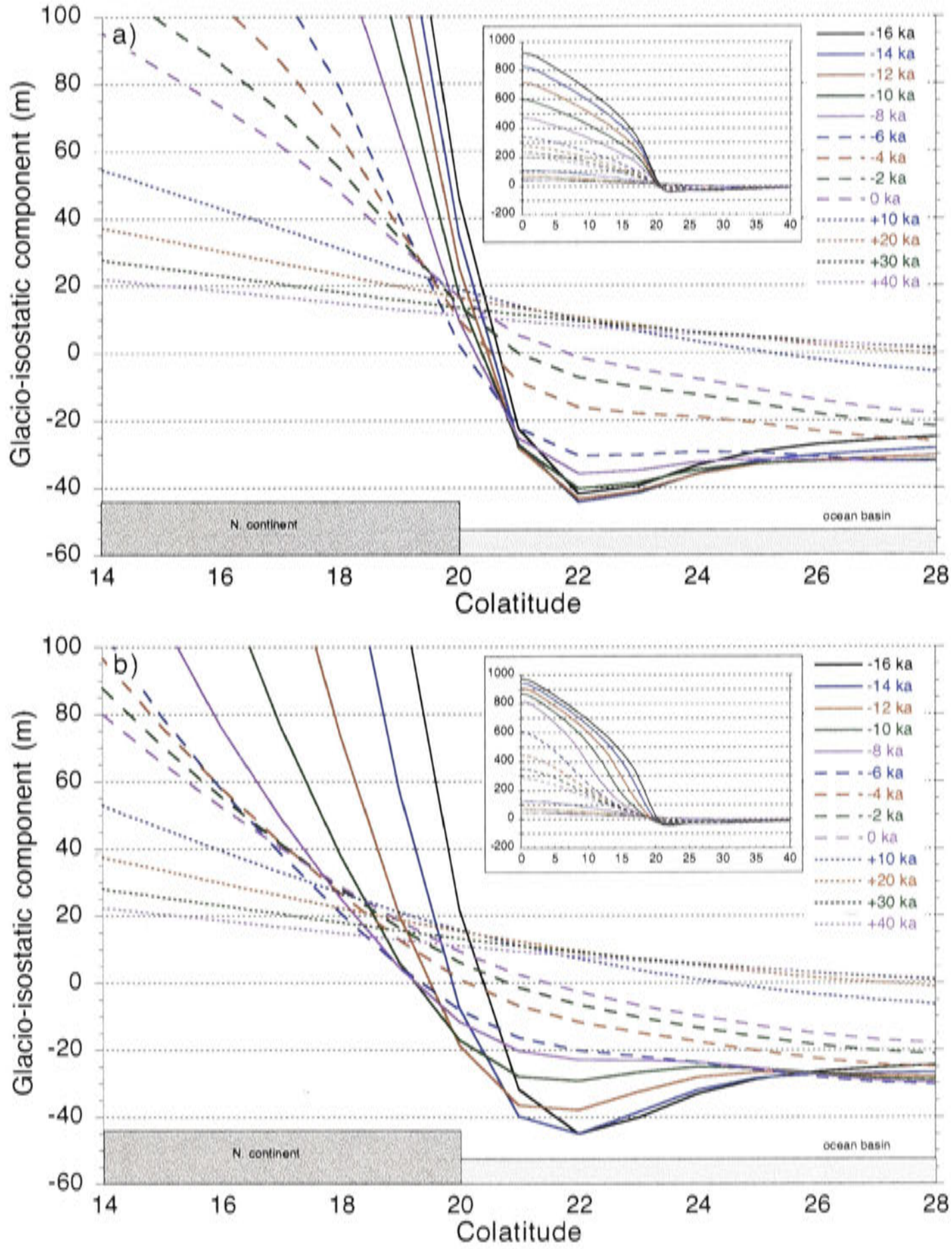

Figure 5.16: Glacio-isostatic component associated with a linear deglaciation between 18 ka and 6 ka, measured relative to equilibrium. The ice sheets in both panels have the same initial size and dimensions, width of ~2000km and central height of ~3.8 km. a) the ice sheet simply thins during the deglaciation. b) the ice sheet margins migrate inwards as the ice sheet thins. The rebound associated with the ice sheet in the upper panel (thinning only) is faster than for the lower panel (migration inwards and thinning) because the ice thickness at the centre of the load decreases more quickly. The glacio-isostatic response in the peripheral regions of the ice sheet are complex and are dependent on the areal extent of the ice sheet during the deglaciation.

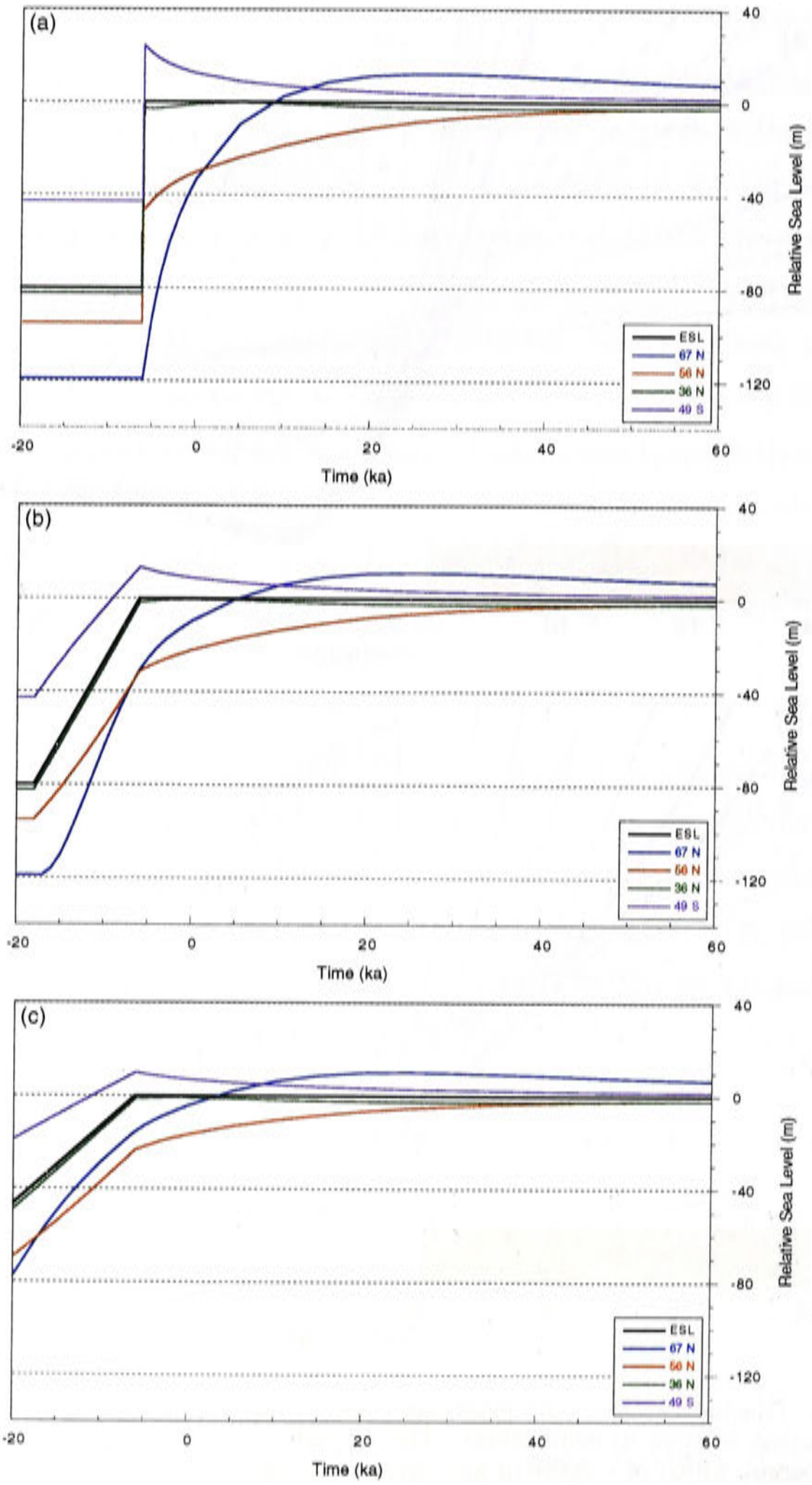

Figure 5.17: Relative sea-level curves at intermediate and far-field sites for different rates of deglaciation: a) near instantaneous (full deglaciation over ~0.1 ka) , b) reference (full deglaciation over 12 ka) and c) slow (full deglaciation over 24 ka).

5.6.5 Superposition of isostatic response

For a complicated surface loading history, relative sea-level results from a linear superposition of the exponentially decaying components of the viscoelastic response to previous surface loading events (equation 5.3). The relative sea-level change at intermediate and far-field sites due to a small oscillation in ice load is shown in figure 5.18a. If an oscillation of this type closely follows a major deglaciation (figure 5.18b), the relative sea-level curves from the two events interfere, producing a more complex response which is a superposition of individual loading histories. In figure 5.18c, the secondary oscillation is delayed. In this case, by the time of the secondary oscillation, the Earth's response to the major deglaciation is more complete and the relative sea-level curve for the secondary oscillation approaches that of the isolated oscillation seen in figure 5.18a.

5.6.6 Present-day deformation

In the previous sections, relative sea-level curves have been plotted relative to a near equilibrium state, where the Earth has relaxed completely following a change in surface loading. However, observations of past sea-level change are measured relative to the present, which is not in an equilibrium state. Figure 5.19 shows the calculation of sea level for a number of intermediate and far-field sites in response to a simple, sawtooth glacial cycle. Near the end of the last interglacial period in this model (at ~120 ka), the sea level at each of these sites is similar to one another (measured relative to the present day). This is because the ice melting history leading up to that time is similar to that leading up to the present and, as a consequence, the deformation at the two times is similar. At other times during the glacial cycle, the deformation of the Earth may be very different to the present day, leading to a large spread of relative sea levels as a function of location.

Because the relative sea level of past events is dependent on the present-day deformation of the Earth, the 'recent' history of surface loading (ie since the LGM) is an important factor in controlling the apparent relative sea level of those events. Changing the magnitude of the LGM ice sheets, or the rate of deglacial melting, affects the rate of glacio-isostatic readjustment and hence the present-day deformation of the Earth. The importance of 'recent' melting history is addressed further in the next chapter.

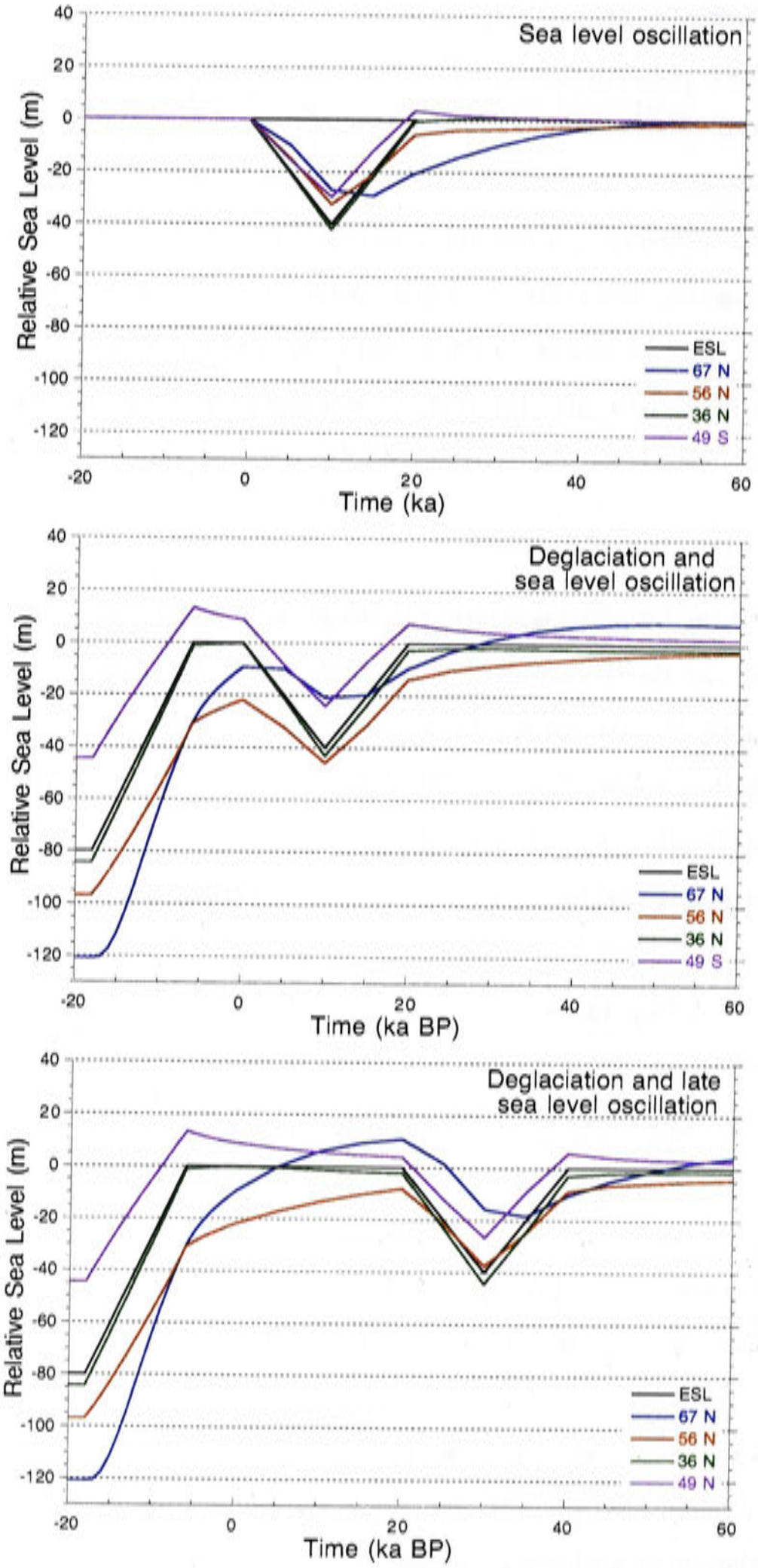

Figure 5.18: Relative sea-level curves for a) a minor oscillation in sea level; b) superposition of major deglaciation and minor oscillation; and c) superposition of major deglaciation and delayed minor oscillation.

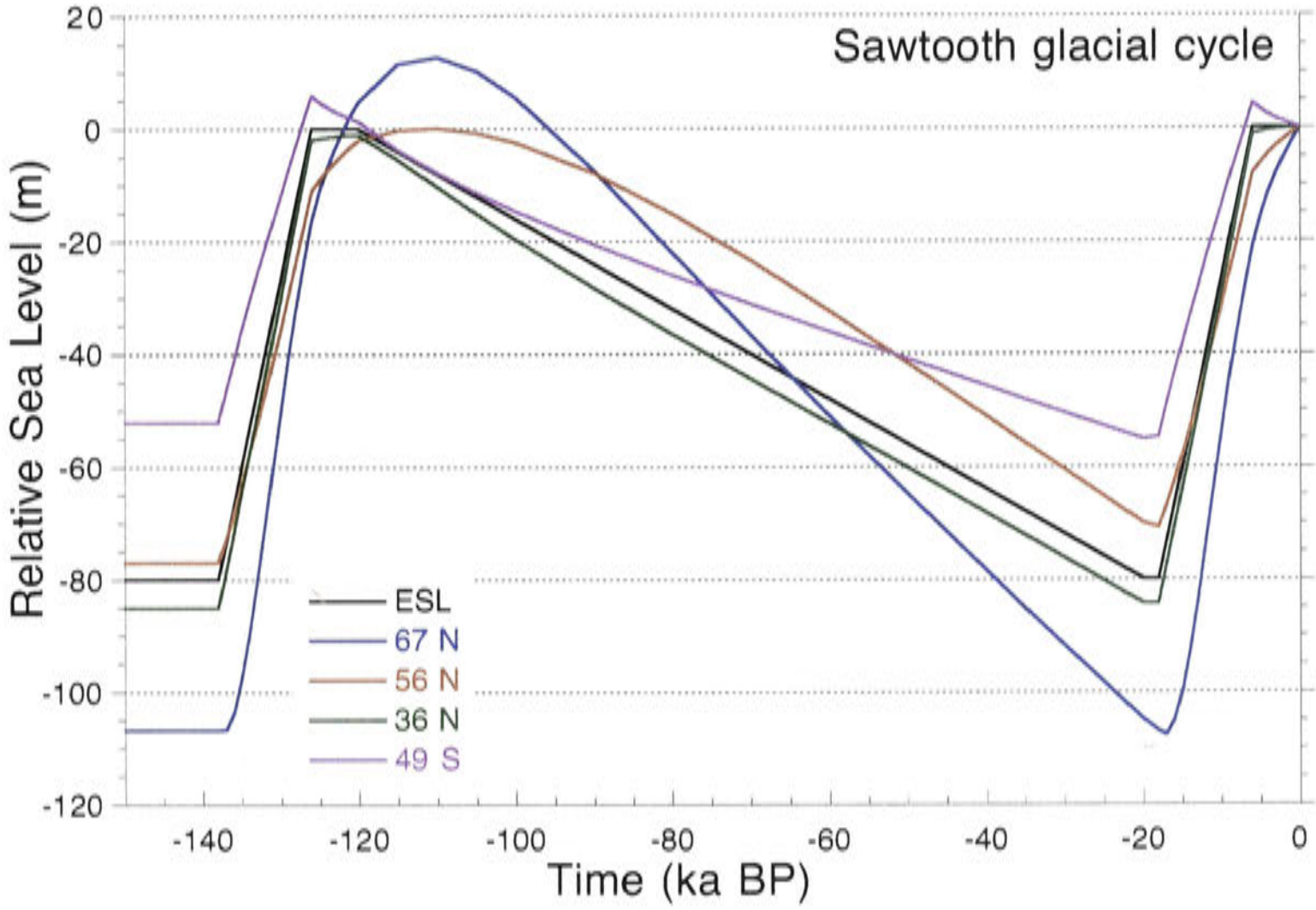

Figure 5.19: Relative sea level for a sawtooth glacial cycle measured relative to present day. Note that at ~120 ka, the sea levels at all the sites are similar because the deformation of the earth was similar to that of today. At other times, the isostatic deformation was different to that of the present day and so there is a spread of relative sea levels at those location.

5.7 Conclusion

In this chapter, I have used a simple axisymmetric model to demonstrate the principles of glacio-hydro-isostasy. Relative sea level at intermediate- and far-field sites is a complex function that is dependent on the rheological properties of the Earth, including the lithospheric thickness and mantle viscosities (section 5.6.3), ice sheet melting history prior to the time of interest (section 5.6.4) and the present-day isostatic state of the Earth (section 5.6.6). Further complexity is introduced when multiple and realistic ice sheets as well as a realistic distribution of ice and water surface loads are considered.

In the next chapter, I compare observations of relative sea-level change in the Caribbean and surrounding region during sub-stages 5a and 5c with predictions made using more realistic glacio-hydro-isostatic models. The sites of interest, between Barbados and the US East Coast, (discussed in chapter 4) lie in the intermediate-field zone of the Laurentide ice sheet. Using the spatially distributed data set of relative sea-level observations for the sub-stage 5a sea-level high-stand, I will explore what constraints may be placed on the rheology of the Earth and the melting history of the Laurentide Ice Sheet.

Chapter 6

Reconciling Sea-Level Observations in the Caribbean Region

6.1 Introduction

In this chapter realistic models of continental coastlines and ice sheet distribution are used to calculate the isostatic contribution to relative sea-level change in the Caribbean and surrounding regions during MIS 5. Redistribution of ice and water surface loads affects relative sea-level change through glacio-hydro-isostatic deformation of the Earth's crust, redistribution of mantle material and perturbation of the geoid (Farrell and Clark, 1976). For the simple axisymmetric models in the previous chapter, these isostatic effects are symmetric about the ice load. Additional complexity in the calculation of relative sea level is introduced by realistic ice melting models and coastlines.

Relative sea-level calculations are dependent on the rheology of the Earth and, in the region of interest to this study, the melting history of the Laurentide Ice Sheet (LIS). A spatially and temporally distributed set of relative sea-level observations is required to establish both the ice distribution and rheological parameters. Preliminary models of ice distribution can be uncertain because they are dependent on limited geological evidence of ice extent and models of ice sheet dynamics. A comparison of sea-level observations with those predicted by isostatic models can be used to improve preliminary ice and earth models.

In this chapter, I demonstrate that the seemingly contradictory observations of relative sea level during sub-stage 5a in the Caribbean region are reconciled by taking into account the effects of glacio-hydro-isostasy. The few observations of relative sea level during this period do not enable a detailed reconstruction of the Laurentide Ice Sheet's melting history.

However, these observations can be used to place some constraints on the ice distribution and earth rheology. In this chapter, I demonstrate how these parameters influence relative sea level during the last glacial cycle.

6.2 Defining a preliminary ice model

One aim of this investigation is to constrain global ice volume during the last glacial cycle by comparing relative sea-level observations with isostatic model predictions. Before this can occur an initial estimate of global ice volume and distribution is required. Absolute changes of global ice volume (ice-equivalent sea level) cannot be measured directly. Far-field sites are, by definition, relatively insensitive to the spatial distribution of ice and are influenced mainly by hydro-isostasy, the effects of which are generally small when compared to the large oscillations in sea level during the last glacial cycle. Therefore, relative sea-level observations at far field sites (such as Huon Peninsula) adjusted for a small hydro-isostatic correction, are a good first approximation to changes in ice-equivalent sea level and global ice volume.

The preliminary ice-equivalent sea-level curve for the last glacial cycle used in the following discussion is based on a number of sources. Sea-level change since the last glacial maximum has been recorded by coral growth at locations such as Barbados, Tahiti and Papua New Guinea (Fairbanks, 1989; Bard *et al.*, 1996; Chappell and Polach, 1991). Micropalaeontological studies of sediment cores from the Northwestern Australian shelf (Yokoyama, 1999) also helps to constrain the sea level during the LGM. With preliminary adjustment for isostatic effects, these records can be combined to define an ice-equivalent sea-level curve since the LGM (Lambeck *et al.*, 2002c).

Evidence of sea-level change prior to the LGM is often overprinted or destroyed by subsequent sea-level oscillations. Even where physical indicators of sea level during the last glacial cycle are preserved, they are often below present sea level and are difficult to access. At tectonically uplifting sites, these deposits can be exposed above present sea level. The best examples of uplifted coral reef deposits during the late Pleistocene are those at Huon Peninsula, Papua New Guinea and the island of Barbados, West Indies (see discussion in chapter 4). At these locations, major coral reefs formed when sea-level rise equalled or exceeded tectonic uplift. These uplifted reef terraces therefore represent reef growth during major interstadial periods. In particular, the high uplift at Huon Peninsula provides access to reef growth features that are not exposed at other locations.

Existing U-Th age data for these reefs has been used to calculate the magnitude of the sea-level high-stands associated with each of the MIS 5 features at Huon Peninsula (chapter 4, Lambeck and Chappell, 2001). The sea-level minima in that curve are based upon the position of stream deltas overlapping the terrace deposits that define sea-level high-stands (Chappell, 1974). Because of the uncertainties in the interpretation of the Huon Peninsula data (section 4.3.2), this sea-level curve may be open to revision. However, it provides a reasonable first estimate of ice-equivalent sea level, which can then be improved by combining further observations at Huon Peninsula and at other locations with models of relative sea-level change at these locations.

A preliminary estimate of the ice distribution of individual ice sheets must be made in order to accurately model the glacio-isostatic component of sea level. The geographical extent of the major ice sheets such as the Laurentide, Antarctic and Fennoscandian, and the smaller Innuitian, Cordilleran and Greenland ice sheets can be partially constrained by geologic indicators. The timing of ice retreat since the last glacial maximum (LGM) can be constrained by Carbon-14 dating of moraine material and cosmogenic exposure dating of rocks in formerly glaciated areas. Striations give an indication of the direction of ice movement. In some locations, trimlines record maximum ice height but observations of this type are not widespread. The total volume of an ice sheet cannot be constrained by geologic indicators alone. Instead, models of ice sheet dynamics are used to constrain the volume and distribution of ice within defined boundaries. However, model parameters such as basal conditions and rates of ablation and precipitation can be uncertain.

While evidence of ice extent and flow directions since the LGM exist in many regions formerly covered by ice, indicators of ice-sheet distribution during earlier periods are often destroyed or hidden by subsequent ice advances. Where physical evidence of ice extent does exist, the timing of deposition can be difficult to constrain. There is often a dearth of material for radiocarbon dating and this method can only be applied to material that is less than 40,000 to 50,000 years old. Electron Spin Resonance (ESR) dating of fossils and Thermoluminescence (TL) dating of sediment are imprecise and are dependent on the availability of suitable material. Because ice extent prior the LGM cannot be constrained directly, preliminary ice-sheet models during these earlier periods are supplemented by knowledge of the ice sheet's behaviour during the last deglaciation, i.e. the relationship between ice volume and ice extent.

Ice Sheet	References	Scaling at LGM
Laurentide	Licciardi *et al.* (1998)	1.3
Fennoscandian	Lambeck *et al.* (1998); Lambeck *et al.* (2000)	1.0
Antarctic	Nakada and Lambeck (1988); Denton and Hughes (1981)	1.2
Greenland	Peltier (1991) (ICE-3G)	1.5
Innuitian	as above	2.0
Cordilleran	as above	1.5

Table 6.1: Summary of ice sheets used in the preliminary model, original references and scaling applied at the LGM. Extra notes: Antarctic ice sheet based on ANT-3 (Denton and Hughes, 1981), scaled to 24 m at LGM and melting in phase with equivalent sea level. The relative sea-level calculations in this chapter are not sensitive to the relative partitioning of ice at far-field ice sheets such as the Antarctic and Fennoscandian.

Partitioning of global ice volume

The isostatic modelling in this chapter includes the effects of the 6 major ice sheets (summarised in figure 6.1 and table 6.1). The spatial distribution of these ice sheets is based on a combination of geologic evidence and, in some cases, the results of previous isostatic studies (references in table 6.1). The sum of the original individual ice sheet models chosen for this analysis was not equal to the global ice volume at the last glacial maximum inferred from sea-level observations, which is equivalent to ~135 m sea level (Yokoyama *et al.*, 2001a). This is not unexpected because of the large uncertainties involved in constraining the volume of individual ice sheets. Each model is, therefore, scaled by an amount that is judged to be within the uncertainties of the observational constraints and so that the total global ice volume at the LGM is consistent with sea-level observations. For the purposes of this chapter, the isostatic contribution to sea-level change in the Caribbean region is most sensitive to the ice volume and distribution of the LIS but relatively insensitive to the global distribution of far-field ice sheets. For this reason, the scaling parameters applied to various other ice sheets are not crucial to the calculations.

The Laurentide Ice Sheet (LIS) provides the most important contribution to the glacio-isostatic component of relative sea level in the Caribbean and surrounding region. The relative sea level at sites near the ice sheet's former margin is very sensitive to the distribution of ice within the ice sheet's boundaries. Models of ice height and total volume vary depending on the basal conditions assumed. Numerical ice growth models by Licciardi *et al.* (1998), show that for a soft bedded base, with water-saturated low viscosity sediments, the LGM Laurentide ice sheet has a multi-domed structure which is thin over the Hudson Bay area and has a relatively low total volume. In the case of a frozen-bedded model,

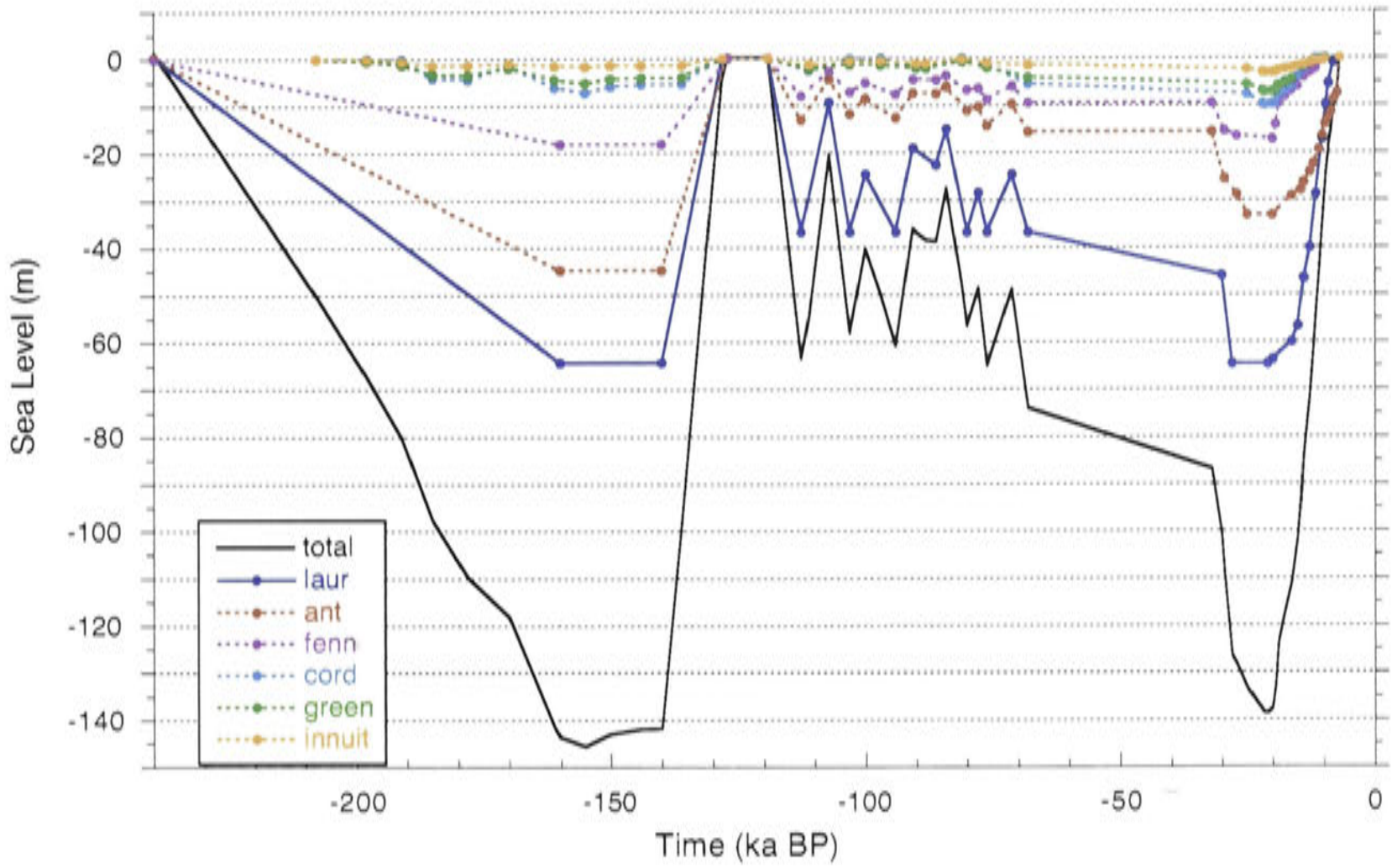

Figure 6.1: Contribution of six major ice sheets to total ice volume expressed in ice-equivalent sea level: Laurentide, Antarctic, Fennoscandian, Greenland, Cordilleran and Innuitian Ice Sheets. References for original ice sheet models are listed in table 6.1 and are scaled to produce a total ice volume at the LGM which is consistent with sea-level observations at that time (Yokoyama, *et al.*, 2001b). The melting history during MIS 7-6 and MIS 3 have been simplified as they do not have a significant effect on the sub-stage 5c and 5a calculations. This preliminary ice model will be referred to as R-0.

the ice sheet approaches a single-domed structure and can achieve a higher volume (e.g. Peltier and Andrews, 1976; CLIMAP Project Members, 1976). Licciardi *et al.* (1998) provide maximum and minimum ice sheet reconstructions since the LGM which are consistent with the available evidence of ice extent during that period (figure 6.2).

Records of the boundaries of the LIS prior to the LGM are scarce, as they have generally been overprinted by subsequent ice sheet advances. During the last interglacial period the Earth's climate was similar to that of today and global ice volume was comparable. Following the last interglacial, constraints on the distribution of the LIS (Clark *et al.*, 1993) are based on limited geological evidence such as glacial sediment. The LIS first developed in the north over Quebec and Baffin Island, and ice volumes may have been small (Clark *et al.*, 1993; Kleman *et al.* 2002). Much of the southern sector of the LIS remained ice-free during stage 5. The onset of major glaciation in the southern region of the Laurentide occurred during MIS 4. Marine records suggest a decrease of glaciation at high latitudes after MIS 5 (Clark *et al.*, 1993). The northern margin of the LIS was more heavily glaciated during MIS 5 than during the subsequent LGM advance.

Licciardi *et al.*'s (1998) maximum ice model defined LIS ice extent and distribution for a series of time steps during the last deglaciation. The Laurentide ice model for the last glacial cycle used in this study is an extension of Licciardi *et al.*'s last deglaciation model to earlier time periods (figure 6.3). Where geological evidence constrains ice extent for a time during MIS 3 and 5, the closest equivalent time step from Licciardi *et al.*'s model was applied while remaining consistent with the MIS 5 geologic evidence. The constraint that the MIS 5 ice sheet remained north of the St Lawrence Lowlands was considered the most important for the preliminary model. A more northerly situated ice sheet MIS 5 ice sheet (suggested by Clark *et al.*, 1993) is investigated later in this chapter. The cyclical nature of global sea level, inferred from sea-level observations, is applied to the growth and decay of the Laurentide during MIS 5. If necessary, the ice model at each time step is scaled to be consistent with the assumed equivalent sea-level contribution of the LIS at that time. For simplicity, in the preliminary model, the north-south balance of Licciardi's last deglaciation ice model is also applied to the corresponding time-step during MIS 5. The effect of changing the distribution of ice within the MIS 5 boundaries is discussed later in this chapter.

The partitioning of ice among the other major ice sheets is also shown in figure 6.1. An accurate global ice distribution among the far-field ice sheets is not crucial to the calcula-

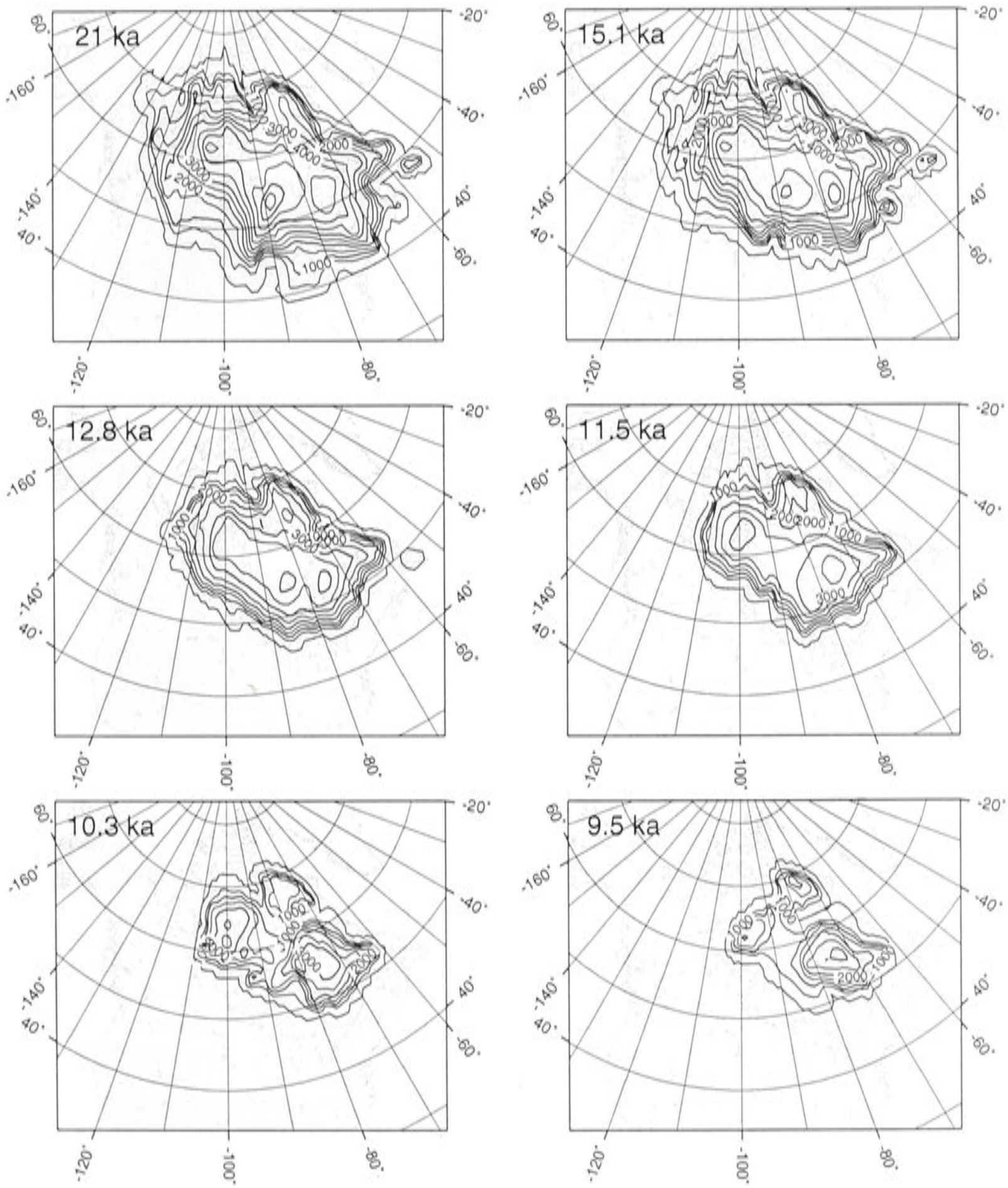

Figure 6.2: Contour plots of LIS ice thickness for timesteps in Licciardi *et al.*'s (1998) ice model (scaled) for the last deglaciation (approx. calibrated years)

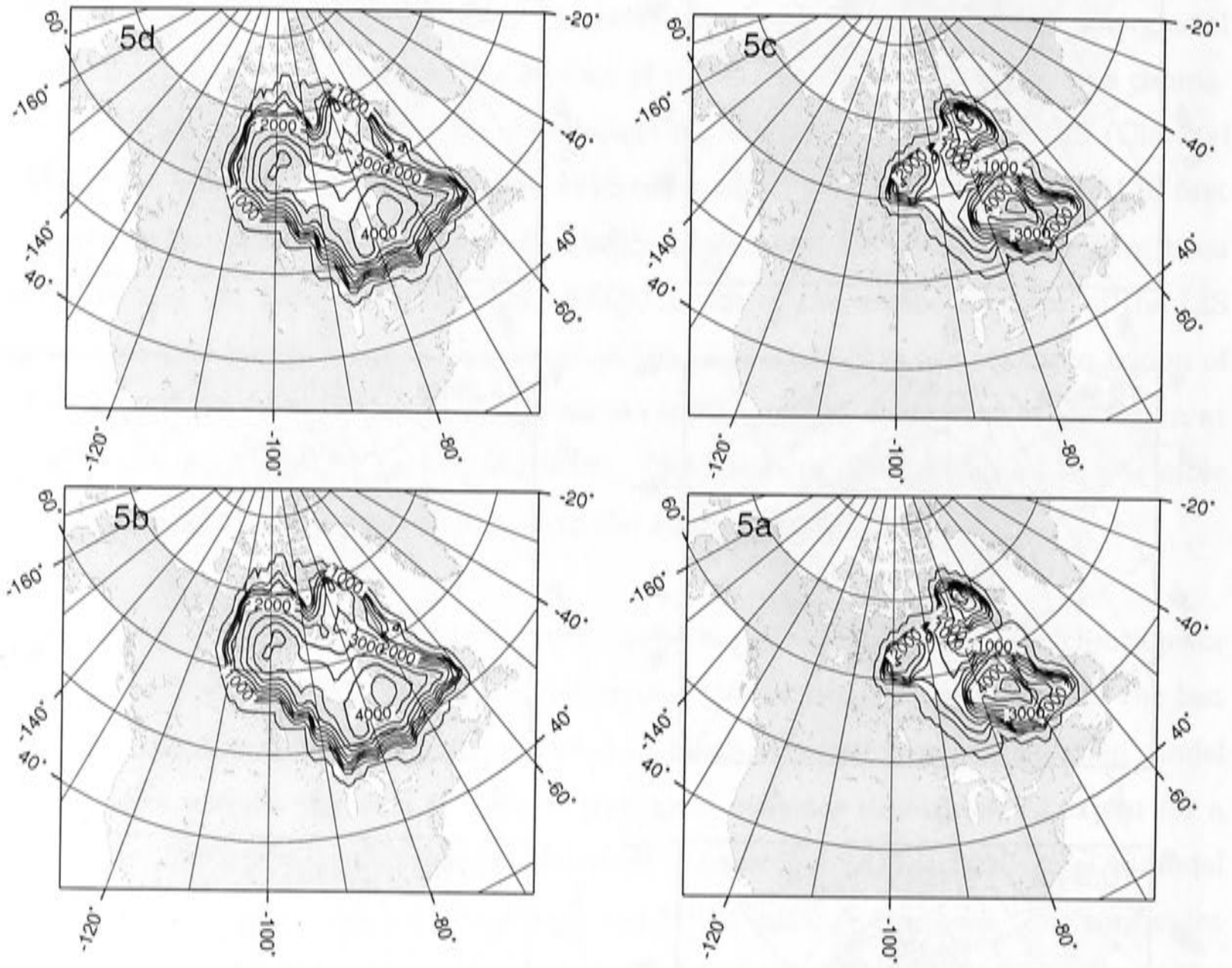

Figure 6.3: Contour plots of LIS ice model during MIS 5 sub-stage 5d, 5c, 5b and 5a, based on the Licciardi *et al.* (1998) last deglaciation model. The ice extent of these models is consistent with the observations that suggest the southern margin of the LIS did not reach the St Lawrence Lowlands during the sub-stage 5d-5a period. The north-south balance of the Licciardi *et al.* model for each corresponding time-step has been maintained. The ice volumes have been scaled up so the contribution of the LIS, as a proportion of global ice volume, during this time period is similar to that of the last deglaciation. This produces large ice thickness, which may not be realistic. In section 6.6.3, I will discuss modifications to this ice model, which include reducing the volume during this period.

tion of sea levels in the Caribbean region. For the modelling in this chapter, the ice sheet melting history during the penultimate glacial cycle (MIS 7-6) and MIS 3 has been simplified because the stage 5a relative sea levels are not particularly sensitive to the details of the ice melting history during those time periods. This preliminary ice model will be referred to as model R-0.

6.3 Components of isostasy during sub-stage 5a

The primary purpose of this chapter is to examine the relative sea level at sites in the Caribbean region at the 84 ka peak of sub-stage 5a. Using the preliminary ice model (R-0) and a reference earth model (ma4A), relative sea level was calculated for the south-eastern US and the Caribbean region (contour plot in figure 6.4a, b). These calculations demonstrate that for the regions both beneath the ice sheet and near its margins where the contours are concentric around the ice sheet, the relative sea level is dominated by the glacio-isostatic response. Relative sea level at intermediate-field sites in the Caribbean region is sensitive to the position of the glacial peripheral bulge, where the contours are still concentric around the ice sheet. Further south, near the coasts of Central and South America, hydro-isostatic effects become more apparent where the contours follow the shape of continental shelf edges.

The total relative sea level at the peak of sub-stage 5a and its glacio- and hydro-isostatic components have been calculated for a series of sites along an arbitrary transect between the southern margins of the Laurentide Ice Sheet and the north coast of South America (figures 6.5 and 6.6). Both the deformation and gravitational effects associated with the LIS load are included in the glacio-isostatic component. The complexity seen in the hydro-isostatic component is due to the geometry of the continental margins and the large island of Haiti and the Dominican Republic. The hydro-isostatic component that is shown is the third iteration of the sea-level calculation and therefore includes the extra water loading effects associated with the glacio-isostatic deformation and gravitation near the LIS margin and coast of the North American continent, as well as the effects of the time-dependence of the shorelines.

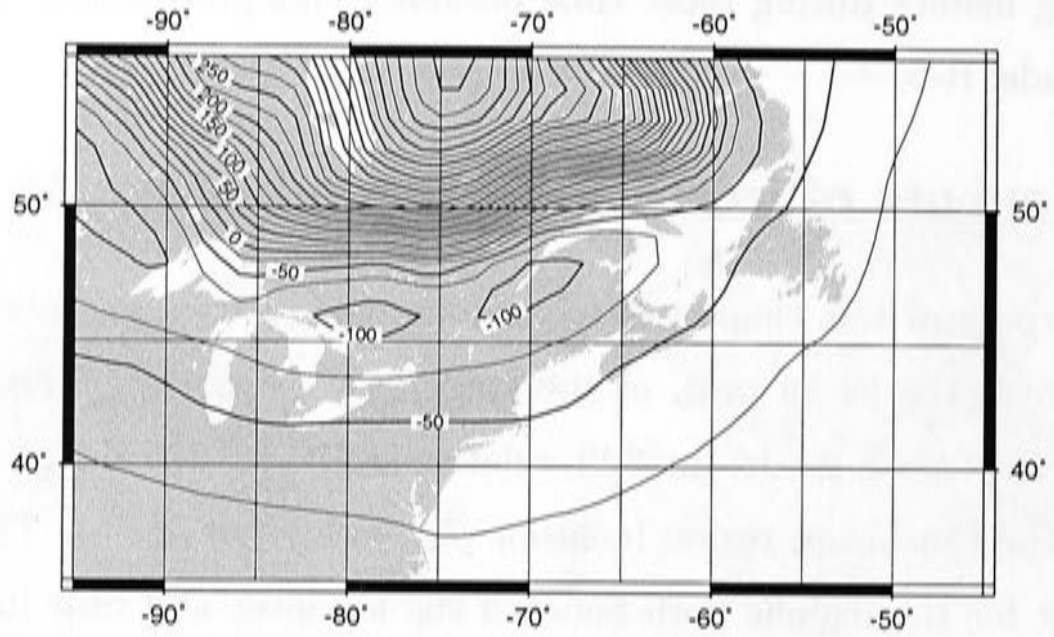

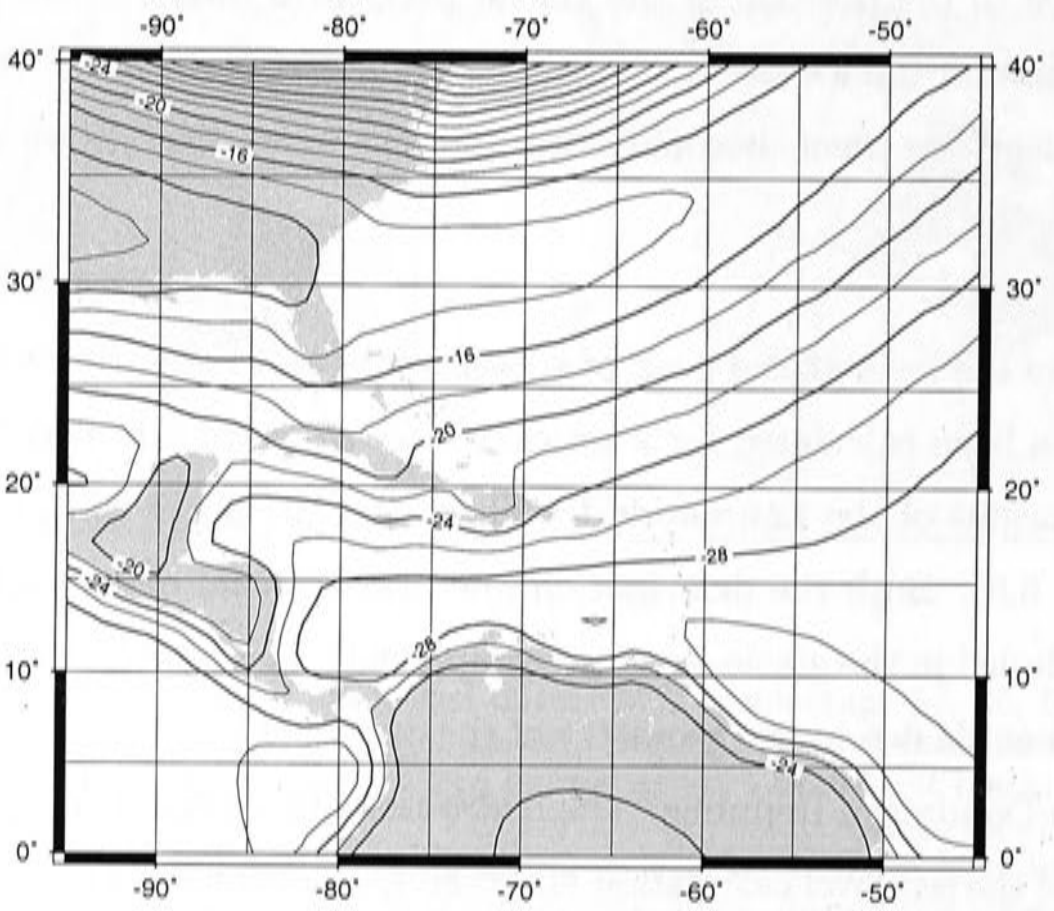

Figure 6.4: Contour plot of relative sea level at the peak of sub-stage 5a (84 ka) relative to the present day in the Caribbean and surrounding regions. The upper panel shows the region occupied by the southern sector of the Laurentide Ice Sheet. The concentric contours around the ice sheet location demonstrate that the glacio-isostatic component dominates in the near and intermediate field. Further south, in the bottom panel, the glacio-isostatic deformation reduces and the contours begin to follow the continental shelf edges, as a consequence of hydro-isostatic deformation. Note the different contour scales in the two plots.

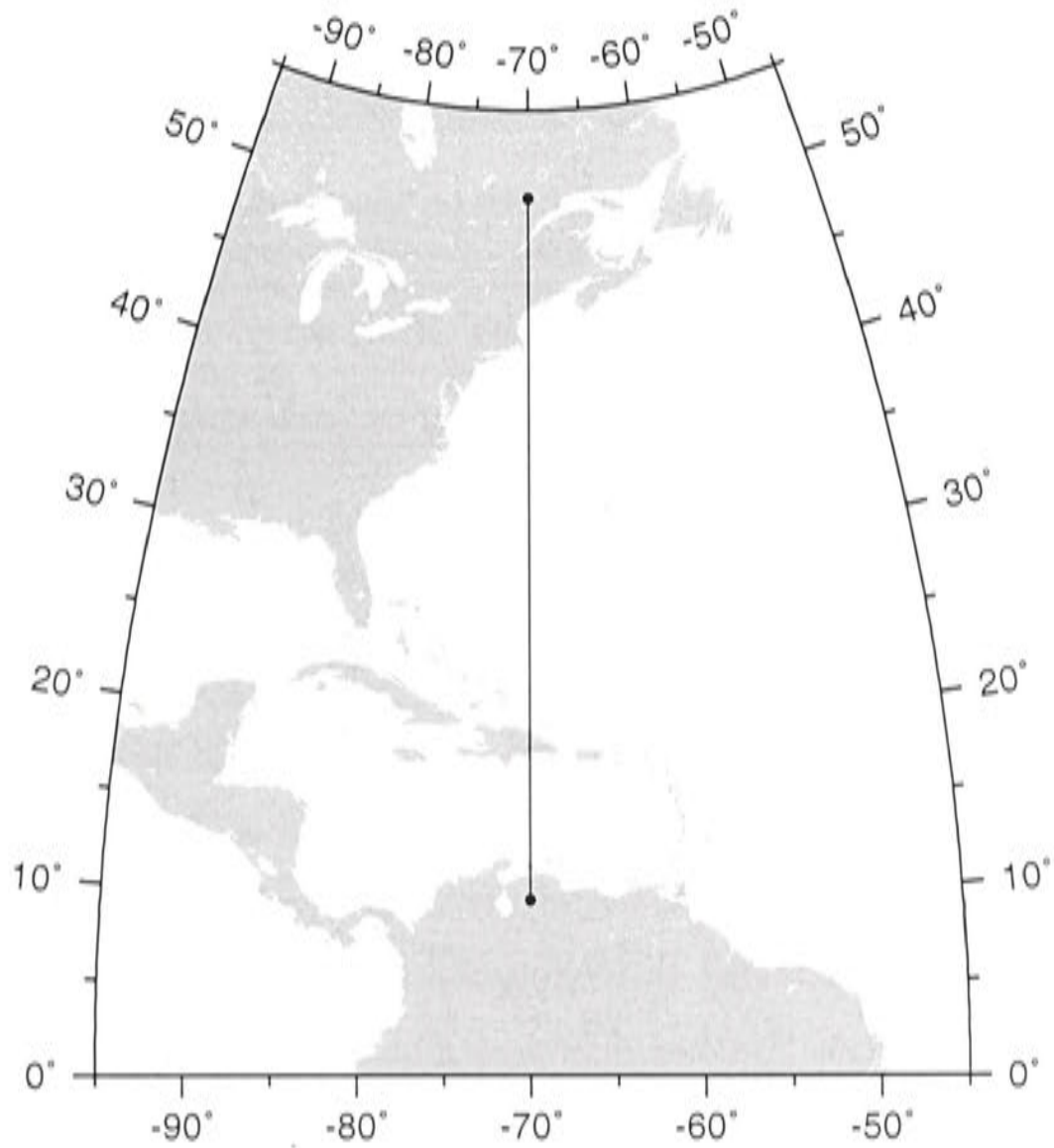

Figure 6.5: This north-south transect through the Laurentide Ice Sheet and Caribbean region is used for the sea level calculations in figures 6.6 and 6.7.

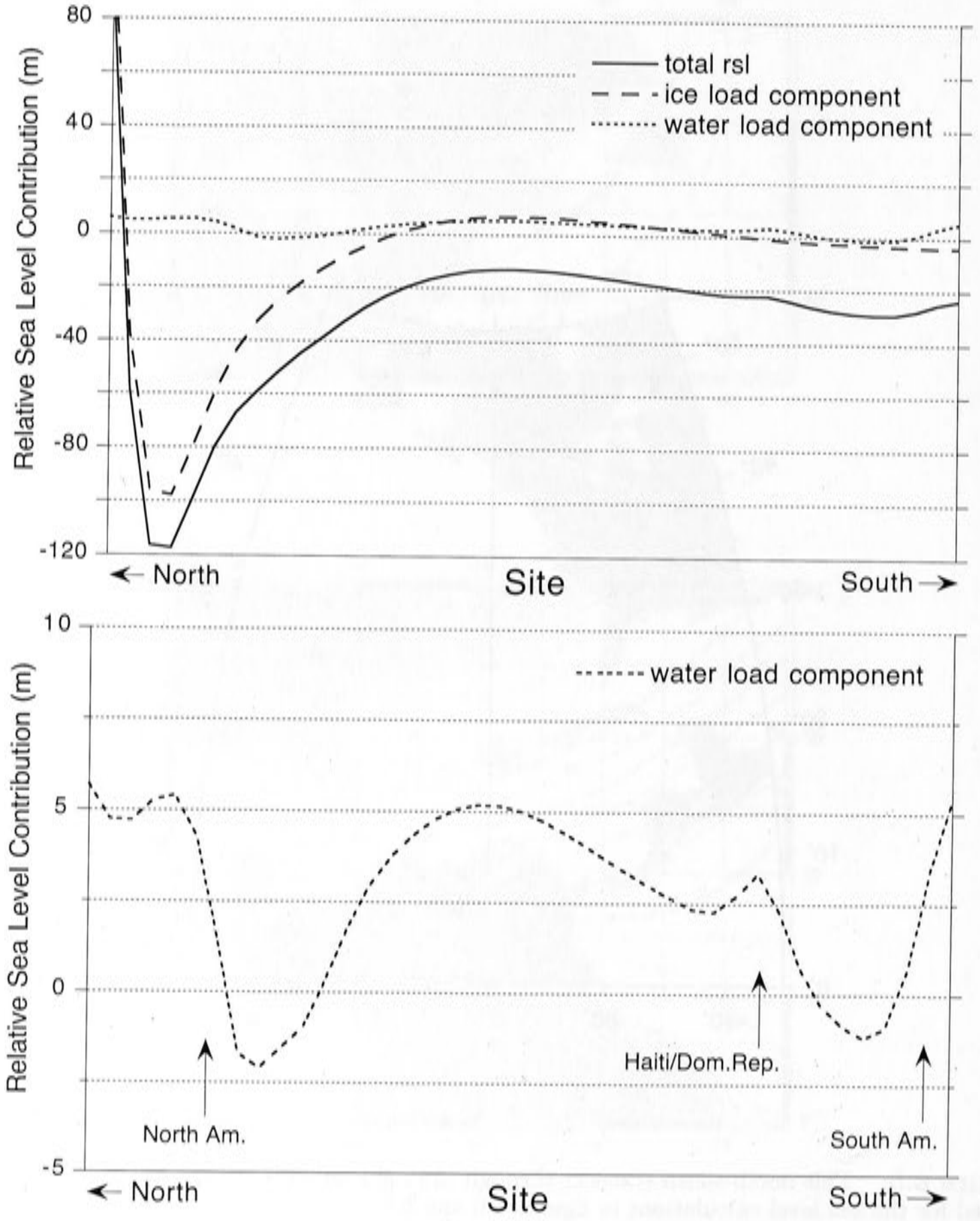

Figure 6.6: Total relative sea level and ice and water components of relative sea level for substage 5a for the N-S transect of figure 6.5. The complexity in the hydro-isostatic component is due to the geometry of the North and South American coastlines and the island of Haiti and the Dominican Republic.

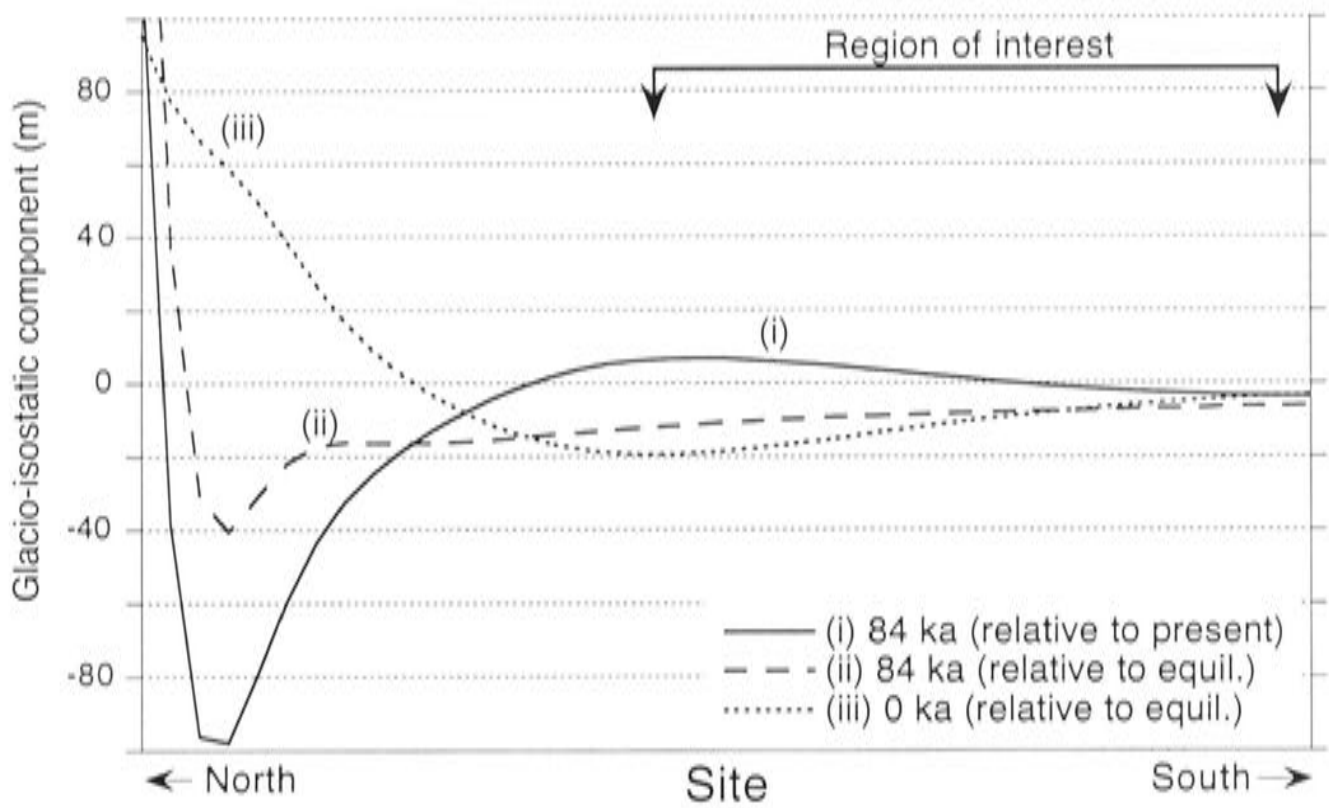

Figure 6.7: The glacio-isostatic component at sub-stage 5a (84 ka BP) relative to present (curve (i)) is equal to the difference between the glacio-isostatic component at sub-stage 5a (84 ka BP) relative to equilibrium (curve (ii)) and the glacio-isostatic component at the present day (0 ka) relative to equilibrium (curve (iii)). This calculation is for the transect of sites shown in figure 6.5. In this region of interest, which corresponds to the Caribbean region, this glacio-isostatic component which has a large gradient across the region.

At the present day, the Earth has not completely relaxed following the last deglaciation, most notably in regions near former ice sheets. The glacio-isostatic component at sub-stage 5a (84 ka BP) relative to present (curve (i) in figure 6.7) is simply equal to the difference between the glacio-isostatic component at sub-stage 5a (84 ka BP), relative to equilibrium (curve (ii) in figure 6.7) and the glacio-isostatic component at the present day, relative to equilibrium (curve (iii) in figure 6.7). The broad present-day collapsing glacial bulge is responsible for a substantial part of the gradient in the glacio-isostatic component (and hence of sea level) at sub-stage 5a relative to the present day in the region of interest.

6.4 Factors controlling sub-stage 5a relative sea-level change

The rate and magnitude of the Earth's response to variations of surface loading in the region of interest is controlled by the melting history of the LIS and the Earth's rheological structure. Before making a direct comparison between observations of sub-stage 5a relative sea level with the isostatic model predictions, I demonstrate these effects for a transect of sites through this region (figure 6.8).

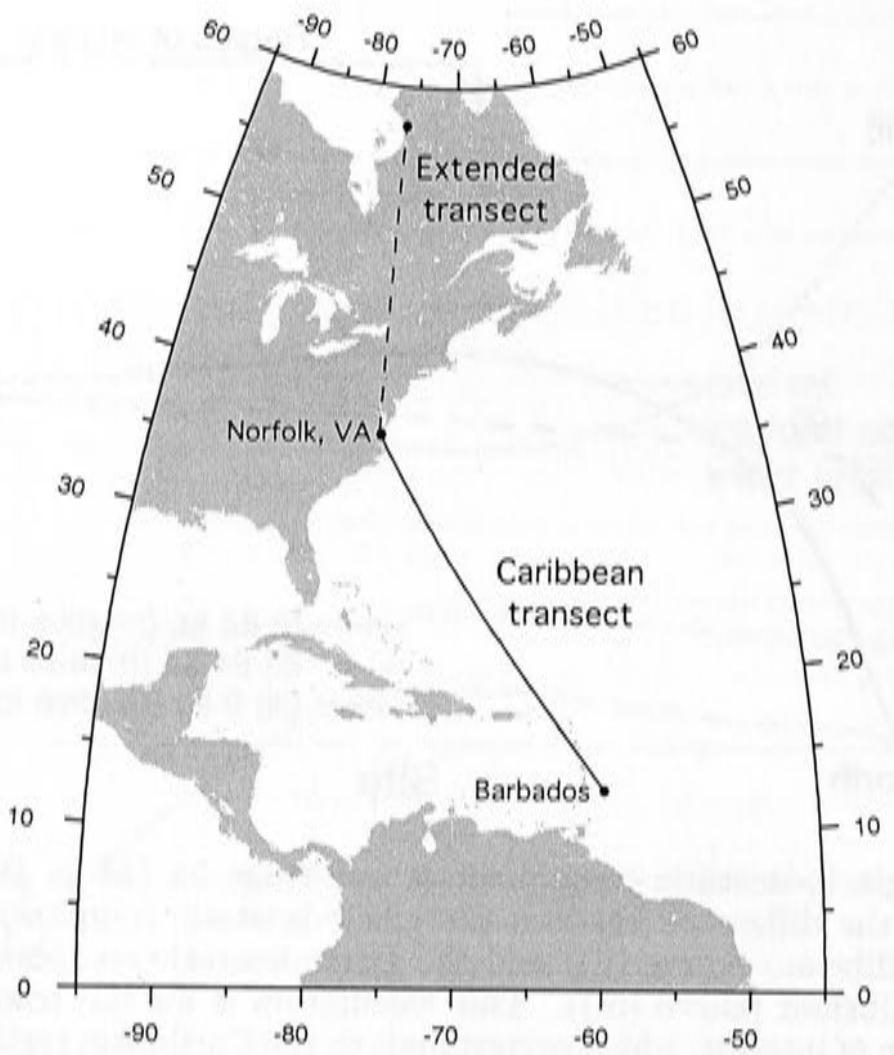

Figure 6.8: Transect of sites through the Caribbean region for demonstrating the behaviour of relative sea level in response to changing ice and earth model parameters. The extended transect in figure 6.8 is used in the following discussion to show the behaviour of glacio-isostasy in the interior and near-field regions of the LIS.

6.4.1 Earth rheology

As discussed before, the glacio-isostatic component of sea-level change in the Caribbean region at the peak of sub-stage 5a is controlled by two factors: i) the deformation of the Earth at 84 ka resulting from the surface load at (and prior to) that time and ii) the present-day deformation of the Earth relative to equilibrium resulting from the more recent melting history of the ice sheet, ie since the LGM. Both of these components are sensitive to the rheological structure of the Earth.

Lithospheric thickness

A change in the effective thickness of the elastic lithosphere between 50 and 80 km (compare mb4A and mc4A in figures 6.9 and 6.10) does not have a significant effect on the calculated gradient in relative sea level for this transect, only modifying the amplitude of relative sea level by a maximum of ~4 m. The reason the effect is small is because the size of the Laurentide Ice Sheet load is very large compared to the flexural wavelength of the lithosphere.

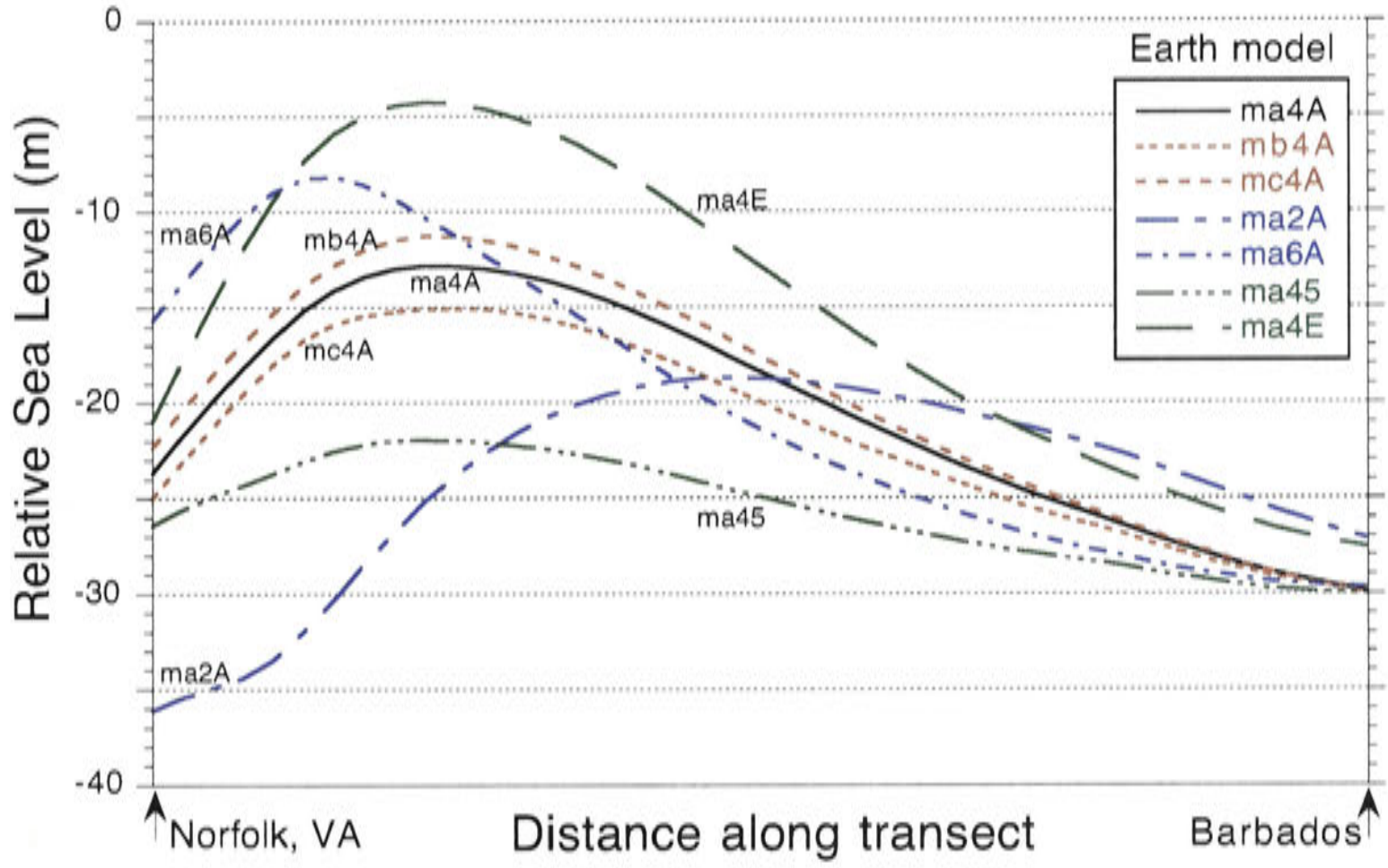

Figure 6.9: The results of relative sea-level calculations for the transect of sites throughout the Caribbean region (figure 6.8) for a series of Earth rheological models (table 6.2). The Earth models, as in chapter 5, are 4 layer models with an elastic lithosphere of thickness, h, two mantle layers with viscosities $\eta_u m$ and $\eta_l m$, and an inviscid fluid core (see table 6.2). The viscoelastic parameters used in the calculations in this chapter bound the range of realistic rheology. The magnitude of the gradient in relative sea level across the region of interest is influenced by rheology. The northern sites, near the ice sheet margin are particularly sensitive to mantle viscosity. See text for discussion.

Model	H_L (km)	η_{um} (Pa s)	η_{lm} (Pa s)
ma4A	65	4×10^{20}	1×10^{22}
mb4A	50	4×10^{20}	1×10^{22}
mc4A	80	4×10^{20}	1×10^{22}
ma2A	65	2×10^{20}	1×10^{22}
ma6A	65	6×10^{20}	1×10^{22}
ma45	65	4×10^{20}	5×10^{21}
ma4B	65	4×10^{20}	2×10^{22}
ma4C	65	4×10^{20}	3×10^{22}
ma4D	65	4×10^{20}	4×10^{22}
ma4E	65	4×10^{20}	5×10^{22}

Table 6.2: Rheological parameters for the earth models used in this study. Lithosphere, with effectively infinite viscosity, with thickness H_L (km); Upper mantle with effective viscosity of η_{um}; Lower mantle with effective viscosity of η_{lm}.

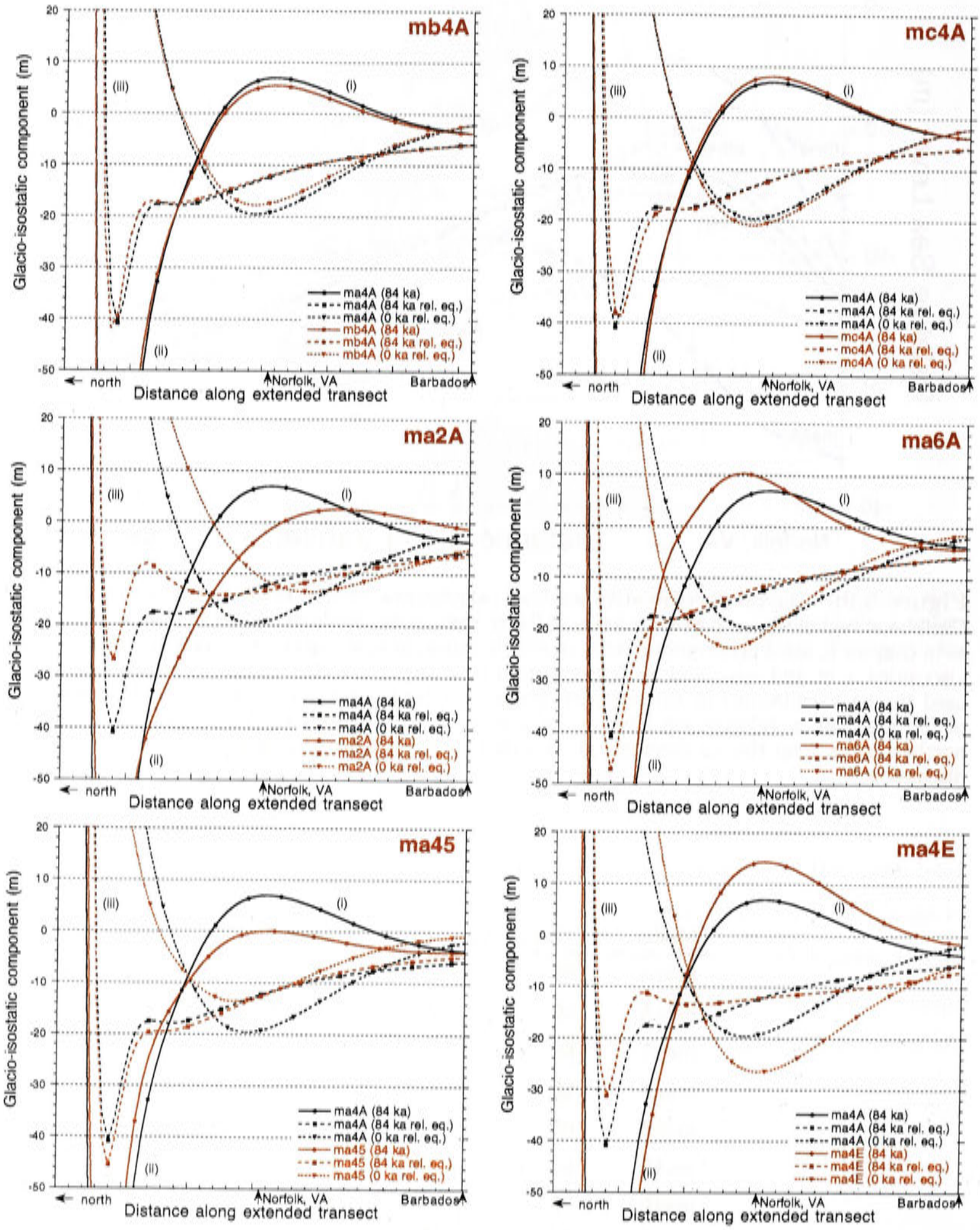

Figure 6.10: For each of the rheological models listed in table 6.2: (i) The glacio-isostatic components at 84 ka relative to the present compared to (ii) the glacio-isostatic component at 84 ka relative to equilibrium and (iii) the present-day deformation relative to equilibrium. The gradient in sea level and the sensitivity of the relative sea-level calculations to changes in Earth rheology, in the region of interest, is contained mainly in the glacio-isostatic component at the present relative to equilibrium.

Upper mantle viscosity

A change in the upper mantle viscosity affects the rate of response of the mantle to changes in surface loading. As upper mantle viscosity is increased (compare ma4A and ma6A in figures 6.9 and 6.10), the Earth's response to unloading is slower and the peripheral bulge is larger at both 84 ka BP and at the present day, relative to equilibrium. Because the glacial peripheral bulge broadens as it collapses as a consequence of the viscosity contrast between the upper and lower mantle (see section 5.6.2 in chapter 5), the position as well as the magnitude of the present-day collapsing glacial bulge relative to the former ice sheet's margin is highly sensitive to the upper mantle viscosity. For an increase in upper mantle viscosity, the peripheral bulge broadens more slowly and its peak remains closer to the former ice sheet margin. Decreasing the upper mantle viscosity (compare ma4A to ma2A) quickens the response of the upper mantle to unloading. As a result, the surface deformation collapses and broadens more quickly.

Lower mantle viscosity

The magnitude and position of the peripheral bulge at 84 ka and at the present day is also sensitive to lower mantle viscosity. An increase in lower mantle viscosity (compare ma4A and ma4E in figures 6.9 and 6.10) leads to a larger and broader present-day collapsing peripheral bulge because the redistribution of lower mantle material does not respond as rapidly to the unloading. Decreasing the lower mantle viscosity (compare ma4A and ma45) leads to a more rapidly collapsing bulge. The location of the peak of the collapsing bulge is not very sensitive to lower mantle viscosity.

Summary

Both the glacio-isostatic component at 84 ka relative to equilibrium and present-day deformation relative to equilibrium are influenced by the Earth's rheology. However, the latter component is more sensitive to changes in viscoelastic parameters and is the dominant factor in controlling the magnitude and location of the relative sea-level spatial maximum in the region of interest. While the magnitude of the gradient in sea level is most sensitive to changes in lower mantle viscosity, it is change in upper mantle viscosity which has the most influence on the location of the relative sea-level peak (figure 6.10).

6.4.2 Laurentide melting history during MIS 5

The glacio-isostatic contribution to relative sea level at the time of interest in the Caribbean region is primarily controlled by the melting history of the Laurentide Ice Sheet. The alternative models discussed in the following sections are designed to test the sensitivity of

the response to aspects of the model and are not necessarily realistic in some cases. Two alternative models of the ice sheet melting history prior to the peak of sub-stage 5a (figure 6.11), in which the ice boundaries and total volume are changed, are compared to the preliminary reference model (R-0, figure 6.12). In alternative 1 (dashed), the transition of ice melting from sub-stage 5b to 5a occurs earlier than the reference model and so the isostatic response to unloading is more complete by the 5a peak (at 84 ka). The effect of this is an increase in the gradient and sea-level values across the region. For alternative 2 (dotted), in which the 5b to 5a transition is delayed, the Earth's response is less complete at the peak of sub-stage 5a and the gradient in sea level is decreased.

Scaling the volume (or ice thickness) of the Laurentide Ice Sheet during the 5d-5a period changes the magnitude of the deformation in the region of interest at the peak of sub-stage 5a. Figure 6.13 shows the effect of decreasing the magnitude of the Laurentide Ice Sheet by 50% during the entire MIS 5 period but increasing the far-field ice volume (ie Antarctic) to maintain the same equivalent sea level throughout that period. The effect of reducing the ice volume during this period is to reduce the glacio-isostatic deformation at 84 ka relative to present and hence increase the total apparent sea level and steepen the gradient across the region of interest.

Following a change in surface loading, the Earth approaches its fluid limit over a period of time defined by its viscous structure. Therefore, the relative sea level at the peak of sub-stage 5a is much more sensitive to the detail of the Laurentide Ice Sheet's melting history during sub-stage 5b than during earlier times. The effect on the predicted sub-stage 5a sea levels by increasing the sub-stage 5b and 5d Laurentide Ice Sheet volume by 30% (figure 6.14) is shown in figure 6.15. Increasing the LIS ice volume during sub-stage 5b by 30% has a much larger effect (3-4 m) than increasing the sub-stage 5d ice volume by the same proportion (~1 m). Changing the stage 6 ice volume by 30% has an insignificant effect on the sub-stage 5a sea level (not shown here) but would be very important in controlling sub-stage 5e relative sea level in the region.

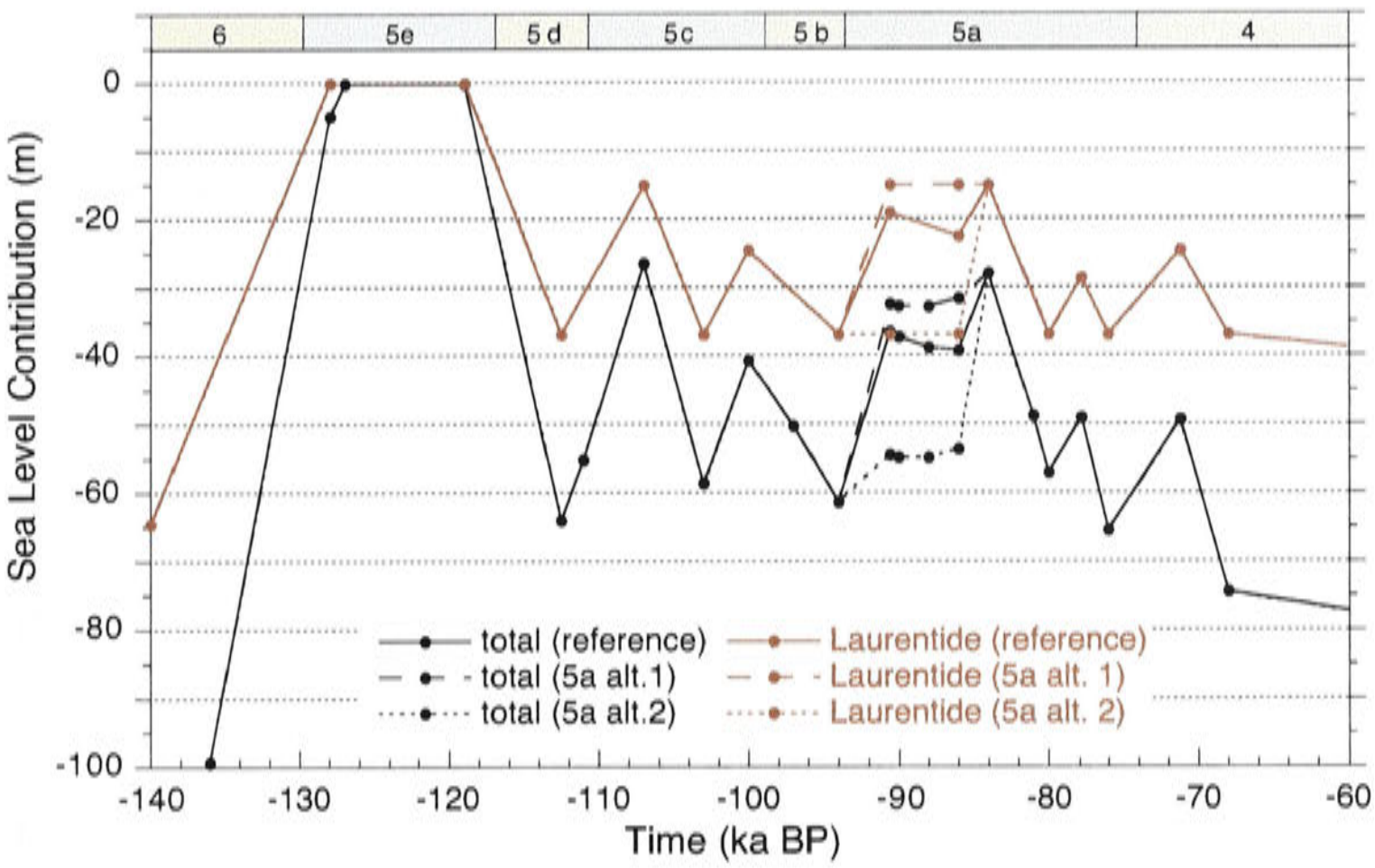

Figure 6.11: Alternative models for the sub-stage 5b to 5a transition. In alternative 1 (dashed), the transition of ice melting from sub-stage 5b to 5a occurs earlier than the reference model. For alternative 2 (dotted), the 5b to 5a transition is delayed.

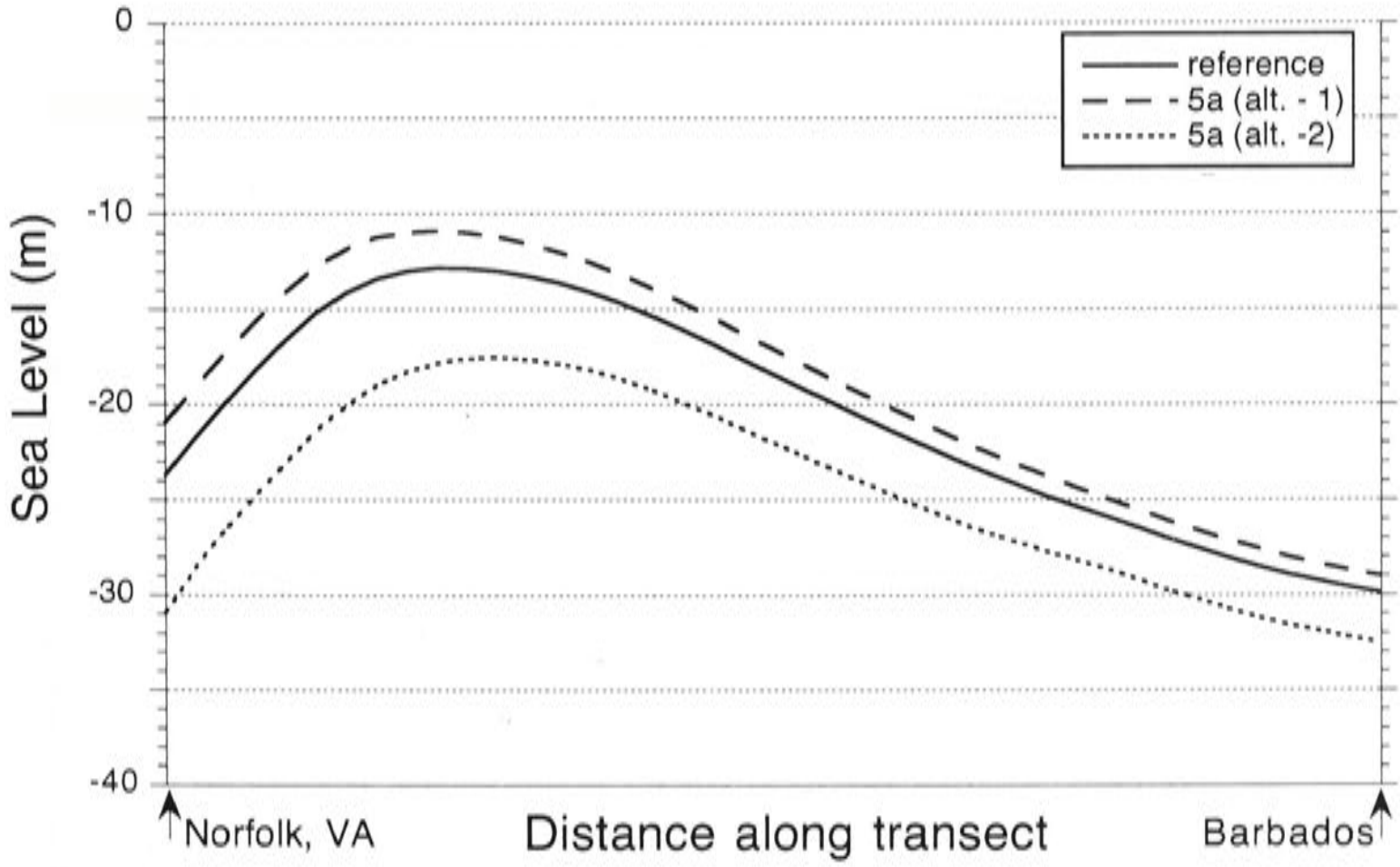

Figure 6.12: Relative sea-level calculations for the alternative sub-stage 5b to 5a alternative melting models defined in figure 6.11. In alternative 1 (dashed) the isostatic response to unloading is more complete by the 5a peak (at 84 ka) and the gradient in sea level is increased. In alternative 2 (dotted) the Earth's response is less complete at the peak of sub-stage 5a and the gradient in sea level is decreased.

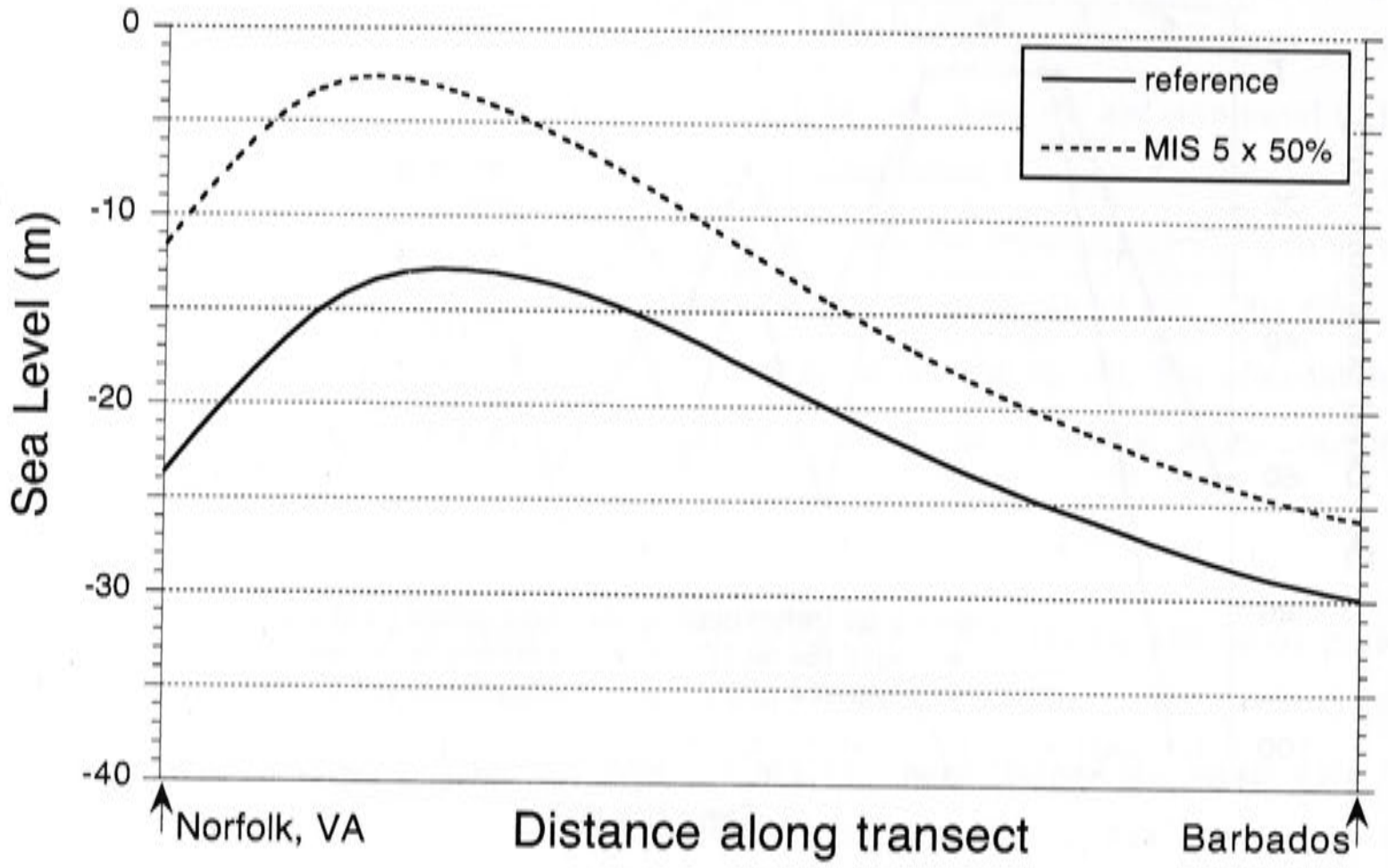

Figure 6.13: Relative sea-level calculations for scaling down of MIS 5 reference model Laurentide ice volume by 50%. This acts to reduce the glacio-isostatic deformation at 84 ka relative to present and increase the total apparent sea levels and steepen the gradient across the region of interest (dashed line).

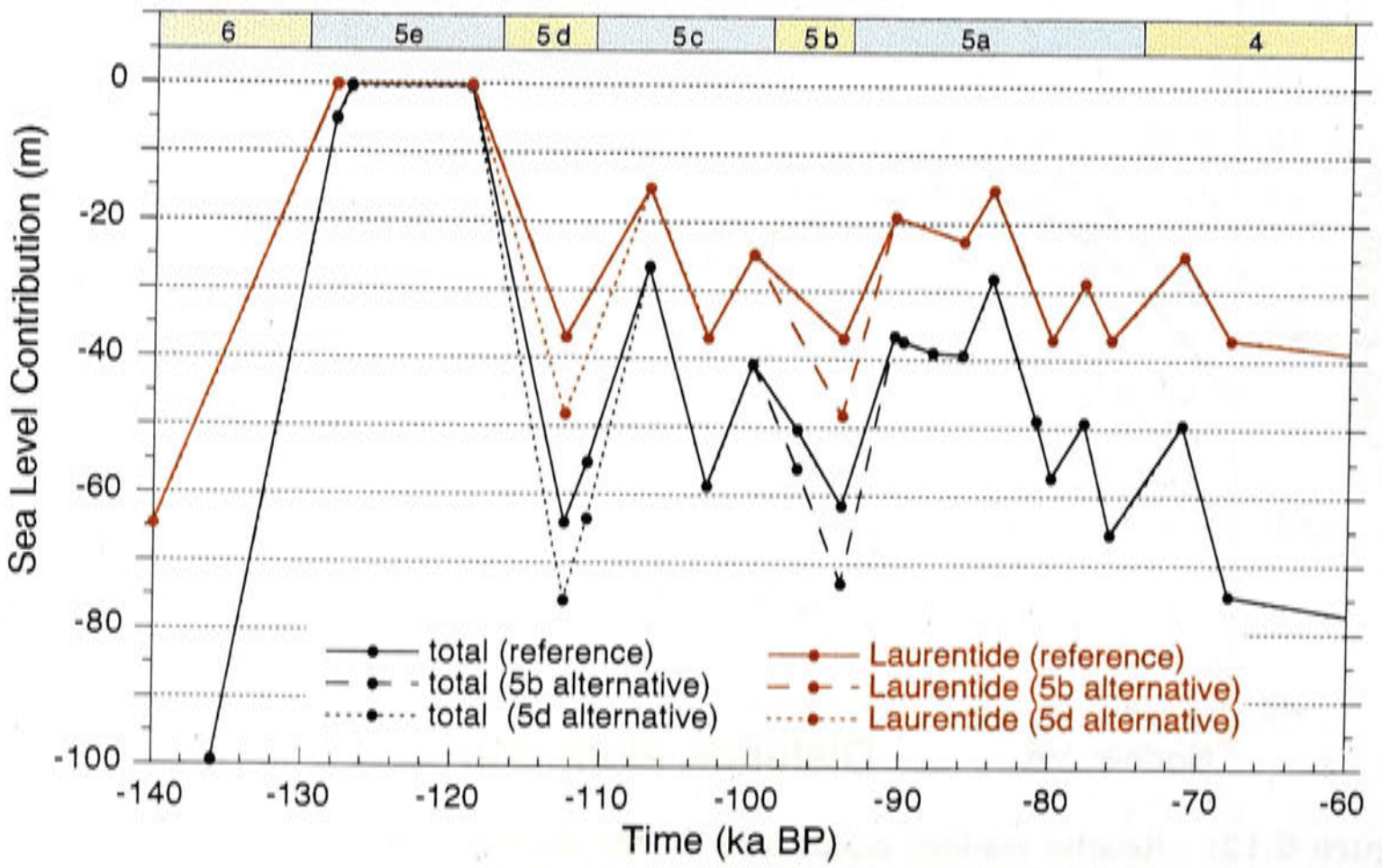

Figure 6.14: Alternative models: Increase of Laurentide ice volume during sub-stage 5b (30%) (dashed); and increase of Laurentide ice volume during sub-stage 5d (30%) (dotted).

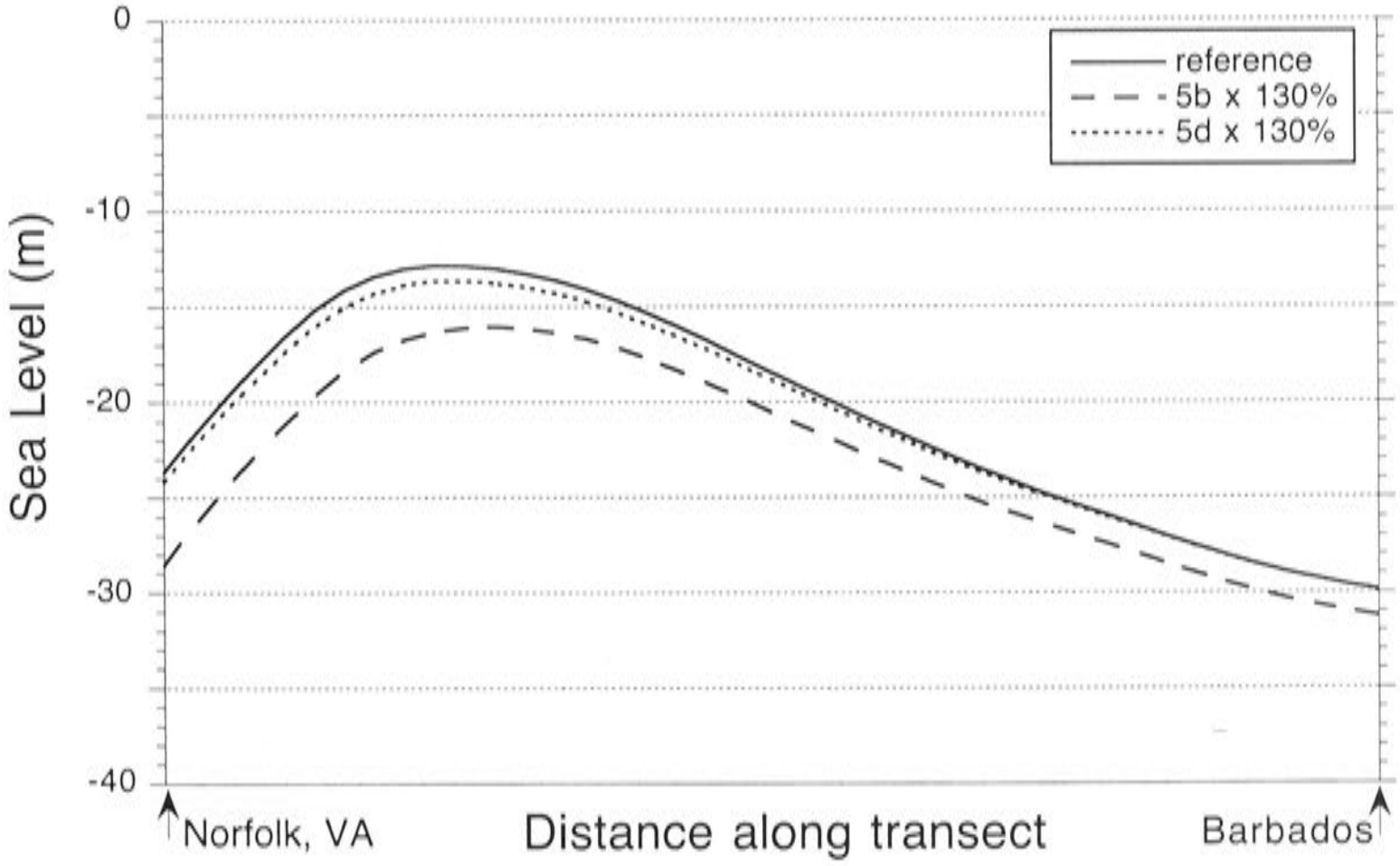

Figure 6.15: Comparison of relative sea-level calculation for the alternative models defined in figure 6.14: An increase of sub-stage 5b Laurentide ice volume (dashed) leads to a larger change in the relative sea-level predictions than for a change in sub-stage 5c ice volume (dotted).

6.4.3 Laurentide melting history since LGM

The gradient in relative sea level at the peak of sub-stage 5a in the Caribbean region is highly dependent on the present-day deformation of the Earth (section 5.6.6). Therefore, the melting history of the Laurentide ice sheet during the last deglaciation is an important factor in these calculations. The sea-level calculations from two alternative models of Laurentide Ice sheet melting history since the LGM (figure 6.16) are compared with the preliminary reference model, R-0. In these two models, the ice volume is scaled but the positions of the ice margins remain unchanged. In alternative model 1, the magnitude of the ice sheet was scaled up by 20% during the last deglaciation, and in alternative model 2, the ice sheet was scaled down by 20%. The relative sea levels calculated for these two alternative models along the transect of sites are shown in figure 6.17. A larger ice sheet during the last deglaciation produces a larger present-day collapsing glacial bulge and therefore increases in the gradient in sea level across the region of interest. A smaller ice volume during the last deglaciation results in a smaller gradient in relative sea level as a consequence of the smaller present-day collapsing glacial bulge.

6.4.4 Ice margins and distribution

Relative sea level at sites near the margins of the former Laurentide Ice Sheet is very sensitive to the location of the ice sheet's margins as well as the distribution of ice within those boundaries. The location of the ice margins during both MIS 5 and the last deglaciation are important factors in controlling of the amplitude and gradient of sea level across the Caribbean region during sub-stage 5a.

The location of the relative sea-level maximum in this region is most sensitive to the position of the present-day collapsing glacial bulge (figure 6.7 in section 6.3), which is determined by the position of the Laurentide Ice Sheet during the last deglaciation. A shift of the Laurentide Ice Sheet southwards or northwards during both the last deglaciation and MIS 5 (figure 6.18) acts to displace the relative sea-level maximum in the same direction, as illustrated in figure 6.19. The shift of ice during the last deglaciation, is intended only to demonstrate the this effect but is not consistent with observations of ice extent during that period.

If the bulk of ice during MIS 5 is located further north than in the reference model (figure 6.20), then the total glacio-isostatic component at 84 ka relative to equilibrium decreases across the region of interest. Consequently, there is an increase in gradient of relative sea level across that region (figure 6.21).

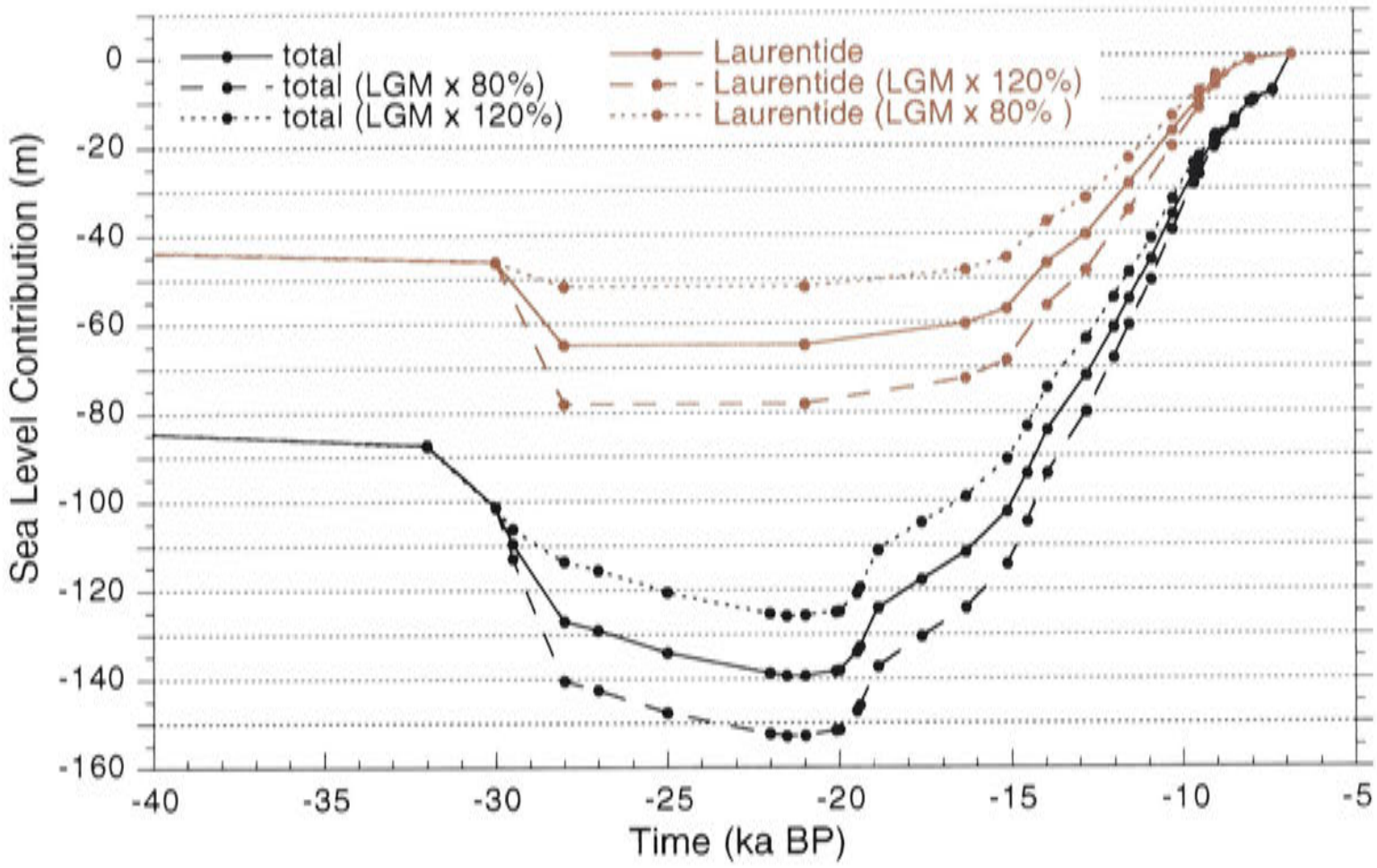

Figure 6.16: Alternative melting histories for the last deglaciation of the Laurentide ice sheet: dashed - increase of Laurentide ice volume by 20% during the LGM and the last deglaciation; and dotted - decrease of Laurentide ice volume by 20% during the LGM and the last deglaciation.

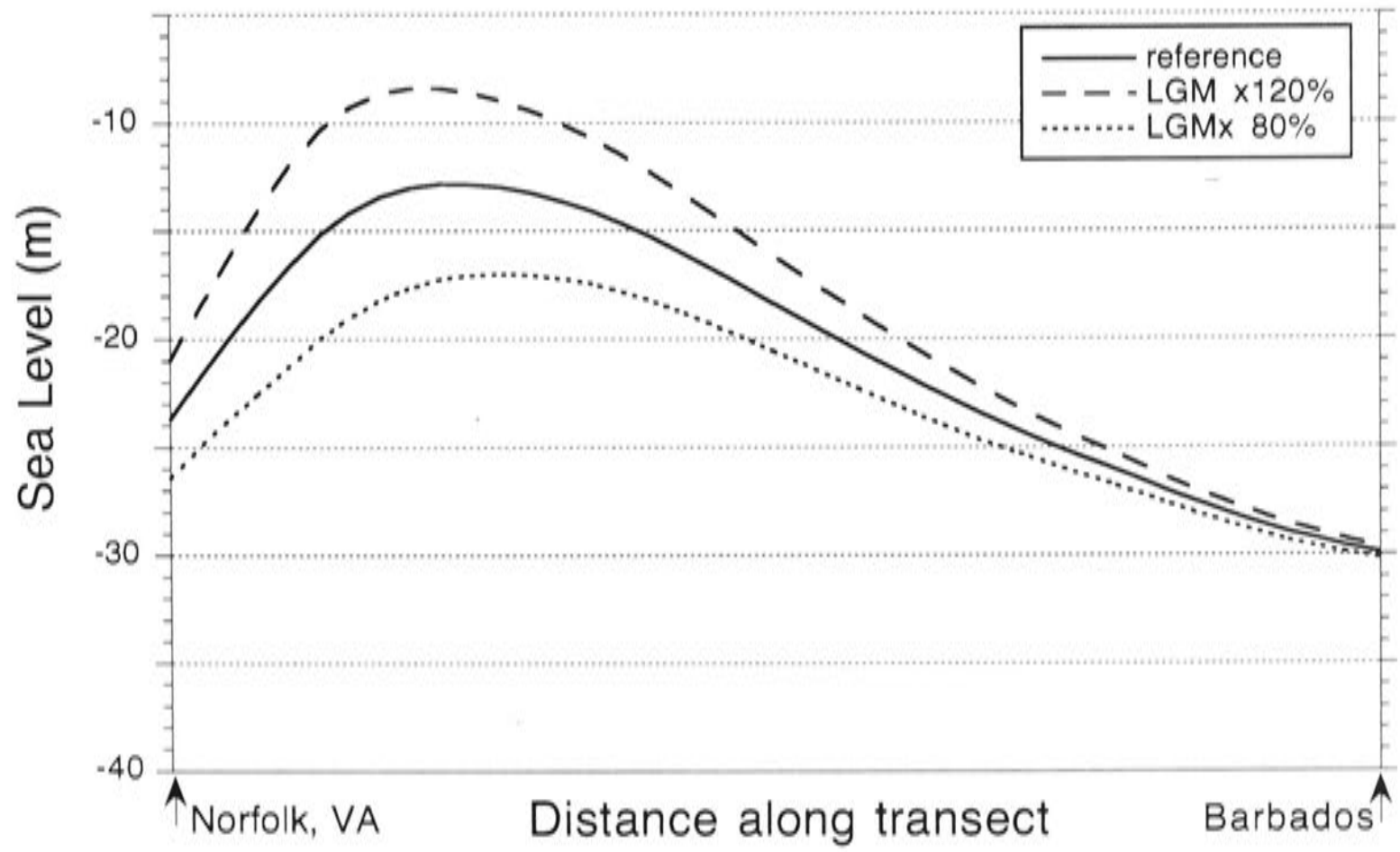

Figure 6.17: Relative sea-level calculations for alternative last deglaciation Laurentide ice volume models defined in figure 6.16. An increase in the volume of the LIS since the LGM increase the gradient glacio-isostatic deformation at the present day and hence relative sea level across the region of interest (dashed). A decrease in ice volume leads to a decrease in the sea-level gradient (dotted).

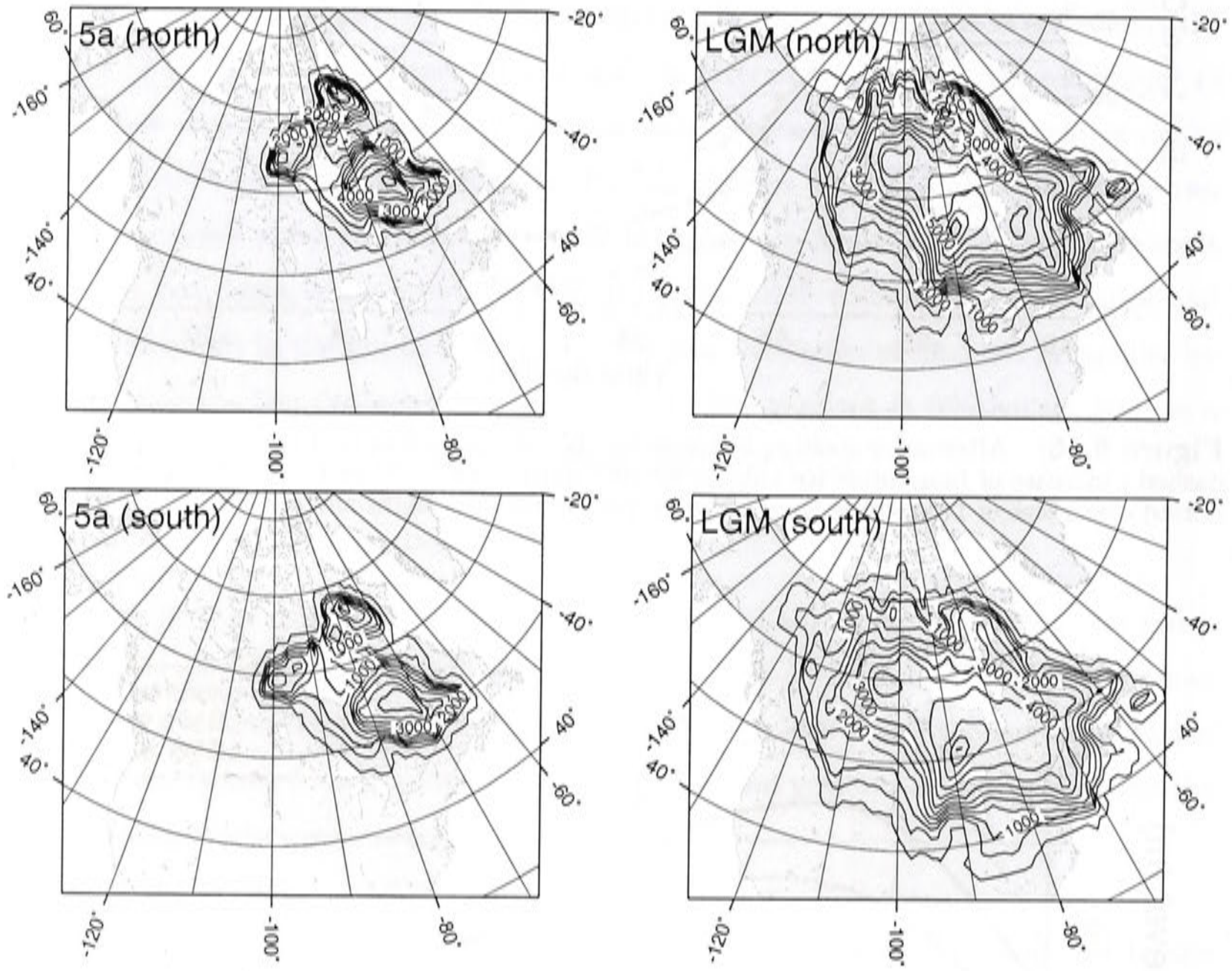

Figure 6.18: Alternative Laurentide ice models: north - ice sheet relocated north by 2.5 degrees latitude during MIS 5 and the last deglaciation (sub-stage 5a and LGM ice distributions shown); and south - ice sheet relocated south by 2.5 degrees latitude during MIS 5 and the last deglaciation (sub-stage 5a and LGM ice distributions shown). In these simple relocations, the ice heights at given latitudes are shifted northwards or southwards by 2.5°. However, this also slightly changes the north-south balance of ice and the total integrated volume. The ice sheets are scaled appropriately to account for this.

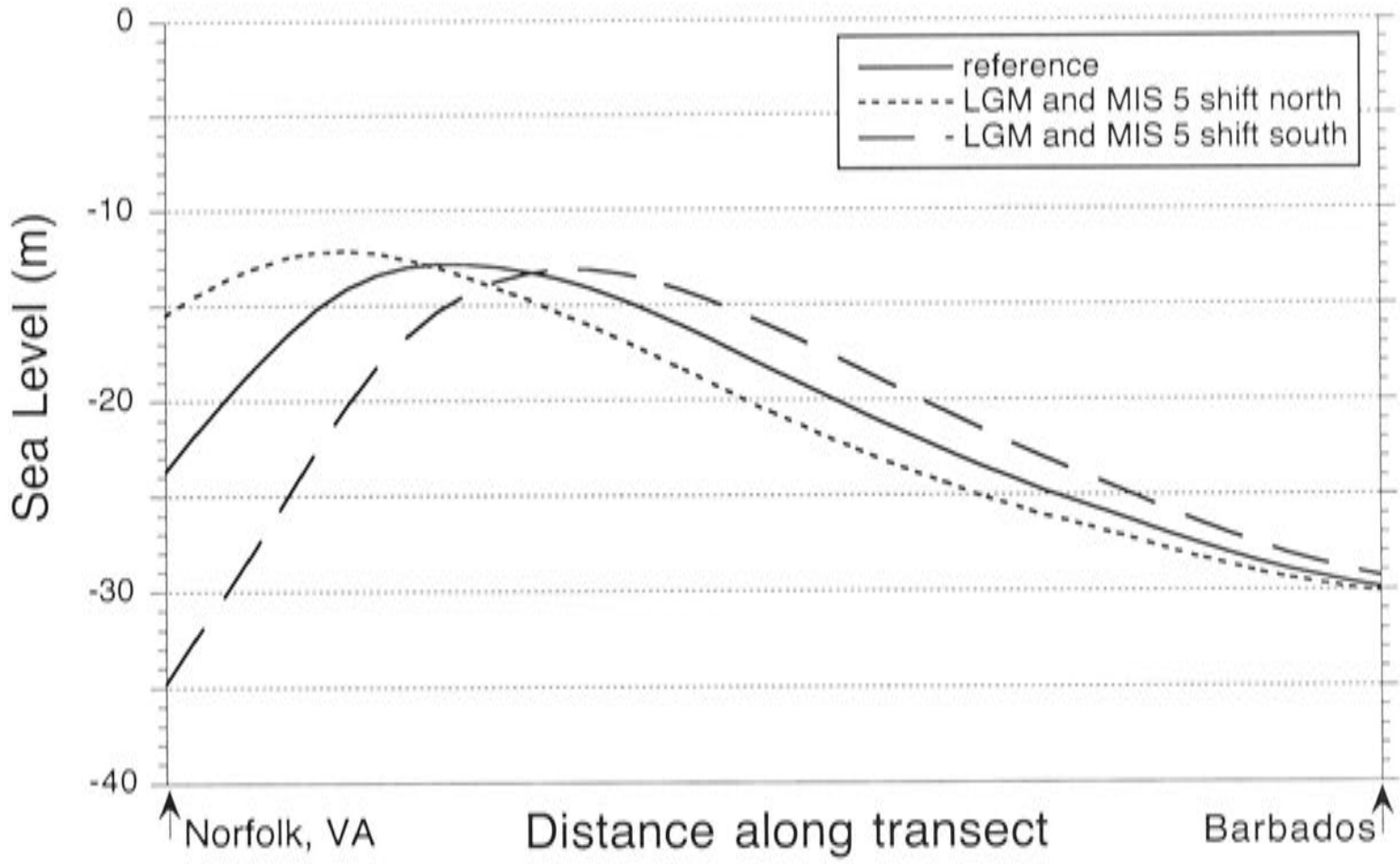

Figure 6.19: Relative sea-level calculations for Caribbean transect for the alternative models shown in figure 6.18 in which the ice was relocated 2.5 degrees latitude north (dotted) and south (dashed). Because the ice was relocated by simply adding or subtracting degrees of latitude onto the existing ice model, the north-south distribution of ice within each model changed. Because of this, sea-level curves were not simply shifted northwards or southwards, but also changed slightly in form, i.e. there is a substantial change in the gradient of sea level in the northern parts of the transect.

The effect of a more northerly redistribution of ice within the prescribed margins during both the last deglaciation and MIS 5 are compared to the reference model in figure 6.21. This result demonstrates that as ice is redistributed northwards, the total present-day deformation in the region of interest is reduced and shifted northward, producing a movement of the relative sea-level maximum in that direction.

In figure 6.22, the melting history of the reference model, which is based on the Licciardi *et al.* (1998) multi-domed model, is replaced with a single domed model with the same volume throughout that period (similar to that from the ICE-1 model defined by Peltier and Andrews, 1976). Because this alternative model has slightly different ice margins and a different internal distribution of ice, it has the effect of shifting the sea-level maximum slightly to the south. In all of these alternative models that involve the redistribution of ice within the prescribed boundaries, the effect on relative sea level becomes less important with distance from the ice sheet.

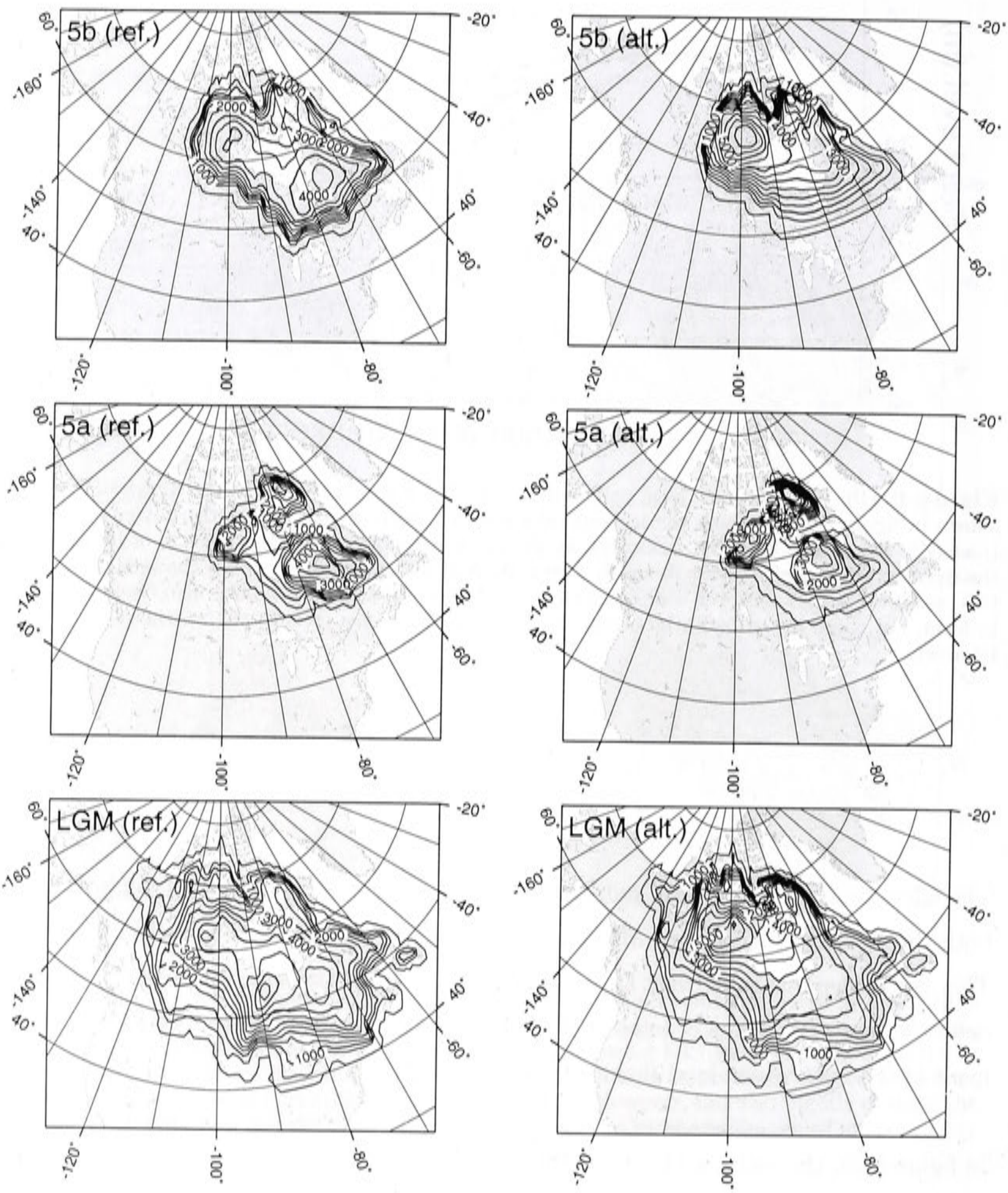

Figure 6.20: Comparison of reference model ice distribution during sub-stage 5b, 5a and the LGM with alternative models in which the ice is scaled down in the south and scaled up to compensate in the north. The results of the sea-level calculations with these alternative scenarios are shown in figure 6.21.

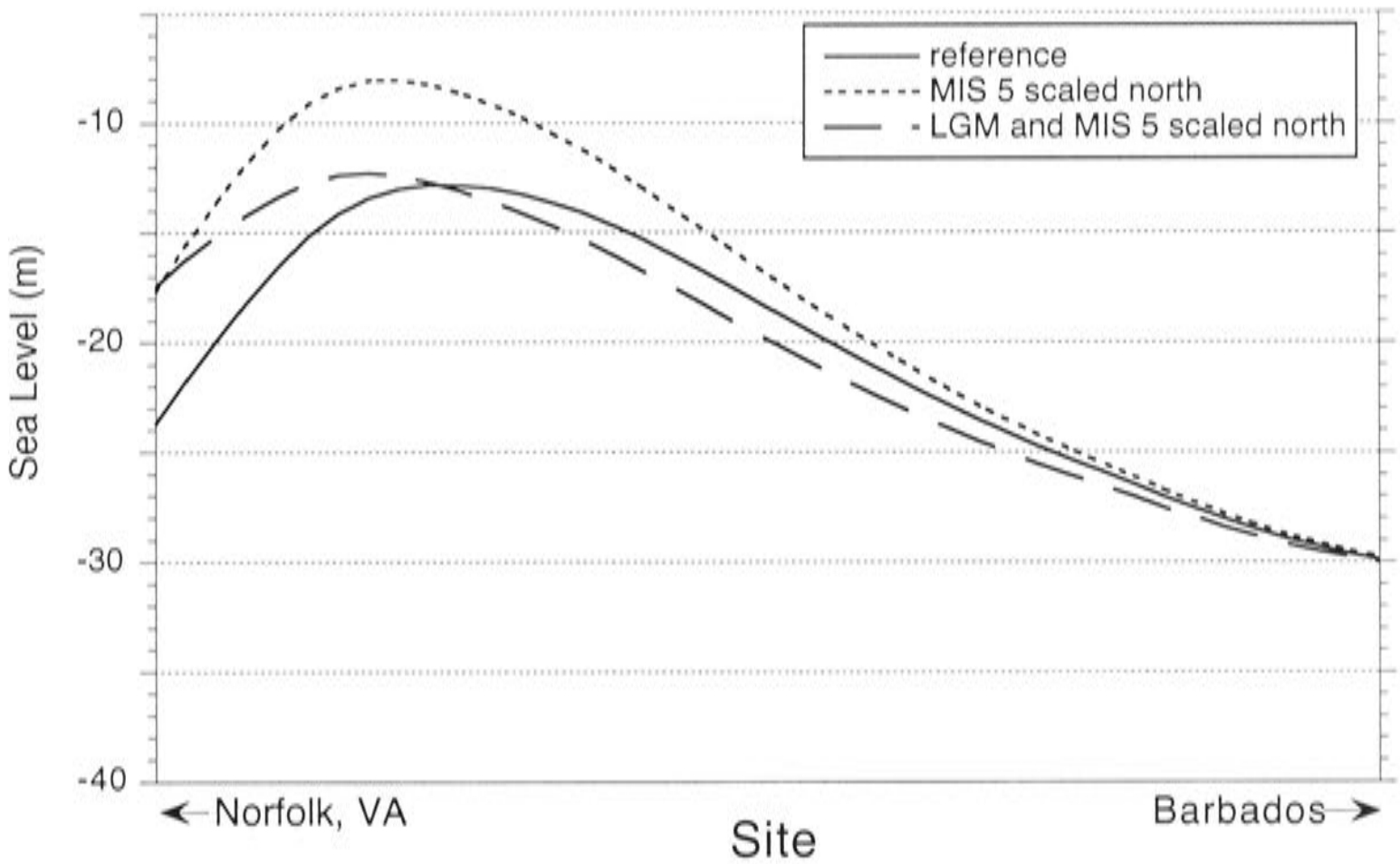

Figure 6.21: Relative sea-level calculations for alternative ice models shown in figure 6.20. For a northward redistribution of ice during MIS 5 and the last deglaciation (dashed) the location of the sea-level maximum is shifted northwards and the fall in sea level at northern sites is reduced. For a northward redistribution of ice during MIS 5 only, there is a minor shift in the sea-level maximum but the total gradient across the region is significantly increased.

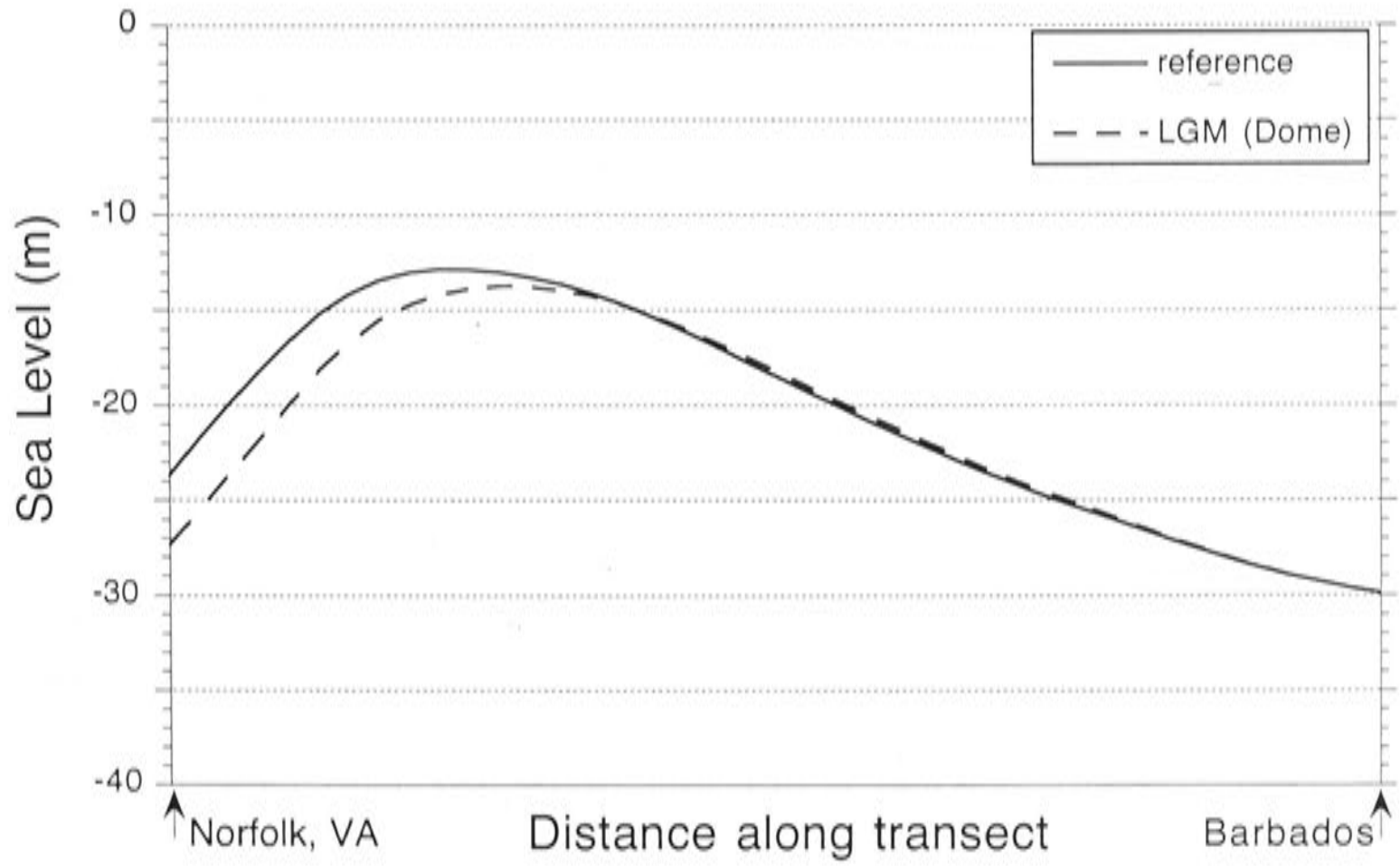

Figure 6.22: Relative sea-level calculations for alternative ice model in which the LIS is a single domed model. As a result, the peak in sea level is shifted slightly to the south.

6.5 Observations versus model predictions

Estimates of the sub-stage 5a sea level in the Caribbean region vary between ~19m below present at Barbados to several metres above present on the US East Coast (see section 4.5 in chapter 4). The highest apparent relative sea level occurs at those sites closest to the former Laurentide and estimates generally decrease with distance from the ice sheet (figure 6.23), with the exception of one observation at Bermuda, which does not fit into this trend and will be disregarded for now. Therefore, there is a roughly north-south gradient in sub-stage 5a sea level across this region. In this section, sub-stage 5a relative sea-level observations from sites across the Caribbean and surrounding regions (discussed in section 4.5 of chapter 4) are compared with model predictions, in order to place constraints on the earth and ice model parameters discussed above.

The preliminary ice model, R-0 (figure 6.1), and reference Earth model (ma4A, table 6.2) were used to calculate the relative sea levels at the peak of sub-stage 5a for each of the study sites. The comparison of predicted sea levels from the preliminary reference model and observations from each site are shown in figure 6.23.

The preliminary reference model produces a general trend of increasing relative sea level from the southern to the northern sites. However, there are some important differences between the calculated and observed trends:

1. the predicted gradient is smaller than observed.

2. the model predicts a relative sea-level maximum in the north of the study region and a fall in sea level at the northernmost site, Norfolk, Virginia, which is not evident in the observations.

3. the predicted relative sea levels at the Caribbean study sites are consistently less than observed

In the following sections, I address each of these observable characteristics and demonstrate how the preliminary reference model can be modified to improve the correspondence of observations and model predictions. In section 6.6, I discuss each of these modifications in more detail.

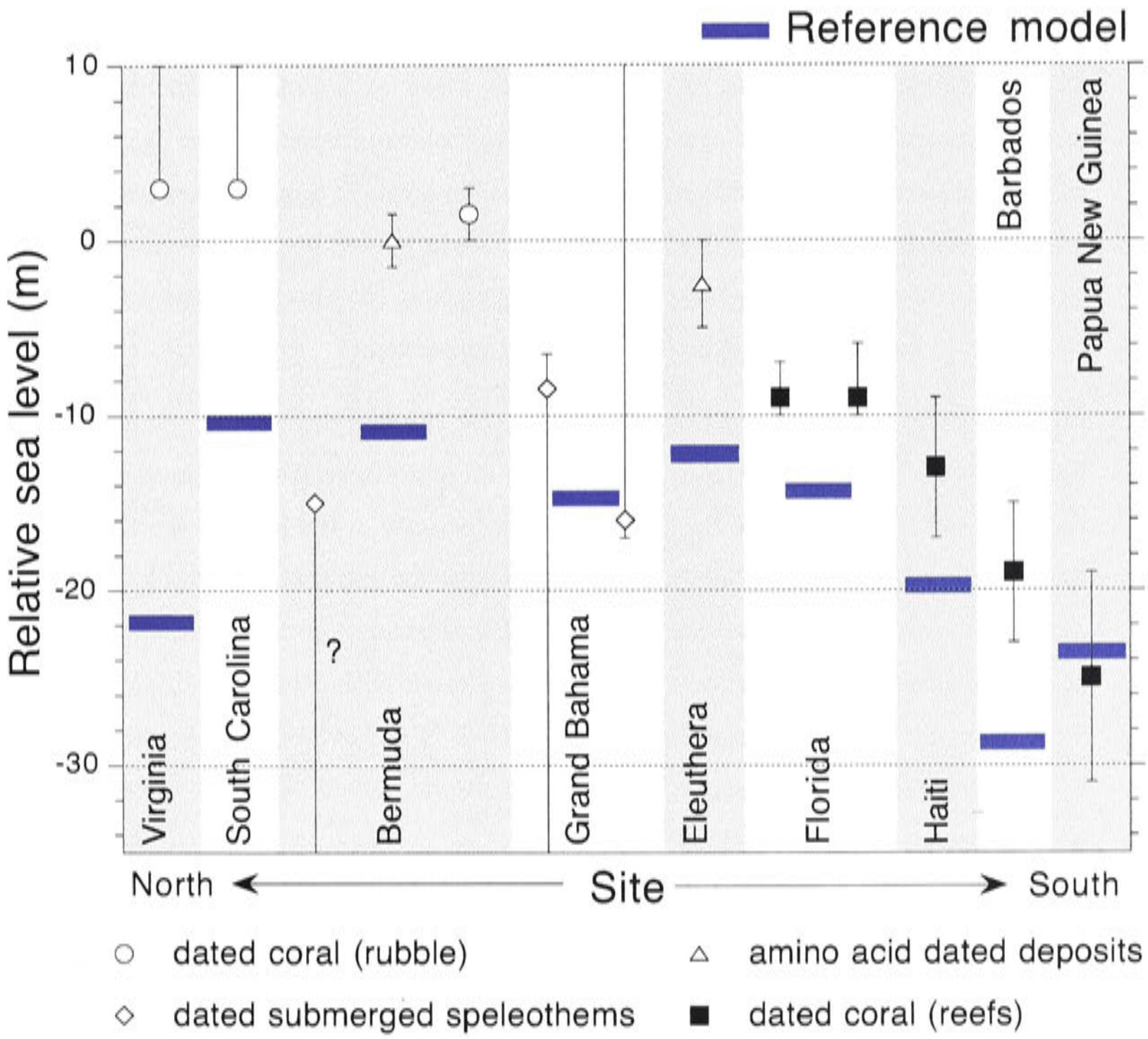

Figure 6.23: Comparison of observations of stage 5a relative sea level in PNG and the Caribbean and surrounding region with predicted sea levels, blue bars, from preliminary reference model, R-0 (figure 6.1). Observations based on dated coral reefs, submerged speleothems, coral rubble units and undated or amino acid racemisation dated stratigraphic units. See section 4.5 in chapter 4 for details. The sea-level prediction for Huon Peninsula is very close to the observed value because the preliminary model was based upon the Huon Peninsula sea-level record.

6.5.1 The gradient

The observed gradient of sub-stage 5a relative sea-level across the central study region (between Barbados and South Carolina) is greater than predicted by the preliminary reference model, R-0 (figure 6.23). The predicted gradient can be increased by any or all of the following four model modifications (figure 6.24):

1. Increasing lower mantle viscosity (e.g. from 1×10^{22} Pa s to 5×10^{22} Pa s, figure 6.24a). This modification increases the predicted sea levels at all of the Caribbean sites, bringing them into better agreement with the observations. There is now good agreement between the predicted and observed sea levels at most of the sites, with the following exceptions: (i) the model still predicts a fall in sea level at the northernmost site of Norfolk, Virginia, which is not observed and (ii) the predicted sea level at Barbados is increased but remains lower than observed.

2. Increasing the magnitude of the ice sheet during the last deglaciation (e.g. by 20%, figure 6.24b). This modification produces an increase in relative sea level at each of the Caribbean sites (except Barbados) and an increase in the general gradient in sea level across the central Caribbean region. In order for the predicted values to better match the observations by only increasing the deglacial ice volumes, the required upward scaling of the ice sheet would be inconsistent with other post-LGM sea level data from the North American region (Lambeck *et al.*, 2002a). Again, a fall in sea level at Norfolk, Virginia is predicted by this model, which does not agree with the observations.

3. A more northerly distribution of ice within the prescribed boundaries during sub-stages 5d-5a (figure 6.24c). This modification also leads to an increase in relative sea-level predictions at each of the Caribbean sites, except Barbados, bringing them into a better agreement with the observations. Again, the model predicts a fall in sea level at Norfolk, Virginia which is inconsistent with the observations. A similar effect occurs if the MIS 5 ice sheet is shifted further north (not shown here).

4. Reducing the Laurentide Ice Sheet volume during sub-stages 5d-5a (compensated by increase in far-field ice volume so that the equivalent sea level during that period remains the same) (e.g. by 50% figure 6.24d). This modification produces a significant increase of the predicted values at all the Caribbean study sites, which are now in better agreement with the observations. The predicted fall in sea level at the northernmost site, Norfolk, Virginia, is also slightly reduced, but not enough to be consistent with the observed trend.

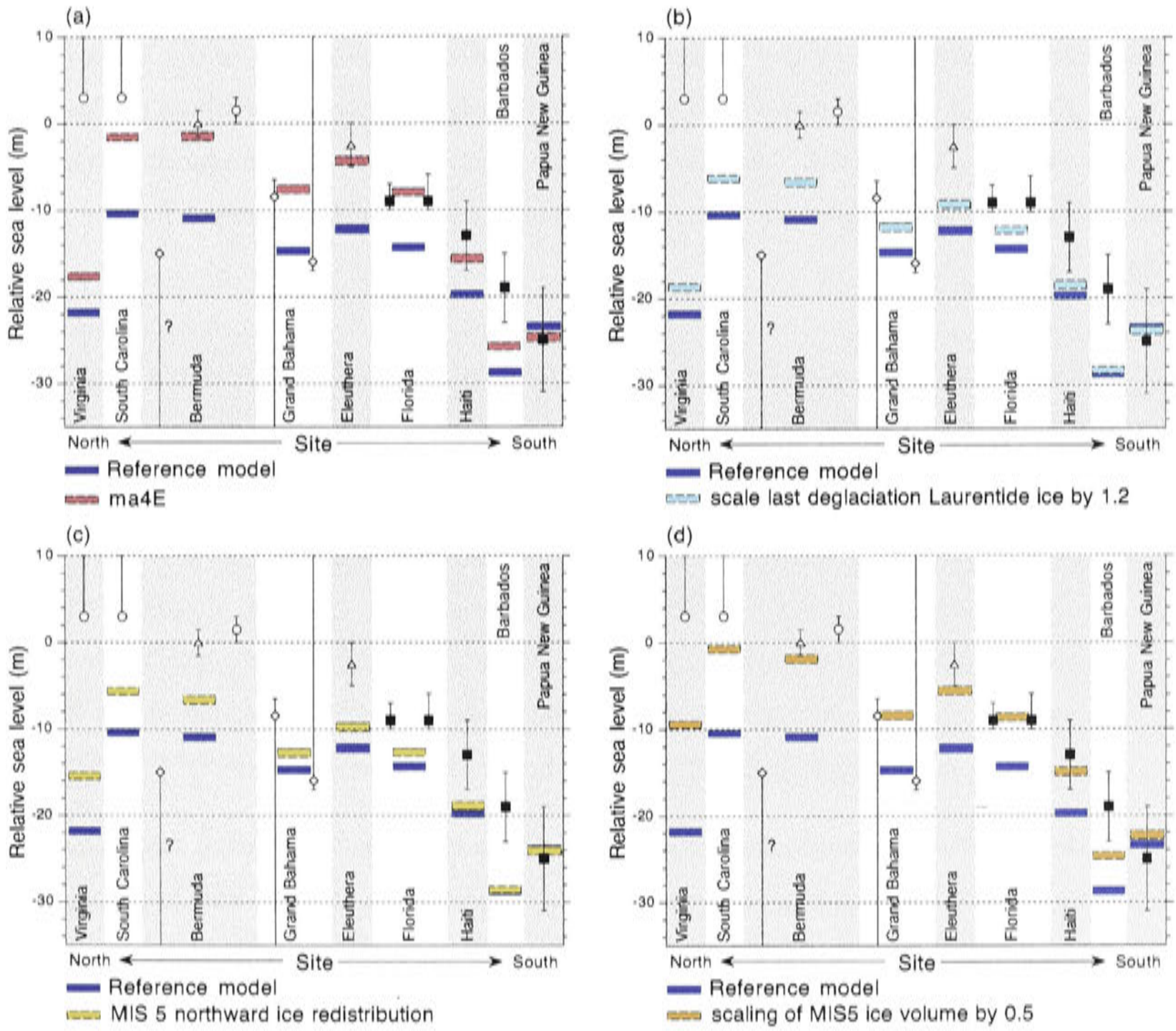

Figure 6.24: Alternative models that increase gradient of relative sea level in the region of interest. a) Increase of lower mantle viscosity 1×10^{22} Pa s to 5×10^{22} Pa s; b) Increase of the magnitude of the Laurentide Ice Sheet during the last deglaciation (scaled by 1.2); c) More northerly distribution (scaling up of ice in north and scaling down in the south) of the Laurentide Ice Sheet during sub-stages 5d-5a, compared to the preliminary ice model (see figure 6.20); d) Scaling down of Laurentide ice sheet volume during 5d-5a, compared to the preliminary ice model (scaled by 0.5).

6.5.2 The fall in sea level at Norfolk, Virginia

The preliminary reference model predicts a spatial maximum in sub-stage 5a relative sea level within the study region, north of which the predicted relative sea level falls. However, a fall in sea level predicted for the northern-most site (Norfolk, Virginia) is not evident in the observations. It must be noted that the mean of the measured ages of the site above present sea level at Norfolk, Virginia is ~71±5 ka BP. Therefore, this deposit does not directly correspond to the 'classic' sub-stage 5a high-stand that is the focus of this study. Rather, it may correspond to the later sub-stage 5a feature identified at Barbados in this study (~77 ka BP). The glacio-isostatic effects for both high-stands at this site are expected to be similar and so the comparison remains valid (discussed further in section 6.7.1).

The fall in sea level at the northernmost site can be reduced by one or both of the following model modifications (figure 6.25):

1. Increasing upper mantle viscosity (e.g. from 4×10^{20} Pa s to 6×10^{20} Pa s, figure 6.25a). This modification produces a significant decrease in the magnitude of the predicted fall in sea level at the northernmost site, Norfolk, Virginia. At some other study sites, this modification decreases the predicted relative sea levels, therefore producing poorer agreement with the observations. The predicted sea level at Barbados using this model remains well below the observed value.

2. More northerly distribution of ice during both the last deglaciation and sub-stages 5d-5a within the prescribed boundaries, (figure 6.25b). This modification also produces a decrease in the predicted fall in sea level at the northernmost study site, whereas the predicted values for the rest of the Caribbean sites are relatively unchanged. The Barbados sea-level prediction is still well below the observed value.

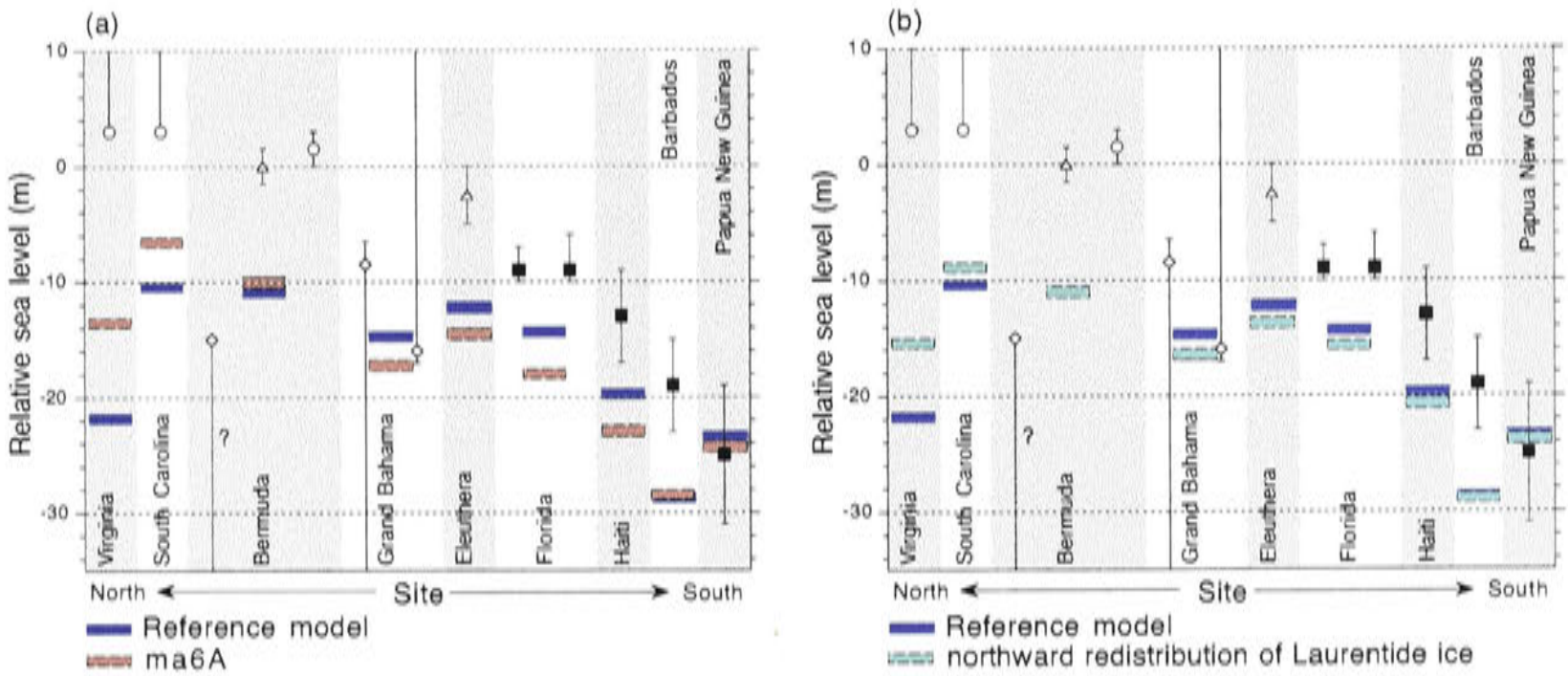

Figure 6.25: Alternative models that act to either shift the spatial maximum in sea level northwards or decrease the rate of sea-level fall north of the maximum. a) increasing upper mantle viscosity from 4×10^{20} Pa s to 6×10^{20} Pa s; b) more northerly distribution of ice during the last deglaciation and MIS5, ie scaling up in the north and scaling down in the southern parts of the ice sheet during those periods (see figure 6.20).

6.5.3 Barbados sea-level offset

Most of the model modifications presented in sections 6.5.1 and 6.5.2 do not result in a significant change in the predicted sea level at Barbados. Any or all of the following model modifications can increase the predicted relative sea level at Barbados (figure 6.26):

1. Decreasing Laurentide Ice Sheet ice volume during the entire sub-stage 5d-5a period (e.g. decrease by 50%, figure 6.26a) This change is compensated by an increase in far-field ice volume so that the equivalent sea level during that period remains the same). This modification (the same as in figure 6.24d) produces an increase in predicted sea level at each of the Caribbean sites, including a several metre increase at Barbados. This modification also produces a small reduction of the fall in sea level predicted for the northernmost study site.

2. Raising ice-equivalent sea level at the peak of sub-stage 5a by introducing:

   (a) Extra far-field melt at the peak of sub-stage 5a (figure 6.26b). This leads to a near constant increase of predicted sea levels at all sites, including PNG, due to the increased equivalent sea level at that time.

   (b) Extra Laurentide Ice Sheet melt at the peak of sub-stage 5a (figure 6.26c). This produces an increase in the predicted sea levels at all sites, including PNG. The offset is not constant because sites close to the LIS experience additional glacio-isostatic effects.

   The increase in equivalent sea level introduced for these models is not sufficient to match the observation at Barbados, but the difference could be made arbitrarily larger.

3. Increasing lower mantle viscosity (e.g. from 1×10^{22} Pa s to 5×10^{22} Pa s, figure 6.26d). This modification (also seen in figure 6.25a) increases the sea level at each of the sites, including Barbados. However, this modification also enhances the predicted fall in sea level at the northernmost site, which is not consistent with the observations.

4. Decreasing upper mantle viscosity (e.g. from 4×10^{20} Pa s to 2×10^{20} Pa s, figure 6.26e). This modification produces an increase in the predicted sea level at Barbados, which is more consistent with the observations. However, this modification shifts the location of the sea-level maximum further south and enhances the fall in relative sea level at the northern sites.

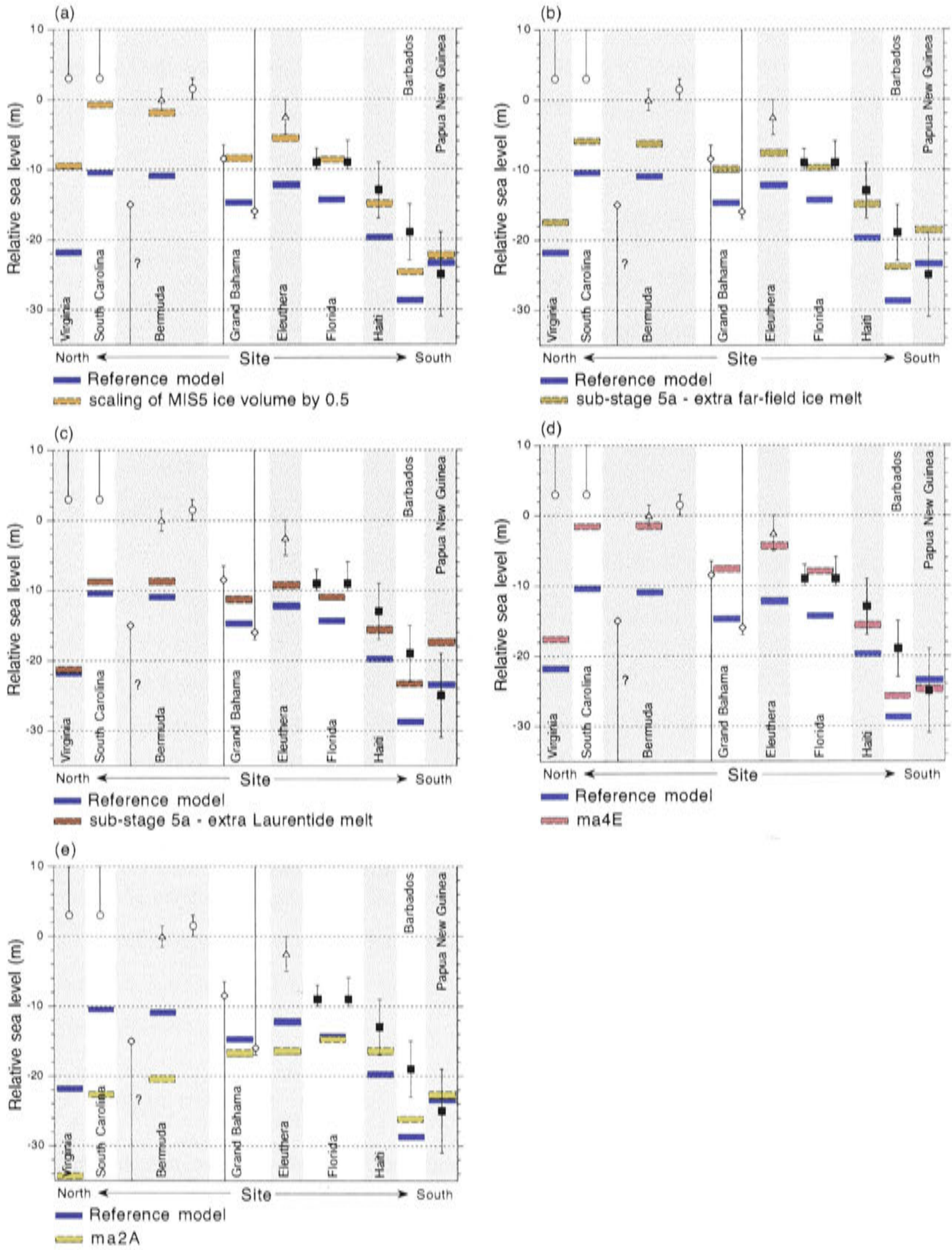

Figure 6.26: Alternative models that act to increase the sea level at each of the study sites: a) decreasing Laurentide Ice Sheet volume by 50% during sub-stages 5d-5a, compensated by an increase in far-field ice volume; b) extra far-field melt at the peak of sub-stage 5a; c) extra Laurentide Ice Sheet melt at the peak of sub-stage 5a; d) increase in lower mantle viscosity from 1×10^{22} Pa s to 5×10^{22} Pa s; e) decrease in upper mantle viscosity from 4×10^{20} Pa s to 2×10^{20} Pa s

6.6 Justification for model modifications

In the previous sections, I have presented a number of alternative models that act to improve the correspondence between predicted and observed sea levels for the sub-stage 5a high-stand at the Caribbean study sites. A summary of these sometimes conflicting model modifications follows:

1. Mantle viscosity changes:
   (a) Increase in lower mantle viscosity
   (b) Increase in upper mantle viscosity
   (c) Decrease in upper mantle viscosity
2. Ice sheet modifications:
   (a) Decrease in Laurentide Ice Sheet (LIS) ice volume during sub-stages 5d-5a
   (b) Northward redistribution (or shift) of LIS during MIS 5
   (c) Northward redistribution of LIS during the last deglaciation
   (d) Increase of LIS volume during last deglaciation
   (e) Extra far-field or LIS ice melt during sub-stage 5a

Table 6.3 summarise the effect each of these model modifications has on each of the three observable characteristics discussed in the preceding sections. The likelihood of each of these model modifications is addressed in the following sections.

6.6.1 Mantle viscosity changes

Lower mantle viscosity increase

An increase in lower mantle viscosity (e.g. from 1×10^{22} Pa s to 5×10^{22} Pa s in figure 6.24a), acts to increase the gradient of predicted relative sea level across the region of interest, hence improving the correspondence between observed and predicted relative sea levels. Okuno and Nakada (2001) suggest lower mantle viscosity is greater than 10^{22} Pa s. Using an inverse modelling technique Kaufmann and Lambeck (2000, 2002) place an upper limit of $1\text{-}3\times10^{22}$ Pa s on the volume-averaged viscosity of the lower mantle. Rotational considerations also place an upper limit on the lower mantle viscosity of around this magnitude (Johnston and Lambeck, 1999). Based on observations of sea level during the last deglaciation from far- and intermediate-field sites, Lambeck *et al.* (2002c) suggest

	Gradient	Local maximum	Barbados sea level
Lower mantle viscosity increase	✓		✓
Upper mantle viscosity increase		✓	
Upper mantle viscosity decrease	✗	✗	✓
MIS 5 LIS volume decrease	✓		
MIS 5 LIS northward shift	✓		
Last deglaciation LIS northward shift		✓	
Last deglaciation LIS volume increase	✓		
Sub-stage 5a ice-equivalent sea level increase			✓

Table 6.3: Summary of the model modifications and their influence on the agreement between the predicted and observed sub-stage 5a sea levels for the region of interest. A tick indicates that the particular modification improves the agreement, a cross indicates that the modification reduces the agreement, and the blank means that there is no significant change.

an appropriate value for the global lower mantle viscosity is 3×10^{22} Pa s. Seismic studies of S-wave velocity and lateral attenuation suggest there is less lateral variability in temperature in the lower mantle than in the upper mantle (Romanowicz, 1998) and therefore lateral variation in lower mantle viscosity may also be less important than in the upper mantle.

Although the above viscosity estimates are dependent on the ice models used in the calculations, it is apparent that lower mantle viscosity may be higher than the 1×10^{22} value used in the reference earth model (ma4A) but not as high as the 5×10^{22} Pa s value invoked in section 6.5.1 (ma4E). I adopt a value of $3\pm1\times10^{22}$ Pa s for lower mantle viscosity in subsequent calculations.

Upper mantle viscosity increase

An increase in upper mantle viscosity (e.g. from 4×10^{20} Pa s to 6×10^{20} Pa s in figure 6.25c) acts to reduce the predicted fall in sea level at the northernmost site of Norfolk, Virginia, producing a result that is more consistent with the observations of sea level at that site (figure 6.25c). However, a decrease in upper mantle viscosity (e.g. from 4×10^{20} Pa s to 2×10^{20} Pa s in figure 6.26e) acts to increase the predicted relative sea levels at the sites in the southern Caribbean, bringing them into better agreement with the observations, while drastically decreasing the estimates for sites on the US East Coast.

The inverse modelling by Kaufmann and Lambeck (2000, 2002), based on deglacial and post-glacial sea-level observations from around the world, suggests upper mantle viscosity lies between 2-10$\times10^{20}$ Pa s (global volume average value of 7×10^{20} Pa s). Okuno and Nakada (2001) also suggest a similar range for upper mantle viscosity (4-10$\times10^{20}$ Pa s) based on observations of sea-level change and other geophysical signals. The Earth models used in the modelling of glacio-hydro-isostatic rebound do not contain lateral mantle viscosity variability. However, seismic shear-wave and attenuation measurements suggest that there are lateral variations in the physical properties of the upper mantle, such as temperature (Romanowicz, 1998). Hence, we expect the viscosity of the mantle may also vary spatially. In particular, seismic studies suggest that the mantle beneath the North American shield region is 'colder', and hence may have a higher viscosity than other parts of the mantle, including the southern Caribbean (Grand, 1994; van der Lee and Nolet, 1997). Indeed, studies of deglacial and Holocene sea-level change suggest that upper mantle viscosity beneath North America is higher than other regions including beneath the southern Pacific, Australasia and northwestern Europe (Nakada and Lambeck, 1991).

It is apparent that higher values of upper mantle viscosity (ie 4-6$\times10^{20}$ Pa s) may be more appropriate for determining the isostatic response at sites in and near the North American shield (the location of the Laurentide Ice Sheet) and that lower values (ie 2-4$\times10^{20}$ Pa s) may be more appropriate for the mantle beneath southern Caribbean sites. Therefore, a single value for upper mantle viscosity may not be representative of the entire study region. As yet, there is no satisfactory earth model formulation that contains lateral mantle variability. In the following calculations, I adopt a range of values for upper mantle viscosity of 2-6$\times10^{20}$ Pa s to allow for uncertainty in the calculated sea levels due to lateral variability in the upper mantle.

6.6.2 Ice model modifications

Marine isotope stage 5

A northward shift of the LIS during sub-stages 5d-5a (or a redistribution of ice within the prescribed boundaries) and a reduction in its volume both lead to an increase in the predicted gradient of sea level across the region of interest at the peak of sub-stage 5a. Because sub-stage 5a sea levels are much more sensitive to the melting history of the LIS immediately prior to this event (i.e. sub-stage 5b) compared to earlier times (5d-5c), this constraint is much stronger for the late MIS 5 period.

Due to the dearth of preserved geologic indicators of ice extent prior to the LGM, the

melting history of the LIS during the sub-stage 5d-5a period is poorly constrained. However, in a review of the geologic evidence of the initiation of the Laurentide Ice Sheet after the last interglacial period, Clark *et al.* (1993) suggest that the LIS first developed in the north, over Keewatin, Quebec and Baffin Island. Soon after the end of the last interglacial period (perhaps during sub-stage 5d), the ice advanced in a northeast to easterly direction across Baffin Island and onto the continental shelf. An advance into the Western Canadian Arctic may have occurred later during MIS 5 (perhaps sub-stage 5b). There is no evidence of southward ice advance into the St Lawrence Lowlands at any time during sub-stages 5d-5a. Only during and after the MIS 5/4 transition did ice advance into the southern sector, across the St Lawrence Lowlands and the Great Lakes region (Clark *et al.*, 1993). Kleman *et al.* (2002) use a 'time-dependent mass-balance driven finite-element model' to calculate a glaciation history for the LIS that is consistent with geologic observations. This model predicts that ice build-up initially occurred over Ellesmere and Baffin Islands and by 90 ka (sub-stage 5b-5a) ice cover remained centred over the central Arctic region (Baffin and Somerset Islands and Melville and Boothia Peninsulas), which is largely consistent with Clark *et al.*'s (1993) constraints. Kleman *et al.*'s (2002) model suggests that during the entire sub-stage 5d-5a period the contribution of the LIS to the global ice volume never exceeded 15 m of equivalent sea level. This suggests that the ~60 m lowering of ice-equivalent sea level during sub-stage 5d, inferred from the Huon Peninsula record, may have been due to a build up of ice in other ice sheets such as the Eurasian and Antarctic ice sheets.

Based on field observations (Clark *et al.*, 1998; Kleman *et al.* 2002), it is apparent that a more realistic model is one in which the sub-stage 5d-5a ice is shifted even further north (figure 6.24c) and the volume is smaller (figure 6.24d and 6.26a) during the entire period than was assumed for the preliminary reference model (R-0, section 6.2).

Ice-equivalent sea level at sub-stage 5a

The observed sub-stage 5a Barbados sea level is significantly higher than the value predicted using the preliminary reference model. If an increase in ice-equivalent sea level alone is invoked to increase the predicted Barbados sea level to be consistent with the observations at that site, then the predicted sea level for Huon Peninsula would no longer match the observed value (see figure 6.26b). However, there are other model modifications that lead to an increase of Barbados sea level without requiring a change in the ice-equivalent sea level such as decreasing MIS 5 LIS ice volume, increasing lower mantle viscosity and decreasing upper mantle viscosity (figure 6.26a, d and e).

The last deglaciation

The alternative models discussed in sections 6.5.1 and 6.5.2 include modifications to the melting history of the LIS during the last deglaciation. The 'recent' melting history of the LIS (during the latter part of the last glacial cycle) is an important part of determining the apparent relative sea level of past events because it controls the present-day deformation of the earth in the region of interest (section 5.6.6).

Increasing the volume of the LIS during the last deglaciation (e.g. in figure 6.24b) improves the correspondence of the predicted and observed sea levels by increasing the predicted gradient in sea level across the study region. The volume of the Licciardi *et al.* (1999) maximum ice model is dependent on the choice of effective viscosity of the underlying till. In the case of the maximum ice volume reconstruction, the viscosities used are within the range reported by Paterson (1994) for till beneath modern glaciers. A hard bedded ice model (Boulton *et al.*, 1985) may allow for an even greater LIS ice volume (equivalent to as much as 80 m sea level), however an increase in the volume during the entire last deglaciation period may be inconsistent with post-LGM sea-level observations (Tushingham and Peltier, 1991; Lambeck *et al.* 2000). The volume of the LIS at the LGM in the preliminary reference model was already scaled up by 30% from Licciardi *et al.*'s (1998) maximum ice reconstruction (to a value of ~65 m equivalent sea level) and I assume no further increase in the following discussion.

A northward shift (or redistribution of ice within the prescribed boundaries) of the LIS during the last deglaciation acts to reduce the predicted fall in relative sea level at the northernmost study sites (figure 6.25b). A shift of the LIS during this period can be ruled out because the ice margins during the last deglaciation are well constrained. The distribution of ice within the given boundaries is not precisely constrained and the preliminary model is dependent on dynamical ice models and is therefore subject to uncertainties. However, it is unlikely that the LGM distribution of ice was centred significantly further north than that suggested by the maximum, multi-domed model proposed by Licciardi *et al.* (1998). A single domed model is centred slightly further south (figure 6.22).

Likely
Increase in upper mantle viscosity (at US coastal sites)
Decrease in upper mantle viscosity (at southern Caribbean sites)
Increase in lower mantle viscosity
Decrease in Laurentide Ice Sheet (LIS) ice volume during MIS 5
Northward shift of LIS during MIS 5

Possible
Increase in ice-equivalent sea level during sub-stage 5a
Increase of LIS volume during last deglaciation

Unlikely
Northward shift or redistribution of LIS during the last deglaciation

Table 6.4: Likelihood of the individual model modifications, relative to the preliminary reference model, dealt with in sections 6.5.1, 6.5.2 and 6.5.3 and discussed in section 6.6.2.

6.6.3 Preferred model for sub-stage 5a

In the previous section, I discussed a number of model modifications that act to improve the correspondence between predicted and observed sea levels in the region of interest. The likelihood of each of these are summarised in table 6.4. The changes in the ice and earth models are with respect to the preliminary ice model R-0 and the reference earth model ma4A. The model modifications that are considered 'likely' or 'possible' are:

1. Increase in upper mantle viscosity (at US coastal sites)
2. Decrease in upper mantle viscosity (at southern Caribbean sites)
3. Increase in lower mantle viscosity
4. Decrease in Laurentide Ice Sheet (LIS) ice volume during MIS 5
5. Northward shift of LIS during MIS 5
6. Extra far-field or LIS ice melt during sub-stage 5a

The estimated range of values for the upper and lower mantle viscosities are 2-6$\times 10^{20}$ Pa (possibly spatially variable) and 3$\pm$1$\times 10^{22}$ Pa s respectively. The results of the comparison of sub-stage 5a observations with predicted sea levels in this chapter are consistent with a LIS that was centred further north during sub-stages 5d-5a than it was after the MIS 5/4 transition and that its volume was significantly smaller than defined in the preliminary ice model, R-0 (figure 6.1 and 6.3). These general conclusions are consistent with additional

field data from this region (Clark *et al.*, 1993). However any further constraints cannot be made based on the existing observations. The modified ice model will be referred to as R-1.

Figure 6.27 shows a comparison of the sub-stage 5a sea-level observations with the sea-level predictions from the preliminary reference model (R-0 and earth model ma4A, blue bars) and the sea-level predictions from an alternative model (R-1, red). The R-1 results in figure 6.27 span the range of predictions for the four earth models at the extreme ends of the viscosity ranges quoted above (ma4B, ma4D, ma2C and ma6C, see table 5.1 for earth model parameters). The sea levels predicted by the alternative model, R-1, are in good agreement with the observations within the range defined by the various earth rheological models. In this ice model, the ice-equivalent sea level at the peak of sub-stage 5a is ~28 m below present.

In this R-1 alternative model the volume of the Laurentide was reduced by 50% during the period 5d-5a and the volume of the Antarctic Ice Sheet was increased to maintain the ice-equivalent sea level defined in the preliminary model. As a result of this scaling, the volume of the Antarctic Ice Sheet approaches that of its LGM size during the stadials 5d and 5b, and the change in ice volume (relative to the present day) is larger than for the LIS during this period. There are few constraints on the magnitude of the Antarctic Ice Sheet prior to the LGM, and although there are suggestions that there was a large expansion of the Antarctic Ice Sheet following the last interglacial period, it is difficult to say whether it reached its LGM size. Alternatively, the same effect could be achieved by relocating the extra ice to other far-field regions such as northern Europe or Russia. Instead, if the volume of extra far-field ice is left unchanged during the stadial events, this raises the ice-equivalent sea-level at those times by ~15 m, but does not have a significant effect on the predicted sea levels for the Caribbean sites (<1.5 m). This is because the most important isostatic contribution to relative sea level in the region of interest at the peak of stage 5a is from glacio-isostatic effects of the Laurentide Ice Sheet. The ice-equivalent sea level for those stadial events was based on the position of raised stream deltas at Huon Peninsula, but the constraints are relatively uncertain (up to ±10 m, Lambeck and Chappell, 2001).

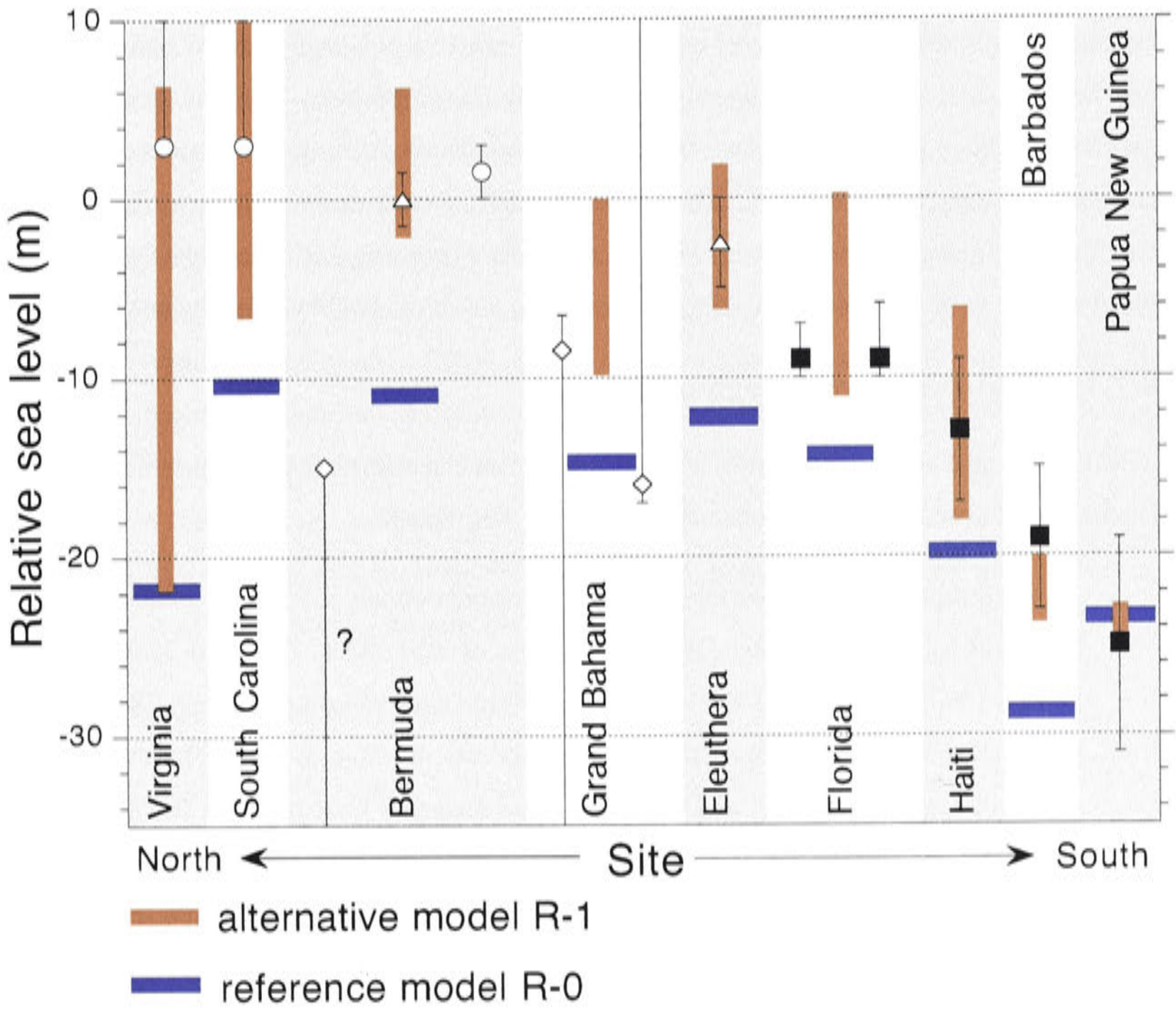

Figure 6.27: Sea-level predictions for sub-stage 5a reference model with earth model (blue) and modified ice model R-1 with a range of reasonable earth rheologies discussed in the text (red). The predicted trend of sea levels across the study region agrees well with the observations. Although many uncertainties remain about the detail of the global ice history during MIS 5, the good agreement between the observed and predicted sea levels indicates that the ice model R-1, discussed in the previous sections is a reasonable alternative for the Laurentide during MIS 5.

6.7 Other time periods

At the peak of the classic sub-stage 5a event, relative sea level in the Caribbean region ranged between ~19 m below present at Barbados to above present sea level in Bermuda and the US East Coast. Therefore, sub-stage 5a deposits are often easily accessible and, as a consequence, are relatively well documented when compared to some of the other interstadial sea levels. For other time periods, other than the Holocene and the last interglacial high-stand (sub-stage 5e), evidence of relative sea-level change has often been overprinted or destroyed by subsequent sea-level transgressions. For the existing documented evidence of the other sub-stage 5a and 5c events, timing constraints and spatial coverage are generally poor. In this section, I briefly examine the evidence of sea level in the Caribbean region during a number of other time periods and comment on how these observations may be used to place constraints on sea-level history during that period.

6.7.1 Additional sub-stage 5a event

The results of the present study indicate a distinct sea-level feature at ~77 ka BP at Barbados. There is some evidence for this event elsewhere:

1. At Bermuda, four samples from the coral rubble deposit just above present sea level analysed by Ludwig *et al.* (1996) have ages of 82.4, 82.3, 77.9 and 77.2 ka. Muhs *et al.*'s (2002) analysis of the same deposit give ages ranging between 78.3 and 84.0 ka. Perhaps this deposit contains corals corresponding to both the sub-stage 5a sea-level events identified at Barbados. This suggests that because the sea levels of both events were similar at this location, they are recorded in the same coral rubble unit, or the two sub-stage 5a events at Barbados may represent a single, prolonged highstand.

2. The analysis of coral samples from the marine facies deposits at >3 m above sea level at Norfolk, Virginia give a mean age of ~71±5 ka (Cronin *et al.*, 1981; Szabo, 1985) or range between 72-84 ka (J. Wehmiller, pers. comm.). Therefore, this deposit appears to correspond to the younger sub-stage 5a deposit at Barbados.

3. The undated, reef Vb terrace at Huon Peninsula, PNG, has been assumed to be related to the ~77 ka event identified at Barbados based on a simple correlation of terrace features. The ice-equivalent sea level (~-49 m) for this event in the preliminary model, R-0 (and R-1) was assigned by Lambeck and Chappell (2001). The sea-level calculations for this event (in chapter 4) differ slightly from the Lambeck and Chappell (2001) value and suggest ice-equivalent sea level was higher (~-40 m)

at that time.

Figure 6.28 shows a comparison of the observations associated with this secondary sub-stage 5a event with the predicted sea levels using the new model (R-1) established in section 6.6.3 (red bars). The predicted sea levels at all the Caribbean sites are well below the observed values. Even increasing the ice-equivalent sea level to ~40 m (as suggested by the revised calculations in chapter 4) does not bring the predicted and observed values into agreement. This implies that there may be a problem either with the chronology assigned to that feature (reef Vb) at Huon Peninsula, or with the elevation used for the calculation of sea level (reef Vb at Huon Peninsula is not well developed). Perhaps the Huon Peninsula reef Vb does not, in fact, represent the same 77 ka BP sea-level event identified at Barbados in this study. Further dating efforts at Huon Peninsula are required to establish the age of the Vb reef. As an alternative, if the equivalent sea level at this time of this event is increased such that the global ice distribution at this time is equal to that of the earlier sub-stage 5a feature (as defined in R-2, figure 6.29), then the predicted sea levels are more consistent with the observed values across the Caribbean region (figure 6.28, blue bars). This is the preferred model for this sub-stage 5a period (R-2). The ice-equivalent sea level associated with this 5a event is ~28 m below present (at ~77 ka BP), which is similar to that of the other 5a feature (at ~84 ka BP).

6.7.2 Sub-stage 5c

Sub-stage 5c deposits are scarce in the Caribbean region, possibly because the relative sea levels associated with the event were slightly lower than during sub-stage 5a and were overprinted or destroyed during the latter sea-level transgression. Evidence of sub-stage 5c sea level is summarised here:

1. Barbados - the results of the present study suggest that sub-stage 5c sea level at ~101 ka reached ~-15±4 m.

2. Haiti - the data of Dodge *et al.* (1983) suggest sea level during sub-stage 5c reached a peak of -10±4 m.

3. Bahamas - a submerged speleothem retrieved from >8.5 m below present sea level, contains a growth hiatus between ~108 ka and 93 ka BP (Lundberg and Ford, 1994; Toscano and Lundberg, 1999). There is no evidence of boring activity in that hiatus, which would indicate submergence in a marine environment. Therefore, Lundberg and Ford (1994) suggest that this hiatus represents inundation with freshwater when sea level rose to (or just above) that level during sub-stage 5c. Richards *et al.* (1994)

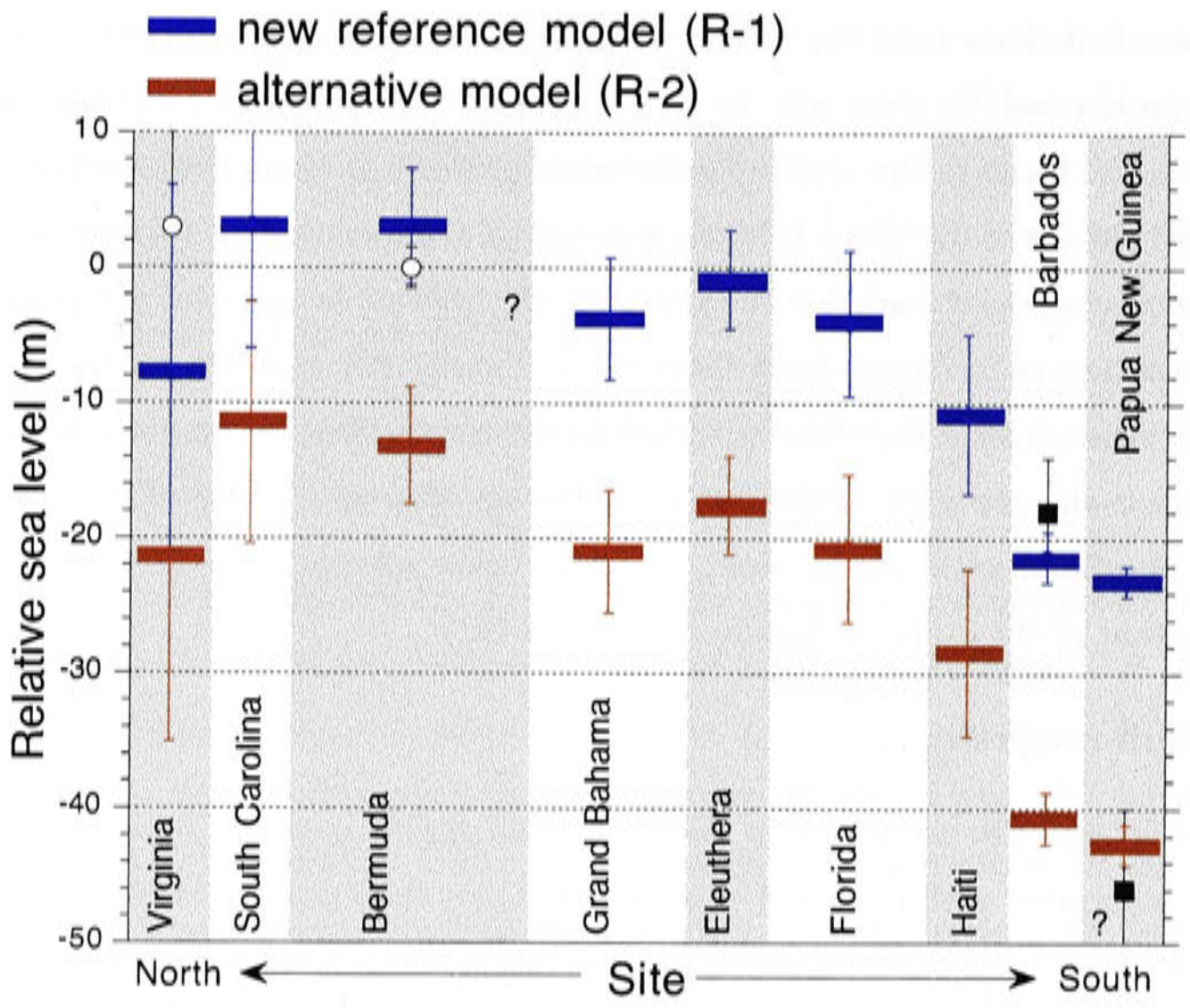

Figure 6.28: Observed and predicted sea levels for the additional sub-stage 5a feature identified in this study (at 77 ka). Red - predicted sea level for the new reference model R-1 and blue - predicted sea level for an alternative model (R-2) in which the global ice distribution is approximately the same for both sub-stage 5a sea-level high-stands. The 'error' ranges represent the range of preferred earth models.

suggests that a hiatus in speleothem growth need not be indicative of submergence, but rather represents a change in ground-water recharge conditions. This leaves open the possibility that sea level may have remained below the level of this speleothem.

4. Bermuda - U-Th dating of submerged speleothems suggest that sea level remained below -15 m during sub-stages 5a and 5c (Harmon *et al.*, 1978, 1983). As I discussed in section 4.5, chapter 4, these age determinations may be uncertain. In contrast, dating of coraliferous samples from a submerged ridge on the Bermuda platform suggests sub-stage 5c sea level rose to at least -12 m below present (Vollbrecht, 1990).

5. The two reefs of sub-stage 5c age (VIa and VIb) at Huon Peninsula (section 4.3.2) suggest that there was more than one sea-level transgression during that interstadial. In the preliminary ice model, R-0, which was based on the Huon Peninsula terraces, these events are assigned ages of 107 ka and 100 ka (see section 4.3.2) and correspond to ice-equivalent sea levels of ~20 m and 40 m respectively. However, these estimates are poorly constrained.

The age constraints for the sub-stage 5c data for many of the Caribbean sites is not sufficient to establish which of these events is being recorded at each of the sites. For this reason, the predicted sea levels for both events are compared with the Caribbean sub-stage 5c observations. Figure 6.30a shows a comparison of the sub-stage 5c observations with the predicted sea levels (for both high-stands) at the Caribbean sites using the new reference model (R-1) proposed in section 6.6.3. Initially, I assume that the reef VIb, which is the minor feature at Huon Peninsula (adopted age of ~100 ka), corresponds to the sub-stage 5c event identified at Barbados (101 ka B) because of the chronology assigned to those deposits. Using the R-1 model, the predicted sea level for the ~101 ka feature at Barbados is well below the observed level (orange bars, figure 6.30a). Figure 6.30b shows the predicted sea level for an alternative model (R-2, defined in figure 6.29) in which global ice distributions are approximately the same at 100 ka and 107 ka (in this case ice-equivalent sea level at both of these times is ~20 m below present). The sea level predictions for the ~100 ka feature are now no longer consistent with the Huon Peninsula reef VIb estimates, but they produce a much better match with the existing Caribbean observations, particularly at Barbados. These changes to sub-stage 5c melting history do not have a significant effect on the predicted sea levels for the sub-stage 5a events.

The reason for the inconsistency between the Huon Peninsula and Barbados sub-stage 5c sea levels may be due to a problem with the chronology assigned to the Huon Peninsula

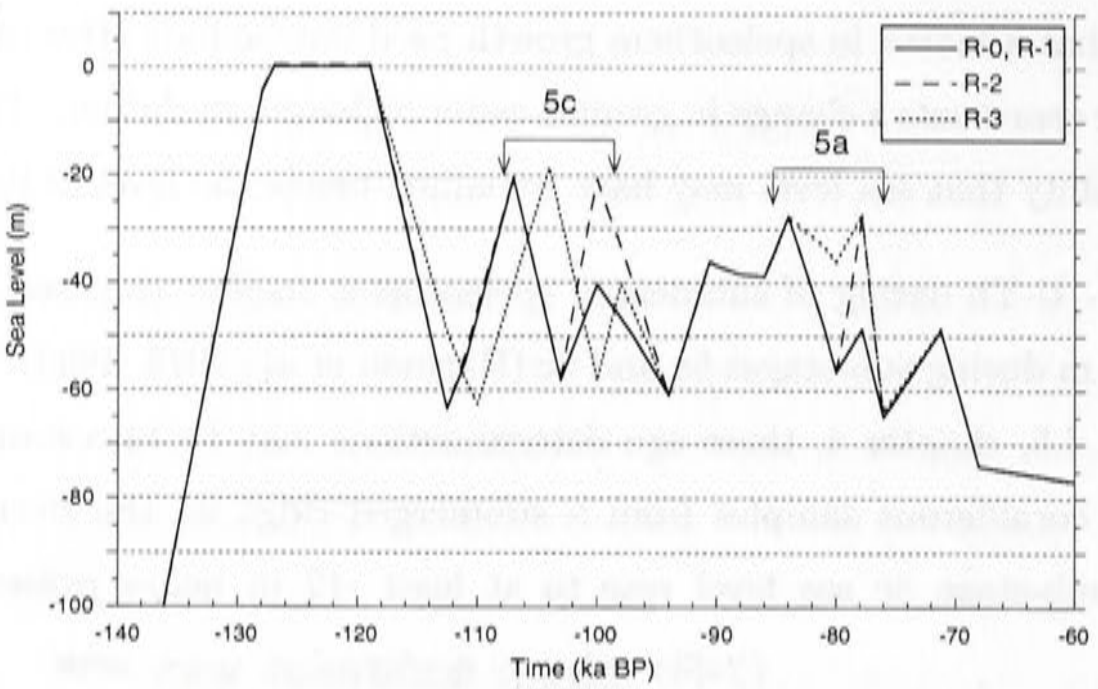

Figure 6.29: Alternative ice equivalent sea-level models. R-0 - preliminary ice model; R-1 - no change in ice-equivalent sea level but a change in the global distribution of ice as discussed in the text in section 6.6.3; R-2 and R-3 - changes to ice-equivalent sea level as shown.

reefs (and/or the Barbados event). The major 5c constructional feature at Huon Peninsula is reef VIa (assigned an age of 107 ka), however the chronology assigned to the Huon reefs suggests that the major 5c Barbados feature (101 ka) corresponds to the minor Huon Peninsula reef VIb ($\sim$ 100 ka). If the Barbados 5c event is instead correlated with the major Huon reef VIa platform, the predicted and observed sea levels at the two locations would be in better agreement. Consider an alternative model (R-3) in which an intermediate age of 104 ka is adopted for the major sub-stage 5a peak at an ice-equivalent sea level of -20 m (figure 6.29). In this model, it is assumed that this high-stand corresponds to the major reef VIa deposit at Huon Peninsula and also to the sub-stage 5c highstand identified at Barbados (this study). This age is within the quoted uncertainty of the Huon Peninsula deposit and would be consistent with an extended age range of the Barbados deposit (assuming the scatter of the U-Th represents a true period of reef growth, section 3.5). In this case, the predicted and observed sea levels for this major sub-stage 5c feature at both sites agree within uncertainties (figure 6.30c).[1] This is the preferred model for this time period. However only further comprehensive dating of the sub-stage 5c terraces at Huon Peninsula will be able to resolve this matter. In model R-3, the second sub-stage 5c event at Huon Peninsula has also been shifted to younger age (figure 6.29).

The predicted gradient in relative sea level across the region of interest is smaller for the sub-stage 5c feature than for the sub-stage 5a event. The peak sub-stage 5c sea level

[1] No alteration to the Huon Peninsula 'observed' sea-level estimate has been made using the new age of 104 ka in this comparison. This change would shift the estimate to a higher sea level but would still be within the quoted uncertainty range. The Barbados estimate has also been left unchanged. This change of age would lower the sea-level estimate at this site by a small amount well within the quoted uncertainty.

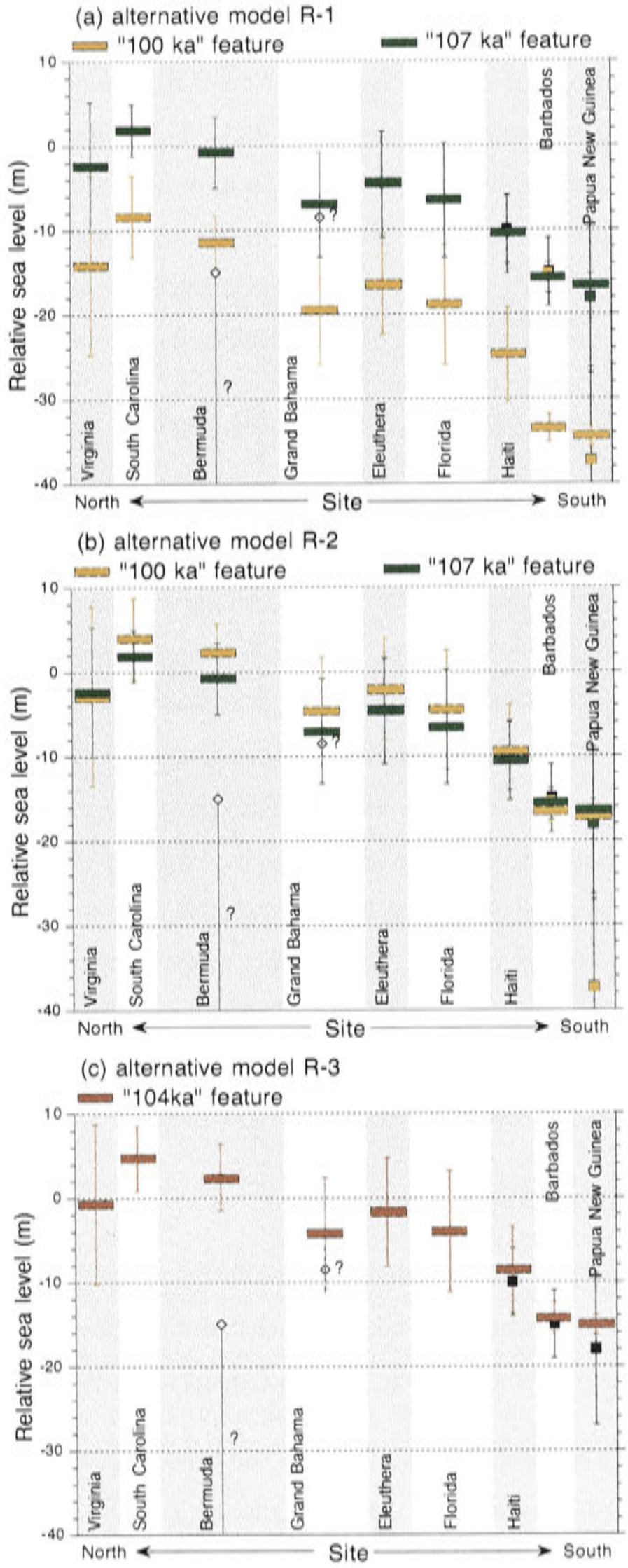

Figure 6.30: Observed and predicted sea levels for the sub-stage 5c sea-level features at ~100 ka and ~107 ka for a) the new reference model R-1; b) an alternative model R-2 in which the global ice distribution for the 107 and 100 ka events are the same; and c) an alternative model R-3 in which the major Barbados and Huon Peninsula events are correlated and assigned an age of 104 ka. The 'error' ranges represent the range of preferred earth models.

in this model occurs immediately following the deglaciation from the sub-stage 5d stadial compared to the 5a peak, which in this model follows a more gradual deglaciation from the 5b stadial. (The effect of the melting history of the LIS immediately prior to a sea-level event of interest was demonstrated in section 6.4.2). This difference may explain why although the ice-equivalent sea level at sub-stage 5c may be higher than at 5a, sub-stage 5a deposits are more commonly found at locations in the northern Caribbean than sub-stage 5c deposits. More spatially distributed sub-stage 5c sea-level observations are required to confirm this suggestion and to place better constraints on the sub-stage 5c melting history.

6.7.3 Sub-stage 5e - the last interglacial period

Sub-stage 5e sea-level observations in the same region do not display the same gradient in sea level as observed for sub-stage 5a deposits (see section 4.5 in chapter 4). Without presenting detailed calculations of sea-level change for the last interglacial highstand, which is beyond the scope of this thesis, there is a simple conceptual explanation for why we expect no significant gradient of 5e deposits across that region. If the penultimate deglaciation of the LIS was roughly similar to the last deglaciation then the isostatic-state of the Earth during the last interglacial period (relative to an equilibrium state) would have been similar to that of the Holocene and the present day. In this case we expect little or no gradient in the peak elevation of last interglacial deposits relative to the Holocene sea levels (see section 5.6.6 in chapter 5). Contour maps of the sea level in the Caribbean region at the peaks of sub-stages 5a and 5c and the end of the last interglacial period are shown in figures 6.31a, b and c and these demonstrate the difference in the behaviour of relative sea level across the region at each of these times.

6.7.4 Preferred MIS 5 sea-level model

Based on the comparison of the observed and predicted sea levels for the sub-stage 5c and 5a events that are recorded at both Huon Peninsula and Barbados the following preferred model of ice equivalent sea level during the last glacial cycle is proposed:

1. An ice-equivalent sea level of ~28 m below the present at 84 ka (peak of 5a) is consistent, within the uncertainties of the earth rheology, with the observations of sea level for that event at Huon Peninsula and across the Caribbean region (section 6.6.3).

2. The paleo-sea level for the secondary sub-stage 5a feature (at ~77 ka) inferred from Huon Peninsula is not well constrained due to the lack of datable material in the reef Vb deposit. In the preliminary model, R-0, the ice-equivalent sea level at that time is assigned a value of -49 m. As a consequence, the sea level predicted for

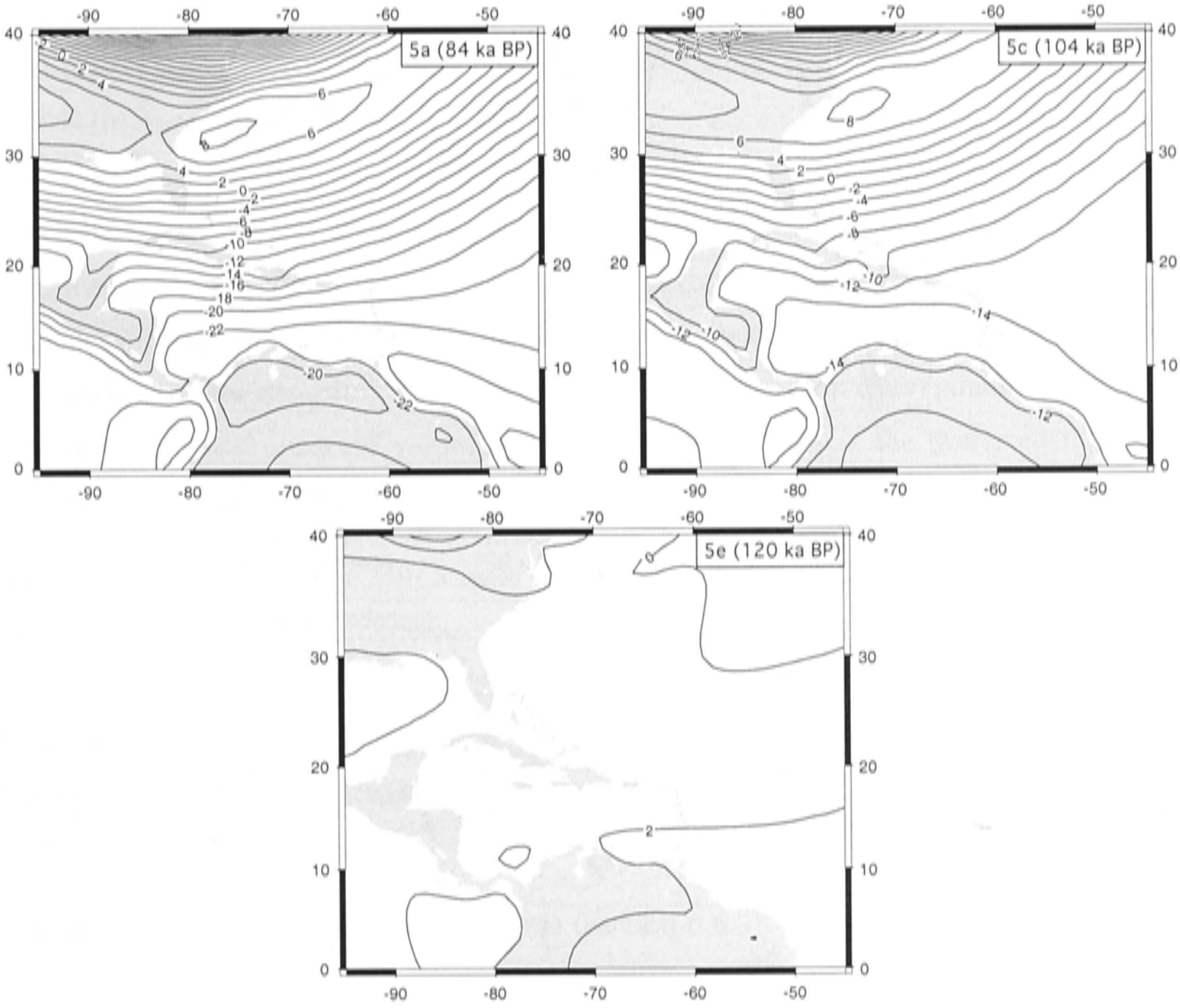

Figure 6.31: Contour plots of relative sea level in the Caribbean region at the peak of sub-stages 5a (84 ka BP) and 5c (104 ka BP) and the end of the last interglacial period, sub-stage 5e (120 ka). The preferred ice model R-3 and earth model ma4C were used for this calculation. There is a significant gradient across the region predicted for the sub-stage 5a and 5c events. This gradient is a consequence of the difference in the glacio-isostatic components at those times relative to the present day. At the end of the last interglacial period, the deformation of the earth in this region was similar to the present day so there is no significant change in the relative sea level across this region at that time.

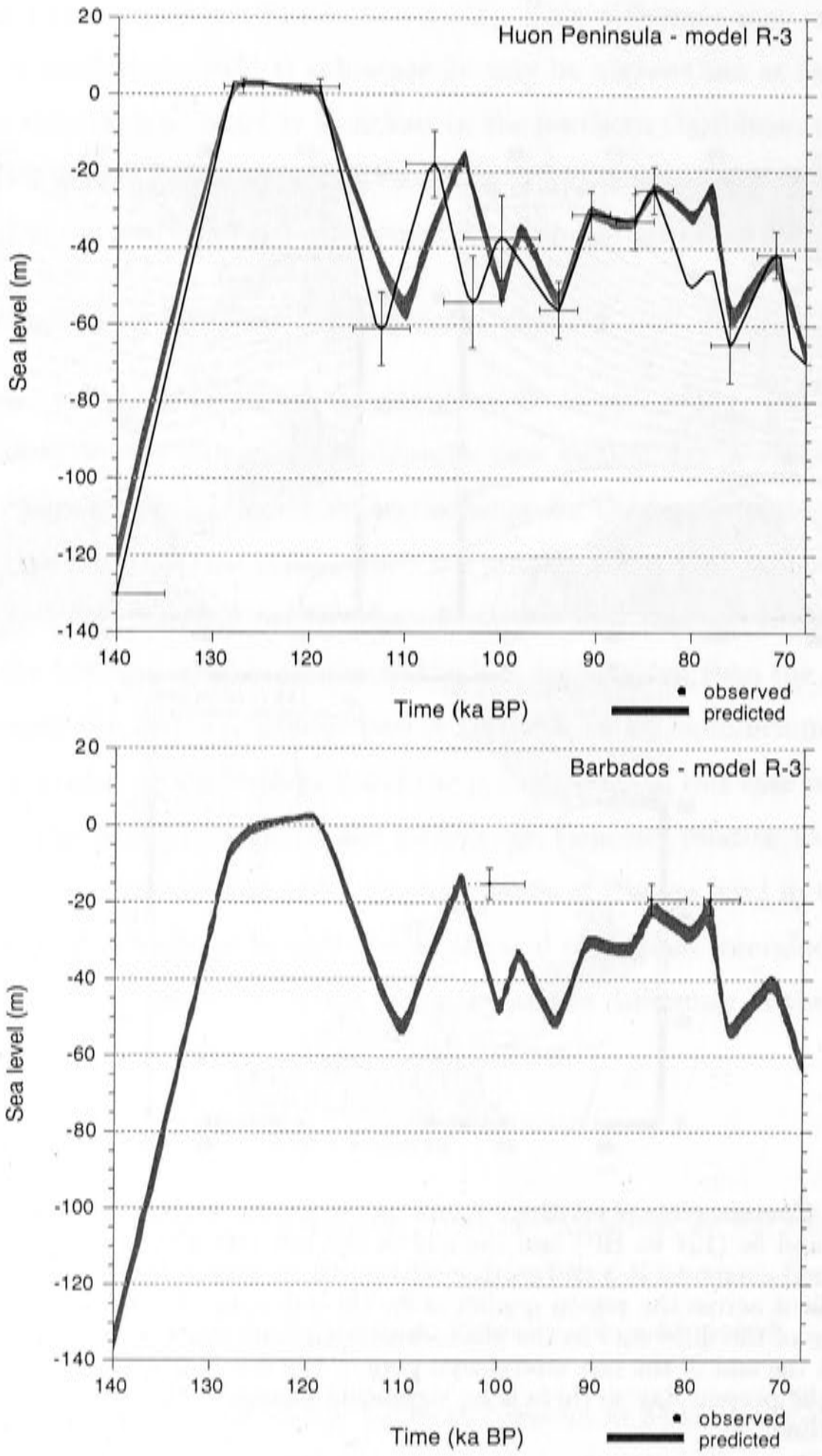

Figure 6.32: Comparison of observed and predicted sea levels at Huon Peninsula and Barbados for the preferred ice model, R-3, and a range of earth model parameters (as for figure 6.27). Notice that the predictions at these locations are not particularly sensitive to the choice of earth model.

this event at Barbados is ~-41 m, which is obviously inconsistent with the observed value at Barbados of ~-19 m (present study). The preferred model is one in which the ice-equivalent sea level and global ice distribution for the secondary sub-stage 5a event (at ~77 ka) is similar to that of the 'classic' sub-stage 5a event (at ~84 ka) and has a value of ~28 m below present. This is the case for the alternative models R-2 and R-3 shown in figure 6.29.

3. Based on the original ice-equivalent sea-level model, the predicted sea level for the ~101 ka event at Barbados is well below the observed value (correlating the minor Huon reef VIb with the sub-stage 5c Barbados event). As an alternative, I suggest that the major reef feature at Huon (reef VIa), originally assigned an age of 107 ka, instead corresponds to the '101 ka' event at Barbados. If an age of ~104 ka is adopted to represent this event at both localities (on the outer limits of the uncertainties for each of these deposits), then there is no longer a major discrepancy between the predicted and observed values for these two sites. This is the preferred model for this event (R-3 in figure 6.29).

Further investigation of the MIS 5 reefs at Huon Peninsula should be conducted to better constrain the ages of these deposits.

A modified ice-equivalent sea-level curve and ice partition model for the preferred model R-3 is shown in figure 6.33 (compared to the preliminary model R-0 described in figure 6.1). This alternative ice model includes the following modifications:

1. A 50% decrease in MIS 5 ice volume (section 6.6.3).

2. Global ice distribution for the two sub-stage 5a events (at 84 ka and 77 ka) have been made approximately equal.

3. The major sub-stage 5c highstand has been shifted from 107 ka to 104 ka BP (and the timing of the minor sub-stage 5c oscillation shifted from 100 ka to 98 ka).

A reduction of the Antarctic ice volume (or other far-field ice sheets) during the *stadial* periods (5d and 5b) can be made without a significant effect on the sub-stage 5a and 5c highstand predictions. Further investigation of MIS 5 sea levels in the region surrounding the Laurentide Ice Sheet is clearly required to establish a more detailed ice melting history for that time period.

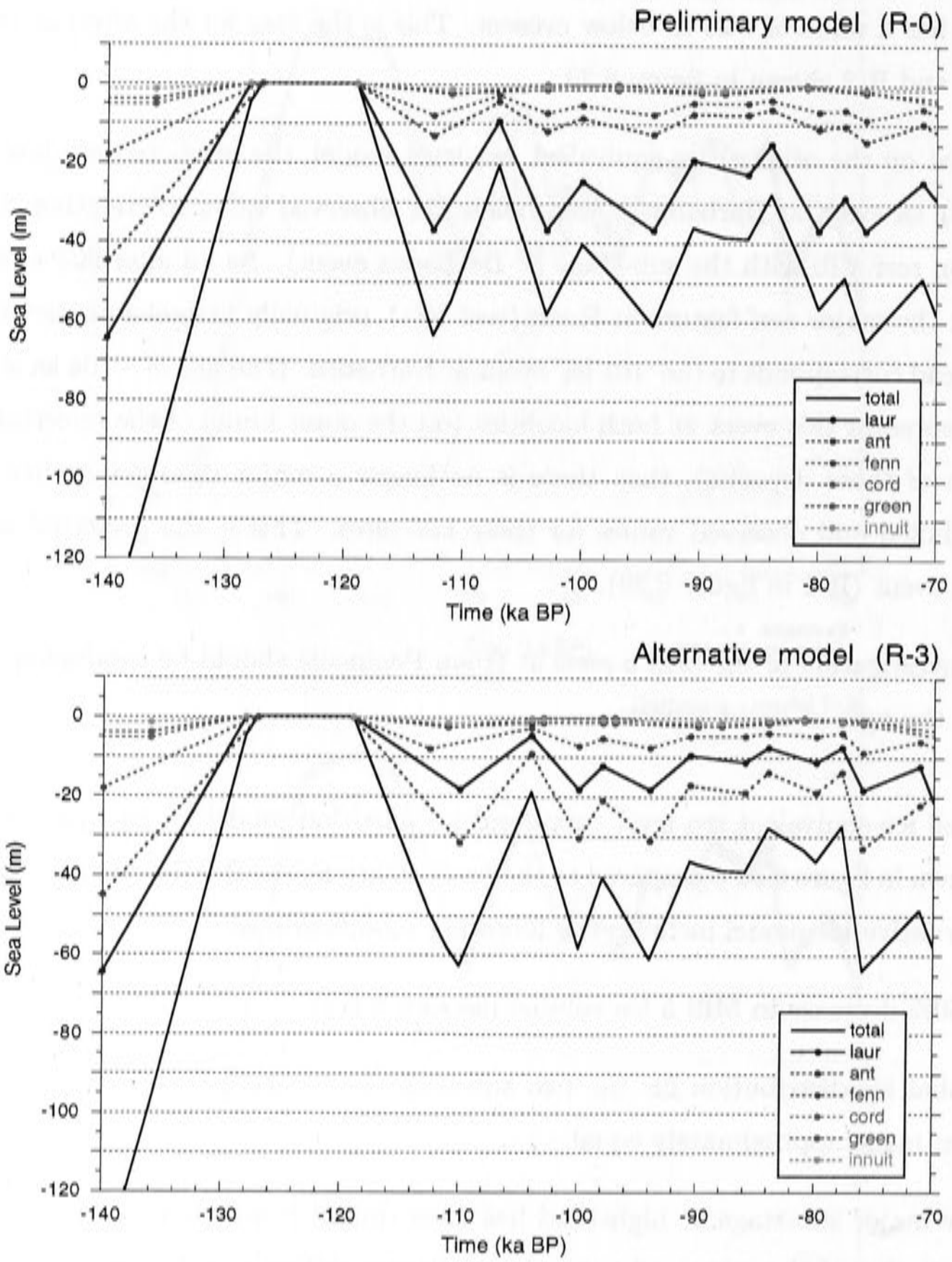

Figure 6.33: Comparison of preliminary ice partition model R-0 with revised model R-3. The R-3 preferred model is described in the text. Contribution of six major ice sheets to total ice volume expressed in ice-equivalent sea level: Laurentide, Antarctic, Fennoscandian, Greenland, Cordilleran and Innuitian Ice Sheets. The volume of the Antarctic Ice Sheet at the stadial events, ie sub-stages 5d and 5a, can be reduced without significantly affecting the sea-level predictions for the interstadial events.

6.8 Conclusions

The apparently conflicting observations of sub-stage 5a sea level in the Caribbean region have been the subject of much controversy in recent years. For example, estimates vary from ~19 m below present sea level in Barbados (this study), to 6-10 m below present at Florida (Ludwig *et al.*, 1996; Toscano and Lundberg, 1999), and to above present sea level at Bermuda and on the US East Coast (Cronin *et al.*, 1981; Szabo, 1985). Researchers have suggested reasons for this range of estimates, including non-*in situ* deposits, poor stratigraphic interpretation and uncertainties in tectonic setting. In this chapter, I have demonstrated that these estimates are reconciled by taking into account the effects of glacio-hydro-isostasy and that this variability can be used to constrain models of the Earth's rheology and ice sheets during the last glacial cycle.

Local sea-level change reflects the superposition of ice-equivalent sea-level variations and the deformation of the Earth's surface and perturbation of the geoid in response to changes in ice and water surface loading. The magnitude of these glacio-hydro-isostatic effects at a given site is a complex function of the melting history of ice sheets, the rheology of the Earth and coastline geometry. The isostatic contribution to sea level at any given time is the difference between the isostatic components at the time of interest (relative to an equilibrium state) and at the present day. At the peak of sub-stage 5a, the glacio-isostatic contribution to sea level across the Caribbean region (relative to an equilibrium state) varies only gradually with distance from the ice sheet. But at the present day, the Earth is still relaxing following the changes in surface loads associated with the last deglaciation. The present day collapsing peripheral bulge contributes a ~20 m gradient in glacio-isostatic component across the Caribbean region and the relative sea level for sub-stage 5a will reflect a similar gradient. The prediction of this gradient is robust but its magnitude varies as a function of the melting history of the Laurentide Ice Sheet both before and after the time of interest and the viscoelastic rheology of the Earth. These same concepts also apply to other time periods such as MIS 3 (section 4.5), but these are not dealt with here.

In this chapter, I have used a preliminary reference model of ice melting history and earth rheology to calculate sub-stage 5a sea-level predictions for a number of sites throughout the Caribbean and surrounding region that were then compared to the observed values at those locations. Although there is a trade-off between the ice and earth model parameters, constraints can be placed on these by combining (i) comparisons of spatially

and temporally distributed relative sea-level observations and predictions, (ii) geological observations of ice extent and (iii) inferences of rheological structure of the Earth from other geophysical observations.

The following modifications to the preliminary reference model (R-0 and ma4A) has led to an improvement of the agreement between the predicted and observed sub-stage 5a sea levels and that are also consistent with the conclusions of other studies.

1. Changes to earth rheology

   (a) Increase in upper mantle viscosity at US coastal sites (from 4×10^{20} Pa s to 6×10^{20} Pa s) - this modification improves the agreement of model predictions with observations by shifting the peak of the predicted maximum sea level towards the ice and is consistent with the results of seismic studies which imply a higher viscosity upper mantle in the North American shield region, beneath the Laurentide Ice Sheet (Grand, 1994).

   (b) Decrease in upper mantle viscosity at southern Caribbean sites (from 4×10^{20} Pa s to 2×10^{20} Pa s) - this modification raises sea-level predictions at the southern Caribbean sites of Barbados and Haiti and is consistent with the conclusions of other LGM and deglacial sea-level studies (Lambeck *et al.*, 2002c).

   (c) Increase in lower mantle viscosity (from 1×10^{22} Pa s to 3×10^{22} Pa s) - this increases sea-level observations at all Caribbean sites so that they are in better agreement with the observations and is also consistent with both the constraints of other relative sea-level studies (Kaufman and Lambeck, 2000, 2002; Lambeck *et al.*, 2002c) and rotational considerations (Johnston and Lambeck, 1999).

2. Changes in Laurentide Ice Sheet melting history

   (a) Decrease in Laurentide Ice Sheet (LIS) ice volume during sub-stages 5d-5a - this modification increases the predicted gradient across the region of interest and is consistent with models and geologic models of ice extent at that time (Clark *et al.*, 1993; Kleman *et al.*, 2002).

   (b) Northward shift of LIS during sub-stages 5d-5a - this modification also increases the predicted gradient and is consistent with geologic evidence of ice extent during that period (Clark *et al.*, 1993).

   (c) Some changes to the ice-equivalent sea level for the sub-stage 5c and secondary 5a sea-level high-stands have been made, as discussed in section 6.7.4. In the preferred model, the classic sub-stage 5c sea-level high-stand occurs at 104 ka

BP and with an ice-equivalent sea level of -20 m. The sub-stage 5a events occur at 84 ka BP and 77 ka BP, both with ice-equivalent sea levels of -28 m.

Further comprehensive studies of sea level during sub-stages 5d to 5a in the regions surrounding the Laurentide Ice Sheet and other ice sheets are required in order to better constrain a detailed global ice melting history during the period following the last interglacial.

Chapter 7

Conclusions

Sea-level change during the last glacial cycle provides constraints on fluctuations in ice volume through time and can be used to examine the factors involved in controlling climate change. The state of climate variability during sub-stages 5a and 5c is of importance because this period represents the transition between the interglacial conditions of sub-stage 5e and the more heavily glaciated period leading into the last glacial maximum. In this thesis, I have adopted a multi-faceted approach to the investigation of sea level and climate change during this period, which includes both geochemical analyses and geophysical techniques. In this way, I have not only established the timing and magnitude of sea-level oscillations during the sub-stage 5a-5c period but have also used these observations to place constraints on ice sheet distribution and melting history as well as on earth rheology. By comparing the sea-level observations with other proxy climate records this study also provides insights into the processes involved in controlling climate variability.

7.1 Barbados U-Th analyses

U-Th dating of corals provides a timescale for changes in sea level during the late Pleistocene. The use of this dating method requires that corals form closed systems with respect to uranium and thorium isotopes. A comparison of a sample's initial activity ratio of ^{234}U to ^{238}U (expressed as $\delta^{234}U$) with that of modern corals ($\sim$148.5‰) is considered the most useful quantitative test for judging the reliability of a coral's measured U-Th age. It has generally been assumed that the $\delta^{234}U$ of the ocean, and hence the initial $\delta^{234}U$ value in corals, has not changed measurably over the last glacial cycle.

In this study, more than 80 U-Th analyses have been conducted on coral samples from sub-stage 5a and 5c deposits on the south and west coasts of Barbados. Within each group of samples from each deposit, there is a range of initial $\delta^{234}U$ values (from 140‰ to >180‰) that are found to vary as a function of measured age (figure 7.1). Possible mech-

anisms leading to initial δ^{234}U values that differ from the observed modern value include variations of the uranium isotopic composition of ocean water during the last glacial cycle and/or mobilisation of uranium and thorium isotopes as a result of diagenetic alteration.

A systematic lowering of oceanic δ^{234}U throughout the last glacial cycle (by 10-15‰), followed by a rapid rise to modern levels is implied by a compilation of coral data from this and other studies (trend 1 in figure 3.16). If ocean water δ^{234}U has varied during the last glacial cycle, this has profound implications for the interpretation of U-Th ages. Such variability could be due to one of several mechanisms including variations in riverine uranium content or isotopic composition, storage and release of ^{234}U from suboxic sediments and/or spatial variability in ocean δ^{234}U. Further investigation of the ocean's uranium budget and isotopic composition is required to establish the relative likelihood of these mechanisms.

Not all of the observed variability of initial δ^{234}U (both the trend within individual deposits and the highly elevated values) can be explained by variations in ocean water δ^{234}U. There are a number of instances where different corals with a similar apparent age have distinctly different initial δ^{234}U values. Furthermore, rapid and large variations in samples from a single stratigraphic horizon cannot be explained by changes in oceanic δ^{234}U. It appears that systematic mobilisation of uranium and/or thorium isotopes during diagenetic alteration can also lead to changes in a coral's initial δ^{234}U. This is a likely explanation for the correlation between apparent age and δ^{234}U observed within individual deposits in this study and other studies. Diagenetic processes that have been proposed to explain this correlation include: (i) the continuous addition of ^{234}U and ^{230}Th in a fixed ratio (Gallup *et al.*, 1994); (ii) the addition of ^{234}Th and ^{230}Th from an α-recoil source or the decay of dissolved uranium (Thompson *et al.*, 2002; Fruijtier *et al.*, 2000); and/or (iii) the net removal of uranium with a preference for ^{238}U and primary ^{234}U relative to secondary ^{234}U (Fruijtier,*et al.*, 2000). Although each of these alternative models predicts similar trends to that observed in the U-Th data, each has unresolved problems. It seems from this work that multiple processes are acting simultaneously, so open system ages cannot be 'corrected' to find a true age based on the predictions of these individual models.

The focus of this work has not been a comprehensive investigation of diagenetic processes leading to the observed correlation of measured age and δ^{234}U in the presented data set. However, the sets of samples analysed here provide the basis for a future detailed study of their physical, chemical and isotopic properties. This will allow a more thorough inves-

Feature	Age (ka)	Sea level (m)
5a-1	$76.8\pm^{0.7}_{3.1}$	-19±4
5a-2	$84.0\pm^{0.4}_{2.7}$	-19±4
5c	$101.0\pm^{1.4}_{3.7}$	-15±4
6	$168.3\pm^{3.7}_{6.1}$	$-35\pm^{10}_{6}$

Table 7.1: Summary of age interpretations and sea-level calculations for the high-stand events identified in this study. The mean ages quoted above are based on the standard reliability criterion of comparing the samples calculated initial δ^{234}U with the modern value (148.5‰). The quoted age uncertainties are asymmetric and take into account both the scatter of data points around the trend-line (which may represent either noise or a finite period of reef growth) and also the possibility of a lower than modern oceanic δ^{234}U at the time these events.

tigation of the effects of diagenesis on a coral's U-Th system, as well as the possibility of δ^{234}U variation in the ocean during the last glacial cycle.

Taking into account the scatter of measured ages and the potential variation in oceanic δ^{234}U, samples from the 'classic' sub-stage 5a and 5c deposits were found to have mean ages of $84.0\pm^{0.4}_{2.7}$ ka and $101.0\pm^{1.4}_{3.7}$ ka respectively (table 7.1). A distinct morphological terrace unit on the south coast was found to have a mean age of $76.8\pm^{0.7}_{3.1}$ ka and is interpreted to represent a secondary sub-stage 5a sea-level event. This is the first time that a distinct period of reef growth of this age has been established using high precision U-Th dating techniques. These results confirm the suggestion of Schellmann and Radtke (2001) that the uplifted terraces at Barbados have a more complex structure than suggested by earlier studies (e.g. Broecker *et al.*, 1968). A deposit with a mean age of $168.3\pm^{3.7}_{6.1}$ ka was also identified and appears to represent a sea-level excursion during MIS 6.

7.2 Sea-level change during sub-stages 5a and 5c

The sea levels associated with each of the sub-stage 5a and 5c deposits identified in this study have been calculated assuming a constant tectonic uplift at Barbados since the last interglacial highstand (table 7.1). The 'classic' sub-stage 5a and 5c events at ~84 ka and ~101 ka BP reached sea levels of ~19±4 m and ~15±4 m below present respectively. The sea level associated with the newly identified ~77 ka BP deposit was calculated to be ~19±4 m below present. The sea levels for the two sub-stage 5a events (at ~84 and ~77 ka BP) are the same, within uncertainties, but it is not clear if or by how much sea level fell between these two events. Because the ages of these features are tightly constrained compared to their age separation of ~7 ka, and considering that they correspond

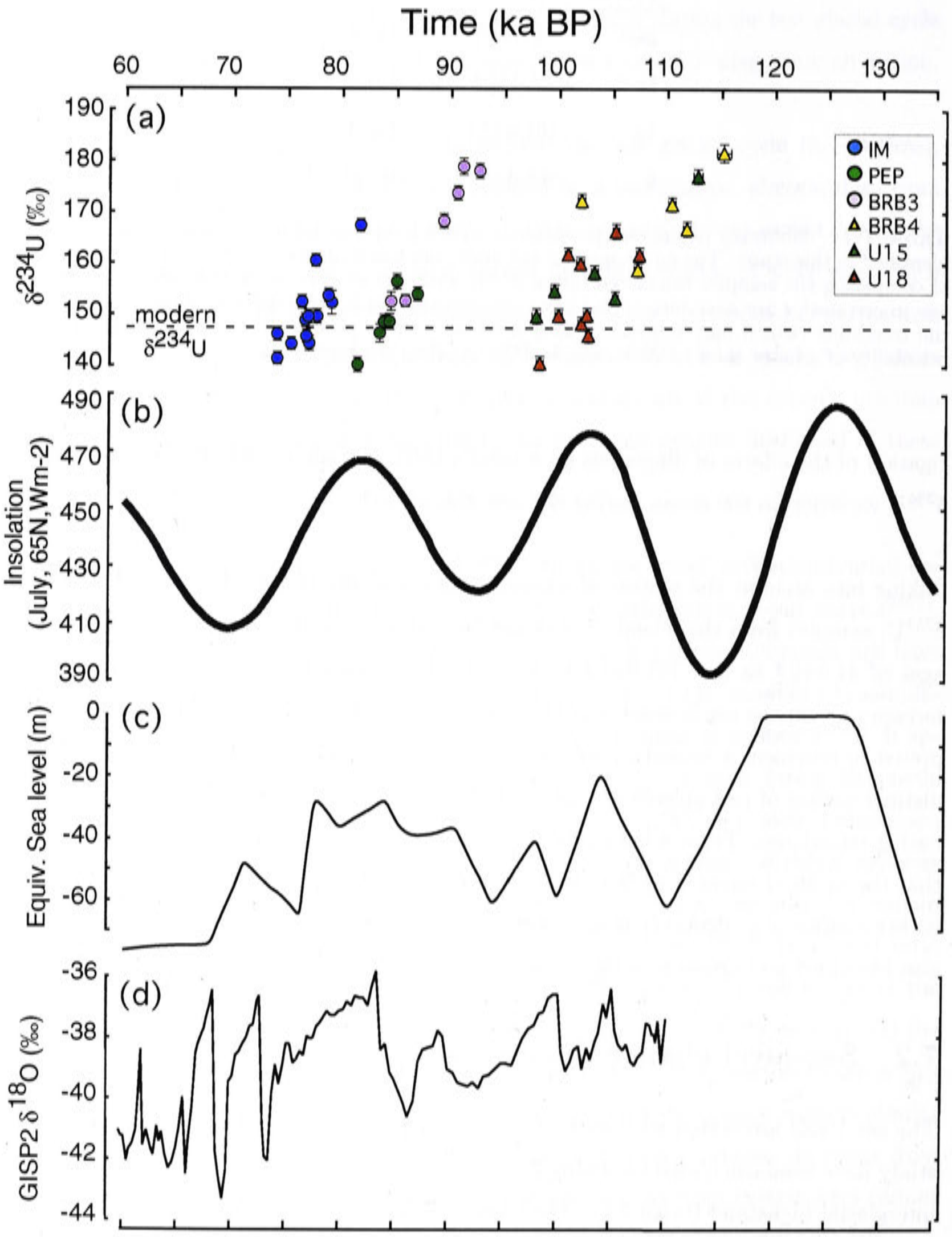

Figure 7.1: (a) U-Th results for the *in situ* Barbados sub-stage 5a and 5c coral samples analysed in this study (chapter 3); (b) 65°N summer insolation (Berger and Loutre, 1991); (c) Ice-equivalent sea-level curve for the preferred model (R-3) established in chapter 6; (d) GISP2 δ^{18}O record (Grootes *et al.*, 1993; Grootes and Stuiver, 1997) plotted on ice core timescale (Bender *et al.*, 1994)

to morphologically distinct deposits, it is likely that they represent two distinct sea-level oscillations.

The MIS 5 Barbados sea-level record presented in this investigation implies a more complex local sea-level history than suggested in earlier studies. By comparing this record with sea-level observations at other locations, a true ice volume signal can be distinguished from local effects. Although the uplifted coral terraces at Huon Peninsula (PNG) also point to multiple sea-level oscillations during this period (Chappell and Shackleton, 1986; Lambeck and Chappell, 2001), a direct comparison of sea level at different sites is not valid, however, because local isostatic effects need to be taken into account.

An important illustration of this is seen in sea-level estimates for the peak of sub-stage 5a across the Caribbean region, which vary by over 20 m (figure 4.15). At Barbados, the peak sub-stage 5a sea level reached ~19±4 m below sea level (this study); at Florida sea level reached 6-10 m below present (Ludwig *et al.*, 1996; Toscano and Lundberg, 1999); estimates in the Bahamas range from ~15 m below present to close to present sea level (Lundberg and Ford, 1994; Richards *et al.*, 1994; Hearty and Kaufmann, 2000; Kindler and Hearty, 1996) and at Bermuda and the US East Coast there is evidence that sub-stage 5a sea level reached above present (Muhs *et al.*, 2002; Cronin *et al.*, 1981; Szabo *et al.*, 1985; Wehmiller, pers. comm.). These apparently conflicting estimates have been the subject of controversy in the literature for many years and are often attributed to poor sample quality, non *in situ* sample collection, uncertainties in tectonic setting and/or poor stratigraphic context.

Local observations of relative sea levels do not simply record changes in ice-equivalent sea level. Instead, local sea-level change reflects the superposition of changes in ice-equivalent sea level and the deformation of the Earth and perturbation of the geoid in response to changing ice and water surface loads (glacio-hydro-isostasy). The sites mentioned above span the outer intermediate-field region associated with the Laurentide Ice Sheet and experience a range of glacio-hydro-isostatic effects, so the relative sea-level histories at these sites are expected to differ. The deformation of the Earth at the peak of sub-stage 5a, relative to an equilibrium state, does not vary significantly across the region of interest. In contrast, the present day deformation of the Earth in that region does have a large gradient (on the order of ~20 m) due to the presence of the collapsing LGM glacial bulge. As a result, we expect a substantial gradient in the glacio-isostatic component of sea-level change at the peak of sub-stage 5a *relative to the present day.*

The isostatic effects are a function of the surface ice and water loading history and of the Earth's rheology. However for any given area or time period these parameters are incompletely known. Temporally and spatially distributed relative sea-level observations provide the opportunity for placing constraints on these parameters. A comparison of isostatic model predictions with observations of sub-stage 5a and 5c sea level for each of the Caribbean sites in chapter 6 has allowed constraints to be placed on both earth rheology and the melting history of the Laurentide Ice Sheet.

Sites close to the Laurentide Ice Sheet's margins are particularly sensitive to the Earth's rheology. The comparison of predicted and observed sea level at sites on the US East Coast favours models with a high upper mantle viscosity ($>4\times10^{20}$ Pa s). However, at southern Caribbean sites, a low upper mantle viscosity ($<4\times10^{20}$ Pa s) is more appropriate. Both of these alternative upper mantle viscosities may be valid because upper mantle viscosity is expected to vary laterally across this region (Grand, 1994). A high lower mantle viscosity (up to 3×10^{22} Pa s) improves the agreement of predicted and observed sea levels across the entire study region, but is particularly important for the southern Caribbean sites. These changes in earth rheology are supported by other observations of geophysical parameters and post-glacial sea-level studies (Kaufmann and Lambeck, 2000, 2002; Okuno and Nakada, 2001; Nakada and Lambeck, 1991).

The comparison between the predicted and observed sea levels indicate that the LIS was located further north during the 5d-5a period and that it contributed less ice (as a proportion of global ice volume) at this time compared to the LGM. This northward shift and smaller volume for the LIS during sub-stages 5d-5a is also consistent with geological observations of ice extent for that period (Clark *et al.*, 1993; and Kleman *et al.*, 2002). In the preferred model, the LIS contributes less than ~20 m to the lowering of ice-equivalent sea level during the entire MIS 5 period. An increase in the volume of the LIS during the LGM and the last deglaciation also improves the agreement between observed and predicted sea levels. A 30% increase of Licciardi *et al.*'s (1999) maximum ice model was made in the preliminary model, but no further increase is required with the MIS 5 ice history discussed above. This is broadly consistent the constraints of post-glacial sea-level studies (Tushingham and Peltier, 1991; Lambeck *et al.* 2000).

The preliminary ice-equivalent sea-level model used in this study was based on the Huon Peninsula sea-level record. The comparison of the observed and predicted sub-stage 5a and

5c sea levels at this location and others (e.g. at Barbados and elsewhere in the Caribbean region) has led to modifications of the preliminary curve. In the preferred ice-equivalent model, sea level reaches ~20 m below the present at the peak of sub-stage 5c and ~28 m below present for each of the sub-stage 5a events identified at Barbados in this study. Opportunities remain for improved spatially and temporally distributed sea-level observations to provide tighter constraints on the melting history of the Laurentide Ice Sheet and changes in ice-equivalent sea level during the last glacial cycle.

7.3 Links between sea level and climate during sub-stages 5a and 5c

The broad trends in stacked $\delta^{18}O$ records (e.g. Imbrie *et al.*, 1984) imply that there were two main oscillations in ice volume during marine isotope sub-stages 5a and 5c. This simple picture is consistent with Milankovitch's (1941) insolation forcing model. However, sea-level observations at Barbados (this study) and Huon Peninsula (Lambeck and Chappell, 2001) suggest that there was more complexity in the sea-level oscillations at that time (figure 7.1). Suborbital climate variability during MIS 5 is also evident in other proxy records of climate change. Discrete episodes of enhanced ice rafted debris (IRD) deposition during MIS 5 are evident in North Atlantic Ocean sediment records (McManus *et al.*, 1994; Chapman and Shackleton, 1999), and have a similar periodicity to the Heinrich events during MIS 3 (Bond *et al.*, 1993). These MIS 5 events can also be linked to episodes of cooling in the North Atlantic ocean (McManus *et al.*, 1994) and Greenland (Chapman and Shackleton, 1999). These observations indicate that other processes, in addition to insolation forcing, are influencing the pattern of glaciation during sub-stage 5a and 5c.

Although there are similarities in the records of climate variability during MIS 5 and MIS 3, such as the frequency of the major ice rafting events and sea-level excursions, there are also some obvious differences: (i) the magnitude of the MIS 5 IRD layers are smaller than during MIS 3 and (ii) the composition of the MIS 5 IRD layers indicates multiple source regions (Chapman and Shackleton, 1999) rather than the predominantly LIS source of the MIS 3 events (Bond and Lotti, 1995). This comparison implies that the ice distribution of the LIS was different during MIS 5 than during later periods. Independent geological observations (Clark *et al.*, 1993) and the conclusions of chapter 6 also suggest that the LIS was located further north and contributed significantly less ice (as a proportion of the global ice volume) during MIS 5 compared to MIS 3 and the LGM. Ice cover in Arctic Russia, including shelf ice, was much more extensive during MIS 5 than later

in the glacial cycle (Svendsen *et al.*, 1999). Perhaps instability of the Russian or other coastal ice sheets, instead of the LIS, was responsible for periodic climate interruptions during the MIS 5 period. Records of MIS 5 ice rafted debris in other regions, such as the Arctic or Southern ocean, may test this possibility.

How are these North Atlantic climate instabilities related to the oscillations in global ice volume observed in the Barbados and Huon Peninsula records? Perhaps insolation-induced melt played a role in destabilising coastal ice sheets in the North Atlantic. In this scenario, the ice rafting triggered by the gradual sea-level rise leads to an interruption of the North Atlantic thermohaline circulation and the subsequent cooling of the region, preventing further insolation melt. Upon a re-start of the thermohaline circulation an enhanced moisture source leads to growth of ice sheets and fall in sea level before insolation-induced melt again dominates. This mechanism, which would be active during periods of high insolation variability may explain why multiple sea-level oscillations are associated with single insolation maxima. However, this scenario cannot explain the early sub-stage 5a sea-level rise, relative to the timing of the insolation rise (figure 7.1) or the additional sea-level oscillation during the sub-stage 5/4 transition. Regardless, sea level during this period is likely to have been the result of a dynamic interplay between insolation forcing and internal climate instabilities. The details of any mechanism are speculative and would, of course, be influenced by the location of the various ice sheets and their susceptibility to destabilisation and collapse. More spatially distributed, high resolution MIS 5 records are required to examine these processes in further detail.

References

Alley, R. B. (1998) Palaeoclimatology - Icing the north Atlantic, *Nature* **392**, 335.

Banner, J. L., Wasserberg, G. J., Chen, J. H., and Humphrey, J. D. (1991) Uranium-series evidence on diagenesis and hydrology in Pleistocene carbonates of Barbados, West Indies, *Earth and Planetary Science Letters* **107**, 129-137.

Bar-Matthews, M., Ayalon, A., and Kaufman, A. (2000) Timing and hydrological conditions of Sapropel events in the Eastern Mediterranean, as evident from speleothems, Soreq cave, Israel, *Chemical Geology* **169**, 145-156.

Bar-Matthews, M., Wasserburg, G. J., and Chen, J. H. (1993) Diagenesis of fossil coral skeletons: Correlations between trace elements, textures, and U-234/U-238, *Geochimica et Cosmochimica Acta* **57**, 257-276.

Bard, E., Antonioli, F., and Silenzi, S. (2002) Sea-level during the penultimate interglacial period based on a submerged stalagmite from Argentarola Cave (Italy), *Earth and Planetary Science Letters* **196**, 135-146.

Bard, E., Hamelin, B., Arnold, M., Montaggioni, L. F., Cabioch, G., Faure, G., and Rougerie, F. (1996) Deglacial sea-level record from Tahiti corals and the timing of global meltwater discharge, *Nature* **382**, 241-244.

Bard, E., Hamelin, B., and Fairbanks, R. G. (1990) U-Th ages obtained by mass spectrometry in corals from Barbados: sea level during the past 130,000 years, *Nature* **346**, 456-458.

Barnes, C. E., and Cochran, J. K. (1990) Uranium removal in oceanic sediments and the ocean U balance, *Earth and Planetary Science Letters* **97**, 94-101.

Belknap, D. F., and Wehmiller, J. F. (1980) Amino acid racemization in Quaternary mollusks: examples from Delaware, Maryland, and Virginia. In: *Biogeochemistry of Amino Acids.* (P. E. Hare, T. C. Hoering, and K. King, Jr., Eds.), pp.401-414. John Wiley, New York.

Bender, M., Sowers, T., Dickson, M. L., Orchardo, J., Grootes, P., Mayewski, P. A., and Meese, D. A. (1994) Climate Correlations between Greenland and Antarctica During the Past 100,000 Years, *Nature* **372**, 663-666.

Bender, M. L., Fairbanks, R. G., Taylor, F. W., Matthews, R. K., Goddard, J. G., and Broeker, W. S. (1979) Uranium-series dating of the Pleistocene reef tracts of Barbados, West Indies, *Geological Society of America Bulletin* **90**, 577-594.

Bender, M. L., Taylor, F. T., and Matthews, R. K. (1973) Helium-Uranium Dating of Corals from Middle Pleistocene Barbados Reef Tracts, *Quaternary Research* **3**, 142-146.

Berger, A. (1988) Milankovitch Theory and Climate, *Reviews of Geophysics* **26**, 624-657.

Berger, A., Loutre, M.-F., and Tricot, C. (1993) Insolation and Earth's Orbital Periods, *Journal of Geophysical Research* **98**, 10341-10362.

Berger, A. L. (1978) Long-Term Variations of Daily Insolation and Quaternary Climatic Changes, *Journal of the Atmospheric Sciences* **35**, 2362-2367.

Berger, A. L., and Loutre, M.-F. (1991) Insolation Values for the Climate of the last 10 million years, *Quaternary Science Review* **10**, 297-317.

Bernal, J. P., Esat, T. M., McCulloch, M. T., and Mortimer, G. E. (2002) Strategies for the determination of the isotopic composition of natural uranium (Goldschmidt 2002, abstract), *Geochimica Et Cosmochimica Acta* **66**, A72.

Blackwelder, B. W., Pilkey, O. H., and Howard, J. D. (1979) Late Wisconsinian Sea Levels on the Southeast US Atlantic Shelf Based on In-Place Shoreline Indicators, *Science* **204**, 618-620.

Blanchon, P., and Eisenhauer, A. (2001) Multi-stage reef development on Barbados during the Last Interglaciation, *Quaternary Science Reviews* **20**, 1903-1112.

Bloom, A. L., Broecker, W. S., Chappell, J., Matthews, R. K., and Mesolella, K. J. (1974) Quaternary Sea Level Fluctuations on a Tectonic Coast: New Th-230/U-234 Dates from the Huon Peninsula, New Guinea, *Quaternary Research* **4**, 185-205.

Bloom, A. L., and Yonekura, N. (1985) Coastal terraces generated by sea level change and tectonic uplift. In: *Models in Geomorphology.* (M. J. Woldenberg, Ed.) pp.139-154. Allen and Unwin, Winchester, Mass.

Bloom, A. L., and Yonekura, N. (1990) Graphic Analysis of Dislocated Quaternary Shorelines. In: *Sea Level Change.* (G. S. C. U.S. National Research Council, Ed.) pp.104-115. National Academic Press, Washington D.C.

Bond, G., Broecker, W., Johnsen, S., McManus, J., Labeyrie, L., Jouzel, J., and Bonani, G. (1993) Correlations between Climate Records from North-Atlantic Sediments and Greenland Ice, *Nature* **365**, 143-147.

Bond, G., Showers, W., Cheseby, M., Lotti, R., Almasi, P., deMenocal, P., Priore, P., Cullen, H., Hajdas, I., and Bonani, G. (1997) A pervasive millennial-scale cycle in North Atlantic Holocene and glacial climates, *Science* **278**, 1257-1266.

Bond, G. C., and Lotti, R. (1995) Iceberg Discharges into the North-Atlantic on Millennial Time Scales During the Last Glaciation, *Science* **267**, 1005-1010.

Broecker, W. S., and Hemming, S. (2001) Climate Swings Come into Focus, *Science* **294**, 2308-2039.

Broecker, W. S., Thurber, D. L., Goddard, J., Ku, T.-L., Matthews, R. K., and Mesolella, K. J. (1968) Milankovitch Hypothesis Supported by Precise Dating of Coral Reefs and Deep-Sea Sediments, *Science* **159**, 297-300.

Cane, M. A. (1998) Climate Change: A role for the Tropical Pacific, *Science* **282**, 59-61.

Cathles, L. M. (1975) *The Viscosity of the Earth's Mantle*, Princeton University Press, New Jersey,

Chapman, M. R., and Shackleton, N. J. (1998) Millenial-scale fluctuations in North Atlantic heat flux during the last 150,000 years, *Earth and Planetary Science Letters* **159**, 57-70.

Chapman, M. R., and Shackleton, N. J. (1999) Global ice-volume fluctuations, North Atlantic ice-rafting events, and deep-ocean circulation changes between 130 and 70 ka, *Geology* **27**, 795-798.

Chapman, M. R., Shackleton, N. J., and Duplessy, J. C. (2000) Sea surface temperature variability during the last glacial- interglacial cycle: assessing the magnitude and pattern of climate change in the North Atlantic, *Palaeogeography Palaeoclimatology Palaeoecology* **157**, 1-25.

Chappell, J. (1974) Geology of Coral Terraces, Huon Peninsula, New Guinea: A study of Quaternary Tectonic Movements and Sea-Level Changes, *Geological Society of America* **85**, 553-570.

Chappell, J. (1983) A revised Sea-level Record for the Last 300,000 Years from Papua New Guinea, *Search* **14**, 99-101.

Chappell, J. (2002) Sea level changes forced ice breakouts in the Last Glacial cycle: new results from coral terraces, *Quaternary Science Reviews* **21**, 1229-1240.

Chappell, J., Omura, A., Esat, T., McCulloch, M., Pandolfi, J., Ota, Y., and Pillans, B. (1996a) Reconciliation of late Quaternary sea levels derived from coral terraces at Huon Peninsula with deep sea oxygen isotope records, *Earth and Planetary Science Letters* **141**, 227-236.

Chappell, J., Ota, Y., and Berryman, K. (1996b) Late Quaternary coseismic uplift of Huon Peninsula, Papua New Guinea, *Quaternary Science Reviews* **15**, 7-22.

Chappell, J., and Polach, H. (1991) Post-glacial sea-level rise from a coral record at Huon Peninsula, Papua New Guinea, *Nature* **349**, 147-149.

Chappell, J., and Shackleton, N. J. (1986) Oxygen isotopes and sea level, *Nature* **324**, 137-140.

Chen, J. H., Curran, H. A., White, B., and Wasserburg, G. J. (1991) Precise chronology of the last interglacial period: U-234-Th-230 data from fossil coral reefs in the Bahamas, *Geological Society of America Bulletin* **103**, 82-97.

Chen, J. H., Edwards, R. L., and Wasserburg, G. J. (1986) 238U, 234U and 232U in sea water, *Earth and Planetary Science Letters* **80**, 241-251.

Cheng, H., Edwards, R. L., Hoff, J., Gallup, C. D., Richards, D. A., and Asmerom, Y. (2000) The half-lives of uranium-234 and thorium-230, *Chemical Geology* **169**, 17-33.

Cherdynstev, V. V., Kazachevski, I. V., and Kuz'mina, Y. A. (1965) Age of Pleistocene carbonates determined from isotopes of Thorium and Uranium, *Geochemistry International* **2**, 749-756.

Clark, P. U., Clague, J. J., Curry, B. B., Dreimanis, A., Hicock, S. R., Miller, G. H., Berger, G. W., Eyles, N., Lamothe, M., Miller, B. B., Mott, R. J., Oldale, R. N., Stea, R. R., Szabo, J. P., Thorleifson, L. H., and Vincent, J. S. (1993) Initiation and Development of the Laurentide and Cordilleran Ice Sheets Following the Last Interglaciation, *Quaternary Science Reviews* **12**, 79-114.

Clark, P. U., Marshall, S. J., Clarke, G. K. C., Hostetler, S. W., Licciardi, J. M., and Teller, J. T. (2001) Freshwater forcing of abrupt climate change during the last glaciation, *Science* **293**, 283-287.

Clark, P. U., Mitrovica, J. X., Milne, G. A., and Tamisiea, M. E. (2002a) Sea-level fingerprinting as a direct test for the source of global meltwater pulse IA, *Science* **295**, 2438-2441.

Clark, P. U., Pisias, N. G., Stocker, T. F., and Weaver, A. J. (2002b) The role of the thermohaline circulation in abrupt climate change, *Nature* **415**, 863-869.

Cochran, J. K. (1982) The oceanic chemistry of the U- and Th-series nuclides. In: *Uranium Series Disequilibrium: Applications to Environmental Problems.* (M. Ivanovich, and R. S. Harmon, Eds.), pp.384-430. Clarendon, Oxford.

Cochran, J. K., Carey, A. E., Sholkovitz, E. R., and Surprenant, L. D. (1986) The geochemistry of uranium and thorium in coastal marine sediments and sediment pore waters, *Geochimica et Cosmochimica Acta* **50**, 663-680.

Cronin, T. M., Szabo, B. J., Ager, T. A., Hazel, J. E., and Owens, J. P. (1981) Quaternary Climates and Sea Levels of the U.S. Atlantic Coastal Plain, *Science* **211**, 233-240.

Dansgaard, W., Johnsen, S. J., Clausen, H. B., Dahljensen, D., Gundestrup, N. S., Hammer, C. U., Hvidberg, C. S., Steffensen, J. P., Sveinbjornsdottir, A. E., Jouzel, J., and Bond, G. (1993) Evidence for General Instability of Past Climate from a 250-Kyr Ice-Core Record, *Nature* **364**, 218-220.

De Bievre, P., Lauer, K. F., LeDuigon, Y., Moret, H., Muschenborn, G., Spaepen, J., Spernol, A., Vaninbroukx, R., and Verdingh, V. (1971) The half-life of 234-U. In: *Proceedings of the International Conference on Chemical and Nuclear Data, Measurements and Applications, Canterbury.* (M. L. Hurrell, Ed.) pp.221-225. Institute of Civil Engineers, London.

Deer, W. A., Howie, R. A., and Zussman, J. (1967) *Rock Forming Minerals*, Longmans, Green and Co Ltd, London.

Denton, G. H., and Hughes T.J. (eds) (1981) *The Last Great Ice Sheets*, Wiley, New York.

Dia, A. N., Cohen, A. S., O'Nions, R. K., and Shackleton, N. J. (1992) Seawater Sr isotope variation over the past 300 kyr and influence of global climate cycles, *Nature* **356**, 786-788.

Dodge, R. E., Faribanks, R. G., Benninger, L. K., and Maurrasse, F. (1983) Pleistocene sea levels from Raised Coral Reefs of Haiti, *Science* **219**, 1423-1425.

Edwards, R. L., Chen, J. H., Ku, T. L., and Wasserburg, G. J. (1987a) Precise Timing of the Last Interglacial Period from Mass Spectrometric Determination of Thorium-230 in Corals, *Science* **236**, 1547-1553.

Edwards, R. L., Chen, J. H., and Wasserburg, G. J. (1987b) ^{238}U-^{234}U-^{230}Th-^{232}Th systematics and the precise measurement of time over the past 500,000 years, *Earth and Planetary Science Letters* **81**, 175-192.

Edwards, R. L., Cheng, H., Murrell, M. T., and Goldstein, S. J. (1997) Protactinium -231 Dating of Carbonates by Thermal Ionization Mass Spectrometry: Implication for Quaternary Climate Change, *Science* **276**, 782-786.

Eisenhauer, A., Wasserburg, G. J., Chen, J. H., Bonani, G., Collins, L. B., Zhu, Z. R., and Wyrwoll, K. H. (1993) Holocene Sea-Level Determination Relative to the Australian Continent - U/Th (Tims) and C-14 (Ams) Dating of Coral Cores from the Abrolhos Islands, *Earth and Planetary Science Letters* **114**, 529-547.

Elliot, M., Labeyrie, L., Bond, G., Cortijo, E., Turon, J. L., Tisnerat, N., and Duplessy, J. C. (1998) Millennial-scale iceberg discharges in the Irminger Basin during the last glacial period: Relationship with the Heinrich events and environmental settings, *Paleoceanography* **13**, 433-446.

Elliot, M., Labeyrie, L., Dokken, T., and Manthe, S. (2001) Coherent patterns of ice-rafted debris deposits in the Nordic regions during the last glacial (10-60 ka), *Earth and Planetary Science Letters* **194**, 151-163.

Esat, T. M. (1995) Charge collection thermal ion mass spectrometry of thorium, *International Journal of Mass Spectrometry and Ion Processes* **148**, 159-170.

Esat, T. M., McCulloch, M. T., Chappell, J., Pillans, B., and Omura, A. (1999) Rapid Fluctuations in Sea Level Recorded at Huon Peninsula During the Penultimate Deglaciation, *Science* **283**, 197-201.

Esat, T. M., and Yokoyama, Y. (1999) Rapid fluctuations in the uranium isotope composition of the oceans (abstract), *EOS Trans. AGU (Fall Meeting Suppl.)* **80**, 581.

Fairbanks, R. G. (1989) A 17,000-year glacio-eustatic sea level record: influence of glacial melting rates on the Younger Dryas event and deep-ocean circulation, *Nature* **342**, 637-642.

Fairbridge, R. W. (1960) The changing level of the sea, *Scientific American* **202**, 70-79.

Farrell, W. E., and Clark, J. A. (1976) On postglacial sea level, *Geophysical Journal of the Royal Astronomical Society* **46**, 79-116.

Faure, G. (1986) *The U-series disequilibrium methods of dating*, John Wiley and Sons, New York.

Finkelstein, K., and Kearney, M. S. (1988) Late Pleistocene barrier-island sequence along the southern Delmarva Peninsula: Implications for middle Wisconsin sea levels, *Geology* **16**, 41-45.

Fleischer, R. L. (1988) Alph-recoil damage: Relation to isotopic disequilibrium and leaching of radionuclides, *Geochimica et Cosmochimica Acta* **52**, 1459-1466.

Fleming, K., Johnston, P., Zwartz, D., Yokoyama, Y., Lambeck, K., and Chappell, J. (1998) Refining the Eustatic sea-level curve since the Last Glacial Maximum using far- and interediate-field sites, *Earth and Planetary Science Letters* **163**,

Fruijtier, C., Elliot, T., and Schlager, W. (2000) Mass-spectrometric 234U-230Th ages from the Key Largo Formation, Florida Keys, United States: Constraints on diagenetic age disturbances, *Geological Society of America Bulletin* **112**, 267-277.

Gallup, C. D., Cheng, H., Taylor, F. W., and Edwards, R. L. (2002) Direct determination of the timing of sea level change during termination II, *Science* **295**, 310-313.

Gallup, C. D., Edwards, R. L., and Johnson, R. G. (1994) The Timing of High Sea Levels Over the Past 200,000 Years, *Science* **263**, 796-800.

Grand, S. P. (1994) Mantle Shear Structure beneath the America and Surrounding Oceans, *Journal of Geophysical Research-Solid Earth* **99**, 11591-11621.

Grootes, P. M., and Stuiver, M. (1997) Oxygen 18/16 variability in Greenland snow and ice with 10(-3)- to 10(5)-year time resolution, *Journal of Geophysical Research-Oceans* **102**, 26455-26470.

Grootes, P. M., Stulver, M., White, J. W. C., Johnsen, S., and Jouzel, J. (1993) Comparison of oxygen isotope records from the GISP2 and GRIP Greenland ice cores, *Nature* **366**, 552- 554.

Hamelin, B., Bard, E., Zindler, A., and Fairbanks, R. G. (1991) U-234/U-238 mass spectrometry of corals: How accurate is the U-Th age of the last interglacial period?, *Earth and Planetary Science Letters* **106**, 169-180.

Harmon, R., Mitterer, R. M., Kriausakul, N., Land, L., Schwarcz, H. P., Garrett, P., Larson, G. J., Vacher, H. L., and Rowe, M. (1983) U-series and Amino-acid racemization geochronology of Bermuda: Implications for eustatic sea-level fluctuation over the past 250,00 years, *Palaeogeography, Palaeoclimatology, Palaeoecology* **44**, 41-70.

Harmon, R. S., Schwarcz, H. P., and Ford, D. C. (1978) Late Pleistocene Sea Level History of Bermuda, *Quaternary Research* **9**, 205-218.

Hays, J. D., Imbrie, J., and Shackleton, N. J. (1976) Variations in the Earth's Orbit: Pacemaker of the Ice Ages, *Science* **194**, 1121-1132.

Hearty, P. J., and Kaufman, D. S. (2000) Whole-Rock Aminostratigraphy and Quaternary Sea-Level History of the Bahamas, *Quaternary Research* **54**, 163-173.

Hearty, P. J., and Kindler, P. (1995) Sea-Level Highstand Chronology from Stable Carbonate Platforms (Bermuda and the Bahamas), *Journal of Coastal Research* **11**, 675-689.

Hearty, P. J., and Kindler, P. (1997) The stratigraphy and surficial geology of New Providence and surrounding islands, Bahamas, *Journal of Coastal Research* **13**, 798-812.

Hearty, P. L., and Vacher, H. L. (1994) Quaternary Stratigraphy of Bermuda: A high resolution pre-Sangamionian rock record, *Quaternary Science Reviews* **13**, 685-697.

Heinrich, H. (1988) Origin and Consequences of Cyclic Ice Rafting in the Northeast Atlantic Ocean during the Past 130,000 Years, *Quaternary Research* **29**, 142-152.

Henderson, G. M. (2002) Seawater (U-234/U-238) during the last 800 thousand years, *Earth and Planetary Science Letters* **199**, 97-110.

Henderson, G. M., Cohen, A. S., and O'Nions, R. K. (1993) U-234/U-238 ratios and Th230 ages for Hateruma Atoll corals: implications for coral diagenesis and seawater U-234/U-238 ratios, *Earth and Planetary Science Letters* **115**, 65-73.

Henderson, G. M., and Slowey, N. C. (2000) Evidence from U-Th dating against Northern Hemisphere forcing of the penultimate degalciation, *Nature* **404**, 61-66.

Imbrie, J., Berger, A., Boyle, E. A., Clemens, S. C., Duffy, A., Howard, W. R., Kukla, G., Kutzbach, J., Martinson, D. G., MacIntyre, A., Mix, A. C., Molfino, B., Morley, J. J., Peterson, L. C., Pisias, N. G., Prell, W. L., Raymo, M. E., Shackleton, N. J., and Toggweiler, J. R. (1993) On the structure and origin of major glaciation cycles 2. The 100,000-Year cycle, *Paleoceanography* **8**, 699-735.

Imbrie, J., Hays, J. D., Martinson, D. G., McIntyre, A., and Mix, A. C. (1984) The orbital theory of Pleistocene climate: support from a revised chronology of the marine $\delta^{18}O$ record. In: *Milankovitch and climate.* (A. L. Berger, Ed.) pp.269-305. D. Reidel Publishing Company, Holland.

James, P. N. (1974) Diagenesis of scleractinian corals in the subaerial vadose environment, *Journal of Paleontology* **48**, 785.

Johnson, R. G., and McClure, B. T. (1976) A model for Northern Hemisphere Continental Ice Sheet Variation, *Quaternary Research* **6**, 325-353.

Johnston, P. (1993) The effect of spatially non-uniform water loads on the prediction of sea-level change, *Geophysical Journal International* **114**, 615-634.

Johnston, P., and Lambeck, K. (1999) Postglacial rebound and sea level contributions to changes in the geoid and the Earth's rotation axis, *Geophysical Journal International* **136**, 537-558.

Johnston, P. J. (1994) *Deformation of the Earth by surface loads*, thesis, Australian National University.

Jordan, T. H. (1975) The Present Day Motions of the Caribbean Plate, *Journal of Geophysical Research* **80**, 4433-4439.

Kaufman, G., and Lambeck, K. (2000) Mantle dynamics, postglacial rebound and the radial viscosity profile, *Physics of the Earth and Planetary Interiors* **121**, 301-324.

Kaufman, G., and Lambeck, K. (2002) Glacial isostatic adjustment and the radial viscosity profile from inverse modelling, *Journal of Geophysical Research* **107**, 2280.

Kindler, P., and Hearty, P. J. (1996) Carbonate petrography as an indicator of climate and sea-level changes: new data from Bahamiam Quaternary units, *Sedimentology* **43**, 381-399.

Kleman, J., Fastook, J., and Stroeven, A. P. (2002) Geologically and geomorphologically constrained numerical model of Laurentide Ice Sheet inception and build-up, *Quaternary International* **95-96**, 87-98.

Klinkhammer, G. P., and Palmer, M. R. (1991) Uranium in the oceans: Where it goes and why, *Geochimica et Cosmochimica Acta* **55**, 1799-1806.

Kolodny, Y., and Kaplan, I. R. (1970) Uranium isotopes in sea floor phosphorites, *Geochimica et Cosmochimica Acta* **34**, 3-24.

Ku, T.-L. (1965) An evaluation of the U234/U238 Method as a Tool of Dating Pelagic Sediments, *Journal of Geophysical Research* **70**, 3457-3474.

Ku, T.-L., Ivanovich, M., and Luo, S. (1990) U-series Dating of Last Interglacial High Sea Stands: Barbados Revisited, *Quaternary Research* **33**, 129-147.

Ku, T.-L., Knauss, K. G., and Mathieu, G. G. (1977) Uranium in open ocean: concentration and isotopic composition, *Deep-Sea Research* **24**, 1005-1017.

Ku, T.-L., Luo, S., Leslie, B. W., and Hammond, D. E. (1992) Decay-series Disequilibria applied to the study of rock-water interactions and geothermal systems. In: *Uranium-series Disequilibrium.* (M. Ivanovich, and R. S. Harmon, Eds.), pp.631-639. Oxford University Press, New York.

Lambeck, K. (1988) *Geophysical Geodesy: The Slow Deformations of the Earth*, Oxford University Press, Oxford.

Lambeck, K., and Chappell, J. (2001) Sea level change through the last glacial cycle, *Science* **292**, 679-686.

Lambeck, K., Esat, T. M., and Potter, E.-K. (2002a) Links between climate and sea levels for the past three million years, *Nature* **419**, 199-206.

Lambeck, K., Johnston, P., Smither, C., and Nakada, M. (1996) Glacial rebound of the British Isles - III. Constraints on mantle viscosity, *Geophysical Journal International* **125**, 340-354.

Lambeck, K., and Nakada, M. (1991) Sea-Level Constraints, *Nature* **350**, 115-116.

Lambeck, K., and Nakada, M. (1992) Constraints on the age and duration of tha last interglacial period and on sea-level variations, *Nature* **357**, 125-128.

Lambeck, K., Purcell, A., Johnston, P., Nakada, M., and Yokoyama, Y. (2002b) Water-load definition in the glacio-hydro-isostatic sea-level equation, *Quaternary Science Reviews* **(in press)**,

Lambeck, K., Smither, C., and Johnston, P. (1998) Sea-level change, glacial rebound and mantle viscosity for northern Europe, *Geophysical Journal International* **134**, 102-144.

Lambeck, K., Yokoyama, Y., Johnston, P., and Purcell, A. (2000) Global ice volumes at the last Glacial Maximum., *Earth and Planetary Science Letters* **181**, 513-527.

Lambeck, K., Yokoyama, Y., and Purcell, T. (2002c) Into and out of the Last Glacial Maximum: sea-level change during Oxygen Isotope Stages 3 and 2, *Quaternary Science Reviews* **21**, 343-360.

Lazar, B., Stein, M., Enmar, R., Bar-Matthews, M., and Halicz, L. (2002) The effect of diagenesis on the U system in live and Holocene corals from the Red Sea (abstract), *Geochimica et Cosmochimica Acta* **66 S1**, A436.

Licciardi, J. M., Clark, P. U., Jenson, J. W., and Macayeal, D. R. (1998) Deglaciation of a soft-bedded Laurentide Ice Sheet, *Quaternary Science Reviews* **17**, 427-448.

Linsley, B. K. (1996) Oxygen-isotope record of sea level and climate variations in the Sulu Sea over the past 150,000 years, *Nature* **380**, 234-237.

Longman, I. M. (1962) A Green's function for determining the deformation of the Earth under surface mass loads 1. Theory, *Journal of Geophysical Research* **67**, 845-850.

Lounsbury, M., and Durham, R. W. (1971) The alpha-half-life of ^{234}U. In: *Proc. Int. Conf. Chem. Nucl. Data, Measurements and Applications, Canterbury.* (M. L. Hurrell, Ed.) pp.215-219. Institute of Civil Engineers, London.

Ludwig, K. R., Muhs, D. R., Simmons, K. R., Halley, R. B., and Shinn, E. A. (1996) Sea-level records at ~80ka from tectonically stable platforms: Florida and Bermuda, *Geology* **24**, 211-214.

Ludwig, K. R., Simmons, K. R., Szabo, B. J., Winograd, I. J., Landwehr, J. M., Riggs, A. C., and Hoffman, R. J. (1992) Mass-Spectrometric Th-230-U-234-U-238 Dating of the Devils-Hole Calcite Vein, *Science* **258**, 284-287.

Lundberg, J., and Ford, D. C. (1994) Late Pleistocene sea level change in the Bahamas from mass spectrometric U-series dating of submerged speleothem, *Quaternary Science Reviews* **13**, 1-14.

Macayeal, D. R. (1993a) Binge/Purge Oscillations of the Laurentide Ice-Sheet as a Cause of the North-Atlantics Heinrich Events, *Paleoceanography* **8**, 775-784.

Macayeal, D. R. (1993b) A Low-Order Model of the Heinrich Event Cycle, *Paleoceanography* **8**, 767-773.

Mann, P., Taylor, F. W., Edwards, R. L., and Ku, T. L. (1995) Actively Evolving Microplate Formation by Oblique Collision and Sideways Motion Along Strike-Slip Faults - an Example from the Northeastern Caribbean Plate Margin, *Tectonophysics* **246**, 1-7.

Marshall, J. F. (1983) Lithology and Diagenesis of the Carbonate Foundations of Modern Reefs in the Southern Great Barrier Reef, *Journal of Australian Geology and Geophysics* **8**, 253-265.

Martinson, D. G., Pisias, N. G., Hays, J. D., Imbrie, J., Moore, J., T.C., and Shackleton, N. J. (1987) Age Dating and the Orbital Theory of the Ice ages: Development of a High-Resolution 0 to 300,000-Year Chronostratigraphy, *Quaternary Research* **27**, 1-29.

Matthews, R. K. (1973) Relative elevation of late Pleistocene high sea-level stands: Barbados uplift rates and their implications, *Quaternary Research* **3**, 147-153.

McConnaughey, T. (1989) ^{13}C and ^{18}O isotopic disequilibrium in biological carbonates: I Patterns, *Geochimica et Cosmochimica Acta* **55**, 151-162.

McManus, J. F., Bond, G. C., Broecker, W. S., Johnsen, S., Labeyrie, L., and Higgins, S. (1994) High-Resolution Climate Records from the North-Atlantic During the Last Interglacial, *Nature* **371**, 326-329.

Meadows, J. W., Armani, R. J., Callis, E. L., and Essling, A. M. (1980) Half-life life of ^{230}Th, *Physical Review C* **22**, 750-754.

Meese, D. A., Alley, R. B., Fiacco, R. J., Germani, M. S., Gow, A. J., Grootes, P. M., Illing, M., Mayewski, P. A., Morrison, M. C., Ram, M. K., Taylor, K. C., Yang, Q., and Zielinski, G. A. (1994) *Preliminary depth-agescale of the GISP2 ice core. Special CRREL Report.*

members, C. p. (1976) The surface of the ice age Earth, *Science* **191**, 1131-1137.

Mesolella, K. J. (1967) Zonation of the Uplifted Pliestocene Coral Reefs on Barbados, West Indies, *Science* **196**, 638-640.

Mesolella, K. J., Matthews, R. K., Broecker, D., and Thurber, L. (1969) The Astronomical Theory of Climatic Change: Barbados data, *Journal of Geology* **77**, 250-274.

Milankovitch, M. (1941) Kanon der Erdbestrahlung (Canon of insolation and the ice age problem, Englich translation by Israel Program for Scientific Translations, Jerusalaem, 1969), *R. Serbian Acad. Special Publ.* **132**,

Milliman, J. D., and Emery, K. O. (1968) Sea Levels during the Past 35,000 years, *Science* **162**, 1121-1123.

Min, G. R., Edwards, R. L., Taylor, F. W., Recy, J., Gallup, C. D., and Beck, J. W. (1995) Annual cycles of U/Ca in coral skeletons and U/Ca thermometry, *Geochimica et Cosmochimica Acta* **59**, 2025-2042.

Mitrovica, J. X., and Peltier , W. R. (1991) On postglacial geoid subsidence over the equatorial oceans, *Journal of Geophysical Research* **96**, 20053-20071.

Morford, J. L., and Emerson, S. (1999) The geochemistry of redox sensitive trace metals in sediments, *Geochimica et Cosmochimica Acta* **63**, 1735-1750.

Muhs, D. R., Simmons, K. R., and Steinke, B. (2002) Timing and warmth of the Last Interglacial period: new U-series evidence from Hawaii and Bermuda and a new fossil compilation for North America, *Quaternary Science Reviews* **21**, 1355-1383.

Muller, R. A., and MacDonald, G. J. (1995) Glacial cycles and orbital inclination, *Nature* **377**, 107-108.

Nakada, M., and Lambeck, K. (1988) The melting history of the late Pleistocene Antarctic ice sheet, *Nature* **333**, 36-40.

Nakada, M., and Lambeck, K. (1991) Late Pleistocene and Holocene Sea-Level Change: Evidence for Lateral Mantle Viscosity Structure? In: *Glacial Isostasy, Sea-level and Mantle Rheology.* (R. Sabadini, K. Lambeck, and E. Boschi, Eds.), pp.79-94. Kluwer Academic Publishing, Dordrecht.

O'Brien, G. W., Veeh, H. H., Milnes, A. R., and Cullen, D. J. (1987) Sea-floor weathering of phosphate nodules off East Australia: Its effect on uranium oxidation state and isotopic composition, *Geochimica et Cosmochimica Acta* **51**, 2051-2064.

Okuno, J., and Nakada, M. (2001) Effects of water load on geophysical signals due to glacial rebound and implications for mantle viscosity, *Earth Planets and Space* **53**, 1121-1135.

Omura, A., Chappell, J., Bloom, A. L., Pillans, B., McCulloch, M. T., Esat, T. M., Sasaki, K., and Kawada, Y. (1994) Alpha-spectrometric 230Th/234U dating of Pleistocene corals. In: *Study on Coral Reef Terraces of the Huon Peninsula, Papua New Guinea.* (Y. Ota, Ed.) pp.95-109. Yokohama.

Opdyke, B. N., and Walker, J. C. G. (1992) Return of the coral reef hypothesis: Basin to shelf partitioning of $CaCO_3$ and its effect on atmospheric CO_2, *Geology* **20**, 733-736.

Oppo, D., and Lehman, S. J. (1995) Suborbital timescale variability of North Atlantic Deep Water during the past 200,000 years, *Paleoceanography* **10**, 901-910.

Oppo, D. W., Keigwin, L. D., McManus, J. F., and Cullen, J. L. (2001) Persistant suborbital climate variability in marine isotope stage 5 and Termination II, *Paleoceanography* **16**, 280-292.

Osmond, J. K., and Ivanovich, M. (1992) Uranium-series Mobilisation and Surface Hydrology. In: *Uranium-series Disequilibrium.* (M. Ivanovich, and R. S. Harmon, Eds.), pp.259-289. Oxford University Press, New York.

Ota, Y., and Chappell, J. (1996) Late Quaternary coseismic uplift events on the Huon Peninsula, Papua New Guinea, deduced from coral terrace data, *Journal of Geophysical Research* **101**, 6071-6082.

Ota, Y., Chappell, J., Kelley, R., Yonekura, N., Matsumoto, E., Nishimura, T., and Head, J. (1993) Holocene Coral-Reef Terraces and Coseismic Uplift of Huon Peninsula, Papua-New-Guinea, *Quaternary Research* **40**, 177-188.

Paine, J. G. (1993) Subsidence of the Texas Coast - Inferences from Historical and Late Pleistocene Sea Levels, *Tectonophysics* **222**, 445-458.

Palmer, M. R., and Edmond, J. M. (1993) Uranium in river water, *Geochimica et Cosmochimica Acta* **57**, 4947-4955.

Pandolfi, J., and Chappell, J. (1994) Stratigraphy and relative sea level changes at the Kanzarua and Bobongara sections, Huon Peninsula, Papua New Guinea. In: *Study on Coral Reef Terraces of the Huon Peninsula, Papua New Guinea.* (Y. Ota, Ed.) pp.119-139. Yokohama.

Peltier, W. R. (1974) The impulse response of a Maxwell Earth., *Reviews of Geophysics* **12**, 649-669.

Peltier, W. R. (1985) The LAGEOS constraint on deep mantle viscosity: Results from a new normal mode method for the inversion of viscoelastic spectra., *Journal of Geophysical Research* **90**, 9411-9421.

Peltier, W. R. (1991) The ICE-3G model of late Pleistocene deglaciation: construction, verification and applications. In: *Glacial isostasy, sea-level and mantle rheology.* (R. Sabadini, K. Lambeck, and E. Boschi, Eds.), pp.95-119. NATO ASI Series-Vol 334. Kluwer Academic Publ., Dordrecht.

Peltier, W. R., and Andrews, J. T. (1976) Glacial-isostatic adjustment - 1. The forward problem, *Geophysical Journal of the Royal Astronomical Society* **46**, 605-646.

Peteet, D. M. (1993) Global Younger Dryas, a special issue of, *Quaternary Science Reviews* **12**,

Pisias, N. G., Martinson, D. G., Moore, T. C., Shackleton, N. J., Prell, W., Hays, J., and Boden, G. (1984) High Resolution Stratigraphic Correlation of Benthic Oxygen Isotopic Records Spanning the Last 300,000 years, *Marine Geology* **56**, 119-136.

Polach, H. A., Chappell, J. M. A., and Lovering, F. (1969) ANU radiocarbon date list III, *Radiocarbon* **11**, 245-252.

Prell, W. L., Imbrie, J., Martinson, D. G., Morley, J. J., Pisias, N. G., Shackleton, N. J., and Streeter, H. F. (1986) Graphic Correlation of Oxygen Isotope Stratigraphy Application to the Late Quaternary, *Paleoceanography* **1**, 137-162.

Radtke, U., and Grun, R. (1990) Revised Reconstruction of Middle and Late Pleistocene Sea-Level Changes Based on New Chronologic and Morphologic Investigations in Barbados, West Indies, *Journal of Coastal Research* **6**, 699-708.

Radtke, U., Grun, R., and Schwarcz, H. P. (1988) Electron Spin Resonance Dating of the Pleistocene Coral Reef Tracts of Barbados, *Quaternary Research* **29**, 197-215.

Richards, D. A., Smart, P. L., and Edwards, R. L. (1994) Maximum sea levels for the last glacial period from U-series ages of submerged speleothems, *Nature* **367**, 357-360.

Robinson, L. F., Henderson, G. M., and Slowey, N. C. (2002) U-Th dating of marine isotope stage 7 in Bahamas slope sediments, *Earth and Planetary Science Letters* **196**, 175-187.

Rodriguez, A. B., Anderson, J. B., Banfield, L. A., Taviani, M., Abdulah, K., and Snow, J. N. (2000) Identification of a -15 m middle Wisconsin shorelines on the Texas inner continental shelf, *Palaeogeography, Palaeoclimatology, Palaeoecology* **158**, 25-43.

Romanowicz, B. (1998) Attenuation tomography of the earth's mantle: A review of current status, *Pure and Applied Geophysics* **153**, 257-272.

Rosenthal, Y., Boyle, E. A., Labeyrie, L., and Oppo, D. (1995) Glacial enrichments of authigenic Cd and U in Subantarctic sediments: A climate control on the elements' ocean budget, *Paleoceanography* **10**, 395-413.

Russell, A. D., Emerson, S., Mix, A. C., and Peterson, L. C. (1996) The use of foraminiferal uranium/calcium ratios as an indicator of changes in seawater uranium content, *Paleoceanography* **11**, 649-663.

Schaffer, J. A., Cerveny, R.S., Dorn, R.I. (1996) Radiation windows as indicators of an astronomical influence on Devil's Hole chronology, *Geology* **24**, 1017-1020.

Schellmann, G., and Radtke, U. (2001) Neue Ergenbnisse zur Verbreitung und Altersstellung gehobener Korallenriffterrassen im Suden von Barbados, *Bamberger Geographische Schriften* **20**, 201-244.

Schellmann, G., and Radtke, U. (2002) *The coral reef terraces of Barbados - a guide*, University of Bamberg, University of Cologne,

Schrag, D. P., Adkins, J. F., McIntyre, K., Alexander, J. L., Hodell, D. A., Charles, C. D., and McManus, J. F. (2002) The oxygen isotopic composition of seawater during the Last Glacial Maximum, *Quaternary Science Reviews* **21**, 331-342.

Schrag, D. P., and DePaolo, D. J. (1993) Determination of dO-18 of seawater in the deep ocean during the last glacial maximum, *Paleoceanography* **8**, 1-6.

Shackleton, N. J. (1987) Oxygen isotopes, ice volume and sea level, *Quaternary Science Reviews* **6**, 183-190.

Shackleton, N. J., and Opdyke, N. D. (1973) Oxygen Isotope and Palaeomagnetic Stratigraphy of Equatorial Pacific Core V28-238: Oxygen Isotope Temperatures and Ice Volumes on a 10^5 Year and 10^6 Year Scale, *Quaternary Research* **3**, 39-55.

Shen, G. T., and Dunbar, R. B. (1995) Environmental controls on uranium in reef corals, *Geochimica et Cosmochimica Acta* **59**, 2009-2024.

Smart, P. L., Richards, D. A., and Edwards, R. L. (1998) Uranium-series ages of speleothems from South Andros, Bahamas: Implications for Quaternary sea-level history and paleoclimate, *Carst and Cave Science* **25**, 67-74.

Smith, J. E., Schwarz, H. P., Risk, M. J., McConnaughey, T. A., and Keller, N. (2000) Paleotemperatures From Deep-Sea Corals: Overcoming 'Vital Effects', *Palaios* **15**, 25-32.

Stein, M., Wasserburg, G. J., Aharon, P., Chen, J. H., Zhu, Z. R., Bloom, A., and Chappell, J. (1993) TIMS U-series dating and stable isotopes of the last interglacial event in Papua New Guinea, *Geochimica et Cosmochimica* **57**, 2541-2554.

Stirling, C. H. (1996) *High-precision U-series dating of corals from Western Australia: Implications for Last Interglacial sea levels*, thesis, Australian National University.

Stirling, C. H., Esat, T. M., Lambeck, K., and McCulloch, M. T. (1998) Timing and duration of the Last Interglacial: Evidence for a restricted interval of widespread coral reef growth, *Earth and Planetary Science Letters* **160**, 745-762.

Stirling, C. H., Esat, T. M., Lambeck, K., McCulloch, M. T., Blake, S. G., Lee, D. C., and Halliday, A. N. (2001) Orbital forcing of the marine isotope stage 9 interglacial, *Science* **291**, 290-293.

Svendsen, J. I., Astakhov, V. I., Bolshiyanov, D. Y., Demidov, I., Dowdeswell, J. A., Gataullin, V., Hjort, C., Hubberten, H. W., Larsen, E., Mangerud, J., Melles, M., Mller, P., Saarnisto, M., and Siegert, M. J. (1999) Maximum extent of the Eurasian ice sheets in the Barents and Kara Sea region during the Weichselian, *Boreas* **28**, 234-242.

Szabo, B. J. (1985) Uranium-series dating of fossil corals from marine sediments of southeastern United States Atlantic Coastal Plain, *Geological Society of America Bulletin* **96**, 398-406.

Szabo, B. J., Ludwig, K. R., Muhs, D. R., and Simmons, K. R. (1994) Thorium-230 Ages of Corals and Duration of the Last Interglacial Sea-Level High Stand on Oahu, Hawaii, *Science* **266**, 93-96.

Teller, J. T., Leverington, D. W., and Mann, J. D. (2002) Freshwater outbursts to the oceans from glacial Lake Agassiz and their role in climate change during the last deglaciation, *Quaternary Science Reviews* **21**, 879-887.

Thom, B. G. (1973) The dilemma of high interstadial sea levels during the last glaciation, *Progress in Geography* **5**, 167-246.

Thompson, W. G., Speigelman, M. W., Goldstein, S. L., and Speed, R. C. (2002) An open-system model for U-series age determinations of fossil corals, *Earth and Planetary Science Letters* (submitted)

Toscano, M. A., and Lundberg, J. (1999) Submerged Late Pleistocene reefs on tectonically stable S.E. Florida margin: high precision geochronology, stratigraphy, resolution of Substage 5a sea-level elevation, and orbital forcing, *Quaternary Science Reviews* **18**, 753-767.

Tushingham, A. M., and Peltier, W. R. (1991) Ice 3G: a new global model of Late Pleistocene deglaciation based upon geophysical predictions of postglacial sea-level change, *Journal of Geophysical Research* **96**, 4497-4523.

Vacher, H. L., and Hearty, P. (1989) History of stage 5 sea level in Bermuda: Review with the new evidence of a brief rise to present sea level during substage 5a, *Quaternary Science Reviews* **8**, 159-168.

van der Lee, S., and Nolet, G. (1997) Upper mantle S velocity structure of North America, *Journal of Geophysical Research-Solid Earth* **102**, 22815-22838.

Veeh, H. H. (1966) Th-230/U-238 and U234-/U-238 Ages of Pleistocene High Sea Level Stand, *Journal of Geophysical Research* **71**, 3379-3386.

Veeh, H. H., and Chappell, J. (1970) Astronomical Theory of Climatic Change: Support from New Guinea, *Science* **167**, 862-865.

Vollbrecht, R. (1990) Marine and Meteoric Diagenesis of Submarine Pleistocene Carbonates from the Bermuda Carbonate Platform, *Carbonates and Evaporites* **5**, 13-95.

Wellner, R. W., Ashley, G. M., and Sheridan, R. E. (1993) Seismic Stratigraphic Evidence for a Submerged Middle Wisconsin Barrier - Implications for Sea-Level History - Reply, *Geology* **21**, 1053-1053.

Winograd, I. J., Coplen, T. B., Landwehr, J. M., Riggs, A. C., Ludwig, K. R., Szabo, B. J., Kolesar, P. T., and Revesz, K. M. (1992) Continuous 500,000-Year Climate Record from Vein Calcite in Devils-Hole, Nevada, *Science* **258**, 255-260.

Yokoyama, Y. (1999) *Sea-level change in Australasia and the radiocarbon time scale during the last 50,000 years*, thesis, Australian National University.

Yokoyama, Y., De Deckker, P., Lambeck, K., Johnston, P., and Fifield, L. K. (2001a) Sea-level at the Last Glacial Maximum: evidence from northwestern Australia to constrain ice volumes for oxygen isotope stage 2, *Palaeogeography Palaeoclimatology Palaeoecology* **165**, 281-297.

Yokoyama, Y., Esat, T. M., and Lambeck, K. (2001b) Coupled climate and sea-level changes deduced from Huon Peninsula coral terraces of the last ice age, *Earth and Planetary Science Letters* **193**, 579-587.

Yokoyama, Y., Esat, T. M., and Lambeck, K. (2001c) Last Glacial sea-level change deduced from uplifted coral terraces of Huon Peninsula, Papua New Guinea, *Quaternary International* **83-85**, 275-283.

Yokoyama, Y., Esat, T. M., Lambeck, K., and Fifield, L. K. (2000a) Last Ice Age Millenial Scale Climate Changes Recorded in Huon Peninsula Corals, *Radiocarbon* **42**, 383-401.

Yokoyama, Y., Lambeck, K., De Deckker, P., Johnston, P., and Fifield, L. K. (2000b) Timing of the Last Glacial Maximum from observed sea-level minima, *Nature* **406**, 713-716.

Zhu, Z. R., Wyrwoll, K.-H., Collins, L. B., Chen, J. H., Wasserburg, G. J., and Eisenhauer, A. (1993) High-precision U-series dating of Last Interglacial events by mass spectrometry: Houtman Abrolhos Islands, western Australia, *Earth and Planetary Science Letters* **118**, 281-293.

Appendix A

Supplementary Huon Peninsula Information

Reef	Bobongara	Kwambu	Kwangam
VIa	Broad platform with 12m shallow water facies	Sharp cliff – several m of shallow water facies	5m of reef platform shallow water facies and further 10-15m of reef crest framework and bioclastic limestone
VIb	~2m of shallow water facies –coral limestone	Irregular discontinuity between upper unit of shallow water facies and lower unit of porites, faviid heads	Thin, 2-3m platform reef crest facies overlying unit with heads then mixed broken material
Va_{main}	Well developed platform , >6m of shallow water coral limestone. Reef platform – massive A.palifera community	-	-
Va_{outer}	Several metres of shallow water facies	7-8 m of shallow water reef crest facies	7-8 m of shallow water facies
Vb	Sandy limestone cap not well developed in some places (<1m). Va appears at some locn to be an erosional bench in Bobo beds	-	2-3 m of rubbly grainstone
IV	Wide platform – shallow water facies	-	-

Table A.1: Summary of field notes for reefs VIa, VIb, Va_{main}, Va_{outer}, Vb and IV from 2001 field expedition to Huon Peninsula

Sample No.*	XRD	H† (m)	^{238}U (ppm)	^{232}Th (ppb)	$\delta^{234}U_m$‡ (‰)	$^{230}Th/^{238}U_{act}$	Age§ (ka)	$\delta^{234}U_i$¶ ‰
HU13-2	-	9.6	2.82	0.14	105.82± 1.02	0.6999± 0.0009	105.9± 0.3	142.9± 1.3
HU13-6	-	11.6	2.2417	0.19	106.14± 1.07	0.8168± 0.0021	140.5± 0.8	158.1± 1.5
HU13-8	-	10.6	2.37	0.15	103.11± 1.02	0.7903± 0.0010	132.8± 0.4	150.2± 1.4

Table A.2: Huon Peninsula, reef VIb, Kwangam: Isotope Ratios and U-^{230}Th age calculations. See table 3.3 caption in chapter 3 for explanation of symbols.

Author	Reef	Sample #	Age	sigma Age	$\delta^{234}U$	Comment
Stein	VIIb	KIL-5(a-1)	119.5	1.2	150	-
Stein	VIIb	KIL-5(a-2)	117.6	1.2	154	-
Stein	VIIb	KIL-5b	116.4	1.8	154	-
Stein	VIIb	HP-47	118.1	1	159	-
Chappell	VIIb	618a	116	7	-	-
Chappell	VIIb	618b	119	7	-	-
Omura	VIIb	KIL-3	116.4	3	167	-
Stein	VIIa	KAM-A-1	118.7	1.4	168	-
Stein	VIIb	HP-22	135.8	1.9	157	-
Stein	VIIb	HP-23a	134.7	1.3	151	-
Stein	VIIb	HP-23b	131.9	1.2	154	-
Stein	VIIc	SIAL-M-3	134	1.9	169	-
Esat	VIIb	HP-23	136.7	1.6	155	-
Bloom	VII	1347G	142	8	-	-
Chappell	VIIa	616a	140	10	-	-
Chappell	VIIa	616b	133	10	-	-
Omura	VIIa	SIAL-M-1	101.4	2.8	156	-
Omura	VIIc	BWW-D-2	148	4.1	154	-
Omura	VIIc	KWAN-U3	147.1	3.5	146	12 m below VIIc

Table A.3: Summary of Huon Peninsula reef VII U-Th age analyses. References - Stein *et al.* (1993), Chappell *et al.* (1996a), Chappell (1974), Omura *et al.* (1994), Esat *et al.* (1999), Bloom *et al.* (1974)

Author	Reef	Sample #	Age	sigma Age	$\delta^{234}U$	Comment
Bloom	VI	1353A	107	9	-	-
Bloom	VI	1347C	107	6	-	-
Esat	VIa	KWAM-U1	113.2	0.8	143	base VIa
Esat	VIa	KWAM-U2	98.8	0.8	151	5m above VIa base, 12 m below in cave
Esat	VIa	KWAM-U12	106.4	1	144	not in situ, 4.5 m below VIa in gravel bed
Esat	VIa	KANZ-U3	92.1	0.7	150	3 m below overhang @ foot of cave
Esat	VIa	KANZ-U4	112.7	0.8	156	11m below VIa crest
Esat	VIa	NAND-U1	118	0.9	154	-
Omura	VI	SIAL-O-2	107.8	2.6	154	-
Omura	VI	SIAL-Q-1	114.4	3.1	167	-
Omura	VIa	KWAM-10	74.4	1.2	140	U conc too high
Omura	VIa	NUZE-1	110	2.1	131	
Esat	VIb	KWAN-U4	89.5	0.7	139	VIIc, 12 m below or KWAM-4, VA, 4.5 m below
Esat	VIb	KWAN-U5	131.6	1	140	VIIc, 5 m below or KWAM-5, 4.5 m below
Esat	VIb	KWAN-U9	128.1	0.9	146	3 m below VIb
Esat	VIb-AC	AC-U12	115	0.9	146	-
Esat	VIb-AC	AC-U17	107.8	0.8	139	-
Esat	VIb-AC	AC-U18	112.2	1	140	-
Omura	VIb	KWAN-U10	131.7	2.7	155	base VIb
Omura	VIb	KWAN-U11	125.6	2.6	145	base VIb
Omura	VIb	KWAN-U11b	128.5	2.8	146	base VIb

Table A.4: Summary of Huon Peninsula reef VI U-Th age analyses. References in caption to table A.3.

Author	Reef	Sample #	Age	sigma Age	$\delta^{234}U$	Comment
Bloom	V	1347F	61	4	-	-
Bloom	V	1347B	84	4	-	-
Bloom	V	1353E	86	4	-	-
Omura	V	KWA-S-1	93.9	2.3	136	-
Omura	Va	KWAM-4	90.9	1.8	151	4.5 m below crest
Omura	Va	KWAN-U18	67.5	1.1	153	U conc to high, 5m below crest
Omura	Vb	BWW-B-1	93.7	2.3	153	-
Omura	Vb	BWW-C-1	105.5	2.8	150	-

Table A.5: Summary of Huon Peninsula reef V U-Th age analyses. References in caption to table A.3.

Author	Reef	Sample #	Age	sigma Age	$\delta^{234}U$	Comment
Omura	IV	FRT-F-1	72.8	2.2	147	-
Chappell	IV	FRT-F-1	72.8	2.2	147	-
Chappell	IV	SIAL-U2	64.9	1.7	138	-
Chappell	IV	SIAL-U4	69.9	1.1	142	-
Chappell	IV	SIAL-U6	71.9	0.5	150	-

Table A.6: Summary of Huon Peninsula reef IV U-Th age analyses. References in caption to table A.3.

Sea level calculation based on reef VIIa at 128 ka BP and 4±2m

	Reef	reef elevation	sigma elev.	age	sigma age	uplift	sigma uplift	rel sl	sigma
BOBO	VIIa	406	0.5	128	2	3.14	0.05	4.0	2.0
BOBO	VIa	326	0.5	107	4	3.14	0.05	-10.0	13.7
BOBO	VIb	286.8	0.5	100	4	3.14	0.05	-27.3	13.6
BOBO	Va,main	264	0.5	90.6	2	3.14	0.05	-20.5	7.8
BOBO	Va,outer	250	0.5	84	2	3.14	0.05	-13.8	7.7
BOBO	Vb	213.8	0.5	77.8	2	3.14	0.05	-30.5	7.5
BOBO	IV	197	0.5	71.2	2	3.14	0.05	-26.6	7.3
KWAMBU	VIIa	240	3	128	2	1.84	0.04	4.0	2.0
KWAMBU	VIa	173.4	0.5	107	4	1.84	0.04	-23.9	8.6
KWAMBU	VIb	144.3	0.5	100	4	1.84	0.04	-40.1	8.4
KWAMBU	Va,main	127.9	0.5	90.6	2	1.84	0.04	-39.1	5.2
KWAMBU	Va,outer	123.6	0.5	84	2	1.84	0.04	-31.3	5.0
KWAMBU	Vb	-	0.5	77.8	2	1.84	0.04		
KWAMBU	IV	88	0.5	71.2	2	1.84	0.04	-43.3	4.7
KWANG	VIIa	204	3	128	2	1.56	0.04	4.0	2.0
KWANG	VIa	140.8	0.5	107	4	1.56	0.04	-26.4	7.4
KWANG	VIb	120.7	0.5	100	4	1.56	0.04	-35.6	7.3
KWANG	Va,main	101.7	0.5	90.6	2	1.56	0.04	-39.9	4.6
KWANG	Va,outer	100.9	0.5	84	2	1.56	0.04	-30.4	4.5
KWANG	Vb	78.5	0.5	77.8	2	1.56	0.04	-43.1	4.3
KWANG	IV	-	0.5	71.2	2	1.56	0.04		

	Reef	Age	rsl	sigma rsl
SUMMARY	VIIa	128	4.0	2.0
	VIa	107	-20.1	10.3
	VIb	100	-34.3	10.1
	Va,main	90.6	-33.2	6.1
	Va,outer	84	-25.1	5.9
	Vb	77.8	-36.8	6.1
	IV	71.2	-34.9	6.1

Table A.7: Summary of sea level calcuations assuming reef VIIa represents growth at 128 ka BP at a paleo-sea level of 4±2 m above present. This is similar to the calculation of Lambeck and Chappell (2001). The paleo-sea level calculated here for reef Vb is ~37 m below present assuming an age of 77.8 ka. Lambeck and Chappell (2001) assumed the same age but the sea level calculated for this feature alone was based on assuming an age of 118 ka for the last interglacial reef (rather than the 128 ka for the other events). The Lambeck and Chappell (2001) sea level curve was used for the basis of sea level calculations in chapter6, but the sea level associated with this feature is eventually revised in the final preferred ice-equivalent sea level model based on a comparison of the predicted and observed sea levels at a number of locations. Because the rear reef elevations were used for the calculations, no allowance for growth depth was included.

Table A.8: Summary of sea level calcuations assuming reef VIIb represents growth at 119 ka BP at a paleo-sea level of 0±2 m. There is much better agreement between the sea level calculations at each transect used this assumed age for the last interglacial reef however, this may be the result of uncertainties in the uplift estimates. Because the rear reef elevations were used for the calculations, no allowance for growth depth was included.

Sea level calculation based on reef VIIb at 119 ka BP and 0±2m

	Reef	reef elevation	sigma elev.	age	sigma age	uplift	sigma uplift	rel sl	sigma
BOBO	VIIb	402	0.5	119	2	3.38	0.06	0.0	2.0
BOBO	VIa	326	0.5	107	4	3.38	0.06	-35.5	14.9
BOBO	VIb	286.8	0.5	100	4	3.38	0.06	-51.0	14.8
BOBO	Va,main	264	0.5	90.6	2	3.38	0.06	-42.1	8.6
BOBO	Va,outer	250	0.5	84	2	3.38	0.06	-33.8	8.4
BOBO	Vb	213.8	0.5	77.8	4	3.38	0.06	-49.0	14.3
BOBO	IV	197	0.5	71.2	2	3.38	0.06	-43.5	8.0
KWAMBU	VIIb	227.6	3	119	2	1.91	0.04	0.0	2.0
KWAMBU	VIa	173.4	0.5	107	4	1.91	0.04	-31.2	9.0
KWAMBU	VIb	144.3	0.5	100	4	1.91	0.04	-47.0	8.8
KWAMBU	Va,main	127.9	0.5	90.6	2	1.91	0.04	-45.4	5.6
KWAMBU	Va,outer	123.6	0.5	84	2	1.91	0.04	-37.1	5.4
KWAMBU	Vb	-	0.5	77.8	4	1.91	0.04		
KWAMBU	IV	88	0.5	71.2	2	1.91	0.04	-48.2	5.0
KWANG	VIIb	197	3	119	2	1.66	0.04	0.0	2.0
KWANG	VIa	140.8	0.5	107	4	1.66	0.04	-36.3	8.0
KWANG	VIb	120.7	0.5	100	4	1.66	0.04	-44.8	7.8
KWANG	Va,main	101.7	0.5	90.6	2	1.66	0.04	-48.3	5.0
KWANG	Va,outer	100.9	0.5	84	2	1.66	0.04	-38.2	4.8
KWANG	Vb	78.5	0.5	77.8	4	1.66	0.04	-50.3	7.4
KWANG	IV	-	0.5	71.2	2	1.66	0.04		

	Reef	Age	rsl	sigma rsl
SUMMARY	VIIa	119	0.0	2.0
	VIa	107	-34.3	11.1
	VIb	100	-47.6	10.9
	Va,main	90.6	-45.2	6.6
	Va,outer	84	-36.3	6.4
	Vb	77.8	-49.7	11.4
	IV	71.2	-45.9	6.7